STUDIES ON SOME IONIC LIQUIDS AS CORROSION INHIBITORS ON 6061 Al-15 VOL. PCT. SiC$_{(P)}$ COMPOSITE IN ACIDIC MEDIA
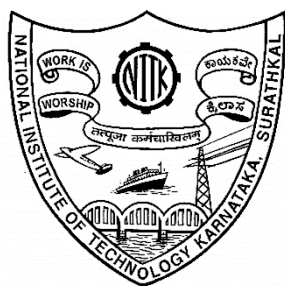
Thesis

Submitted in partial fulfilment of the requirements for the degree of

**DOCTOR OF PHILOSOPHY**

By

KSHAMA SHETTY S.

DEPARTMENT OF CHEMISTRY

NATIONAL INSTITUTE OF TECHNOLOGY KARNATAKA

SURATHKAL, MANGALORE - 575 025

NOVEMBER, 2015

DEDICATION

*To my **DAD**, for being my utmost strength,*
*To my **MOM**, for her unconditional love,*
*To my **SISTER**, for being my confidante,*
*To my **SOULMATE**, for his eternal affection,*
*To my **TEACHERS**, who motivated me,*
*To my **FRIENDS**, who stood by me.*
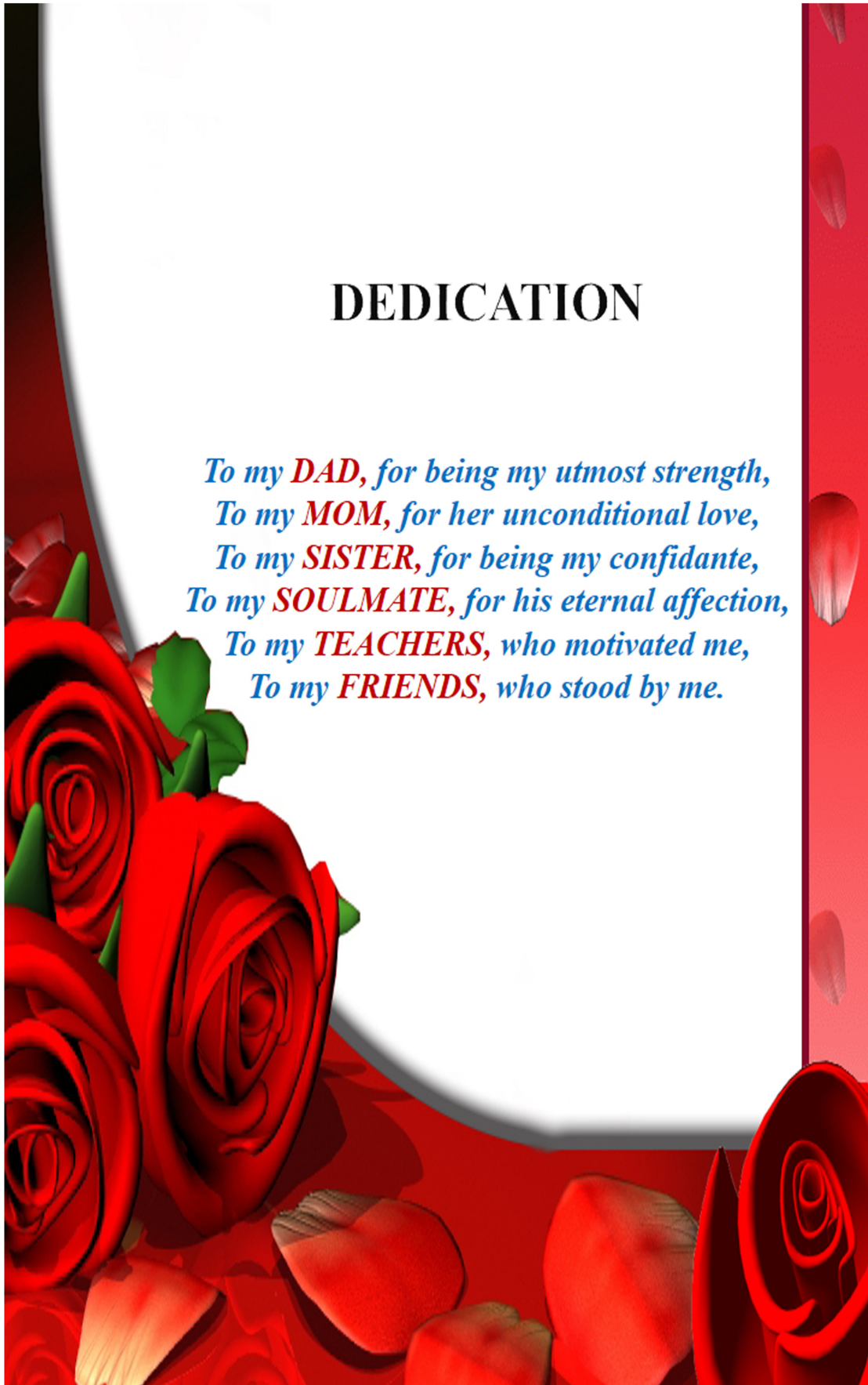
DECLARATION

I hereby *declare* that the Research Thesis entitled "STUDIES ON SOME IONIC LIQUIDS AS CORROSION INHIBITORS ON 6061 Al-15 VOL. PCT. SiC$_{(P)}$ COMPOSITE IN ACIDIC MEDIA" which is being submitted to the **National Institute of Technology Karnataka, Surathkal,** in partial fulfillment of the requirements for the award of the Degree of **Doctor of Philosophy** in Chemistry is a *bona-fide report of the research work carried out by me*. The material contained in this Research Thesis has not been submitted to any University or Institution for the award of any degree.

Kshama Shetty S

Register Number: 121164CY12F02

Department of Chemistry

Place: NITK – Surathkal

Date: 27 November 2015

CERTIFICATE

This is to *certify* that the Research Thesis entitled "STUDIES ON SOME IONIC LIQUIDS AS CORROSION INHIBITORS ON 6061 Al-15 VOL. PCT. $SiC_{(P)}$ COMPOSITE IN ACIDIC MEDIA" submitted by **Ms. Kshama Shetty S (Register Number: 121164CY12F02)** as the record of the research work carried out by her, is accepted as the *Research Thesis submission* in partial fulfilment of the requirements for the award of the Degree of **Doctor of Philosophy**.

(Dr. A. Nityananda Shetty)

Research Guide

Chairman – DRPC

ACKNOWLEDGEMENTS

ABSTRACT

The thesis entitled **"Studies on some ionic liquids as corrosion inhibitors on 6061 Al-15 vol. pct. SiC$_{(P)}$ composite in acidic media"** brings about detailed studies on the corrosion behavior of the composite and also the inhibition studies in hydrochloric acid and sulfuric acid media at different temperatures using electrochemical techniques like potentiodynamic polarization method and electrochemical impedance spectroscopy (EIS). Lately, the composites have replaced pure aluminum in wide variety of applications ranging from house-hold to aerospace applications. The increased strength to weight ratio, density, reduced coefficient of thermal expansion and other valuable attributes make it an engineer's choice over pure aluminum. As a misery to this choice, low corrosion resistance as compared to pure aluminum is the matter of concern among the corrosion engineers. Therefore, study of corrosion rate and developing new methods to control corrosion is inevitable. SiC particle reinforced composites are prone to micro-galvanic corrosion in the presence of strong electrolytes. Bearing in mind the *'go-green'* trend in recent research, four ionic liquids namely, [OPEIm$^+$][Br$^-$], [MPOEIm$^+$][Br$^-$], [OPEBen$^+$][Br$^-$], [MPOEBen$^+$][Br$^-$] were synthesized, characterized and studied for their corrosion inhibition effect on the composite. The activation parameters for the corrosion process and the thermodynamic parameters for the adsorption of inhibitors on the composite surface were evaluated. Surface analyses of the freshly polished surface of the composite and that of the corroded samples in the presence and absence of inhibitors were carried out by scanning electron microscopy (SEM) and the surface compositions were determined by energy dispersive X-ray (EDX) analyses. The synthesized ionic liquids acted as efficient corrosion inhibitors in both the acidic media under study at definite concentrations. [MPOEBen$^+$] [Br$^-$] showed higher efficiency at relatively lower concentrations owing to its macromolecular structure and high electron density, as compared to rest of the ionic liquids. The inhibition was found to be of mixed type with predominant cathodic control. The inhibitors were adsorbed on the composite surface predominantly through chemisorption, following Langmuir adsorption isotherm. Plausible inhibition mechanism is also proposed in the thesis.

Keywords: Al alloy composite, ionic liquids, acid inhibition, EIS, polarization.

CONTENTS

CHAPTER 1
CORROSION OF METALS AND COMPOSITES

CHAPTER 2
MATERIALS AND METHODS

CHAPTER 3
RESULTS AND DISCUSSIONS

CHAPTER 4
SUMMARY AND CONCLUSIONS

LIST OF FIGURES

LIST OF TABLES

NOMENCLATURE

ABBREVIATIONS

[MPOEBen⁺] [Br⁻]   1,3-Bis[2-(4-methoxyphenyl)-2-oxoethyl]-1*H*-benzimidazol-3-ium bromide

[MPOEIm⁺] [Br⁻]   1,3-Bis[2-(4-methoxyphenyl)-2-oxoethyl]-1*H*-imidazol-3-ium bromide

[OPEBen⁺] [Br⁻]   1,3-Bis(2-oxo-2-phenylethyl)-1*H*-benzimidazol-3-ium bromide

[OPEIm⁺] [Br⁻]   1,3-Bis(2-oxo-2-phenylethyl)-1*H*-imidazol-3-ium bromide

¹³C-NMR   Carbon-13 nuclear magnetic resonance

¹H-NMR   Proton nuclear magnetic resonance

A/C   Anode to cathode ratio

AC   Alternating current

ASTM   American society for testing and materials

CPE   Constant phase element

DC   Direct current

DDI   1,2-Dimethyl-3-decylimidazole iodide

EDX   Energy dispersive X-ray analysis

EIS   Electrochemical impedance spectroscopy

EW   Equivalent weight of the corroding material

FT-IR	Fourier transform infra-red
HF	High frequency
ILs	Ionic liquids
IUPAC	International union of pure and applied chemistry
LC-MS	Liquid chromatography-mass spectrometry
LF	Low frequency
MMCs	Metal matrix composites
NACE	National association of corrosion engineers
NASA	National aeronautics and space administration
NIGIS	NACE international gateway India section
OA-TS	Oleylammonium tosylate
OCP	Open circuit potential
ODA-TS	Octadecylammonium tosylate
SCE	Saturated calomel electrode
SCXRD	Single crystal X-ray diffraction
SEM	Scanning electron microscopy
TMA	N-triethylmethylammonium acetate
TML	N-triethylmethylammonium laurate
US	United States

SYMBOLS

E_a	Activation energy
α, β, γ	Angles between the cell edges in single crystal XRD
ω	Angular frequency
$Z_{(\omega)}$	Angular frequency dependent impedance
β_a	Anodic Tafel slope
$\Delta H^{\#}$	Apparent enthalpy of activation
$\Delta S^{\#}$	Apparent entropy of activation
w_i	Atomic weight of alloying element
N	Avogadro number
C_{dl}	Capacitance of the electrical double layer
β_c	Cathodic Tafel slope
R_{ct}	Charge transfer resistance
Q	Charge
C_{inh}	Concentration of the inhibitor
Q_{dl}	Constant phase element associated with electrical double layer capacitance
$i_{corr(b)}$	Corrosion current density in the absence of inhibitor

$i_{corr(inh)}$	Corrosion current density in the presence of inhibitor
E_{corr}	Corrosion potential
v_{corr}	Corrosion rate
n	CPE exponent
ρ	Density of the test specimen
W	Electrical work done
r_{oxd}	Equilibrium oxidation rate
r_{red}	Equilibrium reduction rate
i_0	Exchange current density
F	Faraday's constant
ω_{max}	Frequency at which the imaginary component of the impedance is maximum
Z''	Imaginary impedance
Z	Impedance
Z_{mod}	Impedance modulus
η	Inhibition efficiency
f	Inhibitor interaction parameter
a, b, c	Lengths of the cell edges in single crystal XRD
R^2	Linear regression coefficient

ε	Local dielectric constant
n'	Number of electrons transferred in a reaction
χ	Number of water molecules replaced per molecule of the adsorbed inhibitor
θ'	Phase angle
θ'_{max}	Phase maximum
h	Planck's constant
$R_{P(blank)}$	Polarization resistance in the absence of the inhibitor
$R_{P(inh)}$	Polarization resistance in the presence of the inhibitor
E	Potential
Z'	Real impedance
R_L	Resistance associated with the low frequency inductive loop
E_0	Rest Potential
$V_{(t)}$	Sinusoidal alternating potential signal
R_s	Solution resistance
ΔH^0_{ads}	Standard enthalpy of adsorption
ΔS^0_{ads}	Standard entropy of adsorption
ΔG^0_{ads}	Standard free energy of adsorption
θ	Surface coverage

T	Temperature
d	Thickness of the double layer/surface film
$I_{(t)}$	Time dependent current response
R	Universal gas constant
n_i	Valence of the alloying element
f_i	Weight fraction of the alloying element

Chapter 1
CORROSION OF METALS AND COMPOSITES

1.1 INTRODUCTION

Metals, alloys or composites have a wide array of modern-day as well as historic applications. They are used worldwide as the structural and building materials. Applications of these run from building to household appliances. Road, transport, defense, electronic circuits, machinery, etc., would be a dream without metals. Metals are boon to the society whereas, corrosion is bane.

Corrosion is considered to be the worldwide phenomenon. It is all-pervading and invincible. The word 'corrosion' originated from a Latin word '*corrodere*' which means "gnawing into pieces". Corrosion is defined in numerous ways. Evans (1923), a British Scientist, also known as the 'Father of corrosion' defines corrosion as largely an electrochemical phenomenon, which may be defined as destruction by electrochemical or chemical agents. Fontana (1986) defines corrosion as the destruction or deterioration of a material because of reaction with its environment. Uhlig and Revie (1991) defined corrosion as a destructive attack of a metal by a chemical or electrochemical reaction with its environment. Shreir (1994) defines corrosion as the reaction of an engineering material with its environment with a consequent deterioration in properties of the metal. Constituting all of the definitions, the International Union of Pure and Applied Chemistry (IUPAC) defines corrosion as an "irreversible interfacial reaction of a material (metal, ceramic, and polymer) with its environment which results in its consumption or dissolution into the material of a component of the environment". Often, but not necessarily, corrosion results in effects detrimental to the usage of the material considered. Exclusively, physical or mechanical processes such as melting and evaporation, abrasion or mechanical fracture is not included in the term corrosion. The metals are extracted from their respective ores using the definite amount of energy, an equivalent energy is released during a chemical reaction resulting in corrosion. The process of corrosion converts the metal back to its combined state. A schematic representation of '*metallurgy in reverse*' for iron is depicted in the Figure 1.1. Tarnishing of silver, rusting of iron, etc., are very common instances of

corrosion (Gadag and Shetty 2010). However, certain least active noble metals like gold and platinum are less likely to get corroded.

Corrosion science is linked directly to material science and deals with the study of corrosion of materials, mechanism, consequences and prevention of corrosion. Since the process of corrosion represents a complex interaction of materials across multiple disciplines, characterizing and unravelling corrosion becomes a puzzling, yet a thought-provoking task. The use of chemical thermodynamics in corrosion studies opened a wide field for comparison of thermodynamic parameters like enthalpy, entropy, Gibb's free energy and so on with corrosion phenomenon.
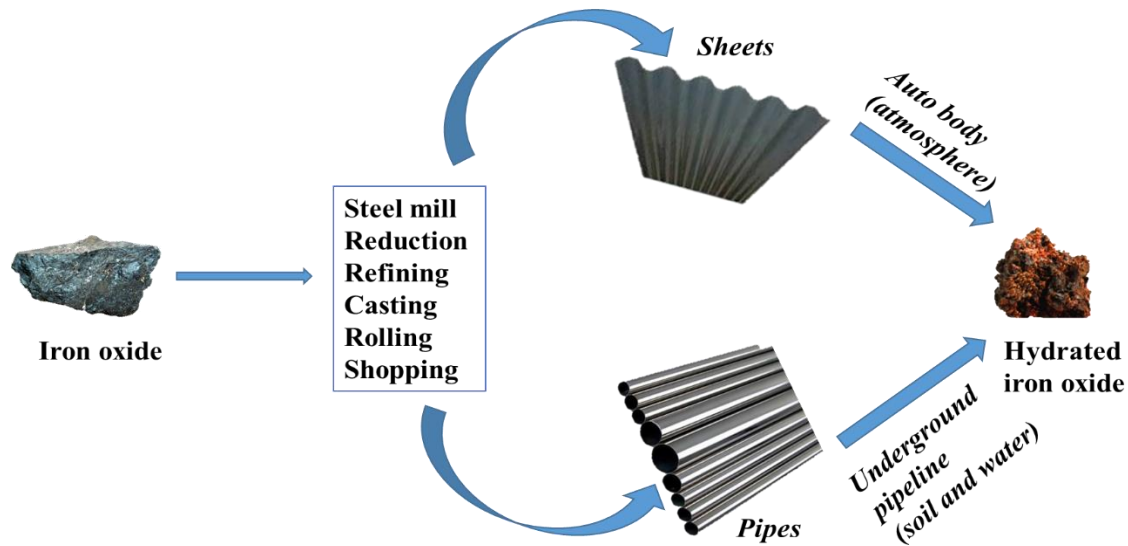
Figure 1.1 Schematic representation of '*metallurgy in reverse*' for iron.

1.2 CONSEQUENCES OF CORROSION

The phenomenon of corrosion may be either constructive or destructive. For example, chemical machining or chemical milling is widely used in aircraft and other applications where the unmasked areas are exposed to acid and excess metal is dissolved. On the other hand, world has witnessed many disasters due to corrosion. The Aloha airlines Flight 243 incident in 1988 where, over 65 passengers and flight attendant were injured killing one (NTSB Report No. NTSB/AAR-89/03). The Bhopal gas tragedy in the year 1984, was a result of corroded pipelines and valves (Cullinan 2004). In 1992, Gudalajara

sewer explosion caused damage to nearly 1600 buildings, injuring over 1500 people (Roberge 2007). In 1992, Boeing 747 freighter crash was fatal to people both on board and on ground and Carlsbad pipeline explosion in the year 2000 claimed about twelve lives (Roberge 2007). However, certain destructive consequences are listed in the following subsections (Fontana 1986).

1.2.1 Environment or health impact

Corrosion may adversely affect the cultural monuments across the world, including treasured articles of the antiquity in the museums. Loss of valuable or hazardous products (like uranium) by leakage due to crevices formed during corrosion may lead to severe loss and damage. In the recent years, use of metal prosthetic devices in the human body has been significant. The devices include pins, plates, hip joints, pacemakers, shoulder prosthesis, dental implants, etc. Corrosion of such bio-medical implants may be fatal to human beings. Despite of numerous better alloying and new technology of implants corrosion seems indomitable.

1.2.2 Economic impact

National Association of Corrosion Engineers (NACE) International Gateway India Section (NIGIS) declares corrosion to be a national calamity with India facing losses in lakhs of crores at World CORCON 2009 (Shetty 2009). Corrosion has both direct and indirect impacts on a country's economy. Leaching of undesirable metal ions due to minute corrosion into the products may lead to heavy losses. For example, the entry of a small metal ion into the solution may cause catalytic decomposition of the product say concentrated hydrogen peroxide or hydrazine, during manufacture and transportation. Loss of valuable products, cost in repairing the instruments, failures in bridge, building materials, machinery, etc., are a big blow to the country's economy causing plant shutdowns. Moreover, modern world hassles need of electronic circuits which are infinitely smaller in dimension for increasing the memory and computational density. Such electronic circuits contribute to evidently increased attack on the circuits by the

environment as the surface to volume ratio surges. Heavy losses may incur due to corrosion in aerospace, defense, automobiles, etc.

1.2.3 Technological impact

The phenomenon of corrosion always leads to overdesign of the metal components or alloying with less corrosive but expensive metals, etc. The designing of metal includes a lot of labor, time, energy and investment in order to prevent corrosion while operating at elevated temperature, pressure, corrosive environment, stress and so on. Such a scenario would be absent if not for corrosion. Technology would be proceeding at a higher rate with relatively lower investment. For example, designing of defense article needs heavy investment depending upon the environment in which the equipment is to be used. The design for a metal article to be used in the air force is different from that which would be used by the navy, the desert operated articles need a different design all the more. Such a demand would have an enormous technological impact.

1.3 ELECTROCHEMICAL THEORY OF CORROSION

The British scientist and the '*Father of corrosion science*' Ulick R. Evans has described '*corrosion*' to be largely an electrochemical phenomenon. Metals have the tendency to react electrochemically with its environment, be it water, oxygen or any other substance in an aqueous electrolyte. In an atmosphere or in an aqueous environment '*corrosion*' is an electrochemical process which involves transfer of electrons between the metal surface and aqueous electrolytes. According to electrochemical theory, corrosion takes place due to the formation of galvanic cells with the formation of anodic and cathodic region either on the same metal surface or when two metals are in contact with each other. Oxidation being the anodic reaction, the metal undergoes oxidation or corrosion at the anodic region. At the cathodic region, the metal is unaffected as it cannot be reduced further.

Any corrosion reaction may be classified into few generalized reactions, considering the oxidation-reduction reactions.

Anodic reaction: Electrons are liberated from the surface of the metal whose number is equivalent to its valance.

$$M \rightarrow M^{n+} + ne^-$$ (1.1)

Cathodic reaction: Various cathodic reactions occur during metallic corrosion, few among them are listed below.

Hydrogen evolution (acidic solutions):

$$2H^+ + 2e^- \rightarrow H_2$$ (1.2)

Hydrogen evolution (neutral or basic solutions):

$$2H_2O + 2e^- \rightarrow H_2 + 2OH^-$$ (1.3)

Oxygen reduction (acidic solutions):

$$O_2 + 4H^+ + 4e^- \rightarrow 2H_2O$$ (1.4)

Oxygen reduction (neutral or basic solutions):

$$O_2 + H_2O + 4e^- \rightarrow 4OH^-$$ (1.5)

Metal ion reduction:

$$M^3 + e^- \rightarrow M^{2+}$$ (1.6)

Metal deposition:

$$M^+ + e^- \rightarrow M$$ (1.7)

Equations 1.2-1.5 are common cathodic reactions. Reactions 1.6 and 1.7 are less common.

Corrosion involving oxygen is called oxygen type corrosion. Iron immersed in water or sea water in the presence of atmospheric oxygen is a common example of this type of corrosion.

The anodic reaction is

$$Fe_{(s)} \rightarrow Fe^{2+} + 2e^-$$ (1.8)

Since the medium is exposed to atmosphere, it contains dissolved oxygen. Water and sea water being nearly neutral, the cathodic reaction is as per Equation 1.4.

The Fe^{2+} ions and OH^- ions diffuse and when they combine ferrous hydroxide gets precipitated.

$$2Fe^{2+}{}_{(aq)} + 2OH^{-}{}_{(aq)} \rightarrow 2Fe(OH)_2 \downarrow \qquad (1.9)$$

If enough oxygen is present, ferrous hydroxide is readily oxidized to ferric hydroxide.

$$4\,Fe(OH)_2 + O_2 + 2H_2O \rightarrow 4Fe(OH)_3 \downarrow \rightarrow 2Fe_2O_3.6H_2O \qquad (1.10)$$
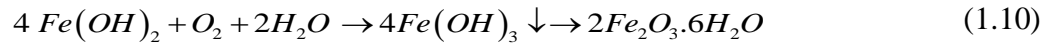
(Yellow rust)

In the presence of limited amount of oxygen, ferrous hydroxide is partially oxidized to form magnetite.

$$3Fe(OH)_2 + \frac{1}{2}O_2 \rightarrow Fe_3O_4.3H_2O \qquad (1.11)$$

(Black rust)

1.4 CLASSIFICATION OF CORROSION

Corrosion may be classified under various sub-headings. However, it may be mainly classified based on three factors as shown in Table 1.1.

Table 1.1 Classification of corrosion.

Inducing Cause	Corrosion Type	Features
Nature of the corrosive species	1. Wet corrosion	Electrochemical attack on the metal by the electrolyte.
	2. Dry corrosion	Chemical attack on the metal in the absence of moisture, usually by gaseous molecules at elevated temperatures.
Mechanism of corrosion	1. Electrochemical corrosion	Electrolytic destruction of the metal.
	2. Chemical corrosion	Direct chemical oxidation of the metal.
Surface appearance of the metal	1. Uniform corrosion	Corrosion rate is uniform.
	2. Localized corrosion	Corrosion in restricted area.

1.4.1 Forms of corrosion

It becomes convenient to classify corrosion based on the forms in which it manifests itself. Hence on the basis of appearance of the corroded material, they can be grouped under eight sub headings, however, all of these are inter-related. The eight forms are as given (Fontana 1986):

1.4.1.1 Uniform corrosion

Uniform corrosion is the most common form of corrosion. It is normally characterized by a chemical or electrochemical attack over a large area of the metal surface which causes thinning of the metal followed by its failure. For uniform corrosion to occur the entire surface should have equal interaction with the environment. However, this type of corrosion is not of great concern from the technical point of view, as one can accurately estimate the rate of corrosion by performing simple tests before designing such materials.

1.4.1.2 Galvanic corrosion

Galvanic corrosion also called as two-metal corrosion, occurs when dissimilar metals with a potential difference between them are immersed in a corrosive or conductive solution. Metal with lower electrode potential acts as anode and undergoes corrosion. Example: Iron sheets with copper screws where iron undergoes corrosion.

1.4.1.3 Crevice corrosion

Crevice corrosion is a form of localized attack that occurs in the narrow openings or spaces between metal to metal or non-metal to metal components. This occurs due to the concentration cell that is formed between the electrolyte within the crevice, which is oxygen deficient and the electrolyte outside the crevice which is rich in oxygen. Thus the material within the crevice acts as the anode and the exterior acts as cathode. Example: Steel corrosion in industries due to moisture in the crevice.

1.4.1.4 Pitting corrosion

Pitting is a localized form of corrosion that produces sharply defined depressions in the material. These depressions may vary from a few diameter to several diameters, but commonly small depressions occur. Pitting results in failure of equipment due to perforations with small percent weight loss of the entire structure. Quantitative assessment of this may not be easy, as the extent of pitting varies even under identical conditions. Example: Aluminum corrosion in chloride environment.

1.4.1.5 Inter-granular corrosion

Inter-granular corrosion is defined as the selective dissolution of grain boundaries or closely adjacent regions, without appreciable attack of the grains themselves. The attack on the metal occurs along the grain boundaries which dissolves as anode and body of the grain remain protected as cathode. The actual mechanism differs with each alloy system. Example: Small amount of iron in aluminum segregates in the grain boundaries and causes inter-granular corrosion.

1.4.1.6 Selective leaching

In selective leaching, a more reactive metal is removed from an alloy, leaving behind a porous weak deposit of the more noble metal. This results in an increase in the concentration of the remaining components, hence, it is also called as parting. This kind of corrosion is highly undesirable as it yields a porous metal with poor mechanical properties. Examples: Dezincification (selective removal of zinc from brass alloys), Graphitization (selective leaching of iron from gray cast iron).

1.4.1.7 Erosion-corrosion

Erosion-corrosion of the metal occurs due to relative motion of corrosive media across the metal surface. All types of equipment exposed to moving fluid are liable to undergo corrosion by erosion. The rate of corrosion is directly proportional to the rate of

flow of the corrosive medium, i.e. higher the flow higher is the corrosion rate and vice versa. Cavitation is a special case of erosion-corrosion. Examples: Propellers, impellers exposed to moving liquids.

1.4.1.8 Stress Corrosion

The cracking of materials by the combined effect of a tensile stress and specific corrosive media is referred as stress corrosion. The metal/alloy remains unaffected virtually, while fine cracks progress in a direction perpendicular to the direction of the tensile stress. Example: Cracking of brass in presence of NH_3.

1.5 FACTORS INFLUENCING THE CORROSION RATE

Despite of a vast number of factors which influences the rate of corrosion. It may be broadly classified as shown in the Figure 1.2. (Gadag and Shetty 2010).
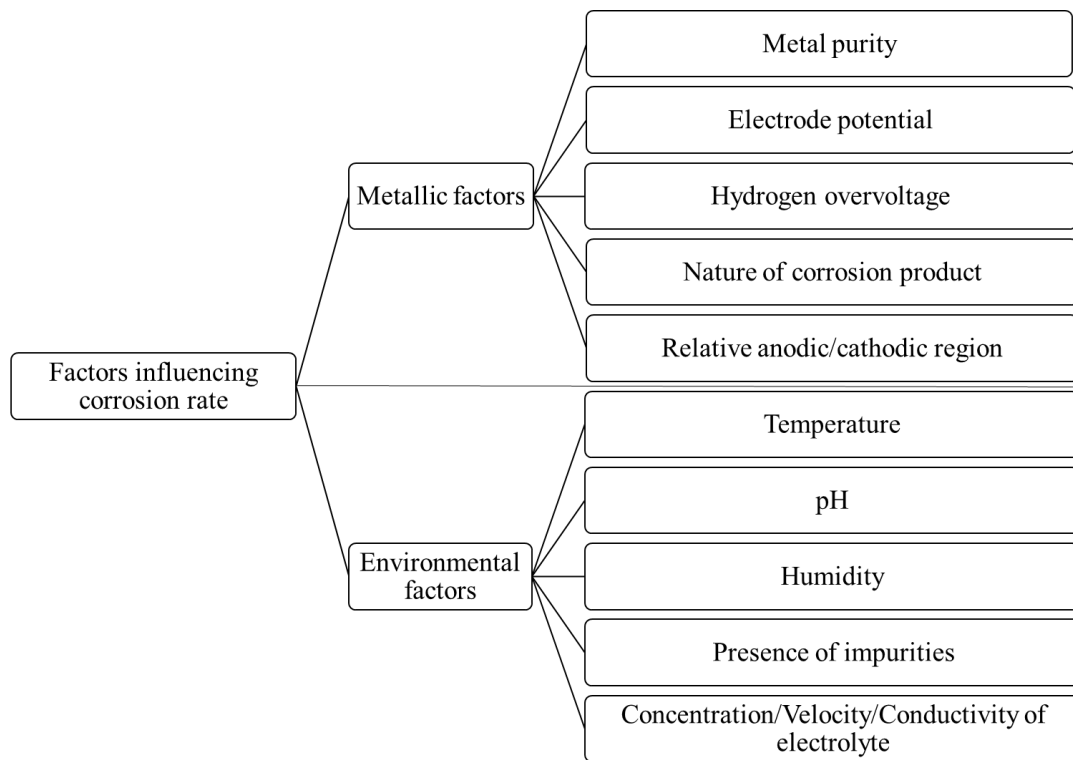
Figure 1.2 Flow chart showing factors influencing the rate of corrosion.

1.5.1 Metallic factors

Various factors of the metal play crucial roles in the understanding the mechanism and rate of corrosion. In the following sub-sections few of such factors are explained.

1.5.1.1 Metal purity

A pure metal is less likely to undergo electrochemical corrosion. However, very pure metals are more often subtle or expensive. To commercialize such metals, the alloying techniques are used. Such techniques are known to increase the strength and thereby used in various applications, ranging from household to aerospace industries.

1.5.1.2 Electrode potential of the metal

The standard electrode potential of the metal determines the susceptibility of metals to undergo corrosion. The metals with lower electrode potentials have greater tendency to undergo corrosion than the metals with higher reduction potentials. Aluminum, having the standard electrode potential of −1.66 V undergoes corrosion forming aluminum oxide. However, at neutral/near neutral solution corrosion doesn't occur due to surface passivation by an oxide layer.

1.5.1.3 Hydrogen overvoltage

When the cathodic reaction is of hydrogen evolution type, the hydrogen overvoltage plays an important role. Higher the overvoltage lesser is the rate of corrosion and vice versa. If the overvoltage is high, then the cathodic reaction is slower, thereby reducing the rate of anodic reaction, which in turn reduces overall corrosion rate.

1.5.1.4 Nature of the corrosion product

Usually, corrosion products are formed on the surface of the metal. If the product is stable, adherent, impervious and non-porous; it serves as a protective barrier to further

action by an electrolyte. However, if the corrosion product is soluble, porous and pervious; corrosion continues to occur at the metal surface.

1.5.1.5 Relative cathodic/anodic area

If the cathodic region is larger than the anode, faster consumption of electrons released by the anode occurs. Practically, anode to cathode (A/C) ratio is considered. If the A/C ratio is small, the corrosion is high.

1.5.2 Environmental factors

The environment in which the metal exists plays a crucial role in determining the corrosion rate. Same metal may show lower or higher corrosion rate based on the environment in which it's present. Few such factors are discussed under the following sub-headings.

1.5.2.1 Temperature

Corrosion is a redox process. Like any other chemical reactions, corrosion is largely influenced by temperature. Increasing the temperature of corrosive medium, the ions would gain excess energy, thereby, increasing its mobility. Increase in ionic mobility leads to the enhanced corrosion rate.

1.5.2.2 Medium pH

Acidic/alkaline pH markedly influences the corrosion rate. Usually, apart from certain metals like aluminum, acidic pH would cause greater corrosion than alkaline pH.

1.5.2.3 Relative humidity

The presence of moisture on the metal surface causes metals to corrode. Certain cases, where two metals with different electrode potentials are placed together, initiation of corrosion reaction occurs if there is any humidity or moisture between the two. Moisture acts as an efficient electrolyte.

1.5.2.4 Presence of impurities

Atmospheric pollutants like dioxide of sulphur combines with moisture and forms sulfuric acid. Such pollutants when comes in contact with metal surface containing moisture, acidic corrosion occurs.

1.5.2.5 Electrical conductivity

Ion migration between anode and cathode governs the reaction rate. Higher the conductivity, greater is the ionic conduction and the corrosion rate. Sea water is therefore more corrosive than fresh water.

1.5.2.6 Concentration of the medium

Concentration of the electrolyte refers to the amount of corrosive species present in an electrolyte. Higher the concentration of the electrolyte, higher is the corrosion rate. But weak acids are corrosive in lesser concentration, this is because at higher concentrations, weak acids undergo lesser ionization therefore rate of corrosion decreases.

1.5.2.7 Presence of oxygen/oxidizers

Presence of oxygen or oxidizers increases the metal corrosion rate. In certain metals, presence of moderate oxygen causes metal passivation. Oxygen undergoes reduction at cathode by consuming electrons released from the anode.

1.6 THERMODYNAMICS OF CORROSION

The study of thermodynamic aspects of corrosion throws light on corrosion process and mechanism. Certain traits of thermodynamics used in corrosion studies are briefly discussed in the following sections.

1.6.1 Free energy change of a corrosion reaction (Sastri et al. 2007)

The electrical work done in the electrical or electrochemical processes is defined as the product of the charges (Q) moved and the potential (E) through which it is moved. If the electrical work is done in an electrochemical cell in which cell potential is E and the charge is that of one mole of reaction in which n moles of electrons are transferred, then the electrical work ($-W$) done by the cell must be nE. In this relationship, Faraday constant F is required to obtain coulombs from moles of electrons. In an electrochemical cell at equilibrium, no current flows and the free energy change (ΔG) occurring in a reaction is expressed in Equation 1.12.

$$W = \Delta G = -nFE \qquad\qquad 1.12$$

For a galvanic cell, the cell potential is given by Equation 1.13.

$$E_{cell} = E_{cathode} - E_{anode} \qquad\qquad 1.13$$

Any spontaneous processes leads the system to thermodynamically stable state with reduced energy. The value of free energy change in a galvanic cell or for spontaneous process is negative and the cell potential is positive. Therefore, corrosion occurs only when the anodic metal dissolution is spontaneously taking place.

1.6.2 Thermodynamics of corrosion reaction: Pourbaix diagram

Marcel Pourbaix has derived and developed a unique, concise method, summarizing the thermodynamics of corrosion of a metal in potential-pH diagram. 'Pourbaix diagrams' are also called as "equilibrium diagrams" as they are applied to systems where metal is in equilibrium with the environment, these diagrams show ranges of potential and pH where the metal undergoes active corrosion or where it remains inactive (McCafferty 2010). The abscissa in the potential-pH plot is the pH of the electrolyte which measures the chemical environment and ordinate is the potential E which is the measure of electrochemical environment. In the Pourbaix diagrams, three possible types of straight lines are present.

- Vertical line: This corresponds to reactions involving only pH and not *E*.

- Horizontal line: This corresponds to reactions involving only *E* and not pH.

- Slanted line: This corresponds to reactions involving both *E* and pH.

1.6.2.1 Pourbaix diagram for aluminum

Pourbaix diagram shows certain distinct regions based on thermodynamic stability of the chemical species. Pourbaix diagram for aluminum is presented in the Figure 1.3, which displays 3 distinct regions mentioned as follows:

- Immunity: When the stable species is the unreacted metal itself.

- Passivity: When the stable species is the solid oxide/hydroxide layer.

- Corrosion: When the stable species is the dissolved ion.
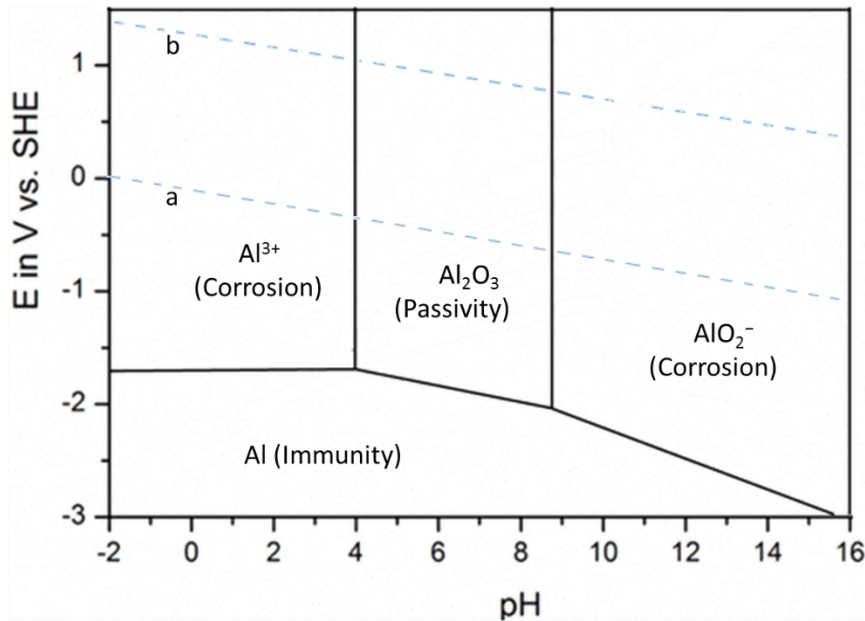
Figure 1.3 Pourbaix diagram of aluminum at 25 °C. Redrawn from (McCafferty 2010).

The advantages of Pourbaix diagrams includes the following:

- Predicting the impulsiveness of the corrosion process.

- Alteration in potential or pH values which would prevent active corrosion.
- Assessing the nature of the corrosion products.

Nothing interesting is ever completely one sided, so are the Pourbaix diagrams which have below mentioned limitations:

- These are purely based on thermodynamic predictions and never accounts for the kinetics of the reaction, which hints the practical values/observations deviating to different extents.
- These conditions refer only to equilibrium state and effects of temperature, velocity, etc., on the rates of corrosion are not accounted for.
- Pourbaix diagrams are usually for pure metals.
- The corrosion products formed are often considered as protective, whereas thickness, porosity, etc., may occur leaving behind non-protective corrosion product.

Although ample number of limitations could be listed, the advantages of Pourbaix diagrams always overshadow its limitations.

1.7 KINETICS OF CORROSION

The kinetics of corrosion process is equally significant like the thermodynamic aspect, as these fail to determine the rates of corrosion and are applied to systems in equilibrium state. Thermodynamics does not help in determining the rate of the corrosion whereas, when certain electrochemical kinetic concepts are applied to the corrosion phenomenon, corrosion rates can be determined. Few among the electrochemical kinetic concepts are briefly explained below.

1.7.1 Polarization

Polarization of an electrode is described as the kinetic deviation of the potential from the equilibrium due to flow of current to or from the electrode surface in a galvanic

cell. The degree of polarization i.e. overpotential or overvoltage is expressed in the Equation 1.14.

$$Overvolatge = E - E_0 \tag{1.14}$$

where, E is the potential during the flow of current and E_0 is the potential at the equilibrium in the absence of flow of current (terms like open circuit potential (OCP), corrosion potential or rest potential are used to denote potential at zero current flow).

1.7.1.1 Activation polarization

The reaction progressing in several successive steps at the electrode/electrolyte interface, results in activation polarization; wherein the rate of the reaction is determined considering the slowest of all the steps. Cathodic activation polarization may occur when the generation of the H atom at the cathodic sites occur at lower rates as compared to that of the supply of electrons to the cathodic sites. Therefore, excess of electrons reside at the cathodic sites which shifts the cathodic potential to more negative direction. Similarly, anodic polarization occurs as the result of slower oxidation at anodic sites which causes shift in the anodic curves to positive values of electrode potential.

1.7.1.2 Concentration polarization

Concentration polarization arises due to the diffusion layer adjacent to the electrode surface where there is gradient of ionic concentration. The ion diffusion through these layers controls the rate of any electrochemical reaction which is crucial for processes like corrosion or electroplating. The anodic polarization arises due to slow diffusion of the metal ions into the bulk electrolyte and cathodic polarization arises due to slow diffusion of cathodic reactants to the cathode surface. However, thermal treatment or mechanical agitation of the electrolyte results in decreased concentration polarization and increases the rate of electrochemical reactions.

1.7.1.3 Resistance/Ohmic polarization

Drop in potential due to resistance offered by the electrolyte surrounding an electrode (IR drop) causes Ohmic polarization. Low conductivity of the electrolyte has higher ohmic resistance unlike those electrolytes with high conductivity. Usually ohmic resistance can be overcome by decreasing the distance between the working and reference electrode by means of Luggin-Haber capillary.

1.7.2 Exchange current density

When a metal dipped in the electrolyte solution is at equilibrium, the rate of metal dissolution and the rate of deposition are equal. When the anodic and cathodic reactions are in equilibrium, the rates which are equal and opposite of each of the two reactions are referred to as exchange current density.

Expression for reaction rates in terms of current density is given by Equation 1.15 based on Faraday's law.

$$r_{\text{oxd}} = r_{\text{red}} = \frac{i_0}{n'F} \tag{1.15}$$

where, r_{oxd} and r_{red} are the equilibrium oxidation and reductions reaction rates, respectively, n′ is the number of electron transferred, F is Faraday's constant and i_0 is the exchange current density in A cm^{-2}.

The exchange current density, i_0 is dependent on below mentioned factors:

- Temperature of the electrolyte, usually i_0 is directly proportional to the electrolyte temperature.
- Concentration ratio of the oxidized to reduced species.
- Electrode surface: a rough electrode surface gives higher surface area therefore higher i_0.

- Electrode composition: The prolonged use of an electrode would cause surface passivation due to adsorption and in such cases i_0 would be different from the unused electrode.

1.7.3 Mixed potential theory

The mixed potential theory consists of two-simple hypothesis:

- Any electrochemical reaction can be divided into two or more partial oxidation-reduction reactions.
- There can be no net accumulation of charges during an electrochemical reaction.

Experimental determinations demonstrate that electrochemical reactions are composed of two or more partial oxidation or reduction reactions. The second hypothesis is a restatement for the law of conservation of charge. This means that the corrosion of an electrically isolated metal sample, the total oxidation rate must be equal to the reduction rate. The IUPAC defines mixed potential as the value of the potential of a given electrode with respect to a suitable reference electrode when appreciable contributions to the total anodic and/or cathodic partial currents are made by species belonging to two or more different couples, but the total current is zero. The mixed potential theory is a modern approach to understand the classical corrosion concepts as it explains the effect of oxidizer addition, cathodic concentration polarization and the influence of galvanic coupling on the rate of corrosion.

1.8 ELECTROCHEMICAL EVALUATION OF CORROSION

Corrosion is an electrochemical phenomenon which involves oxidation-reduction reactions. As corrosion proceeds, the metal undergoing corrosion tends to lose electrons at the anodic region and gets oxidized and the electrons released are consumed by the elements present in the electrolyte undergoing reduction at the cathodic region. Such a flow of electrons from anodic region to the cathodic region, causes current in the system. The current, therefore, can be measured and controlled electronically. This facilitates

electrochemical evaluation of corrosion process. The hardware controlled electrochemical testing methods may therefore be employed for characterization of metal corrosion properties and metal components in the presence of various metal/electrolyte combinations. The corrosion characteristics are specific to metal/electrolyte system.

Usually, the corrosion testing setup consists of a polarization cell consisting of a conducting electrolyte, a standard reference electrode like saturated calomel electrode (SCE) or silver/silver chloride electrode, a counter/auxiliary electrode like platinum, gold, etc., and the desired metal sample called the "working electrode", connected to a specimen holder. The three electrodes are then connected to an electronic instrument referred to as 'potentiostat'. The electrolyte is chosen based on the most resembling environment in which the working electrode is believed to come in contact with. In the electrolyte, an electrochemical potential (also called as voltage) is generated between the electrodes. The corrosion potential, E_{corr} is measured by means of potentiostat as an energy difference between the working and the reference electrode. The schematic representation of a potentiostat is given in the Figure 1.4.

A potentiostatic experiment involves application of a constant potential on the working electrode for a specified period of time. The resultant current is plotted against time. The measurement may be either potentiodynamic or galvanodynamic. In potentiodynamic measurements, the applied potential is increased with respect to time, while current is constantly monitored. The current or current density is then plotted against potential. On scanning the potential up to a pre-determined current density or potential, the potential scan may be reversed while current continues to be measured, such a scan is called as reverse or cyclic polarization.

The current may also be controlled and resulting potential could also be measured. Experiments where current is imposed are called as galvanostatic or galvanodynamic. Galvanodynamic plots include variation of potential against controlled current. Galvanostatic tests maintain a constant current and plot is of change in potential versus time.
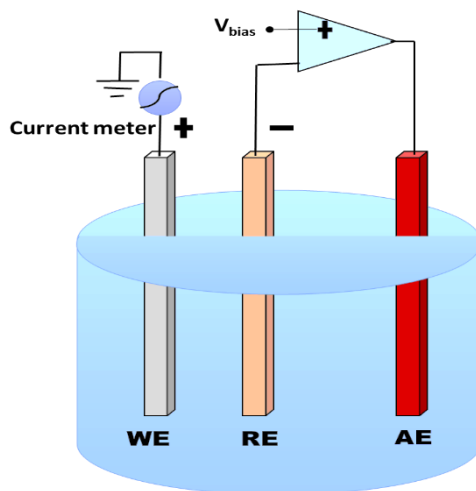
Figure 1.4 A schematic representation of a potentiostat.

The electrochemical measurements include:

- Direct current (DC) corrosion monitoring technique.
- Alternate current (AC) corrosion monitoring technique.

1.8.1 Direct current (DC) corrosion monitoring technique

DC polarization test is a potentiodynamic corrosion testing technique, where the potential of the electrode is varied at a selected rate by the application of a current through the electrolyte. When an electrode is polarized, it can cause current to flow via electrochemical reactions that occur at the electrode surface. The amount of current generated is controlled by the kinetics of the reactions and the diffusion of reactants both towards and away from the electrodes. In a cell where an electrode undergoes uniform corrosion at open circuit, the OCP is controlled by the equilibrium between two different electrochemical reactions.

1.8.1.1 Tafel extrapolation method

In the Tafel extrapolation method, the working electrode would be immersed in the electrolyte and then allowed to attain the steady-state potential or the OCP using an electrochemical workstation. On attaining the OCP, the system will be drifted away from its steady state both anodically and cathodically with regard to the OCP. A plot of logarithm of corrosion current density against the potential thus obtained is called Tafel plot. The anodic and cathodic branches are extrapolated such that their intersection point defines OCP at y-axis and corrosion current density (i_{corr}) at x-axis. However, to ensure accuracy, the linear region at least ±50 mV from the OCP and one decade of linearity is considered to ensure good accuracy in measurements. The corrosion potential (E_{corr}) is a thermodynamic parameter which is specific to sample and i_{corr} is a kinetic parameter which is directly proportional to the rate of corrosion. The anodic and cathodic Tafel slopes or constants are referred to as β_a and $-\beta_c$, respectively. A representative Tafel extrapolation is depicted in the Figure 1.5.
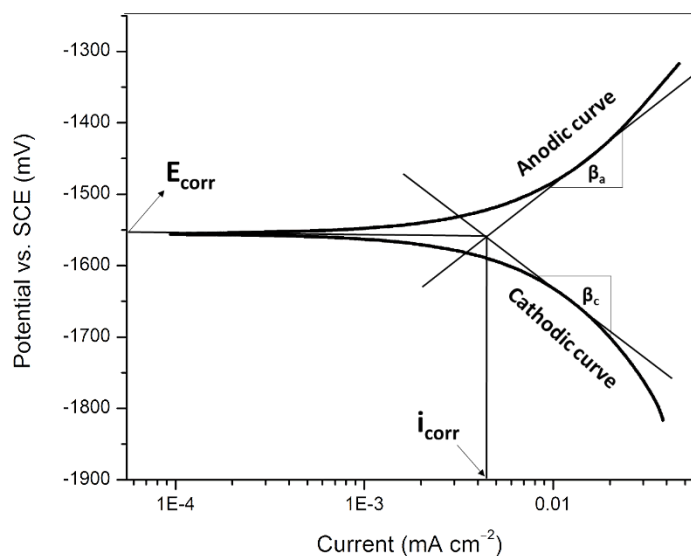
Figure 1.5 Representative Tafel plot showing extrapolation method.

Kinetically controlled electrochemical reaction of an isolated half-cell obeys Tafel Equation 1.16.

$$i = i_0 e^{(2.3(E-E_0)/\beta)} \tag{1.16}$$

where, i is the electrode current density of the reaction, i_0 is exchange current density, E is the electrode potential, E_0 is the equilibrium potential, β is the Tafel constant for a given reaction expressed in units of volts/decade. The combined Tafel equations for both the anodic and cathodic reactions of a corroding system generates the Butler-Volmer Equation 1.17, as mentioned below.

$$i = i_a + i_c = i_{corr}[e^{[2.3(E-E_0)/\beta_a]} - e^{[-2.3(E-E_0)/\beta_c]}] \tag{1.17}$$

where, β_a and β_c are Tafel constants for linear portion of anodic and cathodic Tafel branches up to 1 decade of current, respectively. Tafel constants are related to electrode kinetic parameters and are useful in valuation of polarization resistance (R_P) as described by the Stern-Geary Equation 1.18.

$$R_P = \frac{\beta_a \beta_c}{2.3 i_{corr}(\beta_a + \beta_c)} \tag{1.18}$$

The rate of corrosion is determined by the Equation 1.19.

$$\upsilon_{corr}(mm \quad y^{-1}) = \frac{K \times i_{corr} \times E.W}{\rho \times n} \tag{1.19}$$

where, constant K=0.00327 mm g μA^{-1} cm^{-1} y^{-1}, defining the unit of corrosion rate mm y^{-1}, i_{corr} is the corrosion current density expressed in μA cm^{-2}, $E.W$ is the equivalent weight of the corroding specimen, ρ is the density of corroding specimen.

Advantages of Tafel extrapolation technique:

- A rapid corrosion monitoring technique as compared to conventional weight loss method of analysis.
- Greater accuracy in determined rates of corrosion, even at extremely low corrosion rates.

- Continuous corrosion monitoring in industries are facilitated by Tafel polarization method.

Limitations of Tafel extrapolation technique:

- Is not applicable to the systems with more than one reduction processes, due to distortions in Tafel cathodic region and improper result acquisition.
- Metals exhibiting passivity results in concentration polarization and the Tafel region is not observed for such metals, there by deducing the Tafel constant by extrapolation is more likely to give error in measurement.
- Is a destructive measurement technique.

1.8.2 AC electrochemical monitoring techniques

1.8.1.2 Electrochemical impedance spectroscopy (EIS) measurements

Even in the absence of electrical potential, chemical etching of metal is more likely to occur. Application of an externally-defined potential would change the dynamics of surface chemical reactions. Such dynamics at an interface are extremely non-linear and powerful characterization tools becomes very much essential. For diagnostic reasons like characterizing changes at surface under specific system parameters or application reasons like system parameter tailoring in order to obtain desired effect of surface, EIS comes handy acting as bridge connecting both the purposes. EIS is a tool for unravelling any complex non-linear processes. It's a perturbation characterization of the dynamics of an electrochemical process. Impedance is nothing but AC analogue for DC resistance. A small amplitude (10 mV) ac signal is implied on top of the controlled DC polarization potential. The complex response of the system is obtained usually in Nyquist format, with inverted reactance. The response of the system as a function of the perturbation frequency can reveal the internal dynamics. The representative Nyquist and Bode phase angle and magnitude plots are shown in the Figures 1.6 and 1.7, respectively.
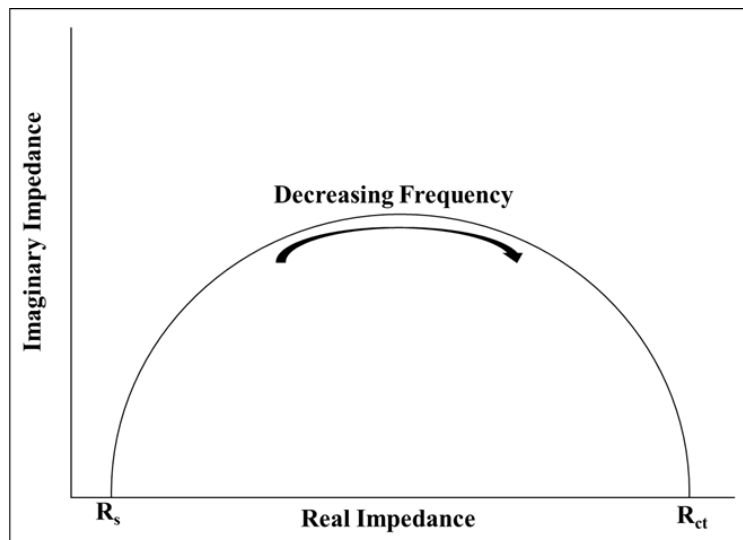
Figure 1.6 Representative Nyquist plot.
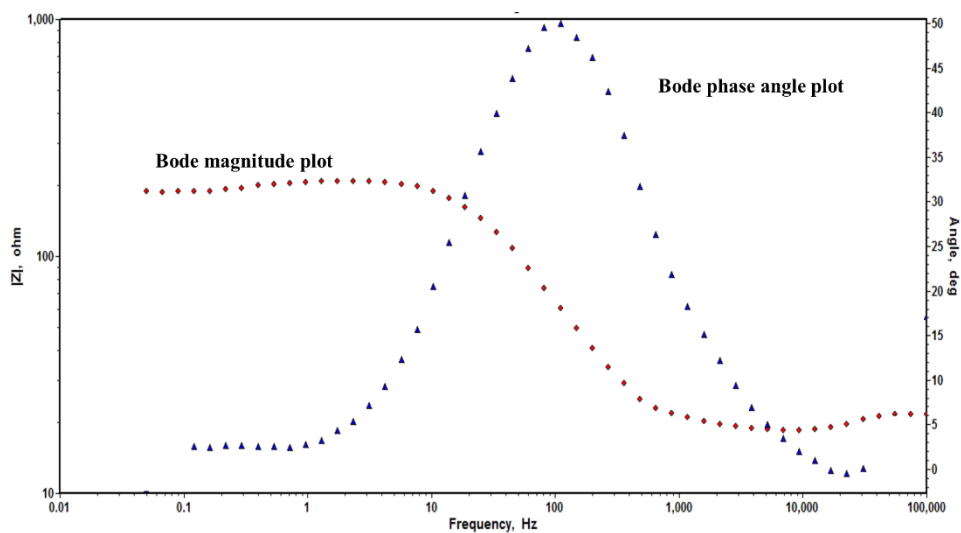
Figure 1.7 Representative Bode plots.

The time dependent current response $I_{(t)}$ of an electrode surface to a sinusoidal alternating potential signal $V_{(t)}$ has been expressed as an angular frequency (ω) dependent impedance $Z_{(\omega)}$ in Equation 1.20.

$$Z_{(\omega)} = V_{(t)} / I_{(t)} \tag{1.20}$$

where, t is time, $V_{(t)} = V_0 \sin \omega t$, $I_{(t)} = I_0 \sin(\omega t + \theta')$, $\theta' =$ phase angle between $V_{(t)}$ and $I_{(t)}$.

Various processes at the surface absorb electrical energy at discrete frequencies, causing a time lag and a measurable phase angle (θ'), between the time dependent excitation and response signals. These processes have been simulated by resistive capacitive electrical networks. The impedance, $Z_{(\omega)}$ may be expressed in terms of real $Z'_{(\omega)}$ and imaginary $Z''_{(\omega)}$ components.

$$Z_{(\omega)} = Z'_{(\omega)} + Z''_{(\omega)} \tag{1.21}$$

The impedance behaviour of an electrode may be expressed in Nyquist plots where $Z'_{(\omega)}$ as a function of $Z''_{(\omega)}$, in Bode plot of log $|Z|$ and θ' versus frequency 'f' in cycles per second (Hz), where $\omega = 2\pi f$. An important part of the EIS analysis is to create an 'equivalent circuit' of the system using resistors and capacitors in series and in parallel. The physical behaviour of the corrosion system can be simulated and quantified with this circuit to gain insight into the important processes in the corrosion system. The impedance spectra are modelled by assuming a circuit made up of resistors, capacitors and inductors and then fitting that circuit to the spectra to extract values of circuit elements. The values may then be related to physical phenomena to try to verify that the circuit model is a reasonable representation of the corrosion process. The Nyquist plot shows a semicircle, with increasing frequency in counter clockwise direction as shown in the Figure 1.6. At very high frequency, the imaginary component $-Z''$ disappears, leaving only the solution resistance, R_s. At very low frequency, $-Z''$ again disappears, leaving a sum of R_s and the Faradaic reaction resistance or polarization resistance (R_P). The Faradaic reaction resistance or polarisation resistance (R_P) is inversely proportional to the corrosion rate. R_s measured at high frequency can be subtracted from the sum of R_P and R_s.

Several advantages of EIS studies are as follows:

- Non-destructive method of analysis as it operates at the open circuit potential.

- Operational at extremely low corroding rates and low conductivity systems.
- Precise estimation of coating quality.

Shortcomings of EIS are as listed below:

- Complicated method of analysis and tedious data interpretation.
- EIS alone cannot fetch sufficient data, therefore usually tested along with other measurement techniques like potentiodynamic polarization.

Equivalent circuit modelling

EIS data analysis is commonly carried out by fitting it to an equivalent electric circuit model. An equivalent circuit model is a combination of resistors, capacitors, and/or inductors, as well as a few specialized electrochemical elements, which produces the same response as the electrochemical system does when the same excitation signal is imposed. Each circuit component comes from a physical process in the electrochemical cell and has a characteristic impedance behaviour. The shape of the model's impedance spectrum is controlled by the style of electrical elements in the model and the interconnections between them. The size of each feature in the spectrum is controlled by the circuit elements parameters. For example, a resistor can be used in places where there are possible conductive paths in the electrochemical reaction.

The electrochemical parameters such as solution resistance (between the reference electrode and the working electrode) and polarization resistance are represented by an equivalent resistor in the model circuit. Capacitors and inductors are used where there are possible space charge polarization region in the electrochemical process. The equivalent circuit should be as simple as possible to represent the electrochemical system and it should give the best possible match between the model's impedance and the measured impedance of the system.

1.9 CORROSION CONTROL/PREVENTION

The corrosion process can be controlled to a larger extent by retarding the anodic or cathodic reaction. This reduction in the reaction rate may be achieved by several ways as mentioned below.

- **Metal conditioning**
a) *Coating of the metal*: A corroding metal can be separated from the corroding environment by effective coating either with another metal, coating derived from metal itself or organic coatings like enamel, grease, oil, paint, etc.
b) *Alloying of the metal*: By producing a more corrosion resistant alloy, Eg: stainless steel, in which ordinary steel is alloyed with chromium and nickel. Stainless steel is protected by an invisibly thin, naturally formed film of chromium sesquioxide (Cr_2O_3).
- **Corrosive environment conditioning**
a) *Removal of oxygen*: Removal of oxygen from the systems by addition of strong reducing agents like sulphite would eliminate the major contributing factor to corrosion in the pH range of 6.5-8.5.
b) *Addition of corrosion inhibitors*: Addition of chemical species in appropriate concentrations would reduce the rate of corrosion by various phenomenon. Detailed explanation would be given in the coming sections.
- **Electrochemical control**: The rate of the corrosion reaction may be controlled by passing anodic/cathodic currents into the metal. Cathodic protection may be achieved by using a DC power supply or by obtaining electrons from the anodic dissolution of a metal with low electrode potential in the galvanic series such as aluminum, zinc or magnesium**.**

1.10 CORROSION CONTROL BY INHIBITORS

Corrosion control by inhibitors has been a most economical and practical method over other methods in industries where pipelines, heaters, boilers, etc., are prone to attack

by corrosive species in the form of contaminants, by-products, cleansing or pickling agents like hydrochloric or sulfuric acid. The inhibitors provide first-line shield against corrosion. Inhibitors are the chemical substances which slow down either anodic, cathodic or both the electrochemical processes when added in suitable concentrations to the corrosive medium. Pre-requisite of an ideal inhibitor are:

- The inhibitor must be chemically inert and must be effective in preventing the dissolution of metal when added in small amounts.
- It must be stable in the medium i.e. should not undergo decomposition.
- It must be cost-effective and eco-friendly.
- It should also inhibit the diffusion of hydrogen ions into the metal.
- Chemisorbing ability for longer protection.
- Must be dispersible in the medium.
- Must be macromolecular.

A corrosion inhibitor can function in two ways. In some cases the inhibitors alter the corrosive environment into a non-corrosive or less-corrosive environment through its interaction with the corrosive species. In other cases the corrosion inhibitor interacts with the metal surface and as a consequence inhibits the corrosion of the metal. Thus, based on the mode of interaction; there are two broad classes of inhibitors which are discussed in the following section.

1.10.1 Types of inhibitors

A flow chart of classification of inhibitors is given in Figure 1.8 (Flick 1993, Papavinasam 1999, Sastri 2012).

1.10.1.1 Environment modifiers

The action of aggressive species on the metals surface is reduced by the addition of environmental modifiers. These inhibitors eliminate corrosive species from the medium

acting as scavengers. A vital constituent that initiates corrosion is removed which reduces one among the anodic or cathodic reactions thereby influencing the overall corrosion rate.
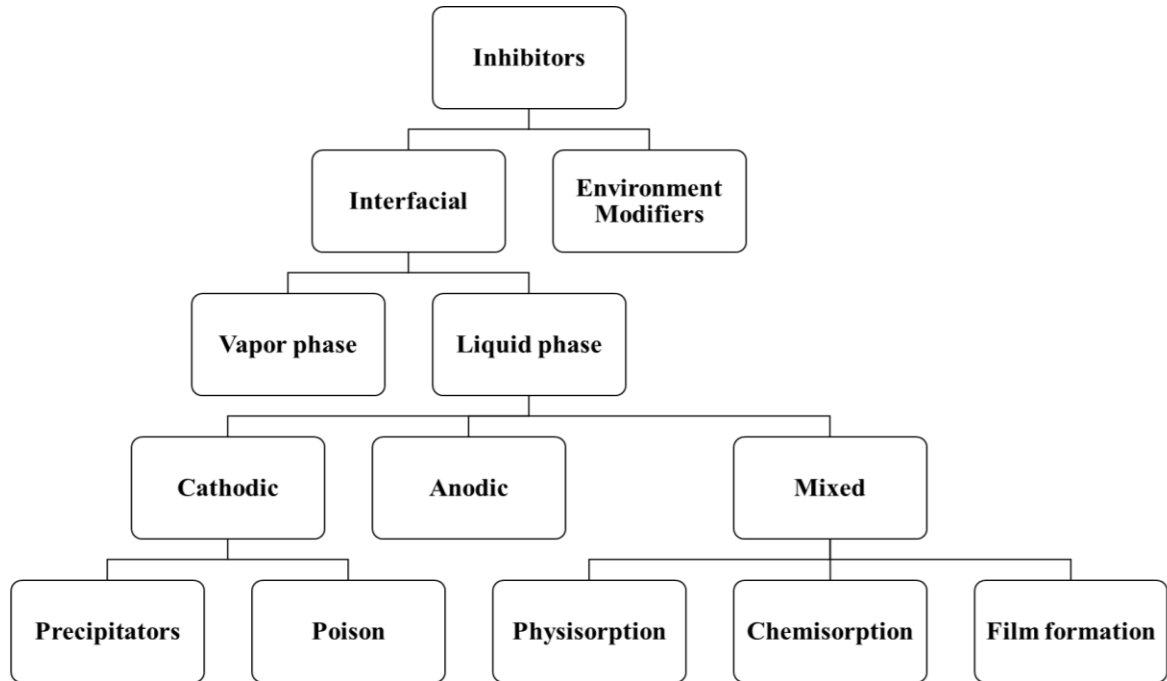
Figure 1.8 Flow chart of classification of inhibitors (Redrawn from Papavinasam (1999)).

1.10.1.2 Interfacial inhibitors

As the name suggests, interfacial inhibition includes inhibitors which can form film on the metal surface and serve as barriers between the metal and corrosive medium. Their further classifications are explained as follows:

a) Vapour-phase inhibitors: These are very similar to the organic adsorption type inhibitors and possess a very high vapour pressure. As a consequence, these materials can be used to inhibit atmospheric corrosion of metals without being placed in direct contact with the metal surface. The inhibitors are placed in the vicinity of the metal to be protected and they are transferred to the metal surface by sublimation and condensation to the metal surface. The vapour-phase inhibitors are usually only effective if used in closed spaces such as inside packages or on the interior of machinery

during shipment (Fontana 1986). On contact with metal surface, vapour of these inhibitors condenses and moisture hydrolyses it to liberate protective ions.

b) Liquid-phase inhibitors: These are the inhibitors that act as barriers between the metal and the electrolyte in the dissolved form. These are further classified follows:

- *Anodic inhibitor*: Anodic inhibitors are those substances which act on the anodic sites. They displace the corrosion potential (E_{corr}) in the positive direction and reduce the corrosion current (i_{corr}), there by retard the anodic reaction and suppress the corrosion rate. Basically, oxyanions such as chromates, molybdates, tungstates and also sodium nitrite are very effective anodic inhibitors. The anodic inhibitors combine with metal ions formed at the anodic region, forming the sparingly soluble respective salts. These compounds formed are deposited on the anodic sites forming the protective films, which act as barriers between the fresh metal surface and the corrosive medium, thereby preventing further anodic reaction. Anodic inhibitors are found to be effective only when sufficient amount of the inhibitor is added into the corrosion medium. When insufficient quantity of an anodic inhibitor is added, corrosion may be more rather than inhibition. The effect of anodic inhibitors on polarization curves is shown in Figure 1.9(a).

- *Cathodic inhibitor*: Cathodic inhibitors are those substances which act on the cathodic sites and polarize the cathodic reaction. They displace the corrosion potential in the negative direction and reduce the corrosion current, there by retard the cathodic reaction and suppress the corrosion rate. Cathodic inhibitors may be divided into three categories viz. (i) those that consume oxygen (deaerators or oxygen scavengers) (ii) those that reduce the area of cathode and (iii) those that increase the hydrogen over potential on the cathode. The effect of cathodic inhibitors on polarization curves is shown in Figure 1.9(b).

- *Mixed inhibitor*: These are substances which affect both the cathodic and anodic reactions. Corrosion potential change in such a case is smaller. Mixed type of inhibitors are generally organic compounds which are adsorbed on the metal surface and suppress

31

both the metal dissolution and the reduction reactions. The effect of mixed inhibitors on polarization curves is shown in Figure1.9(c).

Mixed inhibitors protect the metal in three possible ways:

i. *Physical adsorption*: Physical adsorption is the result of the electrostatic forces of attraction between the inhibiting organic ions or dipoles and the electrically charged surface of the metal. Inhibiting species that undergo physical adsorption interact rapidly with the surface; however they can also be removed easily from the surface. It depends on: a) Structural parameters, such as hydrocarbon chain length and the nature and position of the substituents in the aromatic ring, b) Electrical characteristics of inhibitors i.e. charge on the hydrophilic group, c) Type of ions present in the solution and d) Potential on the metal.

ii. *Chemisorption*: Chemisorption of inhibitor molecules on the metal surface is slow and involves interaction forces stronger than the forces in physisorption. A coordinate type of bond between the metal and the inhibitor is thought to be present with charge transfer from the inhibitor to the metal. Chemically adsorbed inhibitors are the most effective inhibitors.

iii. *Film formation*: During the chemical adsorption adsorbed inhibitor molecules may undergo surface reactions producing films. The properties of films are dependent upon its thickness, composition, solubility, temperature and other physical parameters. Some adsorbed inhibitor molecules produce polymeric films. Corrosion protection increases markedly as the films grow from nearly two-dimensional adsorbed layers to three-dimensional films with a thickness of several hundred Angstroms. Inhibition is effective only when the films are adherent, insoluble and prevent access of the solution to the metal.

- *Precipitation inhibitor*: Precipitation inhibitors are compounds that cause formation of precipitates on the metal surface, by combining with the metal ions, blocking both anodic and cathodic sites. Inhibitors promote the formation of bulky precipitation film over the entire surface. Examples: silicates, phosphates, etc.
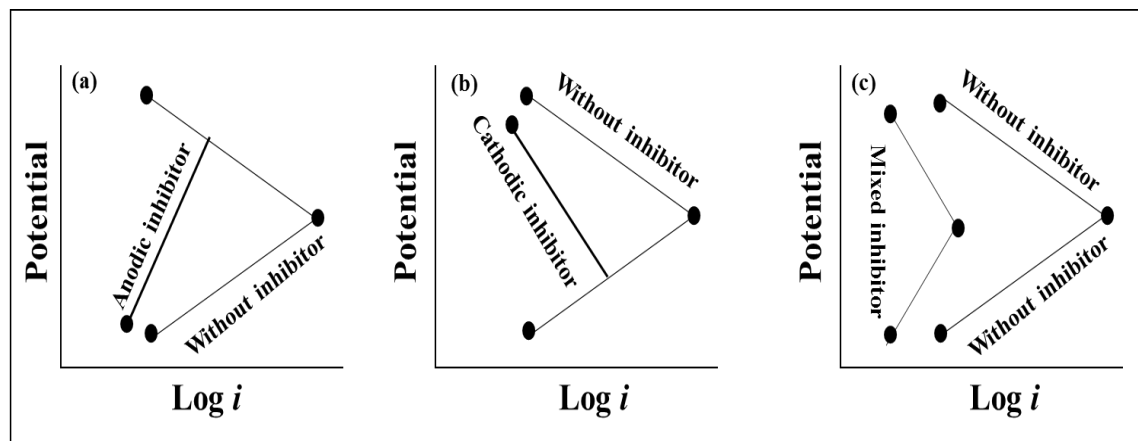
Figure 1.9 Evans diagrams showing the effect of addition of a) anodic inhibitor b) cathodic inhibitor and c) mixed inhibitor (Redrawn from (Fontana 1986)).

1.11 FACTORS GOVERNING THE INHIBITION EFFICIENCY

Organic substances serve extensively as corrosion inhibitors. The efficiency of an inhibitor depends not only on its structure, but also on the characteristics of the environment in which it acts, the nature of the metal and other experimental conditions. Commercial inhibitor packages contain surfactants, de-emulsifiers, carriers and biocides in addition to the active inhibitor. The active ingredient of organic inhibitors invariably contain one or more functional groups containing one or more heteroatoms like N, O, S, P or Se through which the inhibitors anchor to the metal surface. Some common anchoring groups are given in Table 1.2.

The anchoring groups may be attached to the parent chain (backbone), which increases the ability of the inhibitor molecule to cover a large surface area. The backbone may contain additional molecules or substituent groups, to enhance the electronic bonding strength of the anchoring group on the metal and/or to enhance the surface coverage.

Table 1.2 Common anchoring organic groups (Sastri 1998).

Structure	Name	Structure	Name
-OH	Hydroxyl	-CONH$_2$	Amide
—C≡C—	-yne	-SH	Thiol
-C-O-C-	Ether	-S-	Sulfide
-COOH	Carboxy	—S=O	Sulfoxide
-N=C=O	Isocyanate	—C=S—	Thio
-NH$_2$	Amino	—P=O	Phosphonium
-NH	Imino	-P-	Phosphor
-NO$_2$	Nitro	-As-	Arsano
—N=N—N—	Triazole	-Se-	Seleno

The factors that influence the inhibition efficiency are as mentioned below (Knag 2006, Papavinasam 2011):

1. **Structure of the inhibitor**: The substituents, the anchoring element and the core back bone, collectively have the effect on the inhibition efficiency of an inhibitor. The metals act as Lewis acids, which are electron acceptors and therefore, inhibitors must be Lewis bases containing electron donor ability. The backbone or the core moiety which holds the donor atoms or substituents plays a role in supplying electrons to the donor moieties, increasing their electron density and boosting the easy donation. Substituents which are electron donors are preferred for inhibitors.

2. **Temperature of the environment**: If the inhibition is due to the physisorption of the inhibitor on the metal surface, the raise in temperature would have negative impact on inhibition efficiency as the adsorbed inhibitors tend to desorb from the metal surfaces at elevated temperatures. Conversely, chemisorption is favoured at elevated temperature, where a co-ordinate type of bond may be formed between the donor and acceptor. However, under extremely elevated temperatures the inhibitor itself may undergo degradation/decomposition.

3. **Charge on the metal surface**: The metal in contact with the electrolyte develops a charge, based on the type of electrolyte used. The charge on the metal surface is dependent on the difference in the equilibrium corrosion potential and the potential of zero charge. If the metal surface is positively charged, negatively charged inhibitors are preferred and vice versa.

4. **Intermolecular interactions among the adsorbed molecules:** The intermolecular interactions between the adsorbed molecules may be either attractive or repulsive. Attractive interactions would increase the surface coverage thereby increasing the efficiency and repulsive interactions would cause lesser surface coverage.

5. **Synergism and antagonism:** A combination of inhibitor along with other ions can be productive or destructive depending on their mutual interactions. The efficiency, if increased in the presence of an element in addition to the inhibitor than when the inhibitor operates alone is called synergism or the other way round is antagonism.

1.12 MODES OF INHIBITION BY INHIBITORS IN ACID ELECTROLYTES

In acidic media, the main cathodic process is the either the discharge of H^+ ions or the reduction of dissolved oxygen. The anodic reaction is perpetually the dissolution of metal. The adsorbed inhibitor may influence any of these two reactions and control the corrosion in any of the following stated ways.

1.12.1 Blocking of the reaction sites

The main action of the inhibitors is to block the anodic or cathodic sites on the surface by adsorption. This effect is exhibited by aliphatic sulphides or quinoline during corrosion of iron in H_2SO_4. The rate of reaction is proportional to the extent of surface coverage by the adsorbed inhibitor species (Hoar 1948). Hakerman (1962) stated that the inhibitors block the anodic and cathodic sites equally. If the mechanism of corrosion reaction is not affected, the blocking action of the inhibitors can be recognized by the parallel shift in the polarization curves for both anodic and cathodic reactions without the changes in the Tafel slopes (Abdallah 2004).

1.12.2 Participation in the electrode reactions

The adsorbed inhibitors can also retard the corrosion reaction by participating in the electrode reactions thereby affecting the mechanism of inhibition. The electrode reactions of corroding systems are more often multi-step processes involving many intermediate species. The presence of adsorbed inhibitor interferes with the formation of intermediate species, or in some cases the corrosion reaction may proceed through alternative intermediate species involving the inhibitor. The participation of the inhibitor can be characterized by the changes in Tafel slopes of the polarization curves of the reaction (Iofa et al. 1964).

1.12.3 Interfacial inhibition

Interfacial inhibition essentially results in decreasing the rate of physical, electrochemical and/or chemical partial processes of corrosion reaction, which occur in the immediate vicinity of the metal-solution interface. The accumulation of the interface inhibitors in the double layer causes hindrance to the partial reactions of the electrode, which finally decreases the overall electrochemical process (Fischer 1972).

1.13 ALUMINUM/ALLOYS/COMPOSITES

German chemist, Andreas Marggraf first realized an unknown metal in alum in 1746. After over 50 years, Sir Humphry Davy coins the name 'alumium' and later 'aluminium' in the year 1809. Following a series of attempts from the year 1825, finally in the years 1886 and 1889, aluminium was isolated by Hall-Heroult and later by Bayer. These methods are used till date for the production of pure aluminium. Aluminium (renamed as aluminum by the American Chemical Society in the US in 1925) is the third most abundant element (~8.2 wt. %) in the earth's crust following, oxygen (~46wt. %) and silicon (~28.2 wt. %).

Pure aluminum readily reacts with atmospheric oxygen and forms protective aluminum oxide layer on its surface. This layer is highly stable in the neutral and near-

neutral pH environments. Pure aluminum is soft, ductile, recyclable, formable, corrosion resistant and has high electrical and thermal conductivity. Aluminum has density, one-third of steel and used in applications which demand greater strength and lesser weight. Customarily, pure aluminum is alloyed or transformed into composites to boost the strength to weight ratio, enhance the density, improve the performance ability, etc. Alloying is usually done with another metal which can overcome the drawbacks of pure aluminum. Composites are usually made of semi-conducting or ceramic materials. The desired mechanical properties are attained by applying heat treatment to the micro-structure. Ce, Cu, Cr, Fe, Mn, Ti, Zr, Zn are the alloying elements usually added to aluminum (Naeem et al. 2014). These elements either dissolve or transform into compounds in the micro-structure. Composites are made by reinforcing silicon carbide or titanium di-boride, etc. However, corrosion properties may vary depending on the alloying or reinforcing type. Despite of all the pros and cons aluminum/alloys/composites have wide array of applications.

1.13.1 Applications of aluminum/alloys/composites

Owing to the exceptional properties of aluminum/alloys/composites as discussed in the previous section, it encompasses numerous applications ranging from the field of aerospace to day-to-day utilities. Each of them are discussed in detail in the following sub-sections.

1.13.1.1 Transport applications

The airframe of modern flights is composed of 80% aluminum by weight. Aluminum alloys are the irresistible choice for the fuselage, wing and supporting structures of commercial airliners and military cargo/transport aircraft. Structural components of current US Navy aircraft are made up of fabricated wrought aluminum. Ever since the launch of Sputnik a half-century ago, aluminum has been the material of choice for space structures of all categories. Preferred for its light weight and its ability to withstand the stresses occurring during the launch and operation in space, aluminum was used in Apollo

spacecraft, the Skylab, the space shuttles and the International Space Station. Aluminum alloys consistently surpass other metals in areas such as mechanical stability, dampening, thermal conductivity and reduced weight. Attention is now focused towards aluminum casting technology, which offers lower engineering costs, the ability to form complex figures and the suppleness to incorporate innovative design concepts. The primary structures of the Orion spacecraft of National Aeronautics and Space Administration (NASA) are made from an aluminum-lithium alloy and will be covered by an advanced version of the thermal protection tiles used on the space shuttle. After the very earliest days of manned flight, the excellent strength to weight ratio of aluminum have made it the prime material for the construction of aircraft. The properties of aluminum based alloys are also used in passenger and freight rail cars, military vehicles, boats and ships, buses and coaches, bicycles and increasingly in motor cars. The sustainable nature of aluminium with respect to corrosion resistance and recyclability has driven the demand for aluminum vehicle components.

1.13.1.2 Marine applications

Superstructures of ships are mainly made of aluminum plate or extrusions. The usage of these materials consents designers to increase the above waterline size of the vessel without creating stability glitches. The weight benefit of aluminum has allowed marine engineers to gain better performance from the available power by using aluminum in the casings of hovercraft, fast multi-hulled catamarans and surface planing vessels. Also, aluminum has become the established material for helidecks and helideck support structures on offshore oil and gas rigs, ladder, railings, gratings, windows and doors. The alike reasons have resulted in the widespread use of aluminum in telescopic personnel bridges and oil rig stair towers. It's used in deckhouses, hatch covers of ship, etc.

1.13.1.3 Building and architecture

Formability of aluminum into shapes due to ductility has virtues as building material. It includes, roofing, foil insulation, doors, cladding, balustrading, etc.

Recyclability of aluminum has been a windfall to building owners who prefer deconstruction over demolishing of buildings. Such ability saves the *Mother Nature* from being affected due to landfilling from scrap materials. The inherent durability and porosity of anodized aluminum allows it to accept any coloring agents like pigments, dyes, etc., which reduces the maintenance cost. Aluminum endures demand in recent days because it is well-suited with present day's fast-track construction practices.

1.13.1.4 Industrial applications

It's possible to transform aluminum into thin foils of about 6.5 microns which is impermeable to light, oils/fats, gases, moisture and other volatile compounds. These properties along with remarkable heat and cold resistance, non-toxicity, formability, etc. make them extremely useful in industries like food and packaging, pharmaceutical packing, insulation, laminates, electric shielding and so on.

1.13.1.5 Miscellaneous applications

Sports articles, ladders, high pressure gas cylinders, furniture, lithographic printing plates, road barricades and signs, components of machinery, etc. are all the applications of aluminum.

1.14 6061 Al-15 VOL. PCT. SiC$_{(P)}$ COMPOSITE

6061 Al-15 vol. pct. SiC$_{(P)}$ composite is a 'material system' composed of combination of a macro constituent like silicon carbide and aluminum alloy 6061. The base alloy 6061 Al is designated as below:

- The first digit '6' represents the alloying elements Si and Mg.
- The second digit '0' represents no other alloying metals with appreciable quantity.
- The third digit '6' represents 0.6 wt. % Si.
- The fourth digit '1' represents 1.0 wt. % Mg.

The pure aluminum is transformed into an alloy or composite by particle reinforcement to augment its efficacy. The addition of SiC particles into Al alloy is known to enhance fracture toughness, boost strength to weight ratio, reduced thermal expansion coefficient and to ameliorate the stiffness. However, as compared to pure aluminum both alloy and composite are susceptible to corrosion due to micro-galvanic action in the presence of electrolyte/moisture. These composites find vast applications in aviation, marine, defense and other industries.

1.15 LITERATURE REVIEW

1.15.1 Corrosion behavior of pure aluminum/alloys/composites in acidic media

As an established fact, composites are known to corrode faster than the base alloy/pure aluminum although the attack was mainly confined to the interface, resulting in pitting or crevice formation. In the base alloys, the growth of an oxide film on the alloy surface occurs rapidly in acid sulfate and acid chloride solutions (Ford et al. 1980), in the presence of oxygen and water, providing it protection from corrosive species. In SiC reinforced composites, the areas where SiC particles are present, fails to form protective oxide layer and makes the film discontinuous and more corrosion susceptible. The increase in temperature also leads to the increase in the rate of corrosion of aluminum alloys/composites (Bhat et al. 1991, Niel and Garrard 1994).

Studies on aluminum alloys based metal matrix composites (MMCs) have shown that more pits are formed on composites than on unreinforced alloys (Hihara and Latanision 1994). Pitting attack is reported to be the major form of corrosion in SiCp/aluminum MMC (Gnecco and Beccaria 1999). Pitting is the major form of localized attack on Al 6013-20 SiC in chloride solutions (Ahmad et al. 2000). Pits in the SiC/aluminum composites were deeper than those in the Al_2O_3/aluminum composites, probably because the SiC particles acted as efficient cathodic sites (Bobic et.al. 2010).

Studies on corrosion behavior of AA6063/$Al_2O_{3(p)}$ composite in NaCl, NaOH and H_2SO_4 by Alaneme and Bodunrin (2011) conclude that, composites exhibit excellent

corrosion resistance in salt medium than in alkali or acid media. The unreinforced alloy exhibited slightly greater corrosion resistance than the composites in NaCl and NaOH media but the composites had better corrosion resistance in H_2SO_4 medium. Besides, solution heat-treatment resulted in improved corrosion resistance for both the composites and the unreinforced alloy while the effect of volume percent alumina on corrosion resistance did not trail a consistent trend.

Evaluation of the corrosion resistances of aluminum alloy matrix/ 2.5% particulate glass reinforced composite in 5 wt. % NaCl, 10 wt. % HCl and 10 wt. % NaOH were carried out by Ihom et al. (2012). They concluded that the composite could not be used either for holding HCl solution or as a structural material where HCl solution was found. Similarly, it could not be used for holding NaOH solution or environment containing NaOH as it selectively dissolved the composite leaving behind an altered residual structure. However, the composite was recommended to be used in sodium chloride medium as the corrosion rate falls within the recommended range of 1-200 mpy.

Ovat (2012), demonstrated the influence of corrosion on heat treated Al (6063) immersed in 10 wt. % sulfuric acid solution. The results showed that the corrosion susceptibility of heat treated Al (6063) was found to be lesser than the monolithic Al alloy. It was also noted that the passive films formed on the alloy was sufficiently stable which contributed in the reduction of the corrosion rate on the heat treated alloy after 35 days of immersion.

Boukerche et al. (2014) have described the degradation of aluminum in hydrochloric acid, sulfuric acid, nitric acid and sodium hydroxide media. The dissolution of aluminum in acidic solution is more complicated to predict and depends on the combination of several parameters such as the nature of anions/concentration, medium pH and temperature. It was observed that in a chloride-containing liquid media, aluminum dissolution was found to be strongly temperature sensitive. The reactivity of aluminum in acidic media where nitrates and sulfates were present, was very small while their presence with other anions may radically change their behaviors. This was observed with sulfates in

the mixture 4 M H_2SO_4 + 4 M HCl, where a strong synergetic effect on aluminum dissolution was observed.

Ismail (2015) has studied the corrosion behavior of aluminum-silicon-copper-manganese alloy in sulfuric acid medium. At room temperature, for electrolytes containing 10-15% of sulfuric acid, alloy exhibited corrosion resistance. However, at 50 °C, the rate of corrosion was increased. Pitting corrosion was observed.

Since numerous decades, significant efforts were made to study the corrosion behavior of Al 6061/ $SiC_{(p)}$ MMC materials (Ferrando 1989, Hihara and Latanision 1994), but was observed that the results did not match as the corrosion resistance properties of various composites vary with the processing techniques, types of reinforcement techniques and particulate size of the reinforcements. Therefore, very scarce reliable information are available regarding the corrosion resistance of 6061 Al/$SiC_{(P)}$ MMC (Turnbull 1992, Pinto 2010).

1.15.2 Corrosion inhibition of pure aluminum/alloys in acidic media

The review of literature reveals that very few organic inhibitors are reported for 6061 Al-15 vol. pct. $SiC_{(P)}$ composite. Nevertheless, a large number of organic compounds are reported as effective inhibitors for pure aluminum/alloys/composites in acidic media out of which few are listed in the Table 1.3.

Table 1.3 Few reported inhibitors for aluminum/alloys in acidic media.

Specimen	Inhibitor	Medium	Remarks	Reference
Aluminum	1,1(Lauryl amido)propyl ammonium chloride	HCl	Physisorption, Frumkin isotherm, Anodic inhibitor	El Rehim et al. 2001
Aluminum	Vanillin	HCl	99.4% efficiency in 5 M HCl, Langmuir isotherm	El-Etre 2001

Specimen	Inhibitor	Medium	Remarks	Reference
Aluminum	Ethoxylated fatty acids	HCl, H_2SO_4	Flory–Huggins isotherm, Increasing the chain length of the fatty acid is favorable	El-Sherbini et al. 2003
Aluminum	Sulfonic acid, Sodium cumene sulfonate and Sodium alkyl sulfate	HCl	Increasing medium concentration/temperature was unfavorable for inhibition, Temkin isotherm.	Maayta and Al-Rawashde 2004
Aluminum	Alanine, Leucine, Valine, Proline, Methionine, and Tryptophan	HCl + H_2SO_4	Langmuir and Frumkin isotherm, Mixed inhibitor.	Sorkhabi et al. 2005
Aluminum	Benzylidene-(2-methoxy-phenyl)-amine, (2-Methoxy-phenyl)-(4-methyl-benzylidene)-amine, (4-Chloro-benzylidene)-(2-methoxy-phenyl)-amine and (4-Nitro-bezylidene)-(2-methoxy-phenyl)-amine	HCl	Inhibition efficiency depends on the functional group, Langmuir adsorption, Physisorption.	Sorkhabi et al. 2006
Al 2024	Salicylaldoxime, Quinaldic acid and 8-Hydroxyquinoline	Neutral chloride	Chemisorption, Precipitation	Lamaka et.al. 2007
Aluminum	Fluconazole	HCl	Temkin adsorption isotherm, Physisorption	Obot et.al. 2008
Aluminum	2.3-Diaminonaphthalene	HCl	Freundlich isotherm, synergetic inhibition with iodide ions.	Obot et.al 2009
Al 6063	Floxacillin, Dicloxacillin, Cloxacillin and Cefadroxil	H_3PO_4	Frumkin/Temkin isotherm, Moderate inhibitor (50%)	Fouda et al. 2009

Specimen	Inhibitor	Medium	Remarks	Reference
Aluminum	3-Pyridinecarboxaldehyde thiosemicarbazone(meta), Isonicotinaldehyde thiosemicarbazone(para) and 2-Pyridine carboxaldehyde thiosemicarbazone(ortho)	HNO_3	Physisorption, Chemisorption	Khaled 2010
Aluminum	1,2-Diaminoethane	H_2SO_4	Adsorption by ligand exchange mechanism	Mercier et.al. 2010
Aluminum	Diphenolic Schiff bases	HCl	Cathodic inhibitor, Temkin adsorption isotherm, Chemisorption	Yurt et.al. 2011
Aluminum	Schiff bases	HCl	Cathodic inhibitor,Temkin adsorption isotherm	Safak et.al. 2012
Aluminum	Schiff bases	HCl	Mixed inhibitor, Langmuir isotherm, physisorption	Patel et al. 2013
Al-Si	Phenazone and Aminophenazone	HCl	Temkin isotherm, Physisorption	Fouda and Abdallah 2014
AA5052	Triazinedithiol	HCl	Chemisorption, Langmuir isotherm, Cathodic inhibitor	Wang et al. 2014
Aluminum	2-(2,6-Dichloranilino) phenylacetic acid	HCl	Mixed inhibitor, Langmuir adsorption, Physisorption	Hameed et al. 2015

1.15.3 Ionic liquids (ILs) as corrosion inhibitors

The studies by Uerdingen et al. (2005) demonstrated that ionic liquids can be used as corrosion inhibitors on copper, brass, carbon steel, stainless steel, aluminum and aluminum alloys. Their studies on different imidazolium-based ionic liquids having

ethylsulfate, octylsulfate, tosylate and dimethyl phosphate counter ions showed the rate of corrosion of AlMg3 alloy was only 0.03 mm y^{-1}.

Ashassi-Sorkhabi and Es'haghi (2009) have studied 1-butyl-3-methylimidazolium bromide as corrosion inhibitor on mild steel in 1 M hydrochloric acid. The IL acted as a mixed-type inhibitor without modifying the mechanism of hydrogen evolution reaction. The adsorption followed Langmuir adsorption isotherm and 94% inhibition efficiency was attained at about 20 mM concentration of the IL.

Noor (2009) has reported quaternary N-heterocyclic compound as corrosion inhibitor for Al-Cu alloy in HCl medium providing up to 98 % efficiency. It followed Langmuir model of adsorption and the adsorption was by physisorption.

Zhang and Hua (2009) have reported 1-butyl-3-methylimidazolium chloride and 1-butyl-3-methylimidazolium hydrogen sulfate ionic liquids as corrosion inhibitors for mild steel in HCl medium. The ionic liquids acted as mixed inhibitors showing 93.6% efficiency at 30 °C. Inhibition by the ionic liquid with hydrogen sulfate counter ion was more than by the ionic liquid with chloride counter ion.

Zhang and Hua (2010) have reported alkylimidazolium ionic liquids as corrosion inhibitor for aluminum in HCl medium with 93 % of efficiency. The ionic liquids adsorbed on the metal surface through physisorption, obeying Langmuir adsorption isotherm.

Triazolyl blue tetrazolium bromide was investigated as corrosion inhibitor for steel in hydrochloric acid and sulfuric acid media by Li et al. (2011a). The maximum inhibition efficiency in 1 M HCl was 95.1% and in 0.5 M H_2SO_4 was 88.2% at 0.5 mM concentration of the ionic liquid.

Scendo and Uznanska (2011) have reported 1-butyl-3-methylimidazolium chloride (BMIMCl) and 1-butyl-3-methylimidazolium bromide (BMIMBr) as corrosion inhibitors on copper in 1.0 M Cl^- solutions. The ionic liquids showed inhibition efficiency of 95.5 %

and 92 %, respectively. They acted as mixed inhibitors and their adsorption on the metal surface followed Langmuir adsorption isotherm.

Likhanova et al. (2011) have reported corrosion inhibition of carbon steel in 1 M sulfuric acid using imidazolium ionic liquids containing vinyl-hexafluorophosphate as anion inhibitor. The five imidazolium-type ionic liquids containing both, N1-unsaturated and N3-long alkyl saturated chains (cations), and hexafluophosphate as anion, displayed inhibition efficiency in the range of 80-97% when tested on carbon steel surface at 25-40 °C in aqueous 1 M sulfuric acid. They behaved as mixed inhibitors and the adsorption on the steel surface followed Langmuir adsorption isotherm.

Ibrahim et al. (2011) have reported pyridinium and imidazolium based ionic liquids as inhibitors on carbon steel in acidic medium. The inhibitor showed maximum efficiency of upto 75 % and the adsorption of the ionic liquids on the steel surface followed Langmuir adsorption isotherm.

Guzman-Lucero et al. (2011) have reported the five imidazolium type ionic liquids with bromide counter ion as corrosion inhibitors on carbon steel surface in 1 M sulfuric acid medium. Inhibition was attributed to the adsorption of imidazolium molecule on both anodic and cathodic sites.

Zarrouk et al. (2012) have studied imidazolium ionic liquid derivatives as corrosion inhibitors on carbon steel in 1 M HCl. The Langmuir adsorption isotherm was proposed for the adsorption of the ionic liquid on carbon steel surface. The inhibition efficiency of the ionic liquid was up to 97.3%.

Aoun (2013) has studied imidazolium-based ionic liquid as a corrosion inhibitor for carbon steel in hydrochloric acid electrolyte. The ionic liquid showed an inhibition efficiency of 85.5%. The inhibition was of mixed type and the adsorption of the ionic liquid on the steel surface followed Langmuir adsorption isotherm.

Yousefi et al. (2014) studied imidazolium-based ionic liquids as modulators of corrosion inhibition effect of SDS on mild steel in hydrochloric acid solutions. The results showed that the formation of a three-dimensional hydrogen bond network between imidazolium ring and their counter ions could affect the corrosion behavior of mild steel. Solutions of ILs/SDS mixtures showed good inhibition properties compared to solutions of individual surfactant and ILs, due to strong adsorption on the metal surface and formation of protective films.

Olivares-Xometl et al. (2014) have studied adsorption and corrosion inhibition performance of three ionic liquids, namely, 1,2-dimethyl-3-decylimidazole iodide (DDI), N-triethyl methyl ammonium acetate (TMA) and N-triethyl methyl ammonium laurate (TML) on API 5L X52 steel in acid media. The adsorption displayed by DDI, TMA and TML on the API 5L X52 steel surface was both physical and chemical adsorption modes. Efficiency was in the range of 30-70 %.

El Mouden et al. (2014) have examined 1-(2-ethoxy-2-oxoethyl) pyridazinium chloride as corrosion inhibitor for carbon steel in 1 M hydrochloric acid. The IL exhibited an inhibition efficiency of 92.8% in 1 M HCl. The adsorption followed Langmuir adsorption isotherm.

Zheng et al. (2014) have investigated 1-butyl-3-methyl-1H-benzimidazolium iodide as corrosion inhibitor on mild steel in sulfuric acid medium. An inhibition efficiency of 97.2% was obtained and the adsorption of the ionic liquid followed Langmuir adsorption isotherm.

Atta et al. (2015) examined the new hydrophobic ionic liquid derivatives, namely octadecylammonium tosylate (ODA-TS) and oleylammonium tosylate (OA-TS) for corrosion protection of steel in 1 M HCl medium. The inhibition efficiency of ODA-TS was 98.8% and that of OA-TS was 96.6% as given by polarization measurements. The adsorption of the ionic liquids was both by physisorption and chemisorption phenomena, obeying Langmuir adsorption isotherm.

El-Mahdy et al. (2015) have reported the influence of green corrosion inhibitor based on chitosan ionic liquid on the corrosion of steel in chloride solution. Maximum inhibition efficiency obtained was 95%. The adsorption of the inhibitor on the steel surface followed Langmuir isotherm.

Messaadia et al. (2015) studied the adsorption and corrosion inhibition property of pyridazinium-based ionic liquid on carbon steel in 0.5 M sulfuric acid. The maximum inhibition was 91.6%. The adsorption of the ionic liquid on the steel surface was through physisorption phenomenon and followed Langmuir adsorption isotherm.

Hegazy et al. (2015) have studied the corrosion inhibition of carbon steel in hydrochloric acid medium by 1-dodecyl-methyl-1H benzo[d]-[1,2,3] triazole-1-ium bromide. The maximum inhibition efficiency was 94.1%. The adsorption of the inhibitor was by physisorption and followed Langmuir adsorption isotherm.

1.15.4 Studies on corrosion behavior/corrosion inhibition of 6061 Al-15 vol. pct. SiC$_{(P)}$ composite/base alloy in various media

Bhat et al. (1991), have studied the corrosion behavior of 6061 Al/SiC$_{(P)}$ composite in sea water and sulfuric acid medium of different concentrations. It was observed that the composites in the cast form were more prone to corrosion than the extruded forms. The lower corrosion susceptibility of the extruded form was attributed to less defects in the matrix and less agglomeration of SiC particles in the extruded form.

Pinto et al. (2009) have studied the corrosion behavior of 6061 Al-15 vol. pct. SiC$_{(p)}$ composite and its base alloy in 1:1 hydrochloric acid and sulfuric acid mixture. The results indicated that the composites were more prone to corrosion than the base alloys.

Kumari et al. (2012) have reported the corrosion behavior of 6061 Al-15 vol. pct. SiC$_{(p)}$ composite and its base alloy in sodium hydroxide medium. The corrosion rates of both the composite and the base alloy increased with the increase in the concentration of the medium and temperature. The experimental results showed that the composite and the

base alloy did not form the passivation layer in the chosen concentration (0.05-0.5 M) of the corrosion media.

The review of literature reveals that very few organic inhibitors are reported for 6061 Al-15 vol. pct. SiC (P) composite.

Rao et al. (2005) have reported 3-methyl-4-amino-5-mercapto-1,2,4-triazole as inhibitor for the corrosion of 6061 Al-15 vol. pct. SiC(P) composite in hydrochloric acid medium. The inhibition efficiency of 58% at 30 °C was obtained.

Nayak et al. (2008) have studied allyl thiourea and glycyl glycine as corrosion inhibitor for T-6 treated 6061 Al-15 vol. pct. SiC(P) composite in HCl medium. They have reported that the T-6 treatment enhanced the rate of corrosion and also the inhibitors were moderately effective with an inhibition efficiency of 58%.

Pinto et al. (2011a) reported that 4-(N,N-dimethyamino)benzaldehyde thiosemicarbazone as an efficient mixed type of corrosion inhibitor for 6061 Al-15 vol. pct. SiC (p) composite and its base alloy in mixture of sulfuric acid and hydrochloric acid. The adsorption of the inhibitor on the composite and the alloy surface followed Freundlich adsorption isotherm. The inhibition efficiency of the inhibitor on the composite was 77.6% and that on the base alloy was 74.8%.

Pinto et al. (2011b) reported 4-(N,N-dimethyamino)benzaldehyde thiosemicarbazone as an inhibitor for 6061 Al-15 vol. pct. SiC (p) composite and its base alloy in sulfuric acid medium. Inhibitor obeyed Langmuir's model of adsorption, and the adsorption was predominantly through physisorption. The inhibitor exhibited 72% inhibition efficiency.

Pinto et al. (2011c) reported 4-(N,N-diethylamino)benzaldehyde thiosemicarbazone as a corrosion inhibitor for 6061 Al-15 vol. pct. SiC(P) composite and its base alloy in 0.5 M sulfuric acid. The adsorption of the inhibitor on both the composite and the base alloy was through physisorption obeying Langmuir's adsorption isotherm.

Kumari et al. (2011a) reported 3-methyl-4-amino-5-mercapto-1,2,4-triazole as a corrosion inhibitor for 6061 Al-15 vol. pct. SiC $_{(p)}$ composite in NaOH solution. The adsorption of the inhibitor was through physisorption and followed Langmuir adsorption isotherm.

Kumari et al. (2011b) have reported 3-ethyl-methyl-4-amino-5-mercapto-1,2,4-triazole as an inhibitor for 6061 alloy in NaOH medium. The adsorption of the inhibitor obeyed Langmuir adsorption isotherm. The reported inhibition efficiency was 59%.

Kini et al. (2010) studied the corrosion inhibition of 6061 Al-15 vol. pct. SiC $_{(p)}$ composite using ethyl-2-phenyl- hydrozono-3-oxobutyrate in different concentrations of HCl solution. The inhibitor acted as an efficient cathodic inhibitor with a maximum efficiency of 90.62 %. The adsorption of the inhibitor followed Temkin adsorption isotherm.

Kini et al. (2011) used 3-chloro-1-benzothiophene-2-carbohydrazide to inhibit the corrosion of 6061 Al-15 vol. pct. SiC $_{(p)}$ composite in HCl solution. The adsorption was through physisorption, obeying Langmuir and Temkin adsorption isotherms. The inhibition efficiency was reported to be 88.2%.

Kini et al. (2012) reported propanoyl(1Z)-N-(2,6-dimethylphenyl)-2-oxopropanehydrazonoate as corrosion inhibitor for 6061 Al-15 vol. pct. SiC$_{(P)}$ composite in 0.5 M and 1 M HCl medium. The inhibitor was reported to be a cathodic type of inhibitor being adsorbed through physisorption on the composite surface following Temkin adsorption isotherm.

Kumari et al. (2014) have reported 4-amino-5-(4-nitrophenyl)-4H-1,2,4-triazole-3-thiol at different temperatures and concentrations of NaOH by electrochemical techniques. The percentage efficiency was 75 and the inhibitor predominantly controlled the cathodic reaction. The temperature studies showed that increase in temperature was unfavorable to the inhibition.

1.16 SCOPE AND OBJECTIVES

1.16.1 Scope

Aluminum alloy composite materials vaunt wide array of applications ranging from kitchen to aviation applications. As the aviation industries were emergent in larger rates, development of newer materials took the centre-stage and therefore alloying and reinforcement of pure aluminum were carried out for yielding materials of high efficacy. Alloys and composites have been a boon to engineers of various fields for the remarkable properties they possess like enhanced density, fracture resistance, enormous strength to weight ratio, etc. (Campbell 2010, Zhu and Hihara 2010). Nevertheless, the enhanced corrosion susceptibility of the particle reinforced composites is an immense setback to the industries dealing with these composites. 6061 Al-15 vol. pct. SiC $_{(P)}$ composite is prone to micro-galvanic corrosion in the presence of electrolyte at the vicinity of reinforced SiC particles, as the semi-conducting SiC ceramic particles act as efficient cathodic sites and surrounding aluminum acts as anode (Trowsdale et al. 1996, Nunez-Lopez et al. 1996, Winkler and Flower 2004, Pardo et al. 2007).

The pre-finishing techniques of any metal-work-piece is mandatory even for the most expensive coatings. Such pre-finishing operations include, stripping, pickling, cleaning, etc. (Mizuno et al. 2001) using citric acid, lactic acid or even dilute sulfuric or hydrochloric acids (Avci 2008, Xu et al. 2013) where corrosion is likely to occur. Although, several methods like coatings and linings, surface modifications, etc., are adopted for controlling corrosion, inhibitors still persist as relatively economical method for controlling corrosion occurring at lower rates. In recent years, intensifying environmental and health concerns have surged the '*go-green*' concepts in research (Song et al. 2013). An unlimited number of literature exists for organic corrosion inhibitors, containing N, O and S heteroatoms. But, most of these do not account for eco-friendly inhibition. The ongoing green tactic includes use of natural products from fruits, leaves, seeds, flowers, etc. The efficiency of such products are reasonable (Obot et al. 2011 and

Fares et al. 2012). However, they have low stability and are readily biodegradable which make their use at the industrial level limited (Palou et al. 2014).

ILs have been of significant interest among researchers in recent decades due to their remarkable properties like negligible vapor pressure, high thermal stability and high ionic conductivity, large electrochemical window, tunable solubility, etc.(Khupse and Kumar 2010). ILs have anisotropic molecular shape containing both organic and inorganic components of various functional groups. The use of ILs is one of the approaches in green chemistry because they create more clean and sustainable chemistry (Earle and Seddon 2002, Zhang et al. 2014). ILs are known to efficiently inhibit corrosion especially in acidic medium. Significant amount of research has been carried out on ILs as corrosion inhibitors on mild steel, carbon steel, copper, aluminum, etc. Imidazolium compounds are reported as efficient inhibitors on aluminum. Commercially available ILs are expensive (Ku and Lu 2011) therefore, ILs as corrosion inhibitors on metals/alloys/composites seldom appears in the literature as compared to other organic inhibitors (Zarrouk et al. 2012). However, benzimidazolium/imidazolium based ionic liquids as corrosion inhibitors especially on aluminum are yet to be explored in detail. Considering, the pre-requisite for efficient and economic corrosion control approach and the '*go-green*' trend, the present research work was planned.

1.16.2 Objectives

1. To investigate the corrosion behavior of 6061 Al-15 vol. pct. SiC$_{(P)}$ composite in hydrochloric acid and sulfuric acid of different concentrations at different temperatures using potentiodynamic polarisation (PDP) and electrochemical impedance spectroscopy (EIS) techniques.
2. To synthesize ionic liquids and to characterize them using Fourier transform infra-red (FT-IR) spectroscopy, liquid chromatography-mass spectrometry (LC-MS), ^{1}H-NMR (Proton nuclear magnetic resonance) and ^{13}C-NMR (Carbon-13 nuclear magnetic resonance) spectroscopy techniques.

3. To assess the corrosion inhibition efficiency of the synthesized ionic liquids on 6061 Al-15 vol. pct. $SiC_{(P)}$ composite in hydrochloric acid and sulfuric acid media of different concentrations, at different temperatures ranging from 30 °C-50 °C at 5 °C intervals.

4. To determine the surface morphology and surface composition of the corroded surface in the presence/ absence of inhibitors by scanning electron microscopy (SEM) and energy dispersive X-ray (EDX) analyses, respectively.

5. To evaluate the activation parameters of corrosion reaction in the absence/presence of inhibitors.

6. To evaluate the thermodynamic parameters for the adsorption of inhibitors on the composite surface and to propose a plausible corrosion inhibition mechanism in acidic media.

1.17 THESIS FRAMEWORK

The present research work has been presented in the thesis in four chapters, details of each are given below:

Chapter 1 introduces the fundamentals of corrosion, its types, hazards caused and various methods adopted to control corrosion. It also touches upon certain electrochemical methods of analysis to assess the corrosion rates. The chapter also includes the brief literature review pertaining to the work carried out. Scope and objectives of the research work are given in the chapter.

Chapter 2 is on materials and methods, gives the details of materials and methods used in the work. The chapter also discusses the synthesis of inhibitors and the calculation of different parameters associated with the work.

Chapter 3 presents the results and discussion pertaining to the corrosion behavior of 6061 Al-15 vol. pct. $SiC_{(P)}$ composite in acidic media and the inhibition effect of synthesized ionic liquids

Chapter 4 summarizes the present research work and lists the conclusions. The scope for further work is also included the thesis.

2.1 MATERIALS

2.1.1 Specimen

Experiments were carried out using the 6061 Al-15 vol. pct. $SiC_{(P)}$ composite in the extruded rod form whose extrusion ratio was 30:1. Table 2.1 gives the composition of the 6061 Al base alloy. The cylindrical test coupon was obtained from the rod and was molded using epoxy resin approximately about 40 mm height, which is resistant to most of the aggressive medium. Schematic representation of the same is depicted in the Figure 2.1. This molding technique enabled to expose constant surface area of 1.102 cm^2 of the sample to the corrosive media in various studies. As per the customary metallographic practice, test coupon was subjected to belt grinding, polishing over rough to smooth grades of emery papers (180-2000) and mirror finish on disc polishing containing legated alumina. The test coupon was thoroughly cleaned with acetone and double distilled water, which was then dried and immediately subjected to analyses.

Table 2.1 Composition of 6061 Al base alloy.

Element	Cu	Si	Mg	Cr	Al
Composition (wt. %)	0.25	0.6	1.0	0.25	97.9
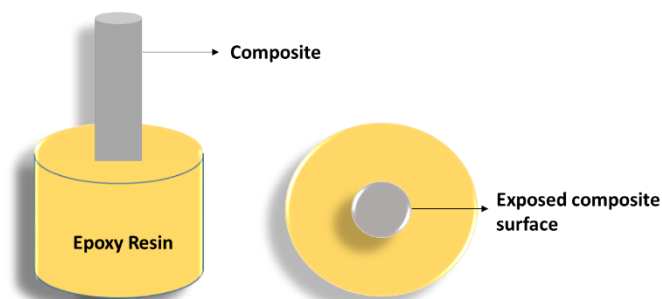
Figure 2.1 Schematic representation of a molded resin.

2.1.2 Media

The tests were performed in two different acidic electrolytes namely, hydrochloric acid and sulfuric acid media. The stock solution of acids were prepared in double distilled water. Both the acids are secondary standards and therefore were standardized by titrimetry against a primary standard like sodium carbonate using methyl orange as indicator. The hydrochloric acid and sulfuric acid solutions of different concentrations were prepared by diluting the stock solution with distilled water. All the measurements were carried out in the temperatures range of 30 to 50 °C (±0.5 °C) with 5 °C increment. The inhibitors were tested in 0.025 M, 0.1 M and 0.25 M of hydrochloric acid and 0.1 M, 0.3 M and 0.5 M of sulfuric acid.

2.1.3 Inhibitors

Four different ionic liquids (ILs) were synthesized using facile synthetic route and were tested for their corrosion inhibition ability on the composite. All the synthesized ILs were characterized using ^{1}H-NMR, ^{13}C-NMR, LC-MS and FT-IR spectroscopic techniques. The synthesized ILs are, 1,3-bis(2-oxo-2-phenylethyl)-1*H*-imidazol-3-ium bromide ([OPEIm$^+$] [Br$^-$]), 1,3-bis[2-(4-methoxyphenyl)-2-oxoethyl]-1*H*-imidazol-3-ium bromide ([MPOEIm$^+$] [Br$^-$]), 1,3-bis(2-oxo-2-phenylethyl)-1*H*-benzimidazol-3-ium bromide ([OPEBen$^+$] [Br$^-$]) and 1,3-bis[2-(4-methoxyphenyl)-2-oxoethyl]-1*H*-benzimidazol-3-ium bromide ([MPOEBen$^+$] [Br$^-$]). Of these, [MPOEBen$^+$] [Br$^-$] is a new molecule and therefore, it was characterized using single crystal X-ray diffractometer (SCXRD) apart from the aforementioned techniques. The inhibition effect of the ILs were studied by dissolving known weights of the ILs in the acid media. Synthesis of ILs were carried out by using the modified procedure from the literature (Roman et al. 2010) and are discussed below.

2.1.3.1 Synthesis of [OPEIm$^+$] [Br$^-$]

The [OPEIm$^+$] [Br$^-$] was synthesized by a two-step synthetic route.

Step 1: Synthesis of 2-(1*H*-imidazol-1-yl)-1-phenylethanone: A mixture containing imidazole (1 g, 14.6 mM) and excess of phenacyl bromide (6.3 g, 32.1 mM) was dissolved in 50 mL dimethyl formamide (DMF) in the presence of 1.5 equivalents of K_2CO_3/KOH in a round bottom flask and the reaction temperature was maintained at 80 °C for 4 h with slight modification in the reported procedure (Roman et al. 2010). The completion of the reaction was checked by thin layer chromatography. The reaction mixture was allowed to attain room temperature and then was poured into a trough containing ice with constant stirring, the orange brown precipitate thus obtained was filtered and washed thoroughly with ice-cold water and dried. The scheme for the synthesis of 2-(1*H*-imidazol-1-yl)-1-phenylethanone is shown in Scheme 1(a).

(a)

1*H*-imidazole   2-bromo-1-phenylethanone   2-(1*H*-imidazol-1-yl)-1-phenylethanone
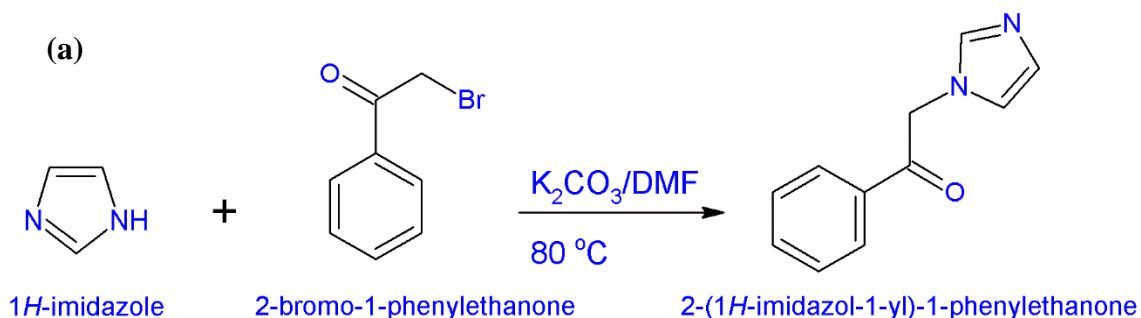
Scheme 1(a) Synthesis of 2-(1*H*-imidazol-1-yl)-1-phenylethanone.

Step 2: Synthesis of [OPEIm$^+$] [Br$^-$]: The orange brown product obtained from step 1 was refluxed with excess phenacyl bromide (6.3 g, 32.1 mM) dissolved in acetonitrile, at 80 °C for 8 h. The product obtained was filtered off and washed thoroughly with hexane and dried. The final product was recrystallized with methanol and was characterized by FT-IR spectrum, ^{1}H-NMR spectrum, ^{13}C-NMR spectrum and LC-MS. The synthetic route for [OPEIm$^+$] [Br$^-$] is shown in **Scheme 1(b)**.
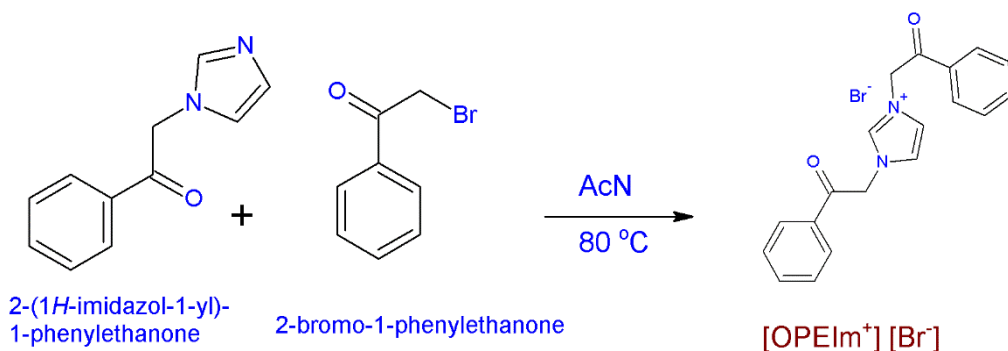
Scheme 1(b) Synthesis of [OPEIm⁺] [Br⁻].

2.1.3.2 Synthesis of [MPOEIm⁺] [Br⁻]

The [MPOEIm⁺] [Br⁻] was synthesized by a two-step synthetic route.

Step (a): Synthesis of 2-(1*H*-imidazol-1-yl)-1-(4-methoxyphenyl)ethanone: A mixture containing 1*H*-imidazole (1.0 g, 14.6 mM) and 2-bromo-1-(4-methoxyphenyl)ethanone (5.0 g, 22.0 mM) was dissolved in 50 mL dimethyl formamide (DMF) in the presence of 1.5 equivalents of K_2CO_3 in a round bottom flask and the reaction temperature was maintained at 80 °C for 4 h (Roman et al. 2010). The completion of the reaction was checked by thin layer chromatography. The reaction mixture was cooled to room temperature and then poured into a trough containing ice, with constant stirring. The orange brown precipitate thus obtained was filtered and washed thoroughly with ice-cold water and dried. Scheme 2(a) shows the reaction.
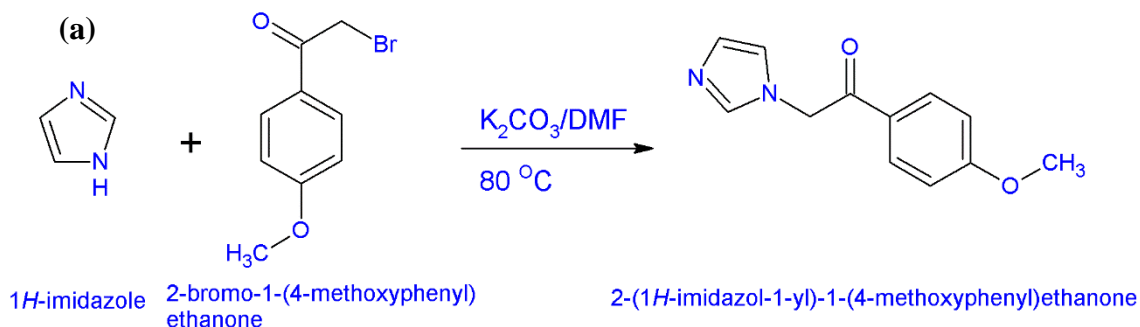
Scheme 2(a) Synthesis of 2-(1*H*-imidazol-1-yl)-1-(4-methoxyphenyl)ethanone.

Step (b): Synthesis of [MPOEIm⁺] [Br⁻]: The orange brown product obtained from step (a) was refluxed with excess 2-bromo-1-(4-methoxyphenyl)ethanone (5 g, 22.0 mM) dissolved in acetonitrile, at 80 °C for 5 h. The product obtained was filtered off and washed thoroughly with hexane and dried. Scheme 2(b) shows the reaction. The final product was recrystallized with methanol and characterized.

(b)

2-(1*H*-imidazol-1-yl)-1-(4-methoxy phenyl)ethanone   2-bromo-1-(4-methoxyphenyl)ethanone   [MPOEIm⁺] [Br⁻]
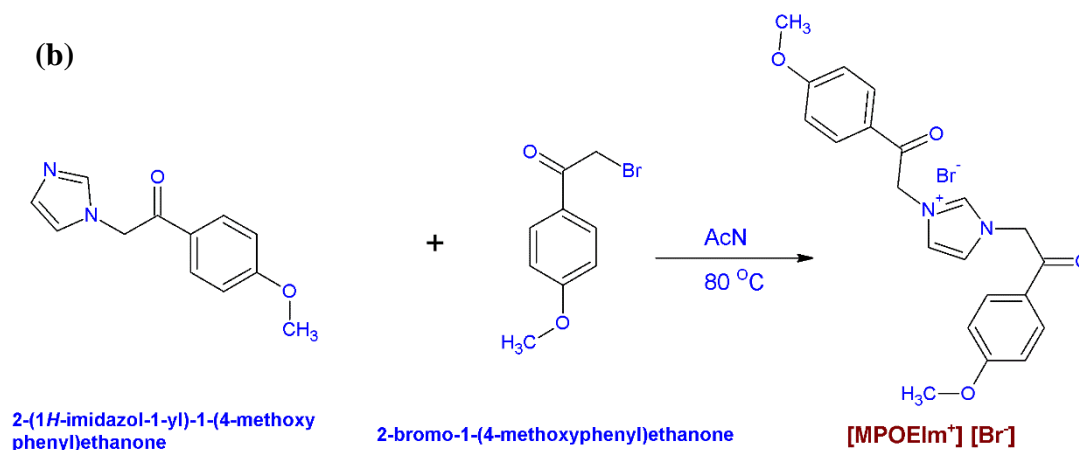
Scheme 2(b) Synthesis of [MPOEIm⁺] [Br⁻].

2.1.3.3 Synthesis of [OPEBen⁺] [Br⁻]

The [OPEBen⁺] [Br⁻] was synthesized by a two-step synthetic route.

Step (a): Synthesis of 2-(1*H*-benzimidazol-1-yl)-1-phenylethanone: A mixture containing 1*H*-benzimidazole (1.0 g, 8.4 mM) and 2-bromo-1-phenylethanone (2.5 g, 12.6 mM) was dissolved in 50 mL dimethyl formamide (DMF) in the presence of 1.5 equivalents of K_2CO_3 in a round bottom flask and the reaction temperature was maintained at 80 °C for 4 h (Roman et al. 2010). The completion of the reaction was checked by thin layer chromatography. The reaction mixture was cooled to room temperature and then was poured into a trough containing ice with constant stirring. The orange brown precipitate thus obtained was filtered and washed thoroughly with ice-cold water and dried. Scheme 3(a) shows the reaction.

(a)

1*H*-benzimidazole   2-bromo-1-phenylethanone

K₂CO₃/DMF
80 ºC

2-(1*H*-benzimidazol-1-yl)-1-phenylethanone
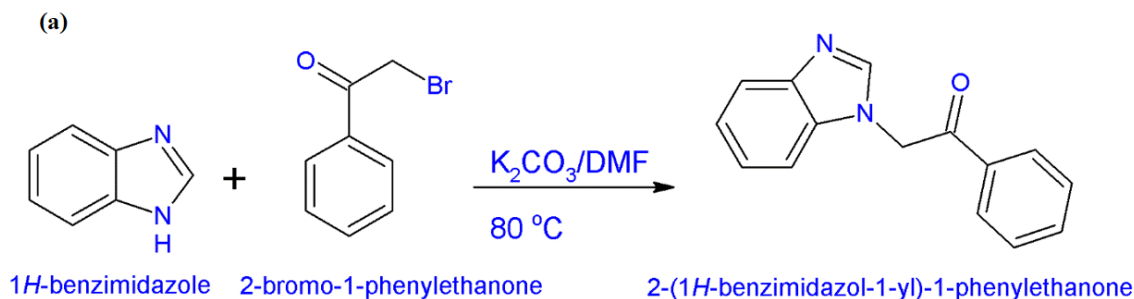
Scheme 3(a) Synthesis of 2-(1*H*-benzimidazol-1-yl)-1-phenylethanone.

Step (b): Synthesis of [OPEBen⁺] [Br⁻]: The orange brown product obtained from step (a) was refluxed with excess and 2-bromo-1-phenylethanone (2.5 g, 12.6 mM) dissolved in acetonitrile, at 80 °C for 5 h. The product obtained was filtered off and washed thoroughly with hexane and dried. Scheme 3(b) shows the reaction.

(b)

2-(1*H*-benzimidazol-1-yl)-1
-phenylethanone

2-bromo-1-phenylethanone

AcN
80 ºC
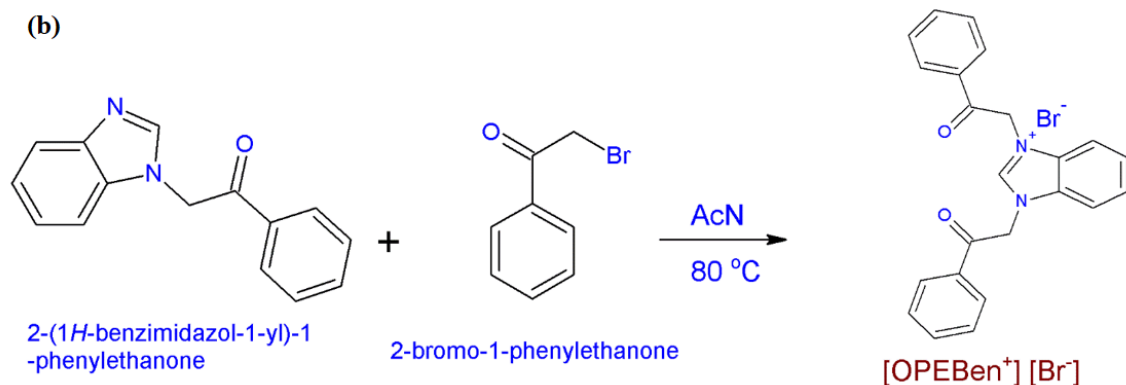
[OPEBen⁺] [Br⁻]

Scheme 3(b) Synthesis of [OPEBen⁺] [Br⁻].

2.1.3.4 Synthesis of [MPOEBen⁺] [Br⁻]

The **[**MPOEBen⁺] [Br⁻] was synthesized by a two-step synthetic route.

Step 1: Synthesis of 2-(1*H*-benzimidazol-1-yl)-1-(4-methoxyphenyl)ethanone: A mixture containing 1*H*-benzimidazole (1 g, 8.4 mM) and 2-bromo-1-(4-methoxyphenyl)ethanone (2.9 g, 12.6 mM) was dissolved in 50 mL dimethyl formamide

(DMF) in the presence of 1.5 equivalents of K_2CO_3 in a round bottom flask and the reaction temperature was maintained at 80 °C for 4 h (Roman et al. 2010). The completion of the reaction was checked by thin layer chromatography. The reaction mixture was allowed to attain the room temperature and then was poured into a trough containing ice with constant stirring. The orange brown precipitate thus obtained was filtered and washed thoroughly with ice-cold water and dried. Scheme 4(a) shows the reaction.
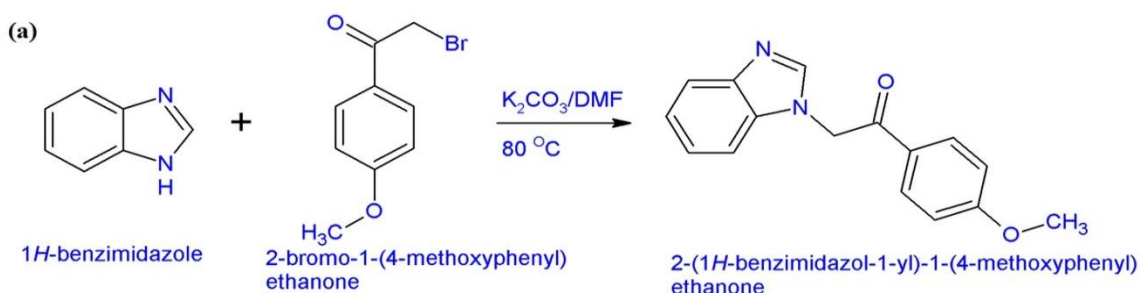
Scheme 4(a) Synthesis of 2-(1H-benzimidazol-1-yl)-1-(4-methoxyphenyl)ethanone.

Step (b): Synthesis of 1,3-bis[2-(4-methoxyphenyl)-2-oxoethyl]-1H-benzimidazol-3-ium bromide: The product obtained from step (a) was refluxed with excess 2-bromo-1-(4-methoxyphenyl) ethanone (2.9 g, 12.6 mM) dissolved in acetonitrile, at 80 °C for 5 h. The product obtained was filtered off and washed thoroughly with hexane and dried. Scheme 4(b) shows the reaction. The final product was recrystallized with acetonitrile-water mixture and was characterized.
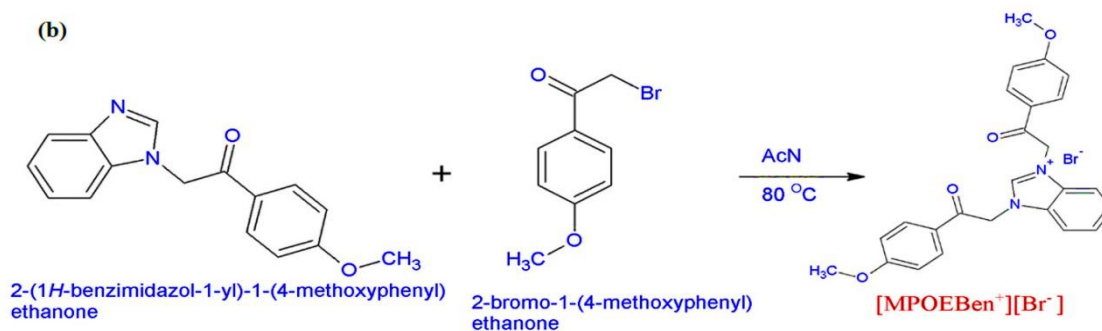
Scheme 4(b) Synthesis of [MPOEBen$^+$] [Br$^-$].

2.2 METHODS

2.2.1 Characterization techniques used for ILs

FT-IR spectrum was recorded using Jasco-4200, Japan FT-IR spectrophotometer. ^{13}C-NMR and ^{1}H-NMR were recorded using Bruker NMR (400 MHz) with dimethyl sulfoxide (DMSO) as solvent and tetra methyl silane (TMS) as internal reference standard. LC-MS was recorded using Agilent ion-trap 3600 liquid chromatography mass spectrometer. Single crystal X-ray diffraction (SCXRD) was recorded using Bruker APEXII DUO CCD diffractometer.

2.2.2 Electrochemical measurements

The electrochemical work station, Gill AC having ACM instrument version 5 software was used to carry out the electrochemical measurements. A conventional three electrode cell was used, the molded test coupon acted as a working electrode, the platinum electrode served as an auxiliary electrode and saturated calomel electrode (SCE) was the reference electrode. The system was allowed to attain the open circuit potential (OCP) following which electrochemical impedance studies were carried out. The test coupon was subjected to potentiodynamic polarization measurements without further surface treatment immediately after EIS analysis. The instrumentation setup used for electrochemical measurements is given in the Figure 2.2.

Figure 2.2 The instrumentation setup used for electrochemical measurements.

2.2.2.1 Potentiodynamic polarization (PDP) measurements

The finely polished test coupon was immersed in the corrosion medium. It was allowed to attain the steady state OCP for 300 s. The potentiodynamic current-potential curves were recorded by polarizing the specimen to −250 mV cathodically and +250 mV anodically with respect to the OCP at a scan rate of 1 mV s^{-1}.

2.2.2.2 Electrochemical impedance spectroscopy (EIS)

The EIS measurements were carried out by impressing a 10 mV amplitude of ac signal and a wide frequency spectrum of 100 kHz-0.01 Hz on the OCP. The impedance data were analyzed by using Nyquist and Bode plots to assess the corrosion characteristics. The impedance parameters were deduced from simulation of Nyquist plot with equivalent circuit using Zsimpwin version 3.21 software.

2.2.3 Surface analyses: SEM and EDX spectroscopy

JEOL JSM-6380LA model SEM was used to image the surface morphology of the polished, corroded and inhibited specimen. EDX was used to determine the surface composition of the specimen through EDX spectra. The sample was subjected to mirror polishing prior to imaging.

2.3 CALCULATIONS

2.3.1 Computation of the corrosion rate

The corrosion current density (i_{corr}) was determined from potentiodynamic polarization plots. The cathodic Tafel slope ($-\beta_c$) and the anodic Tafel slope (β_a) were deduced at approximately ±50 mV from the OCP, where polarization curves remained linear for at least a decade of current to ensure good accuracy and the corresponding corrosion potential (E_{corr}) was determined. The corrosion rate (v_{corr}) was determined using the Equation 2.1 (ASTM Standard G102 1999).

$$\upsilon_{corr}(mm \quad y^{-1}) = \frac{K \times i_{corr} \times E.W}{\rho \times n} \tag{2.1}$$

where, constant K=0.00327 mm g μA^{-1} cm^{-1} y^{-1}, defining the unit of corrosion rate mm y^{-1}, i_{corr} is the corrosion current density expressed in μA cm^{-2}, $E.W$ is the equivalent weight of the corroding specimen, ρ is the density of corroding specimen which is 2.78 g cm^{-3}. The equivalent weight $E.W$ was calculated using the Equation 2.2. (ASTM Standard G102 1999).

$$E.W = \frac{1}{\sum [\frac{n_i f_i}{w_i}]} \tag{2.2}$$

where f_i, w_i and n_i, respectively, are the weight fraction, atomic weight and valence of the ith element of the alloy. Since the weight fraction of Mg alone in the alloy is significant, the equivalent weight of 6061 Al alloy was taken as 9.01.

The equivalent weight of 6061 Al-15 vol. pct. SiC$_{(P)}$ is $0.85 \times 9.01 + 0.15 \times 10 = 9.15$.

Density of 6061 Al alloy = 2.7 g cm^{-3}. Density of SiC = 3.2 g cm^{-3}. Therefore the equivalent density, $2.7 \times 0.85 + 3.2 \times 0.15 = 2.78$ g cm^{-3}.

2.3.2 Calculation of inhibition efficiency

The inhibition efficiency (η) of the ILs was determined as the function of surface coverage (θ) using the Equation 2.3.

$$\eta(\%) = \theta \times 100 \tag{2.3}$$

The surface coverage (θ) was calculated from the results of potentiodynamic polarization studies, using Equation 2.4.

$$\theta = \frac{i_{\text{corr(b)}} - i_{\text{corr(inh)}}}{i_{\text{corr(b)}}} \qquad (2.4)$$

where, $i_{\text{corr(b)}}$ and $i_{\text{corr(inh)}}$ are the corrosion current densities expressed in µA cm^{-2} in the absence and presence of inhibitor, respectively.

The inhibition efficiency from EIS results was calculated using Equation 2.5.

$$\eta\% = \frac{R_{\text{P(inh)}} - R_{\text{P(blank)}}}{R_{\text{P(inh)}}} \times 100 \qquad (2.5)$$

where, $R_{\text{P(inh)}}$ and $R_{\text{P(blank)}}$ are the polarization resistances in the presence and absence of the inhibitor, respectively.

2.3.3 Evaluation of activation parameters

The apparent energy of activation (E_a) for the corrosion process in the absence and presence of IL was deduced from Arrhenius Equation 2.6.

$$\upsilon_{\text{corr}} = Ae^{-E_a/RT} \qquad (2.6)$$

where, υ_{corr} is the rate of corrosion in mm y^{-1}, A is the proportionality constant which is metal specific, R is the universal gas constant, T is the temperature in Kelvin. The slope obtained from Arrhenius plot of ln (υ_{corr}) vs. $1/T$ was used to calculate the energy of activation (E_a).

The apparent enthalpy ($\Delta H^{\#}$) of activation and entropy ($\Delta S^{\#}$) of activation were calculated using transition state theory Equation 2.7.

$$\upsilon_{corr} = \frac{RT}{Nh} e^{\Delta S^{\#}/R} \; e^{-\Delta H^{\#}/RT} \qquad (2.7)$$

where, N is the Avogadro number, T is temperature in Kelvin and h is Planck's constant. From the linear plots of ln (v_{corr}/T) vs. $1/T$, $\Delta H^{\#}$ was calculated using the slope and $\Delta S^{\#}$ was calculated using the intercept.

2.3.4 Evaluation of thermodynamic parameters

Adsorption isotherm represents the variation in inhibitor adsorption on the composite surface with respect to pressure or concentration of the inhibitor (C_{inh}) at constant temperature. The nature of interaction between the adsorbate (IL) and the adsorbent (electrode) may be understood by the adsorption isotherm evaluation. The thermodynamic parameters were calculated from a suitable adsorption isotherm plot. The experimental results were fitted with various adsorption isotherms as mentioned in the Table 2.2. The adsorption isotherm fit with regression value (R^2) close to 1 was considered as the best fit.

Table 2.2 List of adsorption isotherms.

Name	Isotherm	Verification plot
Langmuir	$\dfrac{C_{inh}}{\theta} = C_{inh} + \dfrac{1}{K}$	C_{inh}/θ vs. C_{inh}
Temkin	$\theta = \dfrac{1}{f}(\ln K C_{inh})$	θ vs. log C_{inh}
Freundlich	$\log \theta = \log K + n\log C_{inh}$	$\log \theta$ vs. log C_{inh}
Frumkin	$\dfrac{\theta}{1-\theta}\,e^{f\theta} = \beta C_{inh}$	θ vs. log C_{inh}
Virial Parson	$\theta.e^{2f\theta} = \beta C_{inh}$	θ vs. log θ/C_{inh}
Kinetic Thermodynamic model	$\log \dfrac{\theta}{1-\theta} = \log K + Y \log C_{inh}$	$\log \dfrac{\theta}{1-\theta}$ vs. log C_{inh}
Flory-Huggins	$\log \dfrac{\theta}{C_{inh}} = \log \chi K + \chi \log(1-\theta)$	$\log \dfrac{\theta}{C_{inh}}$ vs. log$(1-\theta)$

where, β is $\Delta G/2.303RT$, ΔG is the free energy of adsorption, R is the gas constant, T is the temperature, C_{inh} is the bulk inhibitor concentration, n is the number of water molecules, f is the inhibitor interaction parameter (0, no interaction; +, attraction; −, repulsion), K is a constant and χ is the number of water molecules replaced by one molecule of the inhibitor (Uhlig and Revie 1991).

The standard free energy (ΔG^0_{ads}) for the adsorption of inhibitors on the composite surface was calculated using Equation 2.8.

$$\Delta G^0_{ads} = -RT \ln 55.5K \tag{2.8}$$

where, $K = \dfrac{55.5\theta}{C(1-\theta)}$ \hfill (2.9)

55.5 is in mol dm^{-3} is the molar concentration of water in solution, R is the universal gas constant, T is temperature in Kelvin. The standard enthalpy (ΔH^0_{ads}) and entropy (ΔS^0_{ads}) were calculated from the linear fit of ΔG^0_{ads} vs. T, using the Equation 2.10.

$$\Delta G^0_{ads} = \Delta H^0_{ads} - T\Delta S^0_{ads} \tag{2.10}$$

3.1 CORROSION BEHAVIOR OF 6061 Al-15 VOL. PCT. SiC$_{(P)}$ COMPOSITE IN HYDROCHLORIC ACID AND SULFURIC ACID MEDIA

3.1.1 Potentiodynamic polarization measurements

The potentiodynamic polarization curves were recorded for the corrosion of the composite in different concentrations of hydrochloric acid and sulfuric acid at different temperatures. Potentiodynamic polarization curves for the corrosion of the composite sample in different concentrations of HCl and H$_2$SO$_4$ at 40 °C are shown in Figures 3.1(a) and 3.1(b), respectively. Similar plots were obtained at other temperatures as well.
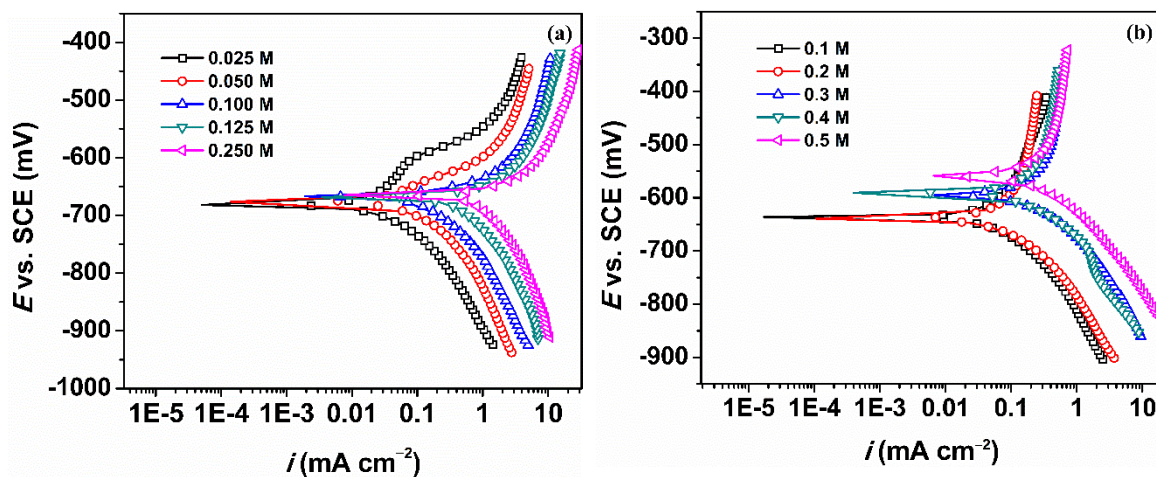
Figure 3.1 Potentiodynamic polarization plots for the corrosion of 6061 Al-15 vol. pct. SiC$_{(P)}$ composite at 40 °C in different concentrations of, (a) HCl and (b) H$_2$SO$_4$.

The anodic regions in the potentiodynamic polarization curves exemplify the metal oxidation and the cathodic regions correspond to the evolution of hydrogen in the case of acidic conditions. Figure 3.1(a) which depicts the Tafel plots for the corrosion of composite in hydrochloric acid medium, show two inflections in the anodic curve, which refers to kinetic barrier effect possibly due to the presence of oxide layer followed by possible partial break down or increased porosity (Dindodi and Shetty 2014). The anodic curve in sulfuric acid medium (Figure 3.1(b)), appears to be more passive, where the anodic region is more or less parallel to the y-axis, which suggests the presence of a less porous oxide

layer. It may be observed from the plots that in both the media, corrosion current density increases when the concentration of acid increases, both the anodic and cathodic polarization curves are shifted towards the higher current density region implying higher rate of corrosion. The trend in the shift of anodic and cathodic polarization curves indicate that with the increase in the concentration of the corrosive electrolyte, both the anodic and the cathodic reactions, responsible for the corrosion of the composite are affected. However, it's evident from the plots that in the case of sulfuric acid medium, that with the increase in the medium concentration, the corrosion potential, E_{corr} is shifted towards the anodic side. The positive shift in the corrosion potential, E_{corr}, with the increase in the concentration of acid indicates that the anodic process is much more affected than the cathodic process (Sato 2012). However, no concrete evidences for direct relation between corrosion potential and current exist in literature.

The electrochemical parameters such as the corrosion potential (E_{corr}), the corrosion current density (i_{corr}), corrosion rate (v_{corr}) and the cathodic Tafel slope ($-\beta_c$) for the corrosion of the composite in hydrochloric and sulfuric acid media are tabulated in Table 3.1 and Table 3.2, respectively. The corrosion rate (v_{corr}) was deduced using the Equation 2.1. Since the anodic polarization curves do not possess well-defined linear Tafel region, the i_{corr} values were determined by the extrapolation of the linear cathode part to the respective corrosion potentials alone (Poornima et al. 2011). The Tafel constant was calculated at -50 mV from the OCP, from the slope value obtained by a tangent drawn where the cathode region remained linear for at least one decade of current density. The corrosion of the composite may be attributed to the discontinuity in the surface protective oxide layer that gives appreciable corrosion resistance to the aluminum alloys (Candan and Bilgic 2004). Also, SiC ceramic particles act as efficient cathodic sites and the region between aluminum metal and the SiC particle are susceptible to undergo micro-galvanic corrosion in the presence of the electrolyte (Nunez-Lopez 1996, Trowsdale 1996, Winkler 2004).

3.1.2 Electrochemical impedance spectroscopy measurements

Nyquist plots for the corrosion of the composite in different concentrations of hydrochloric acid and sulfuric acid at 40 °C are represented in Figure 3.2(a) and Figure 3.2(b), respectively. Similar plots were obtained at other temperatures also.
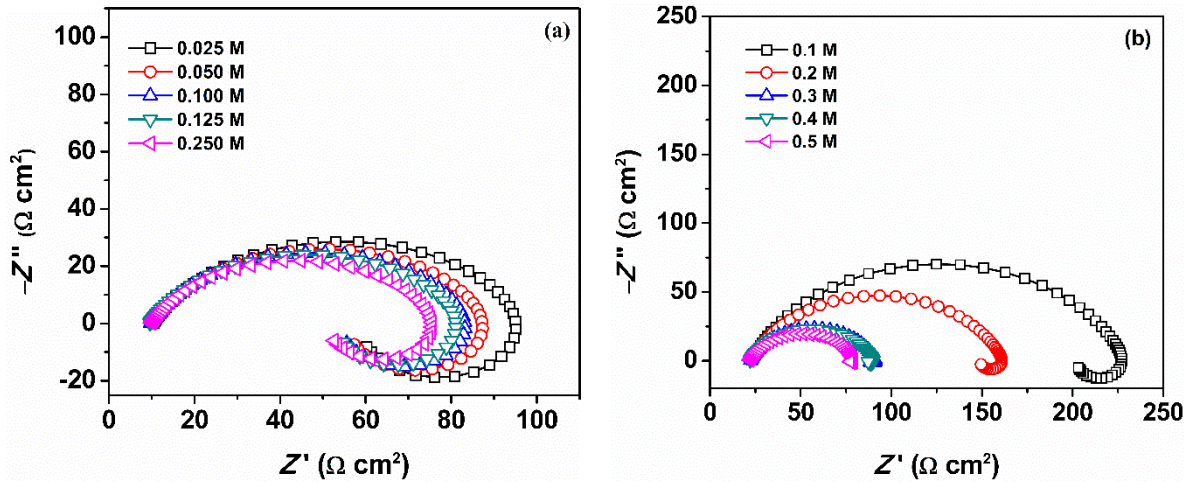
Figure 3.2 Nyquist plots for the corrosion of 6061 Al-15 vol. pct. SiC$_{(P)}$ composite at 40 °C in different concentrations of, (a) HCl and (b) H$_2$SO$_4$.

The semi-circles in the plot demonstrates that the process is mainly charge transfer controlled (Babic et al. 1998, Trabanelli 2005). In either of the plots, there is a capacitive loop in the high frequency region and an inductive loop in the low frequency region. The nature of the plots obtained are in accordance with those reported in literature for aluminum and its alloys in electrolytes containing acid chloride or sulphate medium (Li et al. 2011b, Ismail 2015). The HF capacitive loop indicates the bulk relaxation process of the oxide layer that is present on the surface of aluminum (Pinto 2010). Additional clarification of the presence of HF capacitive loop is imputed to the oxidation of aluminum at the electrode-electrolyte interface (Aytac et al. 2005). The LF inductive loop is ascribed to the adsorption and inclusion of the Cl$^-$/HSO$_4^-$ and H$^+$ ions into the oxide film (Behpour et al. 2009). Aluminum oxide film is regarded to be a parallel circuit of resistor due to the ionic conduction in the oxide film and a capacitor due to its dielectric properties (Pinto 2009, Ravari et al. 2013, Eid et al. 2015). For better interpretation of the EIS data, an equivalent

circuit displayed as an inset in the Figure 3.3, comprising of five circuit elements was derived from the simulation plot shown in the Figure 3.3.The equivalent circuit consists of solution resistance (R_s), a constant phase element (Q) that is parallel to the charge transfer resistance (R_{ct}) and inductive resistance (R_L). The R_L is in series with the inductor L. The constant phase element (Q) replaces an ideal capacitor (C) as the nature of the semi-circle in the Nyquist plot appears to be depressed. This depression in the plot may be attributed to the inhomogeneity of the solid surface of the composite (Lebrini et al. 2008), during reinforcement with SiC particle. The surface inhomogeneity causes frequency dispersion during the impedance analysis and results in depressed semi-circles. The impedance of the constant phase element is given by the Equation 3.1 (Mansfeld et al. 1992).

$$Z_Q = Y_0^{-1}(j\omega)^{-n} \tag{3.1}$$

where, Y_0 is the CPE constant, ω is the angular frequency (in rad s^{-1}), $j^2 = -1$ is the imaginary unit and n is a CPE exponent which reflects the degree of the surface heterogeneity. The value of n ranges from -1 to $+1$. CPE acts as an ideal capacitor when n = 1, an ideal inductor for $n = -1$, and an ideal resistor for $n = 0$. The actual capacitance after taking into consideration the frequency dispersion is calculated using the Equation 3.2 (Mansfeld et al. 1992).

$$C_{dl} = Y_0(\omega_{max})^{n-1} \tag{3.2}$$

where, ω_{max} is the frequency (in Hz) at which the imaginary component of the impedance is maximum.

The polarization resistance (R_P) was calculated using the formula mentioned in Equation 3.3.

$$R_P = \frac{R_L \times R_{ct}}{R_L + R_{ct}} \tag{3.3}$$
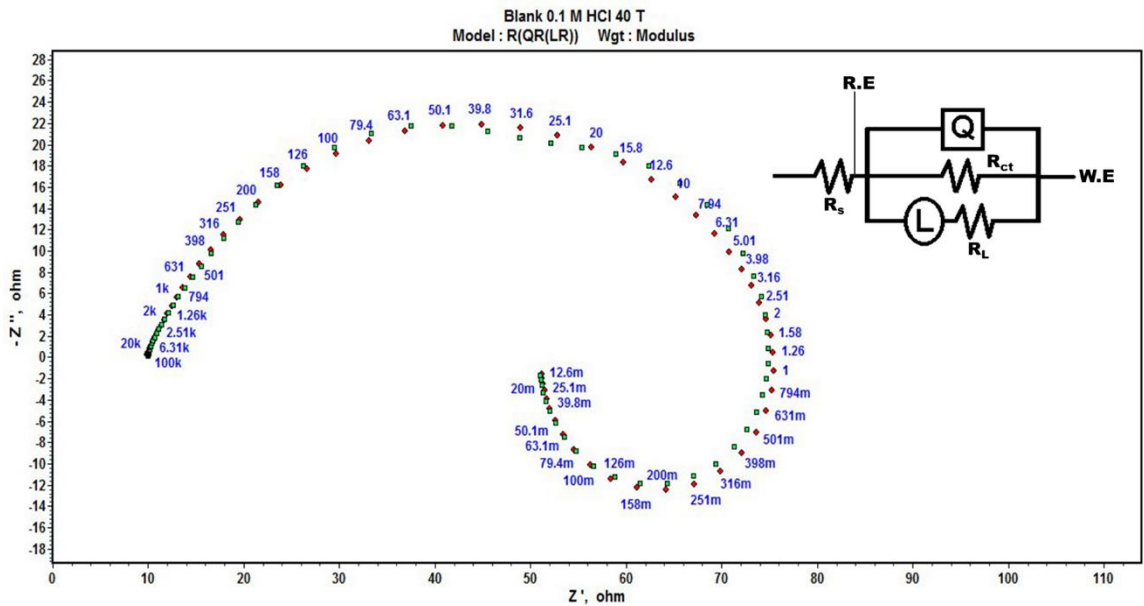
Figure 3.3 Representative simulation plot for the corrosion of 6061 Al-15 vol. pct. SiC$_{(P)}$ composite in 0.1 M HCl at 40 °C.

Table 3.3 and Table 3.4, comprise the results of EIS. From the results it is observed that as the concentration of the acid increases, the value of R_P decreases, which means that the resistance for the process of corrosion is decreased, thereby enhancing the rate of corrosion. Also, with the increase in the concentrations of both the media, the C_{dl} values increase. This is attributed to the decrease in double layer thickness (d) and/or increased local dielectric constant (ε) as per Equation 3.4 (Srinivasan 2006).

$$C = \frac{\varepsilon}{4\pi d} \tag{3.4}$$

EIS results at all other temperatures considered were similar to the one mentioned.

3.1.3 Effect of temperature

The effect of temperature on the corrosion rate of the composite was assessed by running the EIS and analyzing potentiodynamic polarization curves at five different temperatures, starting from 30 °C, with an increment of 5 °C up to 50 °C.

Figure 3.4(a) and Figure 3.4(b) depict the potentiodynamic polarization plots for the corrosion of the composite at different temperatures in 0.1 M HCl and 0.1 M H_2SO_4, respectively. From the Figure 3.4 one can infer that as the temperature rises the polarization curves shift to higher i_{corr} values, indicating an increase in the corrosion rate with the increase in temperature. The Nyquist plots in Figure 3.5(a) and Figure 3.5(b) for the corrosion of the composite in HCl and H_2SO_4 media, respectively, show that the diameters of the high frequency capacitance loop, which contribute to the polarization resistance in the impedance plot, tend to diminish, indicating the increase in the corrosion rate. It is also evident from the Tables 3.3 and 3.4 that the capacitance of the double layer (C_{dl}) also increases indicating higher corrosion at higher temperatures. These observations could be attributed to the fact that as the temperature increases the rate of the corrosion reaction also increases just as in any other chemical or electrochemical reactions.
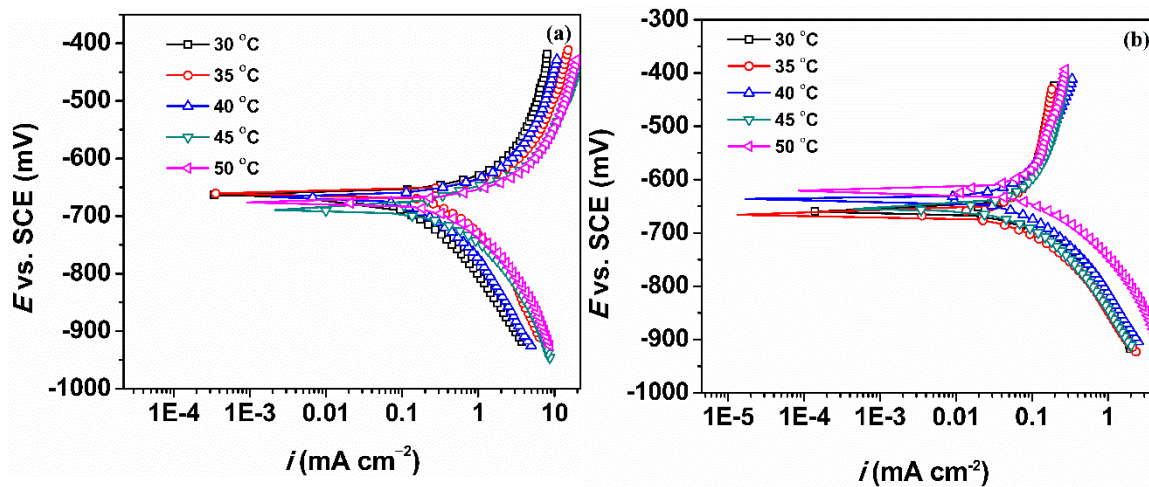
Figure 3.4 Potentiodynamic polarization plots for the corrosion of 6061 Al -15 vol. pct. SiC(P) composite at different temperatures, (a) in 0.1 M HCl and (b) in 0.1 M H_2SO_4 .
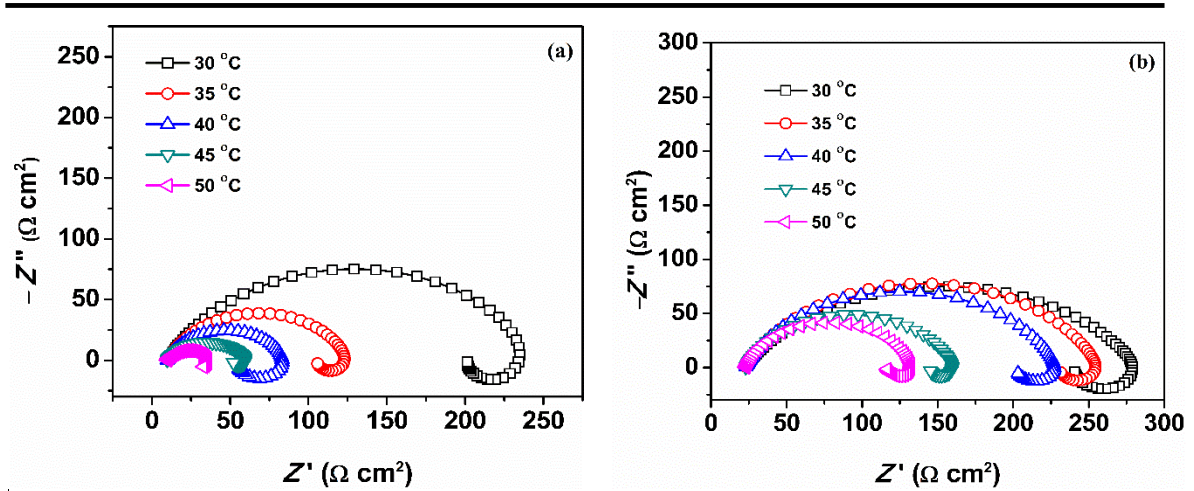
Figure 3.5 Nyquist plots for the corrosion of 6061 Al -15 vol. pct. SiC$_{(P)}$ composite at different temperatures, (a) in 0.1 M HCl and (b) in 0.1 M H$_2$SO$_4$.

The temperature studies enable to calculate the activation parameters like activation energy (E_a), apparent enthalpy ($\Delta H^{\#}$) of activation and entropy of activation ($\Delta S^{\#}$) for the corrosion process. Arrhenius Equation 2.6 was used to calculate the energy of activation (E_a) for the corrosion reaction. The activation energies were calculated using the slope obtained from the linear fit of the Arrhenius plots (Figure 3.6(a) and Figure 3.6(b) for HCl and H$_2$SO$_4$, respectively) (Kumari et al. 2011).
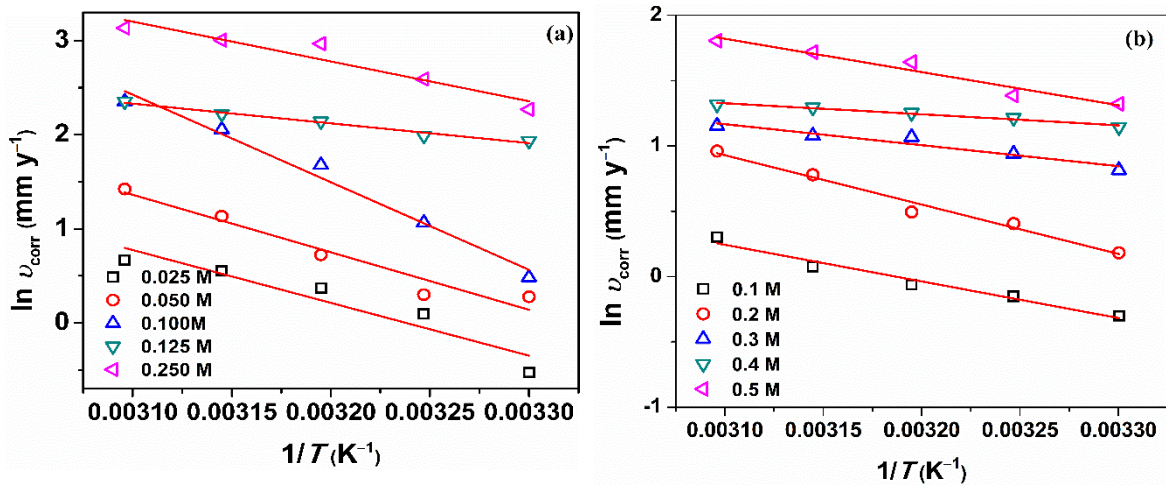
Figure 3.6 Arrhenius plots for the corrosion of 6061 Al -15 vol. pct. SiC$_{(P)}$ composite in different concentrations of, (a) HCl and (b) H$_2$SO$_4$.

The apparent enthalpy of activation ($\Delta H^{\#}$) and entropy of activation ($\Delta S^{\#}$) were calculated from the transition state theory Equation 2.7. The plots of $\ln(v_{corr}/T)$ versus $1/T$ for the corrosion of the composite in HCl media and in H_2SO_4 media of different concentrations are given in Figure 3.7(a) and Figure 3.7(b), respectively. The enthalpy of activation and entropy of activation were then calculated from the slope and intercept values of the linear plots (Deng and Li 2012).
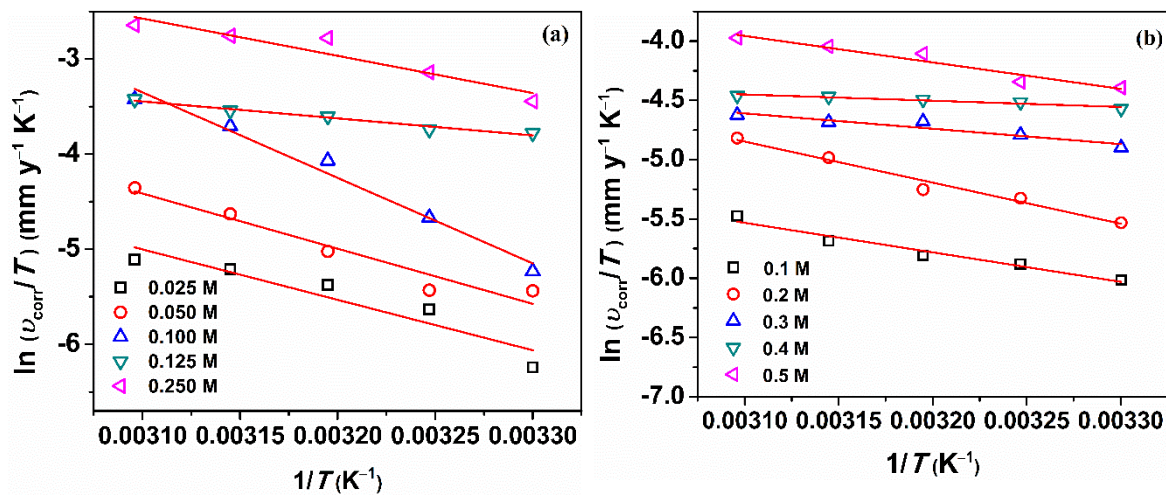
Figure 3.7 Plots of ln (v_{corr}/T) vs. ($1/T$) for the corrosion of 6061 Al -15 vol. pct. SiC$_{(P)}$ composite in different concentrations of, (a) HCl and (b) H_2SO_4 .

Table 3.5 enlists the activation parameters for the corrosion of 6061 Al-15 vol. pct. SiC$_{(P)}$ composite in both the acidic media. It is evident from that Table 3.5 that the value of the activation energy decreases with the increase in the concentration of the acid, which is in line with the increase in the corrosion rate. The entropy of activation ($\Delta S^{\#}$) is negative, indicating decreased randomness in the system which may be due to association process in the formation of the intermediate activated compound (Bentiss et al. 2005, Palou et al. 2014) in the rate determining step of the corrosion reaction.

3.1.4 Mechanism of corrosion of 6061 Al-15 vol. pct. SiC$_{(P)}$ composite in acidic media

The alloy composite comprises of aluminum metal matrix and the ceramic silicon carbide particles. As such, the protective oxide layer (Pilling-Bedworth ratio for pure aluminum~1.38) present on the surface of aluminum becomes discontinuous due to the presence of silicon carbide particles (Trowsdale et al. 1996, Pinto et al. 2009). This discontinuity in the oxide film offers less corrosion resistance to the aluminum metal. Apart from this, the ceramic particles being semi-conductors act as efficient cathodic sites and the aluminum has the natural tendency to undergo oxidation due to its lower standard electrode potential of −1.66 V. The oxidation-reduction processes on the composite surface becomes higher in the presence of strong electrolytes like hydrochloric or sulfuric acids. The electrolyte connects the anode and the cathode forming minute galvanic cells. This results in micro-galvanic corrosion and quickens oxidation of aluminum at the anode and reduction of hydrogen at the cathode (Trowsdale et al. 1996). Uniform and pitting are the common forms of corrosion observed on the composite surface in the presence of chloride, sulfate or bisulfate anions in the electrolyte (Zaid et al. 2008).

In the presence of higher concentrations of HCl, the Cl$^-$ ions are likely to percolate through the oxide film thereby retarding the self-healing ability of the oxide layer on the metal surface. This results in the formation of intermediate soluble complex as given in the Equation 3.5 below.

$$Al_{(s)} + nCl^- \rightarrow [AlCl_n]^{(n-3)^-}{}_{(aq)} + 3e^- \tag{3.5}$$

The complex thus formed enhances the dissolution of the aluminum ions from the lattice into the solution and leads to local thinning of the passive layer making it pervious for further attack by chloride ions leading to severe pitting attack (Al-Turkustani et al. 2010)

The Equation 3.6 and Equation 3.7 represent the anodic and cathodic reaction under acidic condition. The overall reaction involved in the corrosion reaction of the composite is given in the Equation 3.8.

$$(Al_{(s)} \rightarrow Al^{3+} + 3e^-) \times 2 \tag{3.6}$$

$$\underline{(2H^+ + 2e^- \rightarrow H_2 \uparrow) \times 3} \tag{3.7}$$

$$2Al_{(s)} + 6H^+ \rightarrow 2Al^{3+} + 3H_2 \uparrow \tag{3.8}$$

Similarly, in sulfuric acid medium, at the anodic region, aluminum metal gets oxidized into Al^{3+} ions by losing three electrons. At the cathode, the electrons are consumed by H^+ ions resulting in the evolution of hydrogen. The overall reaction is given in the Equation 3.9.

$$2Al_{(s)} + 3H_2SO_{4(aq)} \rightarrow 2Al^{3+}{}_{(aq)} + 3SO_4^{2-}{}_{(aq)} + 3H_{2(g)} \tag{3.9}$$
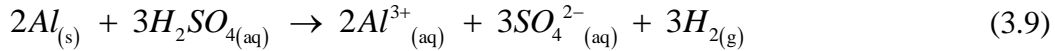
3.1.4.1 Effect of ionic concentration and temperature

As an established fact, aluminum is more corrosion resistant than most of the metals due to its strongly adherent compact surface oxide layer. The existence of surface oxide film is evident in both media for the concentration ranges mentioned in the present study, as shown in Tafel plots. The anodic curve in hydrochloric acid medium shows two inflection points depicting presence of oxide film followed by possible partial breakdown of the oxide film. Similarly, passive anodic curve in sulfuric acid medium shows comparatively persistent oxide film. The aluminum oxide layer is said to be protective in near neutral and neutral pH. However, studies by Al-Turkustani et al. (2010) and also based on the results of present study, one can conclude the presence of oxide film even in hydrochloric and sulfuric acid media for the studied ranges of concentrations. However, the increased corrosion rates with the increase in acid concentrations hints the increased porosity of the surface film followed by partial or complete breakdown. For increasing concentrations of chloride, sulfate or bisulfate anions the oxide film dissolution increases due to more and more adsorption of anions on the surface with the formation of intermediate soluble complex as presented by Equation 3.5 and exposing the composite surface for further attack by the corrosive species. Also, the corrosion rate is more in hydrochloric acid medium than in sulfuric acid medium. This observation is attributed to

the aggressive Cl⁻ ion effect. Studies by Sharma et al. (2012) demonstrates that the rate of corrosion is significantly high in the hydrochloric acid medium with appreciable hydrogen evolution and in the case of sulfuric acid practically less/no evolution of hydrogen was observed for initial exposure period. The increase in temperature brings about the active dissolution of surface oxide film which contributes to the increased rate of corrosion. The increase in temperature also reduces the hydrogen over voltage (Hickling and Salt 1941, Turner 1953), which causes increased evolution of hydrogen causing overall increase in corrosion rate.

3.1.5 Surface analyses

The surface morphology of the freshly polished composite surface was analysed by recording the scanning electron microscopic images. Corresponding EDX spectrum was also recorded for qualitative assessment of surface composition of the sample. Figure 3.8(a) presents the SEM image for freshly polished 6061 Al-15 vol. pct. $SiC_{(P)}$ composite and Figure 3.8(b) shows the corresponding EDX spectrum showing the peaks corresponding to the elements present in the composite. The SEM image of the freshly polished surface of the sample shows uniform metal alloy matrix and dispersed SiC particles. The SEM image showing the metal alloy matrix and SiC interface is shown in Figure 3.8(c) and the corresponding EDX spectrum shown in Figure 3.8(d) gives evidence that the particles appearing on the surface of metal alloy matrix are SiC particles.
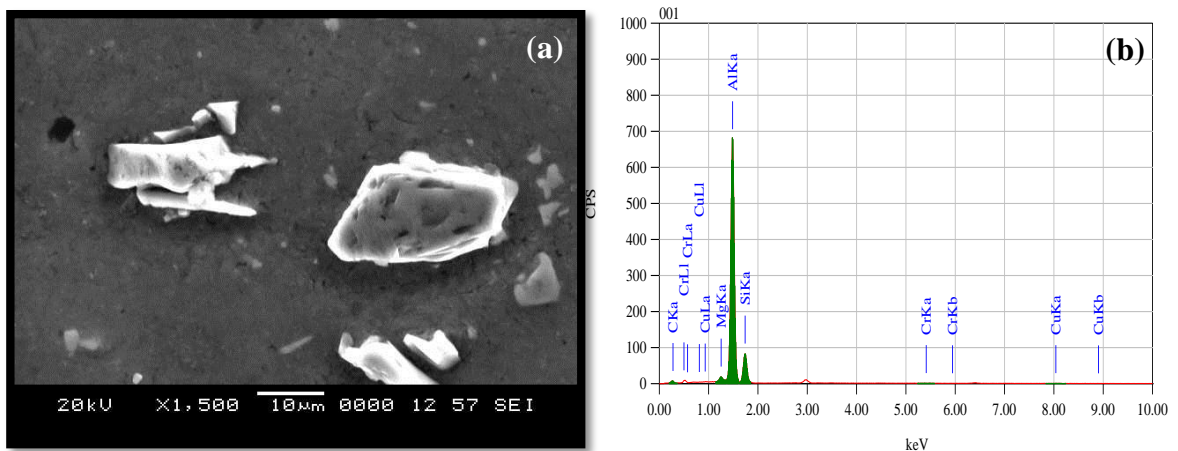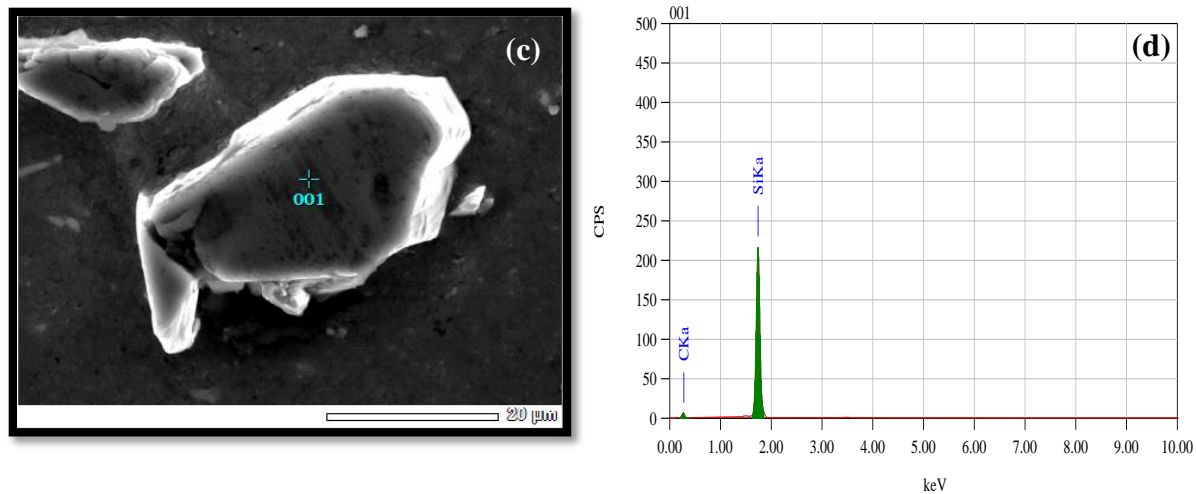
Figure 3.8 (a) SEM image, (b) EDX spectrum of freshly polished 6061 Al-15 vol. pct. SiC(P) composite surface and (c) SEM image, (d) EDX spectrum showing SiC particle and Si and C peak, respectively.

The SEM images were also recorded for samples immersed in 0.25 M hydrochloric acid for two hours and 0.5 M sulfuric acid for 3 hours and are shown in the Figures 3.9(a) and 3.9(b), respectively. It's evident from the surface morphology that apart from uniform corrosion as depicted by the surface unevenness, the regions near the SiC particles show severe pitting corrosion. The corrosion process appears to be severe around the SiC particles due to the formation of minute galvanic cell within the restricted area, SiC ceramic particles acting as cathode and metal acting as anode. The corresponding EDX spectrum are given in the Figures 3.9(c) and 3.9(d), respectively. The additional peaks corresponding to elements Cl in Figure 3.9(c) and S and O in Figure 3.9(d) hints the presence of corrosive species on the surface of the sample.
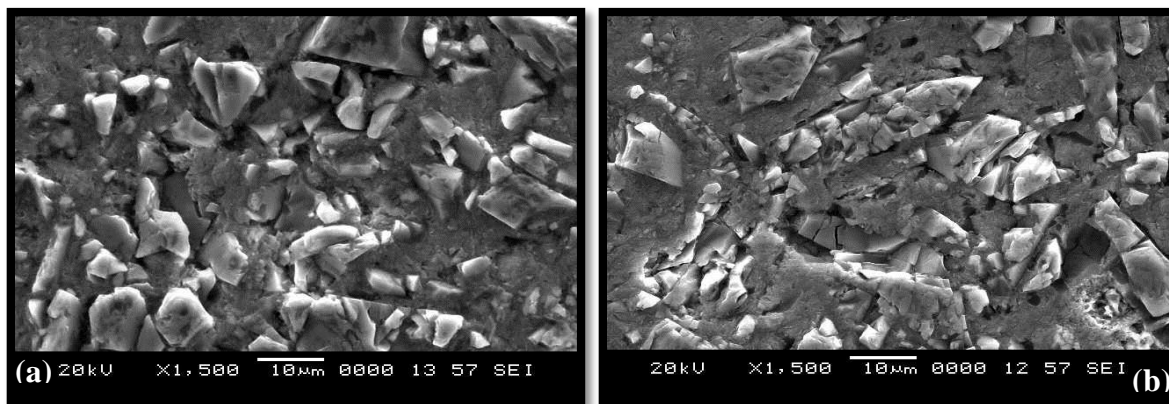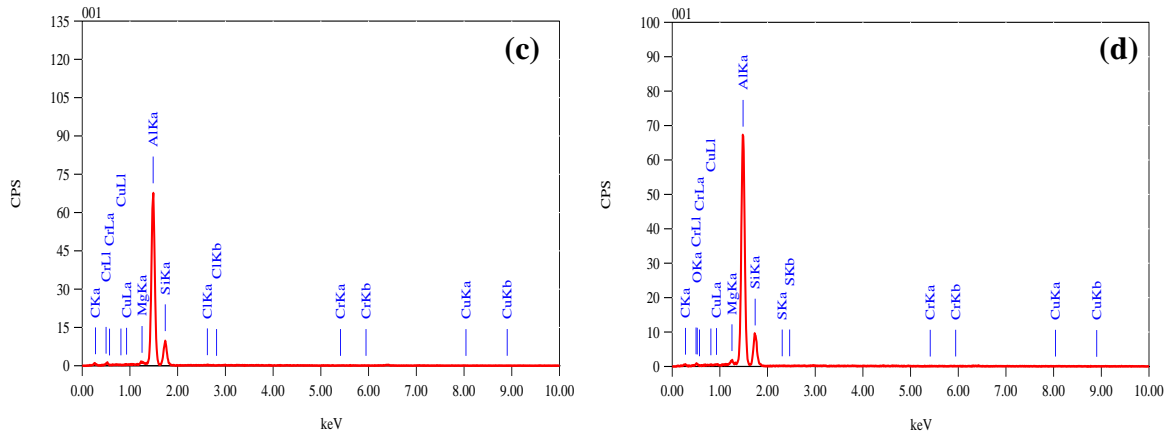
Figure 3.9 SEM images of corroded 6061 Al-15 vol. pct. SiC(P) composite surface immersed in (a) 0.25 M HCl for 2h, (b) 0.5 M H₂SO₄ for 3h and corresponding EDX spectra in (c) 0.25 M HCl and (d) 0.5 M H₂SO₄.

Table 3.1 Potentiodynamic polarization data for the corrosion of 6061 Al-15 vol. pct. SiC(P) composite in hydrochloric acid medium at different temperatures.

Conc. (M)	Temp. (°C)	$-E_{corr}$ (mV vs. SCE)	$-\beta_c$ (mV dec^{-1})	i_{corr} (µA cm^{-2})	v_{corr} (mm y^{-1})
0.025	30	696	215	54.6	0.59
	35	676	192	102.6	1.10
	40	693	216	134.4	1.45
	45	690	225	161.7	1.74
	50	714	224	180.8	1.95
0.05	30	666	209	122.5	1.32
	35	683	207	125.6	1.35
	40	676	204	191.6	2.06
	45	686	198	288.8	3.11
	50	693	217	385.9	4.15
0.1	30	664	166	150.8	1.62
	35	659	199	269.5	2.90
	40	665	188	497.5	5.36
	45	691	204	726.3	7.82
	50	702	223	874.5	9.41
0.125	30	660	270	643.3	6.92
	35	667	290	679.1	7.31
	40	667	247	791.7	8.52
	45	678	321	857.0	9.22
	50	656	220	978.5	10.53
0.25	30	658	293	898.3	9.67
	35	664	224	1239.4	13.34
	40	658	308	1807.0	19.45
	45	684	277	1878.3	20.22
	50	667	246	2135.9	22.99

Table 3.2 Potentiodynamic polarization data for the corrosion of 6061 Al-15 vol. pct. SiC$_{(P)}$ composite in sulfuric acid medium at different temperatures.

Conc. (M)	Temp (°C)	$-E_{corr}$ (mV vs. SCE)	$-\beta_c$ (mV dec^{-1})	i_{corr} (μA cm^{-2})	v_{corr} (mm y^{-1})
	30	659	121	68.5	0.74
	35	665	105	79.5	0.86
0.1	40	636	155	87.3	0.94
	45	655	102	100.1	1.08
	50	653	150	125.7	1.35
	30	629	112	111.8	1.20
	35	628	136	139.8	1.50
0.2	40	635	176	152.7	1.64
	45	657	184	202.5	2.18
	50	652	187	242.8	2.61
	30	595	142	209.6	2.26
	35	595	139	237.6	2.56
0.3	40	592	141	270.5	2.91
	45	603	157	273.1	2.94
	50	605	159	294.8	3.17
	30	578	163	291.3	3.14
	35	575	157	313.3	3.37
0.4	40	587	192	324.7	3.50
	45	581	150	338.8	3.65
	50	584	185	347.3	3.74
	30	560	129	348.7	3.75
	35	559	125	372.1	4.00
0.5	40	557	140	479.8	5.16
	45	562	164	517.9	5.57
	50	565	169	564.7	6.08

Table 3.3 EIS data for the corrosion of 6061 Al-15 vol. pct. SiC$_{(P)}$ composite in hydrochloric acid medium at different temperatures.

Conc. (M)	Temp. (°C)	R_p (Ω cm^2)	C_{dl} (μF cm^{-2})
	30	308.7	55.0
	35	119.0	119.6
0.025	40	64.6	180.4
	45	51.2	251.9
	50	48.6	260.2
	30	228.6	67.5
	35	113.5	129.8
0.05	40	57.1	181.0
	45	45.6	280.4
	50	42.3	291.1
	30	213.7	83.3
	35	100.2	136.5
0.1	40	55.5	201.3
	45	41.3	343.2
	50	21.1	565.1
	30	173.4	89.3
	35	71.8	153.6
0.125	40	53.3	210.4
	45	33.9	351.2
	50	17.2	578.1
	30	126.3	107.8
	35	71.6	177.8
0.25	40	51.4	231.4
	45	21.8	413.8
	50	11.7	589.3

Table 3.4 EIS data for the corrosion of 6061 Al-15 vol. pct. SiC$_{(P)}$ composite in sulfuric acid medium at different temperatures.

Conc. (M)	Temp (°C)	R_P (Ω cm^2)	C_{dl} (μF cm^{-2})
0.1	30	245.5	84.7
	35	221.2	86.4
	40	194.1	120.7
	45	121.4	140.4
	50	101.3	160.4
0.2	30	176.4	94.3
	35	134.0	99.1
	40	132.2	121.4
	45	73.4	143.2
	50	57.4	163.2
0.3	30	103.6	76.5
	35	73.5	147.9
	40	62.8	187.0
	45	59.5	192.7
	50	45.3	234.3
0.4	30	92.7	100.3
	35	69.2	120.3
	40	62.2	176.0
	45	52.6	199.6
	50	34.8	212.1
0.5	30	88.6	122.8
	35	59.6	153.3
	40	53.7	164.4
	45	48.9	180.3
	50	31.2	240.3

Table 3.5 Activation parameters for the corrosion of 6061 Al-15 vol. pct. SiC$_{(P)}$ composite in acidic media.

Medium	Conc. (M)	E_a (kJ mol^{-1})	$\Delta H^{\#}$ (kJ mol^{-1})	$-\Delta S^{\#}$ (J K mol^{-1})
HCl	0.025	46.69	44.09	102.46
	0.05	50.82	48.21	84.74
	0.1	77.40	74.80	26.80
	0.125	17.51	14.98	180.14
	0.25	35.18	32.58	117.96
H$_2$SO$_4$	0.1	23.28	20.63	179.49
	0.2	31.43	28.80	148.64
	0.3	13.33	10.73	202.59
	0.4	6.96	4.43	220.96
	0.5	21.18	18.57	172.84

3.2 CHARACTERIZATION OF SYNTHESIZED IONIC LIQUIDS

The synthesized inhibitors were recrystallized using methanol and characterized by FT-IR, mass spectrometry and NMR techniques and the purity was checked by liquid chromatography. The novel molecule, [MPOEBen⁺] [Br⁻] was characterized by SCXRD analysis to confirm the 3-dimensional structure.

3.2.1 Characterization of [OPEIm⁺] [Br⁻]

Figures 3.10, 3.11, 3.12, 3.13 and 3.14 show IR, ^{1}H-NMR, ^{13}C-NMR, mass spectrum and liquid chromatogram of [OPEIm⁺] [Br⁻], respectively.

Characterization results: White solid, yield: 83%, m.p: 259.2-259.7 °C, (ATR, cm⁻¹): 3085, 3043 (-C-H aromatic stretching), 2836 (-C-H aliphatic stretching) 1689 (C=O), 1596 (C=N), 1446 (C=C), 1229 (C-N), ^{1}H-NMR: (400 MHz, DMSO-d6): d (ppm), 9.12 (s, 1H), 8.09-8.07 (m, 4H), 7.82-7.76 (m, 4H), 7.67-7.63 (m, 4H), 6.20 (s, 4H), ^{13}C-NMR (100 MHz, DMSO-d6) δ (ppm):191.80, 139.06, 134.88, 134.23, 129.58, 128.63, 124.22, 56.12, LC-MS (+ve mode) m/z calculated for $C_{19}H_{17}N_2O_2$: 305.49, Found: 305.5 [M+H]⁺ with 100% purity.
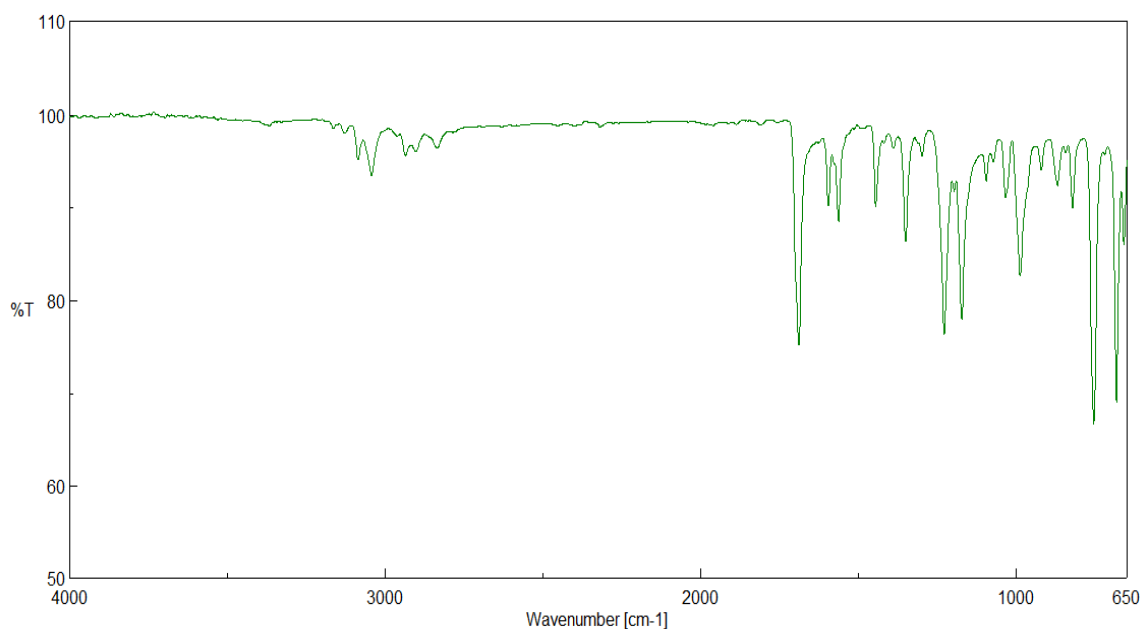
Figure 3.10 FT-IR spectrum of synthesized [OPEIm⁺] [Br⁻].
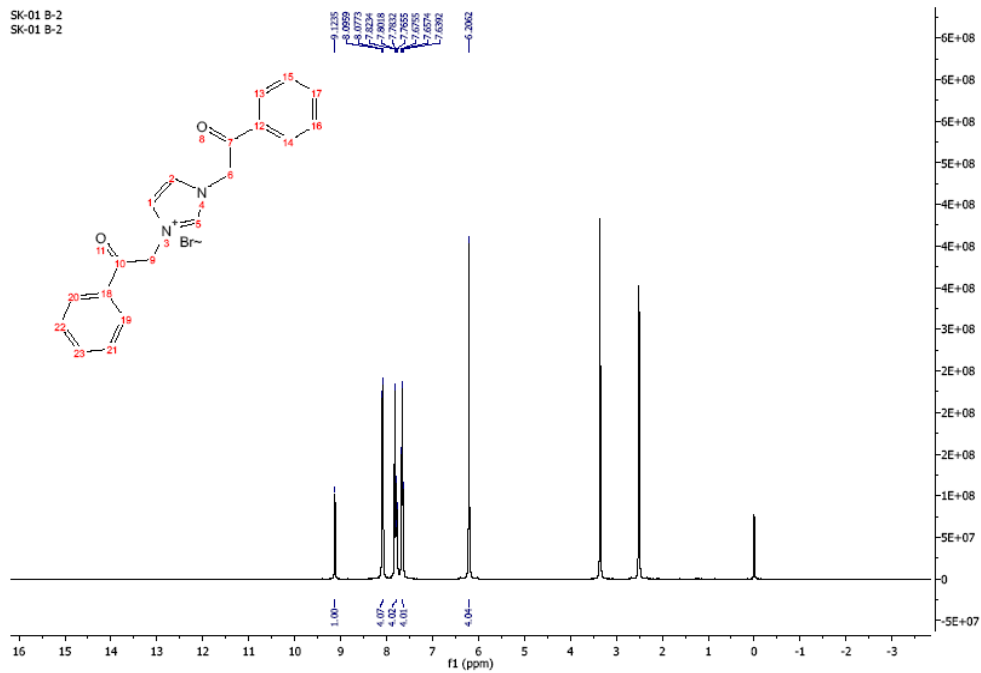
Figure 3.11 ^{1}H-NMR spectrum of synthesized [OPEIm$^+$] [Br$^-$].
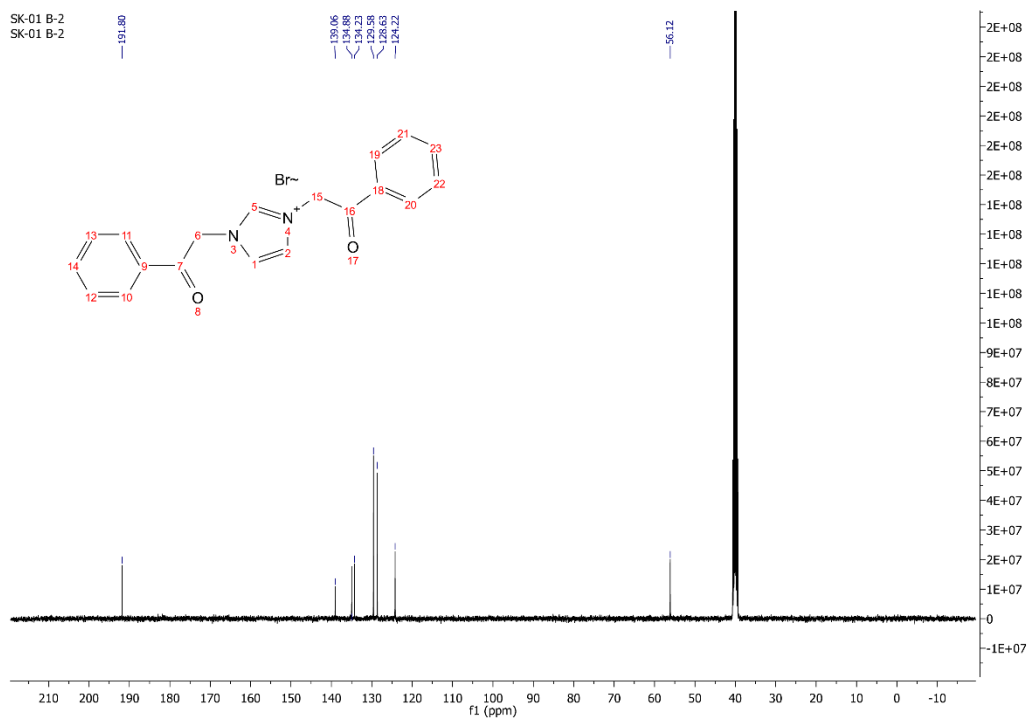
Figure 3.12 ^{13}C-NMR spectrum of synthesized [OPEIm$^+$] [Br$^-$].
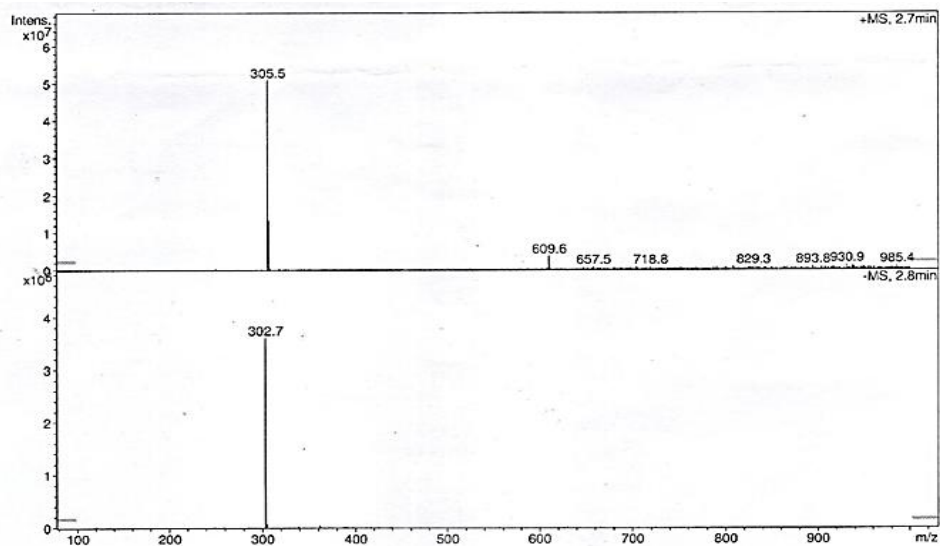
Figure 3.13 Mass spectrum of [OPEIm⁺] [Br⁻].
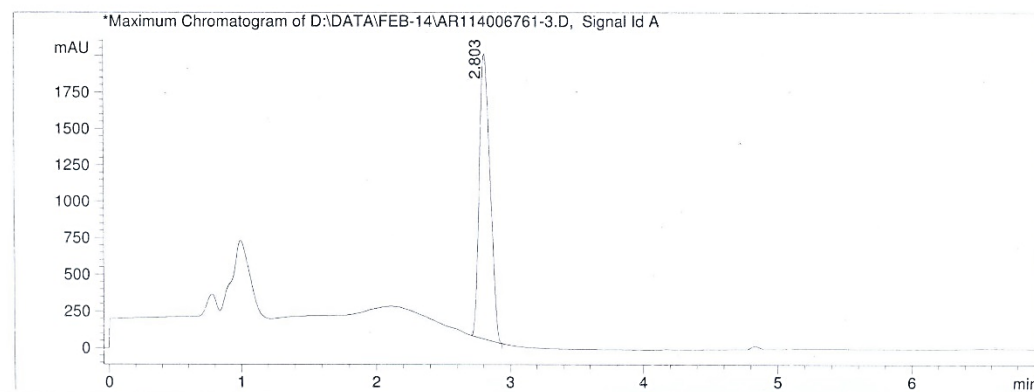
Figure 3.14 Liquid Chromatogram of [OPEIm⁺] [Br⁻].

3.2.2 Characterization of [MPOEIm⁺] [Br⁻]

Figures 3.15, 3.16, 3.17, 3.18 and 3.19 show IR, ^{1}H-NMR, ^{13}C-NMR, mass spectrum and liquid chromatogram of [MPOEIm⁺] [Br⁻], respectively.

Characterization results: White solid, yield: 84%, m.p. 260-262 °C. FT-IR (ATR, cm^{-1}): 3085, 3043 (-C-H aromatic stretching), 2836 (-C-H aliphatic stretching), 1689 (C=O), 1596 (C=N), 1446 (C=C), 1229 (C-N). ^{1}H NMR (400 MHz, DMSO-d6): d (ppm), 9.09 (s, 1H), 8.06-8.04 (d, 4H), 7.79 (s, 1H), 7.78 (s, 1H), 7.18-7.16 (d, 4H, J=8.8), 6.11 (s, 4H), 3.89 (s, 6H). ^{13}C-NMR (100 MHz, DMSO-d6) δ (ppm): 188.94, 163.51, 139.99, 129.98, 125.98, 123.07, 113.75, 55.18, 54.61. LC-MS (+ve mode) m/z calculated for $C_{21}H_{21}N_2O_4$: 365.4, Found: 365.5 [M+H]⁺ with 100% purity.
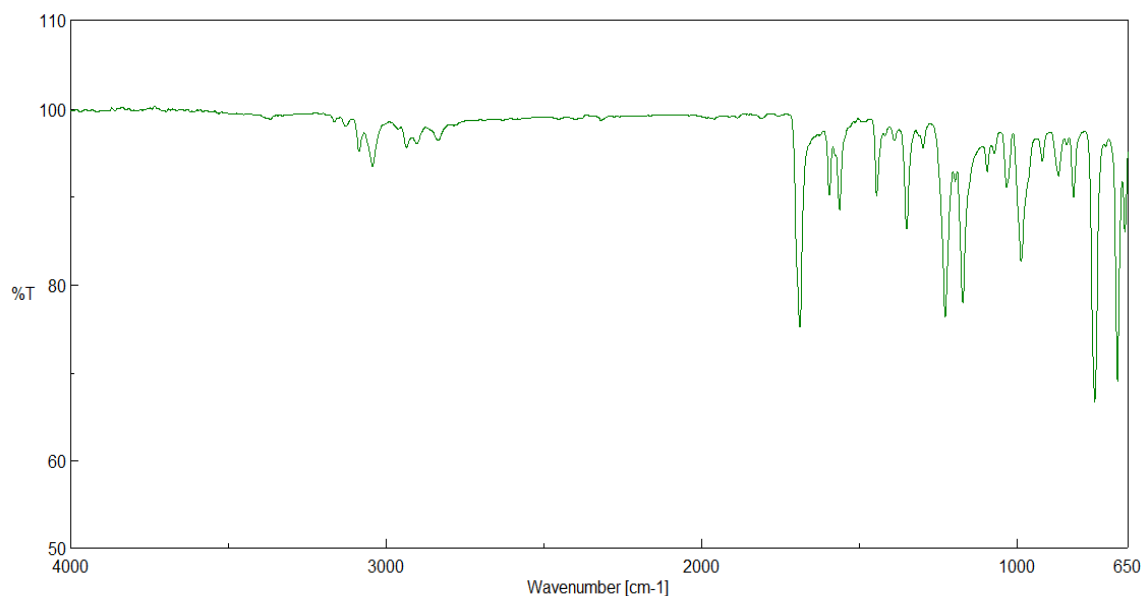
Figure 3.15 FT-IR spectrum of synthesized [MPOEIm⁺] [Br⁻].
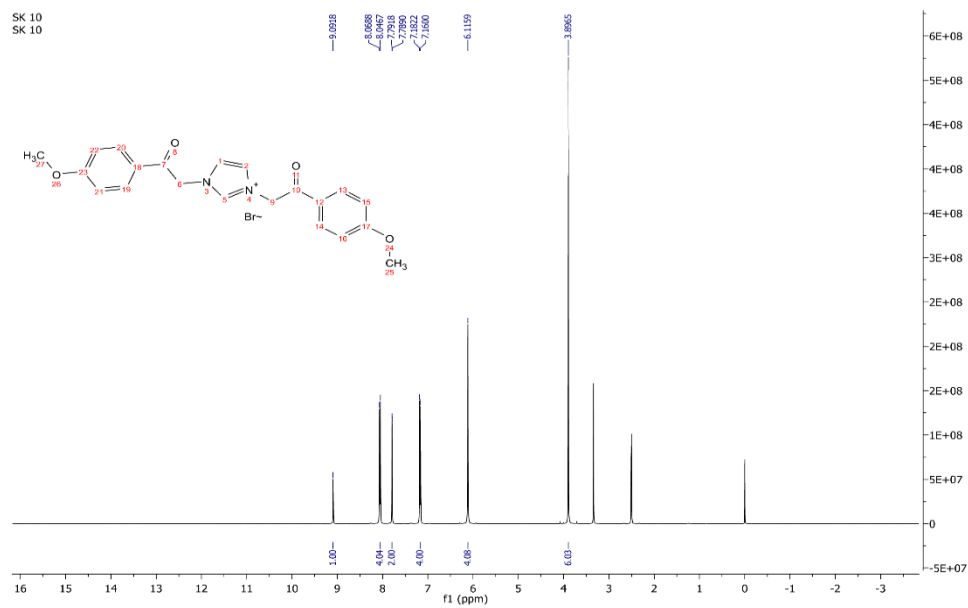
Figure 3.16 ^{1}H-NMR spectrum of synthesized [MPOEIm$^+$] [Br$^-$].
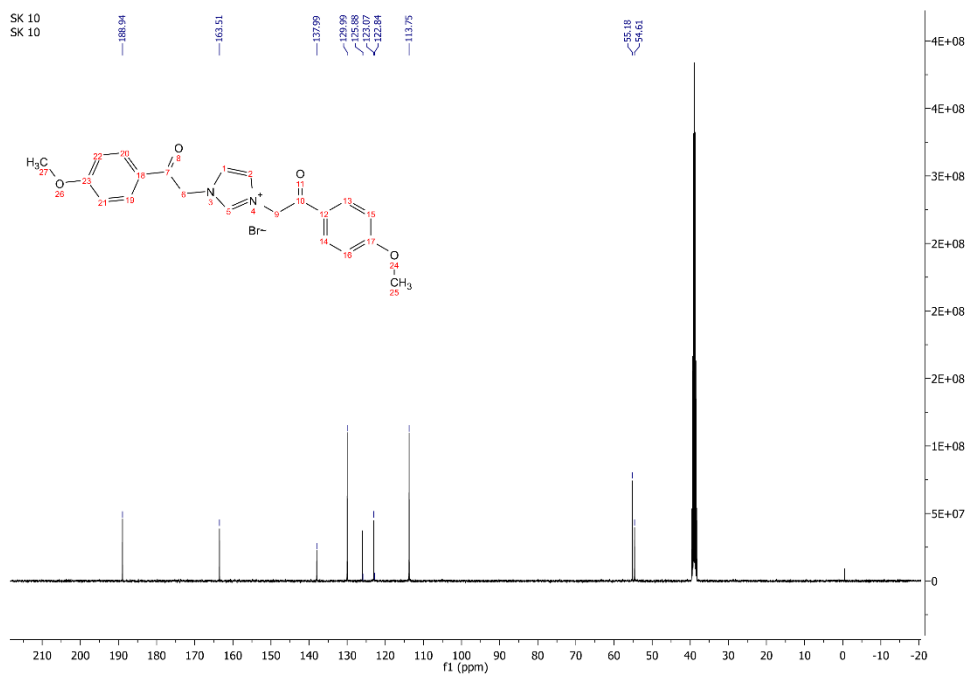
Figure 3.17 ^{13}C-NMR spectrum of synthesized [MPOEIm$^+$] [Br$^-$].
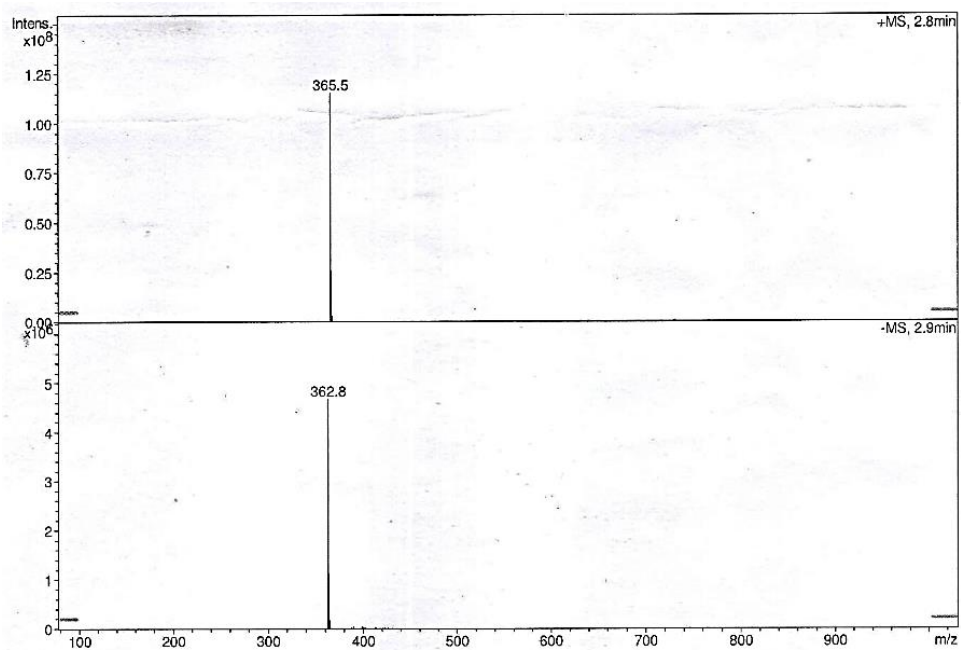
Figure 3.18 Mass spectrum of synthesized [MPOEIm⁺] [Br⁻].
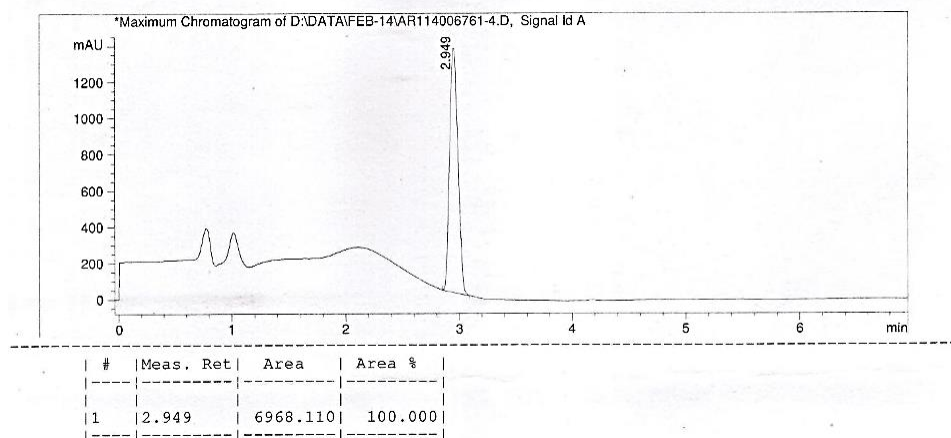
Figure 3.19 Liquid chromatogram of synthesized [MPOEIm⁺] [Br⁻].

3.2.3 Characterization of [OPEBen$^+$] [Br$^-$]

Figures 3.20, 3.21, 3.22, 3.23 and 3.24 show IR, ^{1}H-NMR, ^{13}C-NMR, mass spectrum and liquid chromatogram of [OPEBen$^+$] [Br$^-$], respectively

Characterization results: White solid, yield: 72%, m.p. 240-242 °C. FT-IR (ATR, cm^{-1}): 3085, 3043 (-C-H aromatic stretching), 2836 (-C-H aliphatic stretching), 1689 (C=O), 1596 (C=N), 1446 (C=C), 1229 (C-N). ^{1}H NMR (400 MHz, DMSO-d6): d (ppm), 9.71 (s, 1H), 8.17-8.13 (m, 6H), 7.83-7.67 (m, 8H), 6.56 (s, 4H). ^{13}C-NMR (100 MHz, DMSO-d6) δ (ppm): 191.7, 144.96, 135.04, 134.32, 132.13, 129.53, 129.23, 128.97, 127.23, 114.52, 54.10, 1.71. LC-MS (+ve mode) *m/z* calculated for C$_{23}$H$_{19}$N$_2$O$_2$: 355.4, Found: 355.6 [M+H]$^+$ with 100% purity.
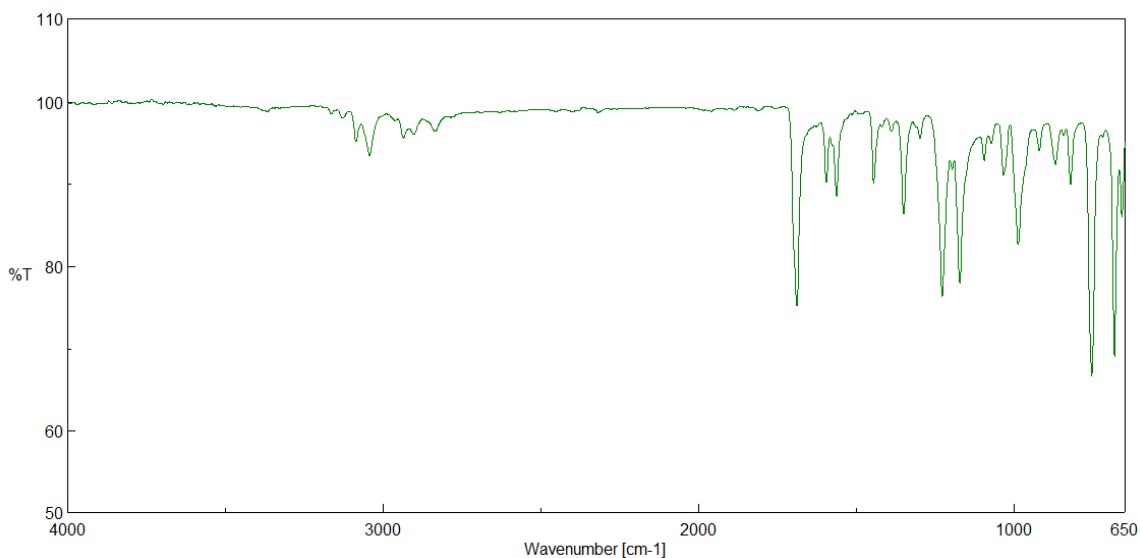
Figure 3.20 FT-IR spectrum of synthesized [OPEBen$^+$] [Br$^-$].
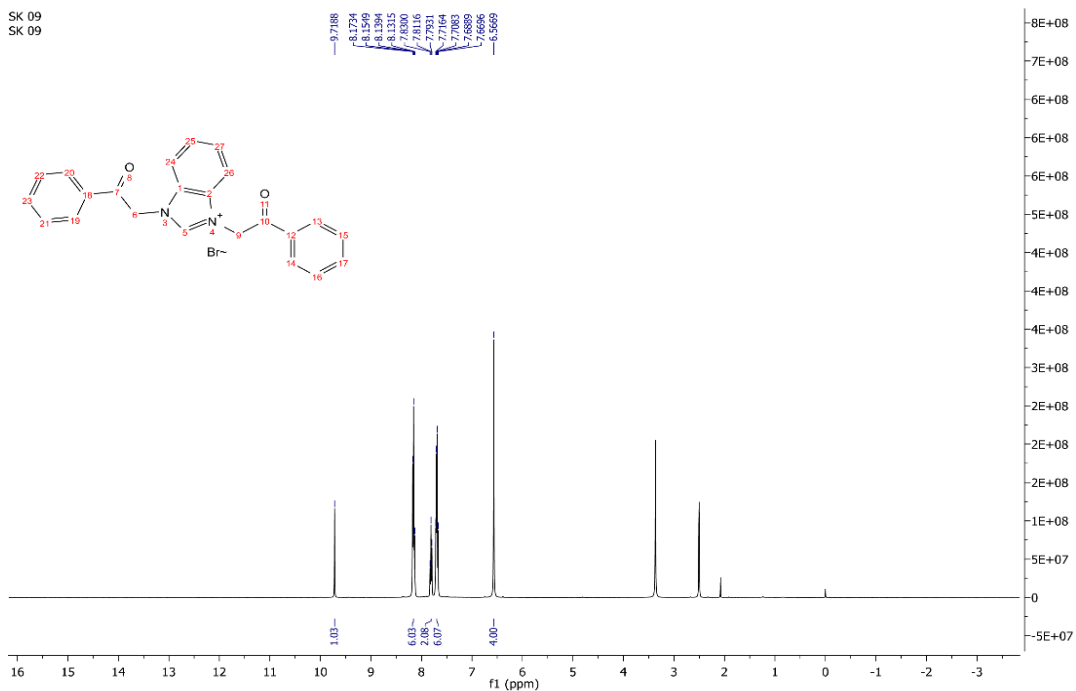
Figure 3.21 ¹H-NMR spectrum of synthesized [OPEBen⁺] [Br^{−}].
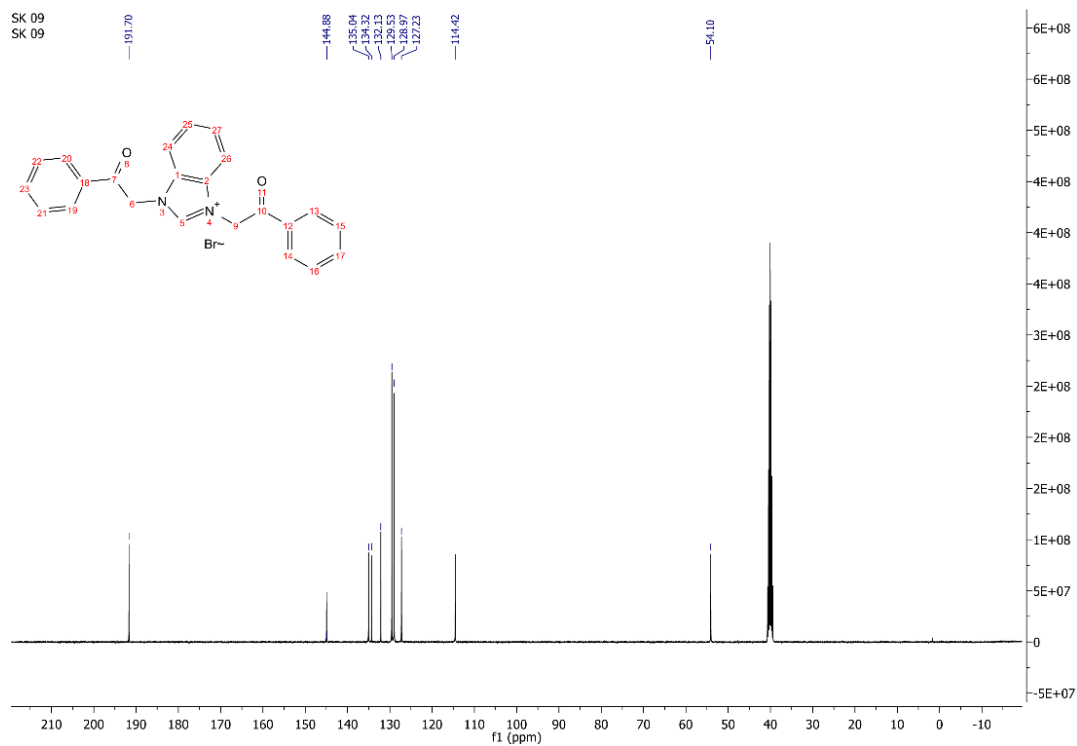
Figure 3.22 ¹³C-NMR spectrum of synthesized [OPEBen⁺] [Br^{−}].
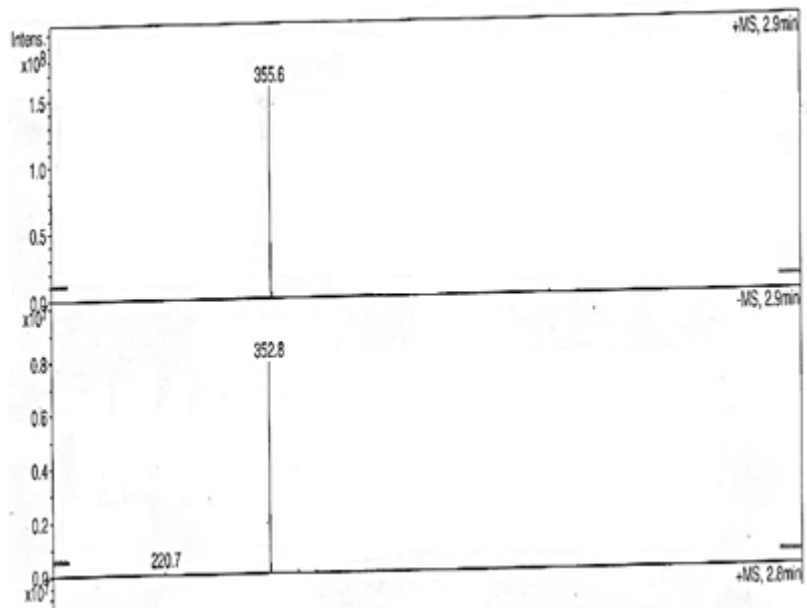
Figure 3.23 Mass spectrum of synthesized [OPEBen$^+$] [Br$^-$].
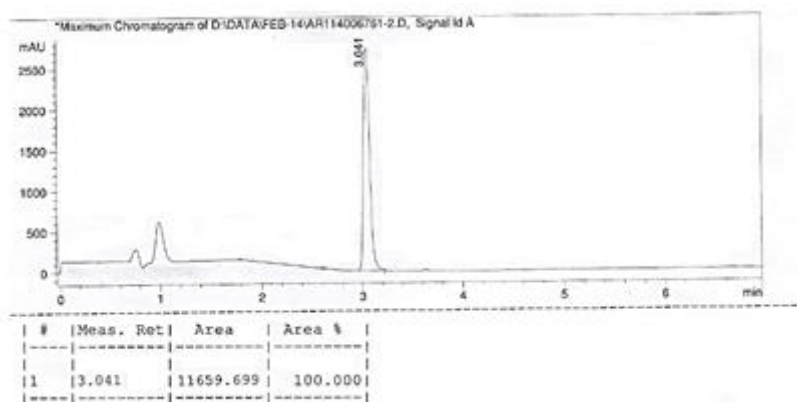
Figure 3.24 Liquid chromatogram of synthesized [OPEBen$^+$] [Br$^-$].

3.2.4 Characterization of [MPOEBen$^+$] [Br$^-$]

Figures 3.25, 3.26. 3.27, 3.28 and 3.29 show IR, ^{1}H-NMR, ^{13}C-NMR, mass spectrum and liquid chromatogram of [MPOEBen$^+$] [Br$^-$], respectively. The crystal structure obtained from SCXRD analysis is depicted in Figure 3.30 and the corresponding data are tabulated in the Table 3.6.

Characterization results: White solid, yield: 76%, m.p. 272-276 °C. FT-IR (ATR, cm^{-1}): 3085, 3043 (-C-H aromatic stretching), 2836 (-C-H aliphatic stretching), 1689 (C=O), 1596 (C=N), 1446 (C=C), 1229 (C-N). ^{1}H NMR (400 MHz, DMSO-d6): d (ppm), 9.68 (s, 1H), 8.13-8.08 (m, 6H), 7.70-7.68 (m, 2H), 7.21-7.19 (d, 4H, J=8.8), 6.47 (s, 4H), 3.91 (s, 6H)). ^{13}C-NMR (100 MHz, DMSO-d6) δ (ppm): 189.88, 164.70, 145.03, 132.11, 131.40, 127.18, 127.13, 114.81, 114.44, 56.32, 53.58. LC-MS (+ve mode) m/z calculated for $C_{25}H_{23}N_2O_4$: 415.6, Found: 415.6 [M+H]$^+$ with 100% purity.
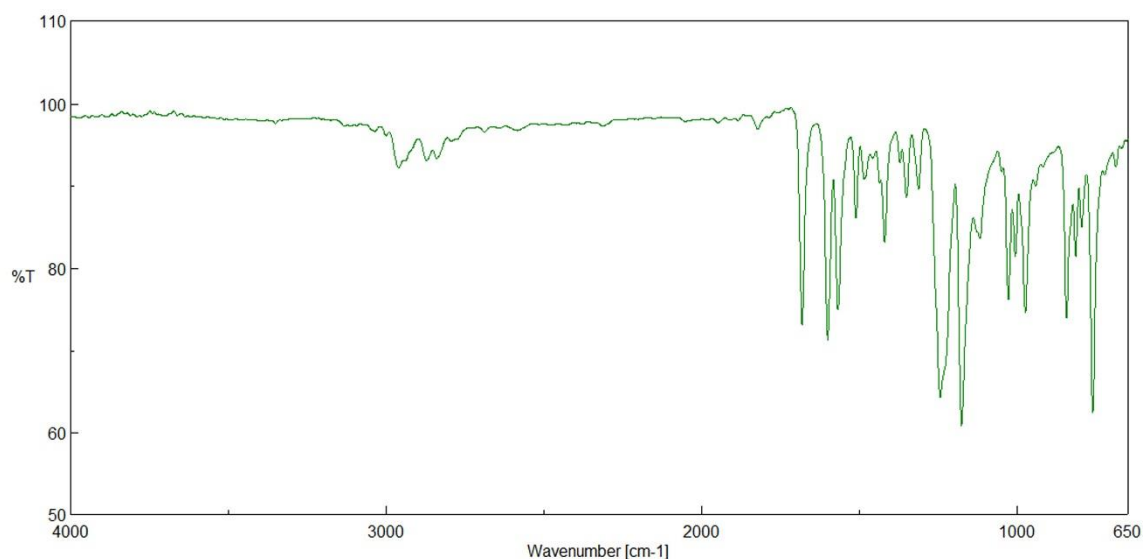
Figure 3.25 FT-IR spectrum of synthesized [MPOEBen$^+$] [Br$^-$].
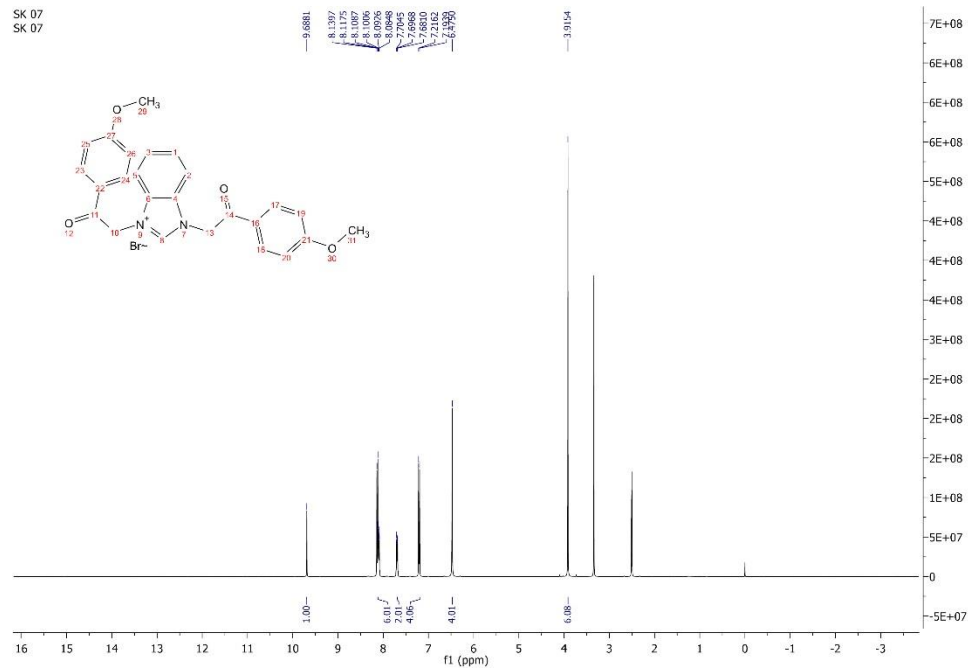
Figure 3.26 ¹H-NMR spectrum of synthesized [MPOEBen⁺] [Br^{−}].
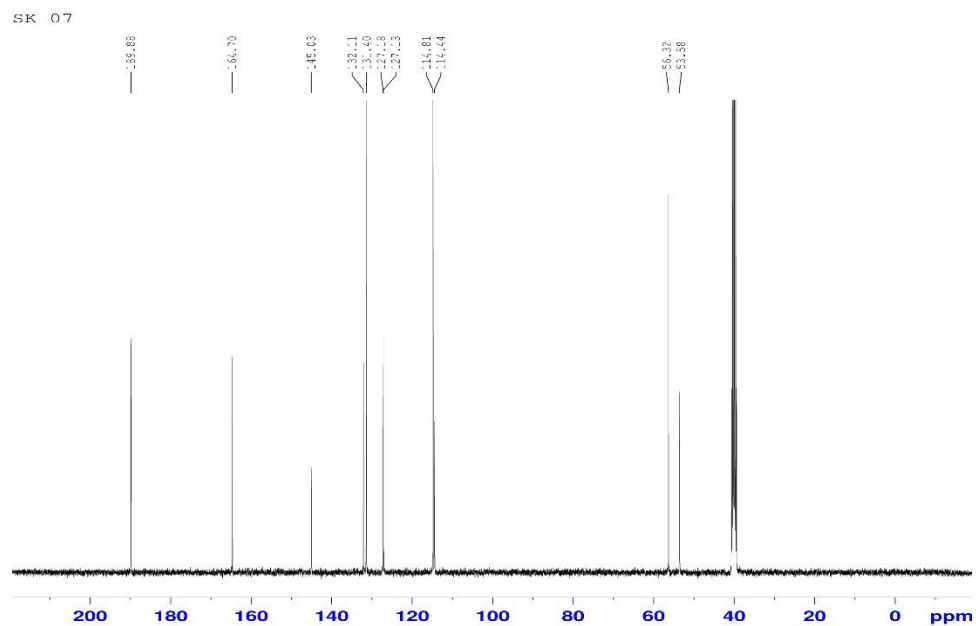
Figure 3.27 ¹³C-NMR spectrum of synthesized [MPOEBen⁺] [Br^{−}].
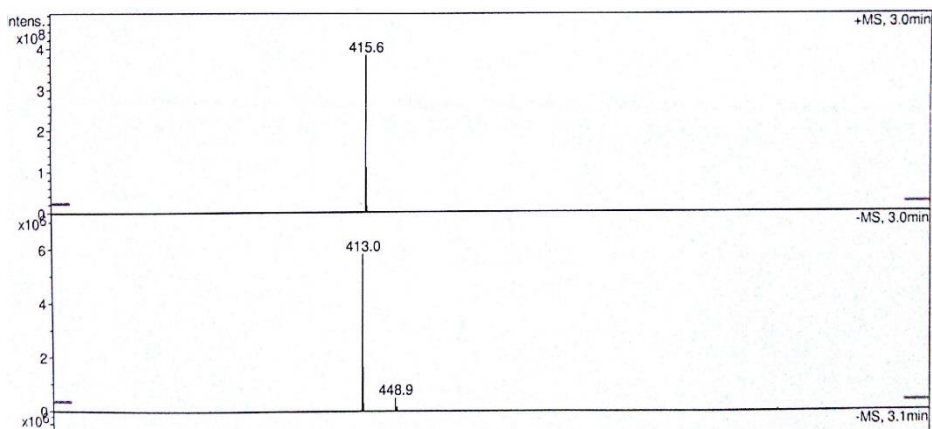
Figure 3.28 Mass spectrum of synthesized [MPOEBen$^+$] [Br$^-$].
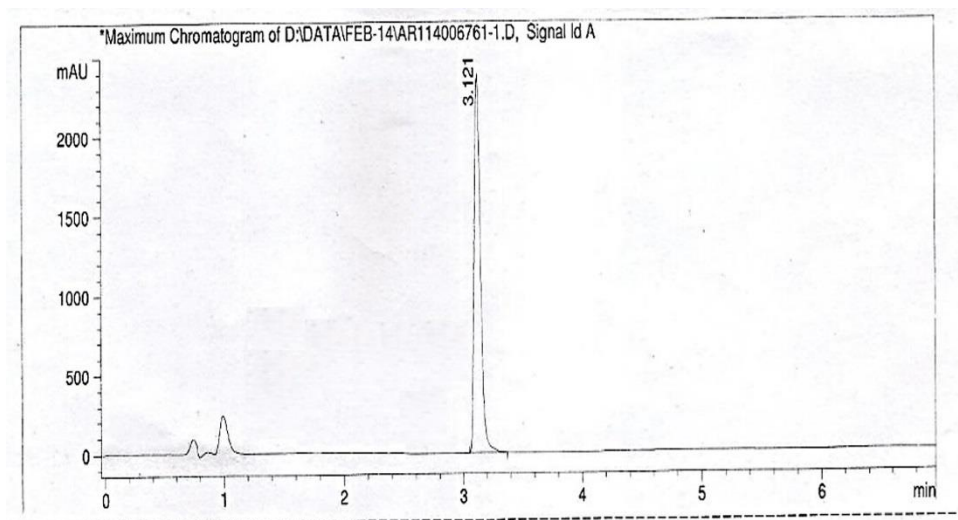
#	Meas. Ret	Area	Area %
1	3.121	14987.503	100.000

Figure 3.29 Liquid chromatogram of synthesized [MPOEBen$^+$] [Br$^-$].
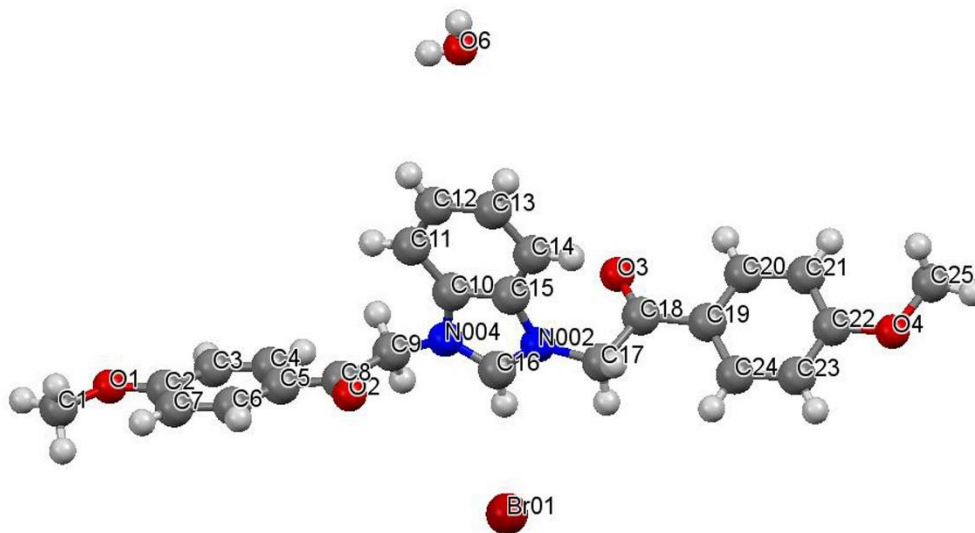
Figure 3.30 SCXRD structure of [MPOEBen⁺] [Br⁻].

Table 3.6 Single crystal XRD data for synthesized [MPOEBen⁺] [Br⁻].

Parameters	Crystal data
CCDC No.	1061620
Chemical formula	$C_{25}H_{23}N_2O_4$
Formula weight	495.36
Crystal system	Triclinic
Space group	P1
a (Å)	8.2011(7)
b (Å)	10.6895(9)
c (Å)	15.0238(13)
Volume (Å³)	1170.45(18)
Angle α, β, γ (°)	70.561 (5), 76.860 (5), 72.118 (5)
Z	2
F_{000}	508
µ (mm⁻¹)	1.789
Temperature	296 K
Radiation wavelength	0.71073
Radiation type	Mo Kα
Radiation source	Fine-focus sealed tube
Radiation monochromator	Graphite
R-factor (%)	7.19

3.3   1,3-BIS(2-OXO-2-PHENYLETHYL)-1*H*-IMIDAZOL-3-IUM   BROMIDE ([OPEIm$^+$] [Br$^-$]) AS CORROSION INHIBITOR ON 6061 Al-15 VOL. PCT. SiC$_{(P)}$ COMPOSITE IN ACIDIC MEDIA

The corrosion inhibition ability of [OPEIm$^+$] [Br$^-$] on 6061 Al-15 vol. pct. SiC$_{(P)}$ composite in hydrochloric acid and sulfuric acid media was tested using potentiodynamic polarization and electrochemical impedance spectroscopy (EIS) methods.

3.3.1 Potentiodynamic polarization measurements

The Figures 3.31(a) and 3.31(b) represent the potentiodynamic polarization curves for the corrosion of Al alloy composite in 0.1 M hydrochloric acid and 0.1 M sulfuric acid, respectively in the presence of different concentrations of [OPEIm$^+$] [Br$^-$] at 40 °C. Similar plots were obtained in other concentrations of the media and at other temperatures.
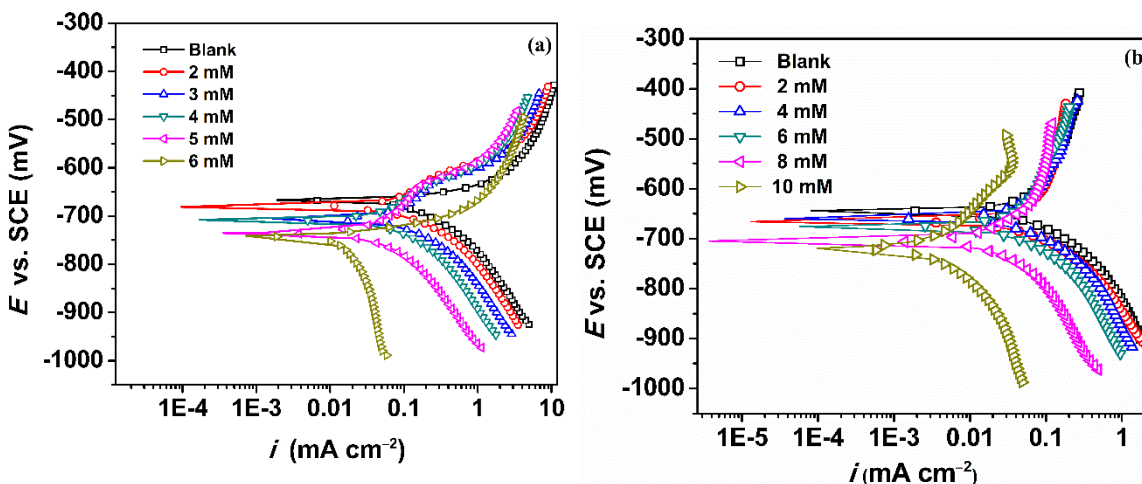
Figure 3.31 Potentiodynamic polarization curves for the corrosion of 6061 Al-15 vol. pct. SiC$_{(P)}$ composite in the presence of different concentrations of [OPEIm$^+$] [Br$^-$] at 40 °C, in 0.1 M (a) HCl and (b) H$_2$SO$_4$.

The anodic branch is attributed to the metal oxidation and cathodic branch defines the evolution of hydrogen in acidic medium (Musa et al. 2011). However, the nature of anodic curve in hydrochloric acid is different from that of the curve obtained in sulfuric acid electrolyte. The anodic curve in HCl shows two inflection points which refers to kinetic barrier effect possibly due to the presence of oxide layer followed by possible partial break down or increased porosity (Dindodi and Shetty 2014). The anodic curve in

sulfuric acid medium appears to be more passive, where the anodic region is more or less parallel to the y-axis, which suggests the presence of a less porous oxide layer. From the plots depicted in the Figure 3.31 it is evident that with the increase in the concentration of [OPEIm$^+$] [Br$^-$], the anodic and cathodic branches shift evidently to lower corrosion current densities (i_{corr}). Also, the corrosion potential (E_{corr}) shifts towards cathodic side with respect to E_{corr} of the blank. The corrosion current density (i_{corr}) was determined by extrapolating the linear cathodic branch up to 1 decade of current at -50 mV from the OCP to ensure accuracy, as the anodic branches in both hydrochloric and sulfuric acid electrolytes do not show linear Tafel region.

Electrochemical polarization parameters, like E_{corr}, i_{corr}, cathodic Tafel slope ($-\beta_c$) and inhibition efficiency (η), calculated from the potentiodynamic polarization studies in hydrochloric and sulfuric acid media, in the presence of different concentrations of [OPEIm$^+$] [Br$^-$] at different temperatures are presented in Tables 3.7, 3.8, 3.9 and 3.10, 3.11, 3.12, respectively.

The inhibition efficiency (η) and the surface coverage (θ) of [OPEIm$^+$] [Br$^-$] were determined using the Equations 2.3 and 2.4 mentioned under chapter 2, section 2.3.2.

From the data tabulated in Tables 3.7-3.9 and 3.10-3.12, certain significant observations could be made. The corrosion potential, E_{corr} shifts towards the cathodic region in the presence of [OPEIm$^+$] [Br$^-$]. But the shift is less than ± 85 mV, which is the widely accepted threshold value for the shift in E_{corr} for an inhibitor to be considered purely anodic or cathodic (Akbarzadeh et al. 2011). The observed shift in the E_{corr} values could be attributed to the mixed type of inhibition, where the inhibitor efficiently controls the metal dissolution at the anode as well as the evolution of hydrogen at the cathode to different extents; however, the predominant control is on the cathodic hydrogen evolution reaction, thereby reducing the overall rate of corrosion (Arukalam et al. 2014). Apart from these observations, the appreciable reduction in the corrosion current density, i_{corr} in the presence of [OPEIm$^+$] [Br$^-$] suggests effective reduction in the rate of corrosion in the presence of [OPEIm$^+$] [Br$^-$]. The rate of corrosion deceases and the inhibition efficiency increases with the increase in the concentration of the inhibitor up to 6 mM and 10 mM in

hydrochloric and sulfuric acid medium, respectively. Beyond the above mentioned concentrations, the increase in the inhibition efficiency was insignificant. It is also clear from the results that inhibition efficiency increases with the increase in medium concentration. The concentration of [OPEIm$^+$] [Br$^-$] required for maximum inhibition efficiency is 6 mM and 10 mM in hydrochloric acid medium and sulfuric acid medium, respectively. It indicates that more economic corrosion control can be achieved in hydrochloric acid medium than in sulfuric acid medium, however, the inhibition efficiencies shows no significant differences. The maximum inhibition efficiencies of 97.9% and 97.3% were obtained in 0.25 M HCl and 0.5 M H$_2$SO$_4$, respectively at 50 °C. The inhibition efficiency increases with the increase in the concentration of the acids in the media.

3.3.2 Electrochemical impedance spectroscopy measurements

Nyquist plots for the corrosion of Al alloy composite in 0.1 M hydrochloric acid and in 0.1 M sulfuric acid in the presence of different concentrations of [OPEIm$^+$] [Br$^-$] at 40 °C are depicted in Figures 3.32(a) and 3.32(b), respectively. Similar plots were obtained at other temperatures and also in other concentrations of the acid media.
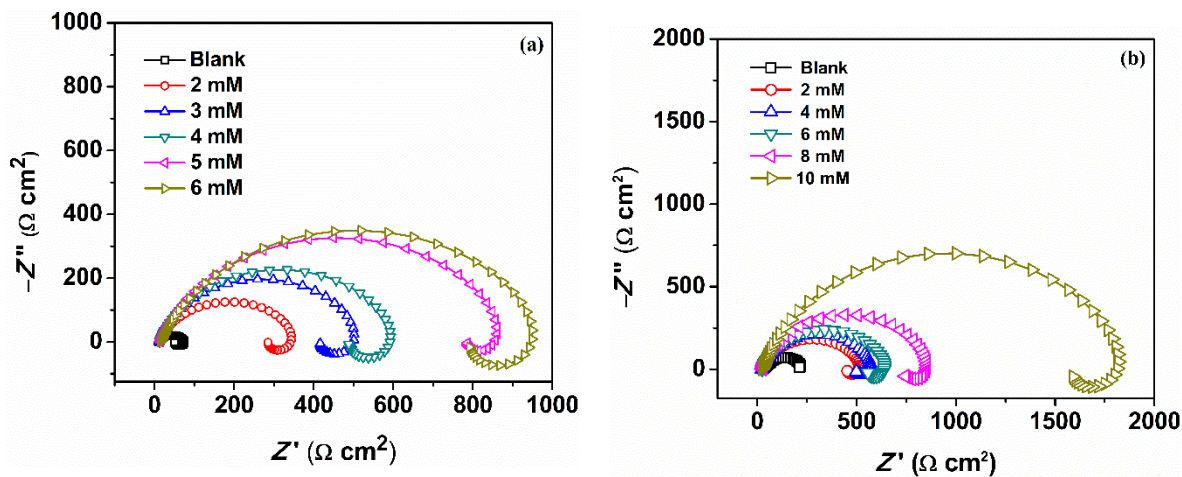
Figure 3.32 Nyquist plots for the corrosion of 6061 Al-15 vol. pct. SiC$_{(P)}$ composite in the presence of different concentrations of [OPEIm$^+$] [Br$^-$] at 40 °C, in 0.1 M (a) HCl and (b) H$_2$SO$_4$.

In both the media, the Nyquist plots are characterized with a high frequency (HF) capacitive loop and a low frequency (LF) inductive loop. Both the loops indicate the resistance offered for corrosion to persevere. Similar plots have been reported in the literature earlier by other researchers, for the corrosion of aluminum/alloy/composite in acidic medium (Pinto et al. 2009, Pinto 2010). The HF loop is often attributed to the resistance for charge transfer of corrosion process and the LF loop is attributed to the relaxation process of H^+ ions and the adsorption of corrosive anions like chloride or sulfate on or into the oxide film (Babic et al. 1998). The aluminum is oxidized to Al^+ ions and the ions migrate to the oxide/electrolyte interface forming oxidized Al^{3+}. Also, at the oxide/electrolyte surface, O^{2-} or OH^- ions are formed. All these processes may be assumed to be represented by a single capacitive loop due to the overlapping of processes or one process dominating the rest (Pinto et al. 2011a). Figures 3.12(a) and 3.12(b) clearly show enlarged capacitive and inductive loops in the presence of $[OPEIm^+]$ $[Br^-]$, which indicate the enhanced resistance for the corrosion to occur. This may be attributed to the formation of a barrier film on the alloy composite surface by $[OPEIm^+]$ $[Br^-]$, which affects the above processes (Ansari et al. 2012).

In order to theoretically fit the impedance behavior obtained practically, the Nyquist plots were simulated using the same equivalent electric circuit shown in the representative simulation plot (Figure 3.3). The percentage inhibition efficiency (η %) is calculated using the Equation 2.5 mentioned in chapter 2, section 2.3.2.

The impedance parameters like R_P, C_{dl} and η in the presence of different concentrations of $[OPEIm^+]$ $[Br^-]$ in different concentrations of HCl and H_2SO_4 at different temperatures are given in the Tables 3.13, 3.14, 3.15 and 3.16, 3.17, 3.18, respectively. It is evident from Tables 3.13-3.15 and 3.16-3.18 that, the concentration of inhibitor required is less in HCl medium than in sulfuric acid medium and also, as the concentration of $[OPEIm^+]$ $[Br^-]$ increases, the R_P value increases and the C_{dl} value decreases. This increase in polarization resistance hints about improved corrosion resistance in the presence of inhibitor probably due to the presence of $[OPEIm^+]$ $[Br^-]$ as a barrier layer on the corroding electrode surface (Ibrahim and Zour 2011). The decrease in

the capacitance of the electrical double layer (C_{dl}) can be attributed to the increase in the double layer thickness (d) or/and reduction in the local dielectric constant (ε), as defined by the Helmhotz model (Equation 3.4, Section 3.1.2) (Srinivasan 2006). The value of R_P increases and that of C_{dl} decreases with the increase in the concentrations of both HCl and H_2SO_4. The optimum concentration of the inhibitor required is less in HCl medium than in H_2SO_4 medium.

In order to overcome the drawback of Nyquist plot, which doesn't account for the frequency specific impedance behavior, Bode magnitude and Bode phase angle plots were also considered. The Figures 3.33(a) and 3.33(b) display Bode magnitude plots for the corrosion of alloy composite in 0.1 M hydrochloric acid and 0.1 M sulfuric acid at 40 °C, respectively. The corresponding Bode phase angle plots for the corrosion of alloy composite in 0.1 M hydrochloric acid and 0.1 M sulfuric acid at 40 °C are shown in the Figures 3.34(a) and 3.34(b), respectively.
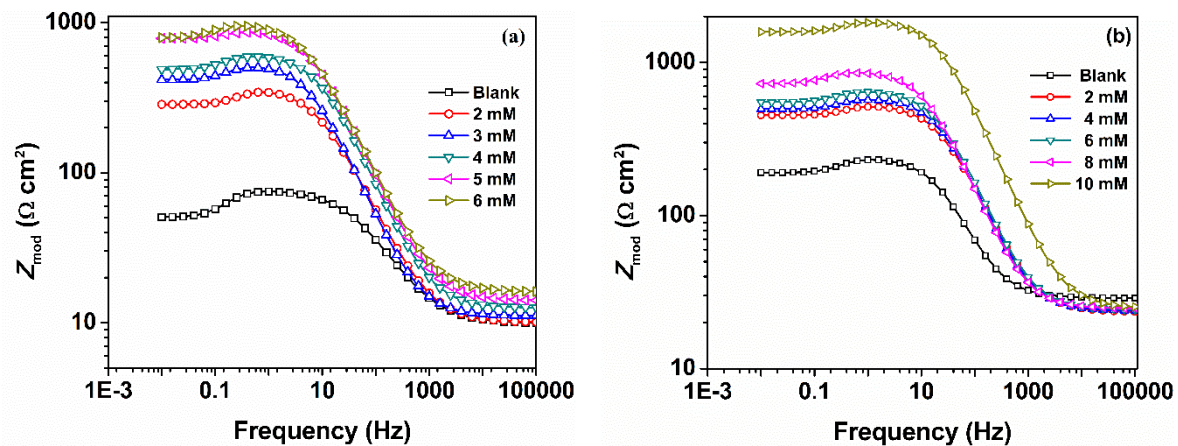
Figure 3.33 Bode magnitude plots for the corrosion of 6061 Al-15 vol. pct. SiC(P) composite in the presence of different concentrations of [OPEIm⁺] [Br⁻] at 40 °C, in 0.1 M (a) HCl and (b) H₂SO₄.
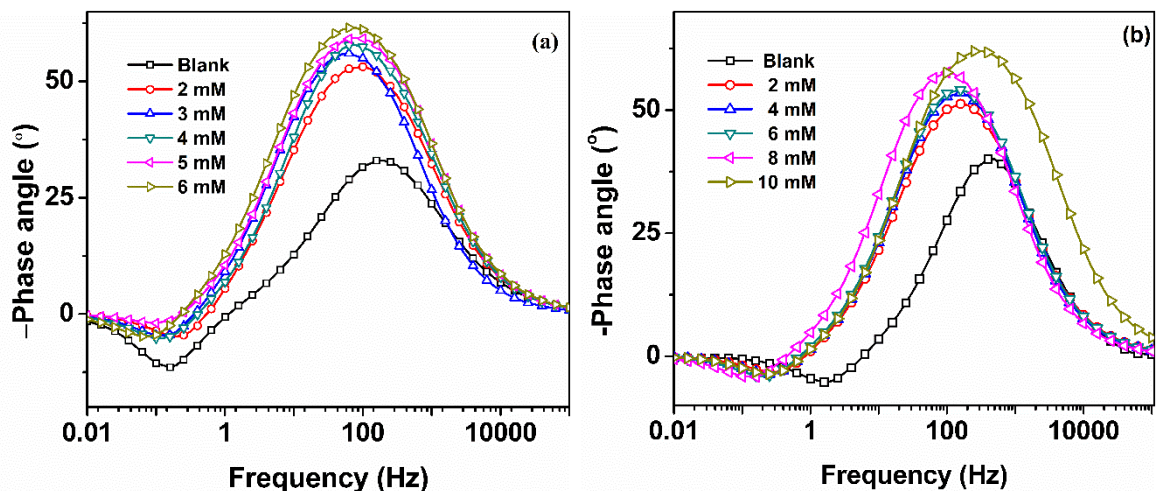
Figure 3.34 Bode phase angle for the corrosion of 6061 Al-15 vol. pct. SiC(P) composite in the presence of different concentrations of [OPEIm$^+$] [Br$^-$] at 40 °C, in 0.1 M (a) HCl and (b) H$_2$SO$_4$.

From Bode magnitude plots, it may be observed that, with the increase in the concentration of [OPEIm$^+$] [Br$^-$], the low frequency impedance modulus (Z_{mod}) increases, indicating better corrosion protection (Gao et al. 2010). Similarly, in Bode phase angle plots, a shift in mid frequency phase maximum (θ'_{max}) towards lower frequency, along with an increase in θ'_{max} with the increase in the concentration of [OPEIm$^+$] [Br$^-$] implies an improved corrosion protection. As the mid frequency behavior accounts for the diffusion of corrosive species through the surface oxide layer, increase in the values of θ'_{max} reflects the decrease in the diffusion of corrosive species into the oxide film and thereby protects the surface of the composite (Hu et al. 2013).

3.3.3 Effect of temperature

The effect of temperature on the corrosion process in the presence of different concentrations of [OPEIm$^+$] [Br$^-$] was studied and the activation parameters were derived. It is evident from the potentiodynamic polarization measurements and EIS studies and the data summarized in the Tables 3.7-3.18 that, the inhibition efficiency increases with the increase in temperature. It is known that if the inhibition efficiency increases with the increase in temperature, the inhibitor species may have adsorbed via chemisorption

phenomenon on the electrode surface (Noor 2007, Adejo et al. 2013). Adsorption of the inhibitor on the electrode surface through physisorption, would cause the decrease in the efficiency as the temperature is increased due to the probable desorption of the weakly adsorbed inhibitors through electrostatic interactions with the electrode surface, on gaining extra kinetic energy. However, when it is chemisorption through relatively strong chemical interactions between the inhibitor and the corroding specimen, the extent of adsorption increases with temperature. As a result, more and more inhibitor molecules in the electrolyte would come in contact with the electrode surface and adsorb via chemisorption phenomenon. Chemisorption is an irreversible process unless and until some harsh reagent or extreme conditions of temperature is used to remove the adsorbed molecules.

The apparent energy of activation (E_a) in the presence of different concentrations of [OPEIm$^+$] [Br$^-$] was deduced from Arrhenius Equation 2.6 mentioned in chapter 2, section 2.2.3. The slopes obtained from Arrhenius plots of ln (v_{corr}) vs. 1/T were used to calculate the energies of activation (E_a). The Arrhenius plots for the corrosion of the composite in 0.1 M HCl and 0.1 M H$_2$SO$_4$ in the presence of [OPEIm$^+$] [Br$^-$] are given in the Figures 3.35(a) and 3.35(b), respectively.
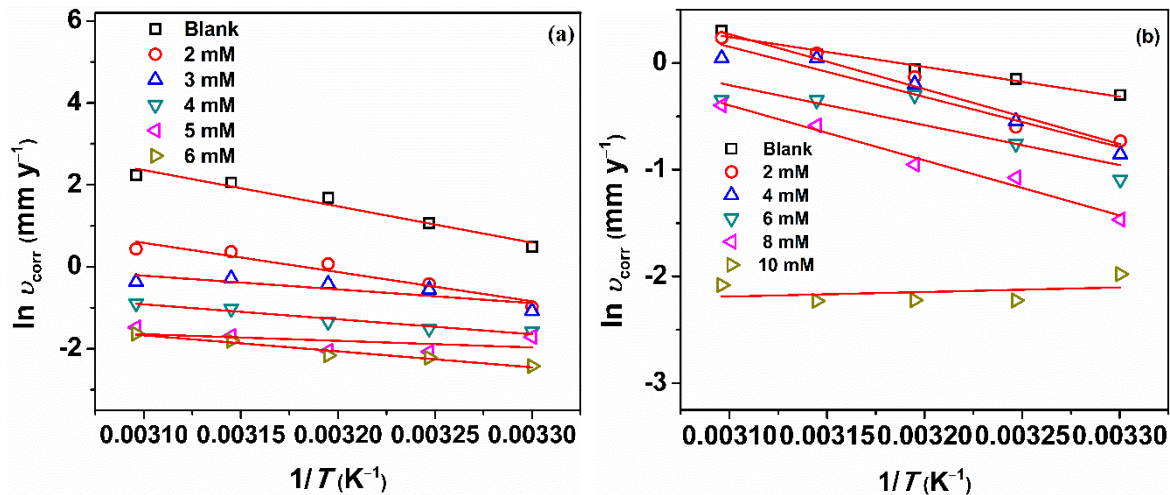
Figure 3.35 Arrhenius plots for the corrosion of 6061 Al-15 vol. pct. SiC$_{(P)}$ composite in the presence of different concentrations of [OPEIm$^+$] [Br$^-$] in 0.1 M (a) HCl and (b) H$_2$SO$_4$.

The apparent enthalpy of activation ($\Delta H^{\#}$) and entropy of activation ($\Delta S^{\#}$) were calculated using transition state theory Equation 2.7 mentioned in chapter 2, section 2.2.3. From the linear plots of $\ln(v_{corr}/T)$ vs. $1/T$, the values of $\Delta H^{\#}$ were calculated using the slopes and the values of $\Delta S^{\#}$ were calculated using the intercepts obtained by the linear fit. The plots of $\ln(v_{corr}/T)$ vs. $1/T$ for the corrosion of the composite in 0.1 M HCl and 0.1 M H_2SO_4 in the presence of [OPEIm$^+$] [Br$^-$] are shown in Figures 3.36(a) and 3.36(b), respectively. The calculated activation parameters are presented in Tables 3.19 and 3.20.
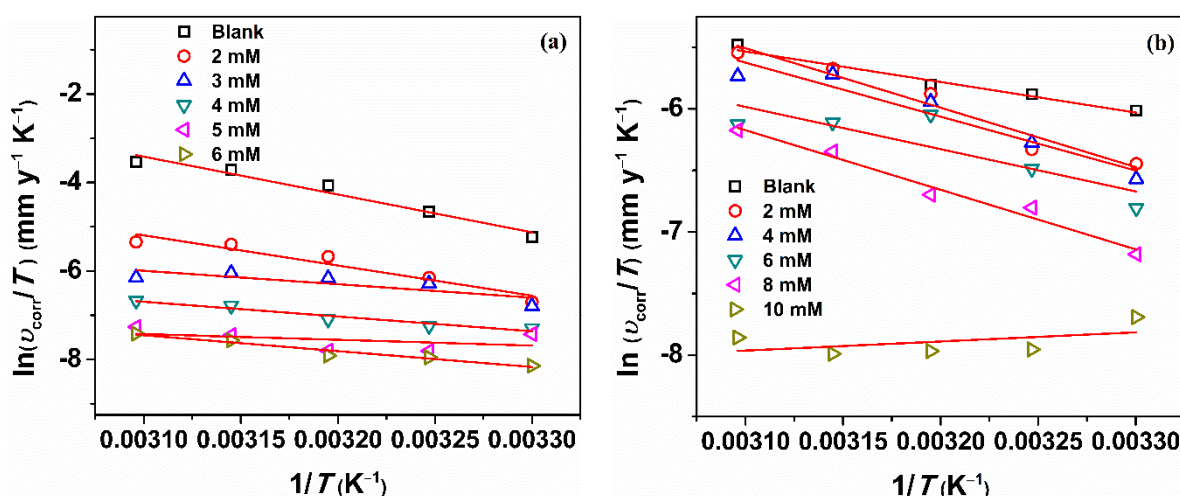
Figure 3.36 Plots of ln (v_{corr}/T) vs. $1/T$ for the corrosion of 6061 Al-15 vol. pct. SiC$_{(P)}$ composite in the presence of different concentrations of [OPEIm$^+$] [Br$^-$] in 0.1 M (a) HCl and (b) H$_2$SO$_4$.

It is seen from Tables 3.19 and 3.20, that the values of E_a obtained in the presence of inhibitor are lower than that obtained in the absence of inhibitor. The decrease in E_a in the presence of [OPEIm$^+$] [Br$^-$] is also suggestive of the possible chemisorption phenomenon (Stoyanova et al. 1997, Cicek et al. 2013, Ameer et al. 2014). Also, it's noteworthy that some of the values of apparent activation energy and activation enthalpy are negative, which is less common. However, studies by Han et al. (2013) state that practically, when the reaction rate varies inversely with temperature, there is a possibility of negative enthalpy values which would also result in negative values of activation energy. Hence, it may be concluded that since the rate of corrosion decreases with the increase in

temperature, which is reflected in increasing inhibition efficiencies with temperature, negative values of activation energies obtained by plots are valid. Also, studies by Shimomura (1967) states that the potential-energy barrier for any elementary process cannot be negative; and, therefore, a "*negative*" activation energy indicates some complexity of the process. The negative values of $\Delta S^{\#}$ indicates association process in the formation of the activated intermediate complex in the rate determining step of the corrosion reaction (Borsato et al. 2014).

3.3.4 Adsorption isotherms

Adsorption isotherm represents the variation in the extent of inhibitor adsorption on the composite surface with respect to pressure or concentration of the inhibitor (C_{inh}) at constant temperature. The nature of interaction between the adsorbate (inhibitor) and the adsorbent (electrode) may be understood by the analysis of adsorption isotherms. The electrode surface is previously adsorbed with water molecules. The adsorption of the inhibitor (*Inh)* occurs by the displacement of water molecules as shown in Equation 3.10.

$$Inh_{(sol)} + \chi H_2O_{(ads)} \rightarrow Inh_{(ads)} + \chi H_2O_{(sol)} \tag{3.10}$$
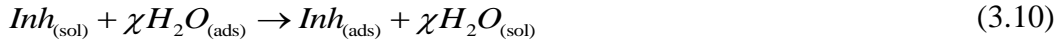
where, χ is the number of water molecules displaced by one molecule of the inhibitor. The value of χ is inhibitor and metal charge specific.

The efficiency of an inhibitor depends on the surface coverage, θ of the composite surface by the inhibitor. The values of θ at different concentrations of inhibitor (C_{inh}), were calculated according to Equation 2.4 mentioned under section 2.2.2 of chapter 2. The linear relation between C_{inh} and θ was obtained graphically by linear fit of parameters to various adsorption isotherms which include, Langmuir, Temkin, Freundlich and Frumkin adsorption isotherms. The adsorption isotherm with linear regression coefficient (R^2) close to 1 was considered as the best fit. The best fit in the present study was obtained with Langmuir adsorption isotherm, mathematical expression of which is given in the Equation 3.11.

$$\frac{C_{inh}}{\theta} = C_{inh} + \frac{1}{K} \tag{3.11}$$

where, K is the equilibrium constant for the process of adsorption-desorption. Langmuir adsorption isotherm plots for the adsorption of [OPEIm$^+$] [Br$^-$] on the composite surface in 0.1 M HCl and 0.1 M H$_2$SO$_4$ are given in Figures 3.37(a) and 3.37(b), respectively. K was calculated as reciprocal of the intercept values from the plot.

The value of K was substituted in Equation 2.8 mentioned under section 2.2.4 of chapter 2 to calculate the standard free energy of adsorption (ΔG^0_{ads}). The standard enthalpy of adsorption (ΔH^0_{ads}) and standard entropy of adsorption (ΔS^0_{ads}) were calculated from the linear fit of ΔG^0_{ads} vs. T, using the Equation 2.9 mentioned under section 2.2.4 of chapter 2.
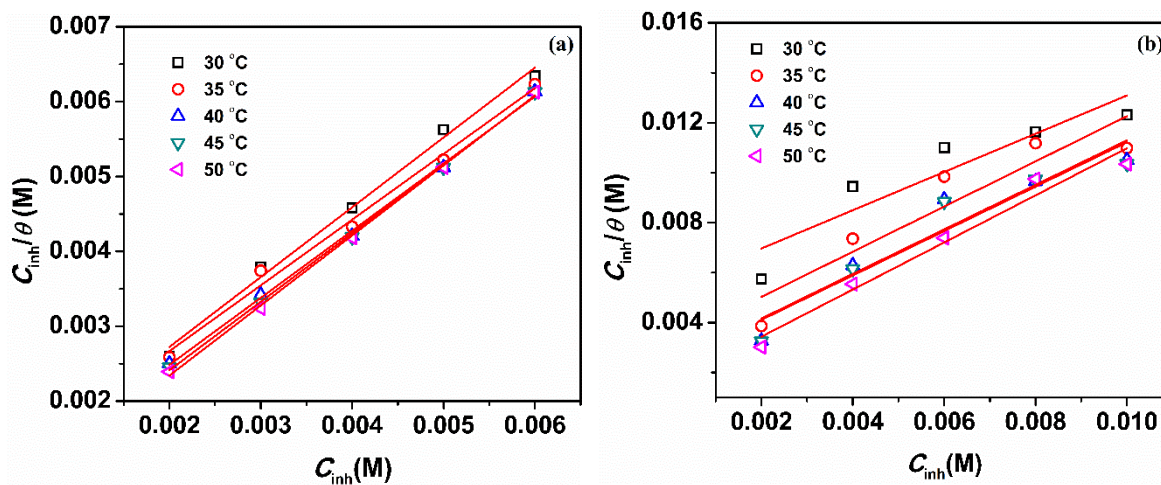
Figure 3.37 Langmuir adsorption isotherms for the adsorption of [OPEIm$^+$] [Br$^-$] on the surface of 6061 Al-15 vol. pct. SiC$_{(P)}$ composite in 0.1 M (a) HCl and (b) H$_2$SO$_4$.

The calculated thermodynamic parameters for the adsorption of [OPEIm$^+$] [Br$^-$] on the composite surface in hydrochloric and sulfuric acid media of different concentrations are listed in Tables 3.21 and 3.22. The deviation of slope values from unity suggests the possible intermolecular interactions between the adsorbed inhibitor molecules on the composite surface which are forbidden interactions as per the assumptions for the statistical derivation of Langmuir equation (Masel 1996). The values of standard free energy, ΔG^0_{ads} are negative and are in the range of approximately −27.5 to −32.0 kJ mol^{-1} in HCl and   to −23.3 to −28.7 kJ mol^{-1} in H$_2$SO$_4$ for the adsorption of [OPEIm$^+$] [Br$^-$] on the composite

surface. The widely accepted threshold for standard free energy of adsorption is −20 kJ mol^{-1} for physisorption and more negative than −40 kJ mol^{-1} for chemisorption and in between these two threshold values both the processes are likely to occur (Bentiss et al. 2005). The obtained values of standard free energy for the adsorption of [OPEIm$^+$] [Br$^-$] on the composite surface in both the media are suggestive of chemisorption and physisorption phenomena. Also, the values of ΔH^0_{ads} is positive suggesting endothermic reaction during adsorption. The negative values of standard enthalpy is associated with both the chemisorption and the physisorption and positive value of standard enthalpy is associated exclusively with chemisorption processes (Zarrouk et al. 2013). It was also observed that with the increase in temperature the value of ΔG^0_{ads} becomes more and more negative, which indicates that the adsorption process is spontaneous and thermodynamically favorable at higher temperatures (El Bribri et al. 2013, Arshadi et al. 2014). From the values of standard free energy of adsorption, standard enthalpy of adsorption and the trends in the variation of inhibition efficiency with temperature, it can be concluded that the adsorption of the inhibitor is predominantly through chemisorption and the contribution by physisorption is to a lesser extent. The values of ΔS^0_{ads} in both the electrolytes are positive, suggesting increased randomness in the system which may be due to desorption of water molecules and displacement with [OPEIm$^+$] [Br$^-$] (Manamela et al. 2014).

3.3.5 Surface analyses

An even and smooth morphology may be observed in the SEM images in Figures 3.38(a) and 3.38(b) which depict the specimen morphologies of samples immersed in 0.1 M hydrochloric acid and 0.1 M sulfuric acid containing 6 mM and 10 mM of [OPEIm$^+$] [Br$^-$] for 2 and 3 hours at 30 °C, respectively. Also, the qualitative support to the visual assessment is fetched by EDX spectra shown in Figures 3.39(a) and 3.39(b), which show additional N peaks apart from C, O and other peaks from the metal, which supports the adsorption of inhibitor on the composite surface.
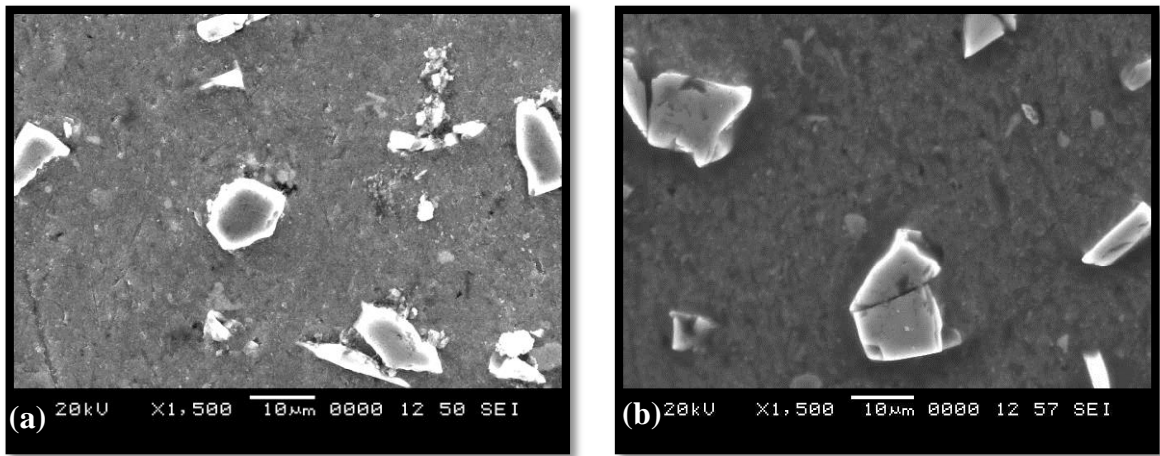
Figure 3.38 SEM images of the 6061 Al-15 vol. pct. SiC$_{(P)}$ composite surface immersed in 0.1 M (a) HCl containing 6 mM [OPEIm$^+$] [Br$^-$] for 2 hand (b) H$_2$SO$_4$ containing 10 mM [OPEIm$^+$] [Br$^-$] for 3 h.
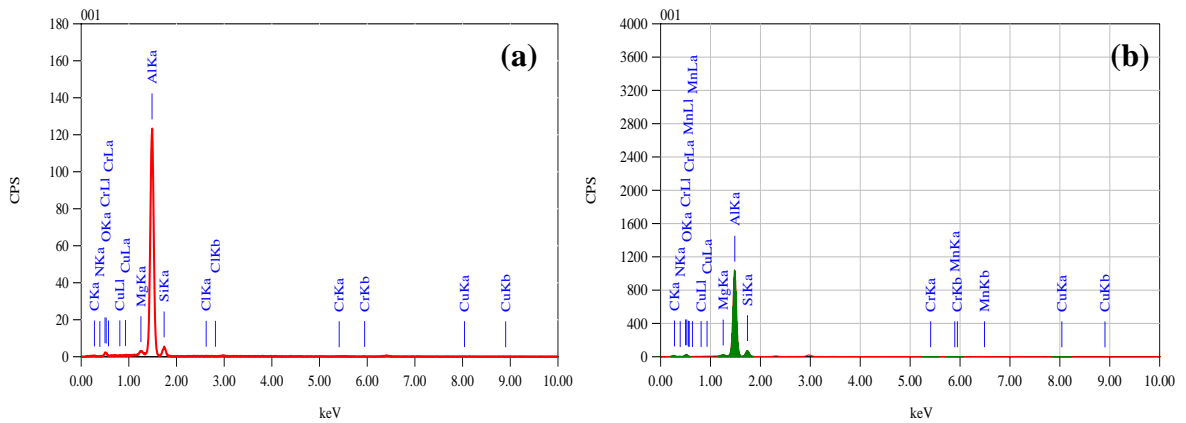
Figure 3.39 EDX spectra of 6061 Al-15 vol. pct. SiC$_{(P)}$ composite surface immersed in 0.1 M (a) HCl containing 6 mM [OPEIm$^+$] [Br$^-$] for 2 h and (b) H$_2$SO$_4$ containing 10 mM [OPEIm$^+$] [Br$^-$] for 3 h.

Table 3.7 Potentiodynamic polarization data for the corrosion of 6061 Al-15 vol. pct. SiC$_{(P)}$ composite in 0.025 M HCl solution containing different concentrations of [OPEIm$^+$] [Br$^-$] at different temperatures.

Temp (°C)	Inh. Conc. (mM)	$-E_{corr}$ (mV vs. SCE)	$-\beta_c$ (mV dec^{-1})	i_{corr} (μA cm^{-2})	η (%)
	Blank	696	215	54.6	-
	2	696	198	15.2	72.2
30	3	699	192	12.0	78.0
	4	702	198	7.0	87.2
	5	709	193	6.2	88.7
	6	711	196	3.7	93.2
	Blank	676	192	102.6	-
	2	680	146	26.9	73.8
35	3	689	144	21.9	78.6
	4	693	150	9.1	91.1
	5	698	142	4.7	95.4
	6	699	145	4.1	96.0
	Blank	693	216	134.4	-
	2	701	177	34.9	74.1
40	3	709	173	16.9	87.5
	4	712	176	6.9	94.9
	5	727	179	3.3	97.5
	6	732	179	3.0	97.8
	Blank	690	225	161.7	-
	2	699	195	39.2	75.8
45	3	708	193	17.7	89.1
	4	719	198	7.3	95.5
	5	727	194	4.0	97.5
	6	735	190	3.6	97.8
	Blank	714	224	180.8	-
	2	720	179	42.7	76.4
50	3	734	173	26.2	85.5
	4	737	172	16.6	90.8
	5	738	176	6.6	96.3
	6	740	172	5.0	97.2

Table 3.8 Potentiodynamic polarization data for the corrosion of 6061 Al-15 vol. pct. SiC$_{(P)}$ composite in 0.1 M HCl solution containing different concentrations of [OPEIm$^+$] [Br$^-$] at different temperatures.

Temp (°C)	Inh. Conc. (mM)	$-E_{corr}$ (mV vs. SCE)	$-\beta_c$ (mV dec^{-1})	i_{corr} (μA cm^{-2})	η (%)
	Blank	664	166	150.8	-
	2	668	142	34.8	76.9
30	3	669	166	31.6	79.1
	4	690	125	19.1	87.3
	5	698	133	16.8	88.9
	6	723	185	8.2	94.6
	Blank	659	199	269.5	-
	2	673	156	61.2	77.3
35	3	695	153	53.4	80.2
	4	702	159	20.6	92.4
	5	703	158	11.7	95.7
	6	734	154	10.1	96.3
	Blank	665	188	497.5	-
	2	683	148	99.9	79.9
40	3	705	153	61.2	87.7
	4	708	154	24.3	95.1
	5	735	156	11.9	97.6
	6	741	156	10.7	97.9
	Blank	691	204	726.3	-
	2	675	192	134.2	81.5
45	3	698	198	69.9	90.4
	4	708	197	33.5	95.4
	5	710	195	17.2	97.6
	6	737	196	15.3	97.9
	Blank	702	223	874.5	-
	2	682	192	143.6	83.6
50	3	709	199	64.3	92.6
	4	714	194	38.1	95.6
	5	738	196	21.1	97.6
	6	741	193	18.1	97.9

Table 3.9 Potentiodynamic polarization data for the corrosion of 6061 Al-15 vol. pct. SiC$_{(P)}$ composite in 0.25 M HCl solution containing different concentrations of [OPEIm$^+$] [Br$^-$] at different temperatures.

Temp (°C)	Inh. Conc. (mM)	$-E_{corr}$ (mV vs. SCE)	$-\beta_c$ (mV dec^{-1})	i_{corr} (μA cm^{-2})	η (%)
	Blank	658	293	898.3	-
	2	676	276	191.3	78.7
30	3	687	274	129.5	85.6
	4	689	273	113.0	87.4
	5	690	278	93.5	89.6
	6	692	275	45.5	94.9
	Blank	664	224	1239.4	-
	2	674	198	256.4	79.3
35	3	679	197	163.0	86.8
	4	681	199	90.4	92.7
	5	683	197	53.1	95.7
	6	684	196	45.2	96.4
	Blank	658	308	1807.0	-
	2	678	273	325.2	82.0
40	3	681	275	181.8	89.9
	4	681	276	84.1	95.3
	5	684	274	43.8	97.6
	6	687	278	37.7	97.9
	Blank	684	277	1878.3	-
	2	689	246	299.8	84.0
45	3	690	243	159.4	91.5
	4	694	245	80.3	95.7
	5	695	244	43.9	97.7
	6	697	241	39.8	97.9
	Blank	667	246	2135.9	-
	2	685	204	292.9	86.3
50	3	687	203	121.8	94.3
	4	689	205	91.3	95.7
	5	695	208	49.7	97.7
	6	699	206	45.3	97.9

Table 3.10 Potentiodynamic polarization data for the corrosion of 6061 Al-15 vol. pct. SiC$_{(P)}$ composite in 0.1 M H$_2$SO$_4$ solution containing different concentrations of [OPEIm$^+$] [Br$^-$] at different temperatures.

Temp (°C)	Inh. Conc. (mM)	$-E_{corr}$ (mV)	$-\beta_c$ (mV dec^{-1})	i_{corr} (μA cm^{-2})	η (%)
	Blank	659	121	68.5	-
	2	659	121	44.7	34.8
30	4	660	123	39.5	42.4
	6	672	124	31.2	54.5
	8	710	166	21.4	68.7
	10	714	188	12.9	81.2
	Blank	665	105	79.5	-
	2	666	105	38.2	51.8
35	4	667	124	36.3	54.4
	6	677	129	31.1	61.0
	8	705	185	22.8	71.6
	10	714	185	7.0	91.0
	Blank	636	155	87.3	-
	2	645	155	34.0	61.1
40	4	665	157	32.1	63.6
	6	681	160	28.7	67.2
	8	713	161	14.9	82.9
	10	718	165	4.2	95.2
	Blank	655	102	100.1	-
	2	658	106	38.7	61.3
45	4	660	156	35.0	65.1
	6	681	159	32.1	67.9
	8	730	209	17.8	82.2
	10	735	218	3.4	96.6
	Blank	653	150	125.7	-
	2	656	151	41.9	66.3
50	4	662	161	34.9	72.2
	6	689	185	23.7	81.2
	8	732	207	22.5	82.1
	10	740	214	4.1	96.7

Table 3.11 Potentiodynamic polarization data for the corrosion of 6061 Al-15 vol. pct. SiC$_{(P)}$ composite in 0.3 M H$_2$SO$_4$ solution containing different concentrations of [OPEIm$^+$] [Br$^-$] at different temperatures.

Temp (°C)	Inh. Conc. (mM)	$-E_{corr}$ (mV vs. SCE)	$-\beta_c$ (mV dec^{-1})	i_{corr} (μA cm^{-2})	η (%)
	Blank	595	142	209.6	-
	2	596	110	132.2	36.9
30	4	596	126	113.5	45.8
	6	606	118	93.1	55.6
	8	608	110	61.0	70.9
	10	610	118	35.7	83.0
	Blank	595	139	237.6	-
	2	596	117	111.9	52.9
35	4	598	108	107.7	54.7
	6	599	103	86.0	63.8
	8	602	108	59.6	74.9
	10	604	115	16.9	92.9
	Blank	592	141	270.5	-
	2	594	125	102.0	62.3
40	4	596	120	96.1	64.5
	6	600	124	84.0	69.0
	8	601	109	44.7	83.5
	10	606	102	11.0	95.9
	Blank	603	157	273.1	-
	2	604	105	99.2	63.7
45	4	605	101	94.6	65.4
	6	606	103	85.9	68.5
	8	609	104	46.7	82.9
	10	617	107	8.6	96.8
	Blank	605	159	294.8	-
	2	606	111	88.2	70.1
50	4	608	117	75.5	74.4
	6	609	112	50.7	82.8
	8	610	115	49.9	83.1
	10	613	114	9.4	96.8

Table 3.12 Potentiodynamic polarization data for the corrosion of 6061 Al-15 vol. pct. SiC$_{(P)}$ composite in 0.5 M H$_2$SO$_4$ solution containing different concentrations of [OPEIm$^+$] [Br$^-$] at different temperatures.

Temp (°C)	Inh. Conc. (mM)	$-E_{corr}$ (mV vs. SCE)	$-\beta_c$ (mV dec^{-1})	i_{corr} (μA cm^{-2})	η (%)
	Blank	560	129	348.7	-
	2	563	100	202.0	42.1
30	4	565	113	174.5	49.9
	6	567	113	149.8	57.0
	8	572	114	100.3	71.2
	10	573	120	58.7	83.2
	Blank	559	125	372.1	-
	2	565	113	163.6	56.0
35	4	570	104	155.0	58.3
	6	572	110	132.5	64.4
	8	576	110	92.1	75.2
	10	580	99	23.8	93.6
	Blank	557	140	479.8	-
	2	567	124	164.2	65.8
40	4	568	114	162.8	66.1
	6	574	105	132.2	72.5
	8	575	109	76.2	84.1
	10	578	113	16.6	96.5
	Blank	562	164	517.9	-
	2	570	136	166.9	67.8
45	4	574	131	154.4	70.2
	6	574	135	133.0	74.3
	8	577	133	75.6	85.4
	10	582	136	14.8	97.1
	Blank	565	169	564.7	-
	2	567	149	162.5	71.2
50	4	575	146	128.1	77.3
	6	584	141	95.4	83.1
	8	585	144	64.0	88.7
	10	590	148	15.3	97.3

Table 3.13 EIS data for the corrosion of 6061 Al-15 vol. pct. SiC$_{(P)}$ composite in 0.025 M HCl solution containing different concentrations of [OPEIm$^+$] [Br$^-$] at different temperatures.

Temp (°C)	Inh. Conc. (mM)	R_P (Ω cm^2)	C_{dl} (μF cm^{-2})	η (%)
	Blank	308.7	55.0	-
	2	1129.1	37.2	72.7
30	3	1551.2	29.7	80.1
	4	1770.4	28.0	82.6
	5	1950.1	21.5	84.2
	6	2798.0	16.9	89.0
	Blank	119.0	119.6	-
	2	470.2	43.3	74.7
35	3	705.3	42.9	83.1
	4	902.1	41.1	86.8
	5	1113.3	39.4	89.3
	6	1334.2	36.9	91.1
	Blank	64.6	180.4	-
	2	311.9	42.6	79.3
40	3	509.3	40.8	87.3
	4	596.5	39.6	89.2
	5	898.2	35.2	92.8
	6	932.3	34.3	93.1
	Blank	51.2	251.9	-
	2	311.3	58.8	83.6
45	3	698.7	44.1	92.7
	4	726.3	41.1	93.0
	5	884.4	34.6	94.2
	6	1080.0	32.0	95.3
	Blank	48.6	260.2	-
	2	384.1	53.7	87.3
50	3	686.9	47.0	92.9
	4	753.2	34.2	93.5
	5	877.6	35.8	94.5
	6	1302.2	33.7	96.3

Table 3.14 EIS data for the corrosion of 6061 Al-15 vol. pct. SiC$_{(P)}$ composite in 0.1 M HCl solution containing different concentrations of [OPEIm$^+$] [Br$^-$] at different temperatures.

Temp (°C)	Inh. Conc. (mM)	R_P (Ω cm^2)	C_{dl} (μF cm^{-2})	η (%)
	Blank	213.7	83.3	-
	2	800.3	54.4	73.3
30	3	1169.3	53.5	81.7
	4	1232.9	52.7	82.7
	5	1587.3	47.6	86.5
	6	2314.2	37.9	90.8
	Blank	100.2	136.5	-
	2	425.8	50.2	76.5
35	3	629.8	45.7	84.1
	4	802.2	38.9	87.5
	5	1036.9	35.3	90.3
	6	1339.3	32.5	92.5
	Blank	55.5	201.3	-
	2	311.2	70.4	82.2
40	3	469.7	68.7	88.2
	4	551.8	64.1	90.0
	5	811.6	58.9	93.2
	6	893.2	49.0	93.8
	Blank	41.3	343.2	-
	2	263.8	58.2	84.3
45	3	604.9	57.5	93.2
	4	684.1	53.5	94.0
	5	770.3	50.3	94.6
	6	960.1	41.7	95.7
	Blank	21.1	565.1	-
	2	197.1	66.0	89.3
50	3	344.0	62.3	93.9
	4	378.6	53.4	94.4
	5	410.1	49.1	94.9
	6	650.4	44.5	96.8

Table 3.15 EIS data for the corrosion of 6061 Al-15 vol. pct. SiC$_{(P)}$ composite in 0.25 M HCl solution containing different concentrations of [OPEIm$^+$] [Br$^-$] at different temperatures.

Temp (°C)	Inh. Conc. (mM)	R_P (Ω cm^2)	C_{dl} (μF cm^{-2})	η (%)
	Blank	126.3	107.8	-
	2	543.9	67.4	76.8
30	3	836.6	61.3	84.9
	4	944.3	58.7	86.6
	5	1238.0	55.3	89.8
	6	1643.7	53.2	92.3
				-
	Blank	71.6	177.8	
	2	336.9	124.2	78.7
35	3	540.6	117.3	86.8
	4	638.9	115.2	88.8
	5	821.6	111.1	91.3
	6	961.6	109.3	92.6
	Blank	51.4	231.4	-
	2	328.2	134.2	84.3
40	3	527.9	128.4	90.3
	4	624.5	126.3	91.8
	5	891.6	123.2	94.2
	6	947.6	122.5	94.6
	Blank	21.8	413.8	-
	2	156.9	298.3	86.1
45	3	323.8	292.1	93.3
	4	422.1	290.3	94.8
	5	523.3	288.3	95.8
	6	625.3	287.2	96.5
	Blank	11.7	509.3	-
	2	124.7	303.4	90.6
50	3	222.9	299.4	94.8
	4	346.2	297.3	96.6
	5	463.0	295.3	97.5
	6	583.3	294.1	98.0

Table 3.16 EIS data for the corrosion of 6061 Al-15 vol. pct. SiC$_{(P)}$ composite in 0.1 M H$_2$SO$_4$ solution containing different concentrations of [OPEIm$^+$] [Br$^-$] at different temperatures.

Temp (°C)	Inh. Conc. (mM)	R_P (Ω cm^2)	C_{dl} (μF cm^{-2})	η (%)
	Blank	245.5	84.7	-
	2	380.3	74.0	35.4
30	4	387.0	45.2	36.6
	6	453.0	42.0	45.8
	8	515.7	40.7	52.4
	10	1724.0	35.9	85.8
	Blank	221.2	86.4	-
	2	507.3	57.8	56.4
35	4	672.9	45.1	67.1
	6	773.7	41.7	71.4
	8	984.1	39.0	77.5
	10	1612.3	33.2	86.3
	Blank	194.1	120.7	-
	2	476.9	45.8	59.3
40	4	534.4	44.5	63.7
	6	604.3	41.4	67.9
	8	814.6	38.7	76.2
	10	1768.6	32.9	89.0
	Blank	121.4	140.4	-
	2	582.3	45.8	79.2
45	4	616.1	42.8	80.3
	6	862.8	40.9	85.9
	8	989.7	38.1	87.7
	10	1090.4	25.7	88.9
	Blank	101.3	160.4	-
	2	341.0	45.5	70.3
50	4	368.0	42.5	72.5
	6	396.7	40.8	74.5
	8	556.3	37.1	81.8
	10	1680.3	23.1	94.0

Table 3.17 EIS data for the corrosion of 6061 Al-15 vol. pct. SiC$_{(P)}$ composite in 0.3 M H$_2$SO$_4$ solution containing different concentrations of [OPEIm$^+$] [Br$^-$] at different temperatures.

Temp (°C)	Inh. Conc. (mM)	R_P (Ω cm^2)	C_{dl} (μF cm^{-2})	η (%)
	Blank	103.6	76.5	-
	2	166.1	70.2	37.6
30	4	178.8	65.1	42.1
	6	222.2	61.9	53.4
	8	290.4	58.0	64.3
	10	785.1	52.8	86.8
	Blank	73.5	147.9	-
	2	177.5	81.2	58.6
35	4	227.2	69.4	67.7
	6	262.8	67.6	72.0
	8	361.0	60.1	79.6
	10	592.8	59.0	87.6
	Blank	62.8	187.0	-
	2	162.9	106.1	61.5
40	4	185.3	105.1	66.1
	6	206.9	75.9	69.7
	8	274.8	75.6	77.2
	10	892.5	71.9	93.0
	Blank	59.5	192.7	-
	2	288.4	95.0	79.4
45	4	322.7	93.2	81.6
	6	437.8	86.0	86.4
	8	489.3	82.3	87.8
	10	926.0	76.4	93.6
	Blank	45.3	234.3	-
	2	227.5	145.3	80.1
50	4	268.5	88.5	83.1
	6	332.4	87.9	86.4
	8	445.3	87.1	89.8
	10	766.4	78.5	94.1

Table 3.18 EIS data for the corrosion of 6061 Al-15 vol. pct. SiC$_{(P)}$ composite in 0.5 M H$_2$SO$_4$ solution containing different concentrations of [OPEIm$^+$] [Br$^-$] at different temperatures.

Temp (°C)	Inh. Conc. (mM)	R_P (Ω cm^2)	C_{dl} (μF cm^{-2})	η (%)
	Blank	88.6	122.8	-
	2	169.7	107.0	47.8
30	4	183.9	106.3	51.8
	6	196.0	104.9	54.8
	8	275.5	102.5	67.8
	10	658.1	94.0	86.5
	Blank	59.6	153.3	-
	2	148.4	120.9	59.8
35	4	192.9	116.6	69.1
	6	233.4	112.8	74.5
	8	295.6	106.2	79.8
	10	467.8	102.4	87.3
	Blank	53.7	164.4	-
	2	146.2	118.5	63.2
40	4	189.6	114.9	71.6
	6	230.0	103.7	76.6
	8	302.2	94.8	82.2
	10	918.7	94.0	94.1
	Blank	48.9	180.3	-
	2	236.8	105.2	79.3
45	4	275.3	103.6	82.2
	6	384.8	99.6	87.3
	8	494.7	93.3	90.1
	10	901.1	89.0	94.6
	Blank	31.2	240.3	-
	2	166.2	215.5	81.2
50	4	197.7	102.2	84.2
	6	242.0	99.3	87.1
	8	350.7	83.4	91.1
	10	661.4	82.4	95.3

Table 3.19 Activation parameters for the corrosion of 6061 Al-15 vol. pct. SiC$_{(P)}$ composite in HCl solutions of different concentrations containing [OPEIm$^+$] [Br$^-$].

Medium Conc. (M)	Inh. Conc. (mM)	E_a (kJ mol^{-1})	$\Delta H^{\#}$ (kJ mol^{-1})	$-\Delta S^{\#}$ (J K^{-1} mol^{-1})
	Blank	**46.69**	**44.09**	**102.46**
	2	40.09	37.49	134.92
	3	22.00	19.39	196.84
0.025	4	24.14	21.54	196.06
	5	−0.69	−3.30	280.47
	6	7.20	4.60	257.15
	Blank	**77.40**	**74.80**	**26.80**
	2	59.25	56.64	65.13
	3	27.85	25.25	169.11
0.1	4	30.31	27.71	167.31
	5	13.43	10.83	225.70
	6	32.45	29.85	166.96
	Blank	**35.18**	**32.58**	**117.96**
	2	16.66	14.05	191.57
	3	−2.09	−4.69	256.38
0.25	4	−9.01	−11.62	282.62
	5	−24.08	−26.68	335.08
	6	−2.30	−4.90	267.49

Table 3.20 Activation parameters for the corrosion of 6061 Al-15 vol. pct. SiC$_{(P)}$ composite in H$_2$SO$_4$ solutions of different concentrations containing [OPEIm$^+$] [Br$^-$].

Medium Conc. (M)	Inh. Conc. (mM)	E_a (kJ mol^{-1})	$\Delta H^{\#}$ (kJ mol^{-1})	$-\Delta S^{\#}$ (J K^{-1} mol^{-1})
	Blank	23.28	20.63	179.49
	2	42.74	40.14	118.91
	4	39.06	36.46	131.30
0.1	6	31.13	28.53	158.86
	8	42.84	40.24	124.15
	10	−3.57	−6.17	282.90
	Blank	13.33	10.73	202.59
	2	−15.21	−17.81	301.24
	4	−15.33	−17.93	302.31
0.3	6	−19.66	−22.27	317.91
	8	−10.62	−13.23	292.42
	10	−55.03	−57.63	445.26
	Blank	21.18	18.57	172.84
	2	−6.83	−9.43	270.40
	4	−10.07	−12.68	281.63
0.5	6	−14.55	−17.15	297.55
	8	−17.87	−20.48	311.96
	10	−51.99	−54.60	431.80

Table 3.21 Thermodynamic parameters for the adsorption of [OPEIm$^+$] [Br$^-$] on 6061 Al-15 vol. pct. SiC$_{(P)}$ composite in HCl solutions of different concentrations.

Medium Conc. (M)	Temp (°C)	R^2	Slope	$-\Delta G^0_{ads}$ (kJ mol^{-1})	ΔH^0_{ads} (kJ mol^{-1})	ΔS^0_{ads} (J K^{-1} mol^{-1})
	30	0.996	0.912	27.52		
	35	0.989	0.851	27.78		
0.025	40	0.993	0.856	28.72	9.90	123.2
	45	0.994	0.875	29.50		
	50	0.998	0.879	29.74		
	30	0.991	0.932	27.90		
	35	0.989	0.877	28.21		
0.1	40	0.997	0.896	29.39	27.03	180.4
	45	0.998	0.915	30.31		
	50	0.998	0.935	31.36		
	30	0.995	0.963	28.60		
	35	0.999	0.918	28.98		
0.25	40	0.998	0.916	29.86	25.02	176.0
	45	0.999	0.934	30.82		
	50	0.999	0.956	32.08		

Table 3.22 Thermodynamic parameters for the adsorption of [OPEIm$^+$] [Br$^-$] on 6061 Al-15 vol. pct. SiC$_{(P)}$ composite in H$_2$SO$_4$ solutions of different concentrations.

Medium Conc. (M)	Temp (°C)	R^2	Slope	$-\Delta G^0_{ads}$ (kJ mol^{-1})	ΔH^0_{ads} (kJ mol^{-1})	ΔS^0_{ads} (J K^{-1} mol^{-1})
	30	0.820	0.785	23.25		
	35	0.856	0.903	24.98		
0.1	40	0.885	0.891	26.17	46.02	229.6
	45	0.884	0.888	26.65		
	50	0.960	0.942	28.16		
	30	0.832	0.791	23.51		
	35	0.864	0.866	25.00		
0.3	40	0.897	0.890	26.28	48.34	237.6
	45	0.886	0.895	26.76		
	50	0.965	0.960	28.57		
	30	0.869	0.888	24.04		
	35	0.848	0.900	25.33		
0.5	40	0.921	0.904	26.60	44.95	228.0
	45	0.938	0.917	27.37		
	50	0.983	0.939	28.72		

3.4   1,3-BIS[2-(4-METHOXYPHENYL)-2-OXOETHYL]-1*H*-IMIDAZOL-3-IUM BROMIDE ([MPOEIm$^+$] [Br$^-$]) AS CORROSION INHIBITOR ON 6061 Al-15 VOL. PCT. SiC$_{(P)}$ COMPOSITE IN ACIDIC MEDIA

3.4.1 Potentiodynamic polarization measurements

The potentiodynamic polarization curves for the corrosion of 6061 Al-15 vol. pct. SiC$_{(P)}$ composite in 0.1 M hydrochloric acid and 0.1 M sulfuric acid media containing different concentrations of [MPOEIm$^+$] [Br$^-$] at 40 °C are given in Figures 3.40(a) and 3.40(b), respectively. Similar plots were obtained at different temperatures and in different concentrations of the acid media.
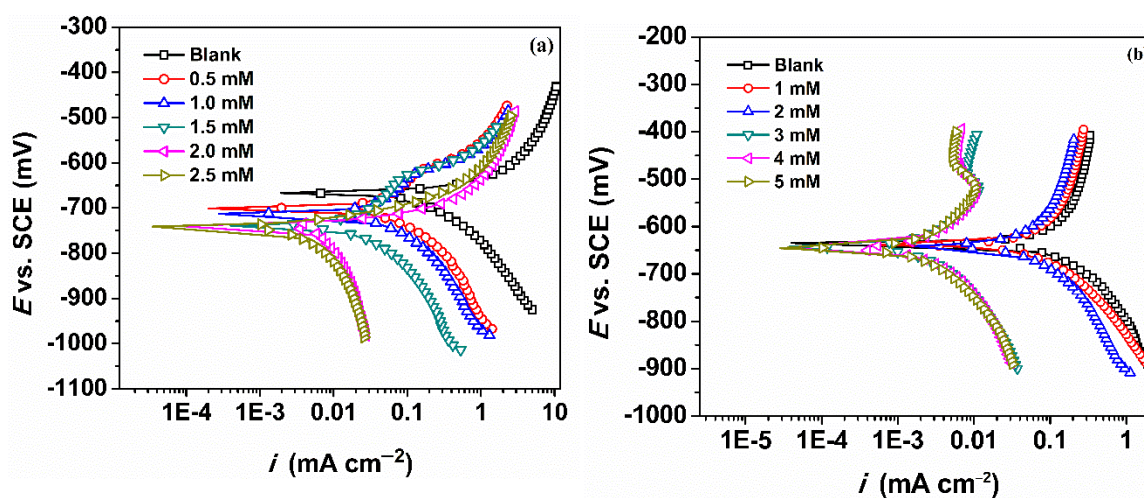
Figure 3.40 Potentiodynamic polarization curves for the corrosion of 6061 Al-15 vol. pct. SiC$_{(P)}$ composite in the presence of different concentrations of [MPOEIm$^+$] [Br$^-$] at 40 °C, in 0.1 M (a) HCl and (b) H$_2$SO$_4$.

It may be observed in both the figures that the curves shift towards lower corrosion current density in the presence of inhibitors, indicating decreased corrosion rate in the presence of inhibitors. Also, the cathodic branch seems to be more affected than the anodic branch. The anodic curves in hydrochloric acid containing [MPOEIm$^+$] [Br$^-$] show two inflection points and in sulfuric acid show passivation. The two inflection points suggest the dissolution of the existing surface oxide film and in the case of sulfuric acid medium (Dindodi and Shetty 2014), the oxide film provides surface protection from the corrosive species to some extent. The values of corrosion potential (E_{corr}), cathodic slope ($-\beta_c$),

corrosion current density (i_{corr}) and percentage inhibitor efficiency (η %) in hydrochloric acid and sulfuric acid media are tabulated in Tables 3.23, 3.24. 3.25 and 3.26, 3.27, 3.28, respectively. It may be observed that, with the increase in the concentrations of [MPOEIm$^+$] [Br$^-$], the inhibition efficiency increases. The insignificant change in Tafel slope values suggest that there is no change in the mechanism of the corrosion reaction in the presence of inhibitor. The shift in corrosion potential is more towards cathodic end but less than -85 mV as compared to corrosion potential without the inhibitor. This indicates mixed control on both the anodic and the cathodic reactions with predominant control on cathodic hydrogen evolution reaction (Akbarzadeh et al. 2011). Also, for the range of medium concentrations studied, the increase in ionic concentration of both the electrolytes increase the inhibition efficiencies. Similar to previous section, amount of inhibitor required in the hydrochloric acid medium is less than that in the sulfuric acid medium, however, the inhibition efficiencies are more or less comparable. The maximum efficiencies of about 97% and 96.9% were obtained in 0.25 M HCl and 0.5 M H$_2$SO$_4$, respectively at 50 °C containing 2.5 mM and 5 mM [MPOEIm$^+$] [Br$^-$].

3.4.2 Electrochemical impedance spectroscopy measurements

The Nyquist plots for the corrosion of 6061 Al-15 vol. pct. SiC$_{(P)}$ composite in 0.1 M hydrochloric acid and 0.1 M sulfuric acid media containing different concentrations of [MPOEIm$^+$] [Br$^-$] at 40 °C are given in the Figures 3.41(a) and 3.41(b), respectively. Similar plots were obtained at different temperatures and in different concentrations of the acid media. As the concentration of the inhibitor increases, the diameter of the semi-circles in the Nyquist plot increases, indicating a decrease in the corrosion rate (Ibrahim and Zour 2011).

The Nyquist plots were simulated with the same equivalent circuit model shown in Figure 3.3. The impedance parameters in hydrochloric acid medium are listed in Tables 3.29, 3.30, 3.31 and in sulfuric acid medium are listed in Tables 3.32, 3.33, 3.34. The observations and inference follow the discussions under section 3.3.2.

The inhibition efficiency of [MPOEIm$^+$] [Br$^-$] was optimum at 2.5 mM and 5 mM concentrations of the inhibitor. The inhibitors act as barriers between the composite surface and corrosive electrolyte.

Bode plots were also analyzed to further support the observation of impedance results. Figures 3.42(a) and 3.42(b) display Bode magnitude plots for the corrosion of alloy composite in 0.1 M hydrochloric acid and 0.1 M sulfuric acid at 40 °C, respectively. The corresponding Bode phase angle plots are shown in Figures 3.43(a) and 3.43(b), respectively. The Figures 3.42 and 3.43 clearly show increased impedance modulus (Z_{mod}) and phase maxima (θ'_{max}) in the presence of increasing concentrations of the inhibitor (Gao et al.2010, Hu et al. 2013).
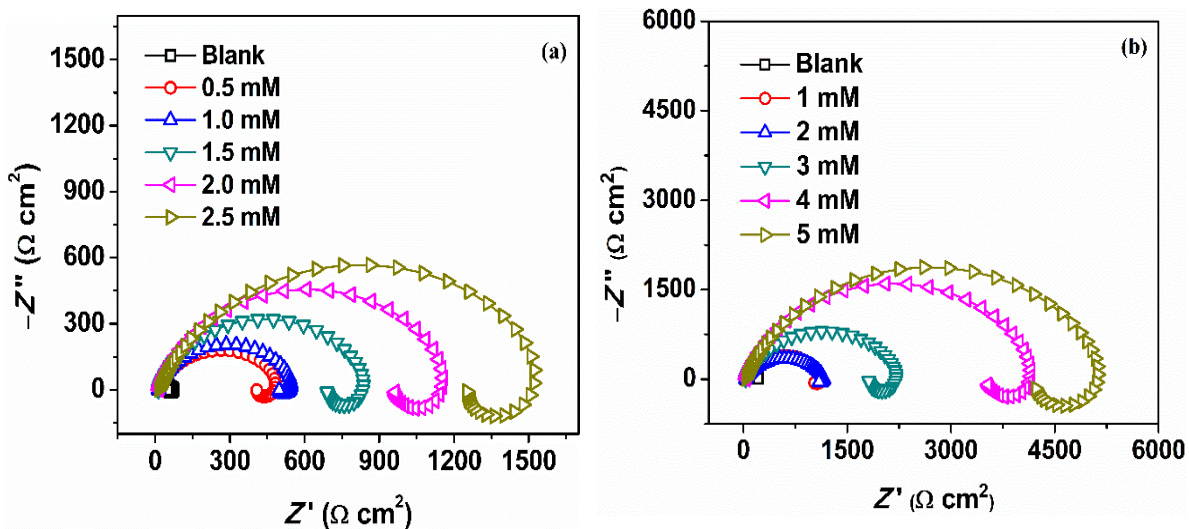
Figure 3.41 Nyquist plots for the corrosion of 6061 Al-15 vol. pct. SiC$_{(P)}$ composite in the presence of different concentrations of [MPOEIm$^+$] [Br$^-$] at 40 °C, in 0.1 M (a) HCl and (b) H$_2$SO$_4$.
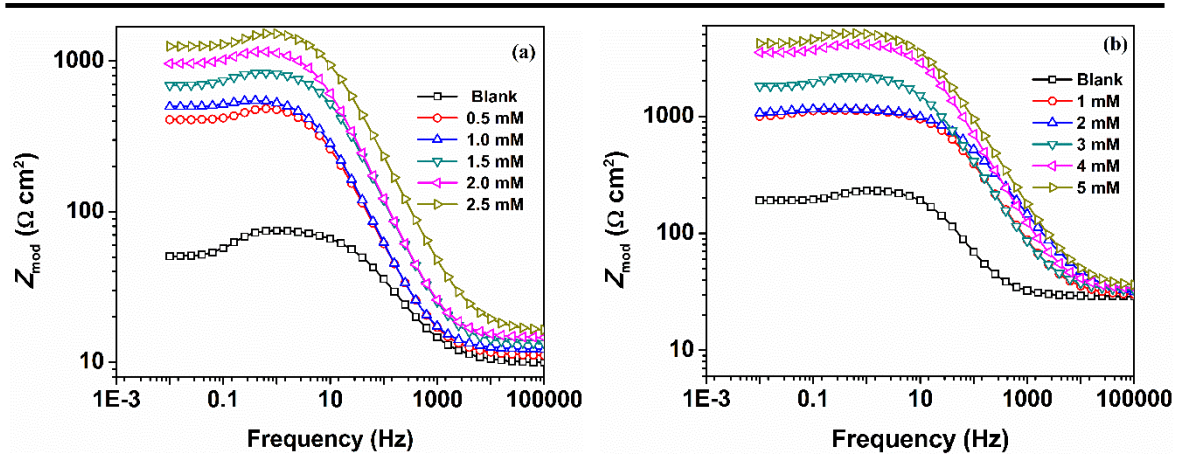
Figure 3.42 Bode magnitude plots for the corrosion of 6061 Al-15 vol. pct. SiC(P) composite in the presence of different concentrations of [MPOEIm+] [Br−] at 40 °C, in 0.1 M (a) HCl and (b) H2SO4.
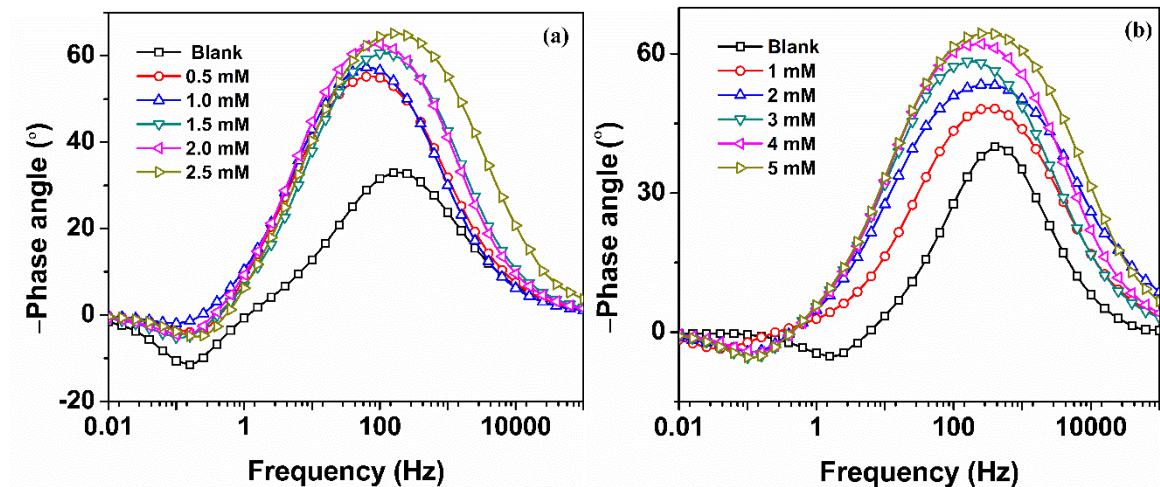
Figure 3.43 Bode phase angle plots for the corrosion of 6061 Al-15 vol. pct. SiC(P) composite in the presence of different concentrations of [MPOEIm+] [Br−] at 40 °C, in 0.1 M (a) HCl and (b) H2SO4.

3.4.3 Effect of temperature

For the temperature range studied at 5 °C intervals between 30-50 °C, it was observed that the inhibition efficiency increases with the increase in temperature (Tables

3.23-3.34). The trend suggest the chemisorption mode of adsorption of the inhibitor on the composite surface (Noor 2007, Adejo et al. 2013). The Arrhenius plots for the corrosion of the composite in 0.1 M hydrochloric acid and 0.1 M sulfuric acid containing different concentrations of [MPOEIm$^+$] [Br$^-$] are shown in Figures 3.44(a) and 3.44b), respectively. The slopes and intercept values of plot of $\ln(\upsilon_{corr}/T)$ vs. $1/T$ were used to deduce the enthalpy of activation and entropy of activation (Figures 3.45(a) and 3.45(b)). The activation parameters for the corrosion of the composite in hydrochloric acid and sulfuric acid media in the presence of the inhibitor are listed in Tables 3.35 and 3.36, respectively. The activation energy in the presence of inhibitor is less and in some cases it is negative as compared to that in the blank media (Stoyanova et al. 1997, Cicek et al. 2013, Ameer et al. 2014). The change in activation enthalpy is analogous to the change in energy of activation. Large negative values of activation entropy suggest association step in the formation of reaction intermediates in the rate determining step of the corrosion reaction (Borsato et al. 2014).
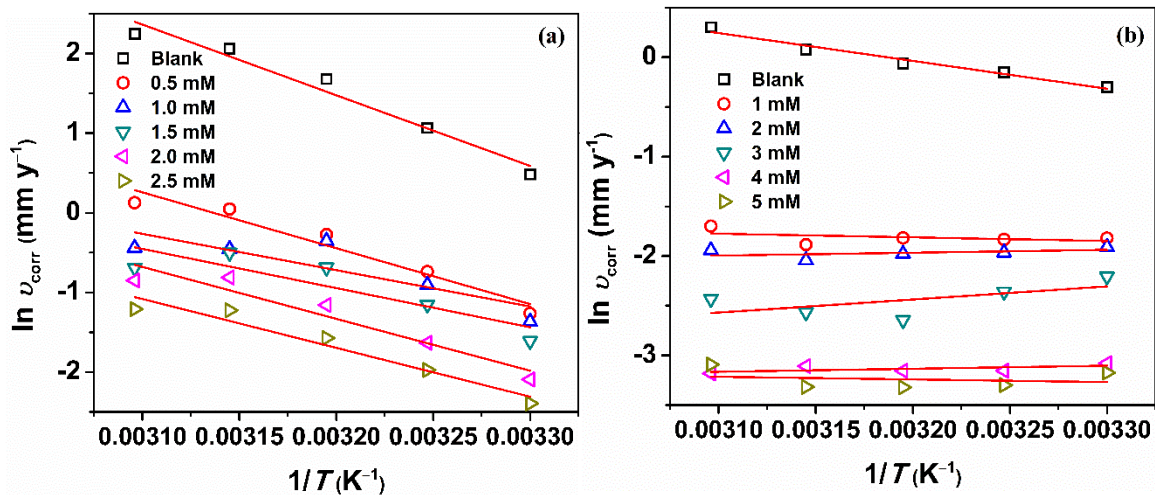
Figure 3.44 Arrhenius plots for the corrosion of 6061 Al-15 vol. pct. SiC$_{(P)}$ composite in the presence of different concentrations of [MPOEIm$^+$] [Br$^-$] in 0.1 M (a) HCl and (b) H$_2$SO$_4$.
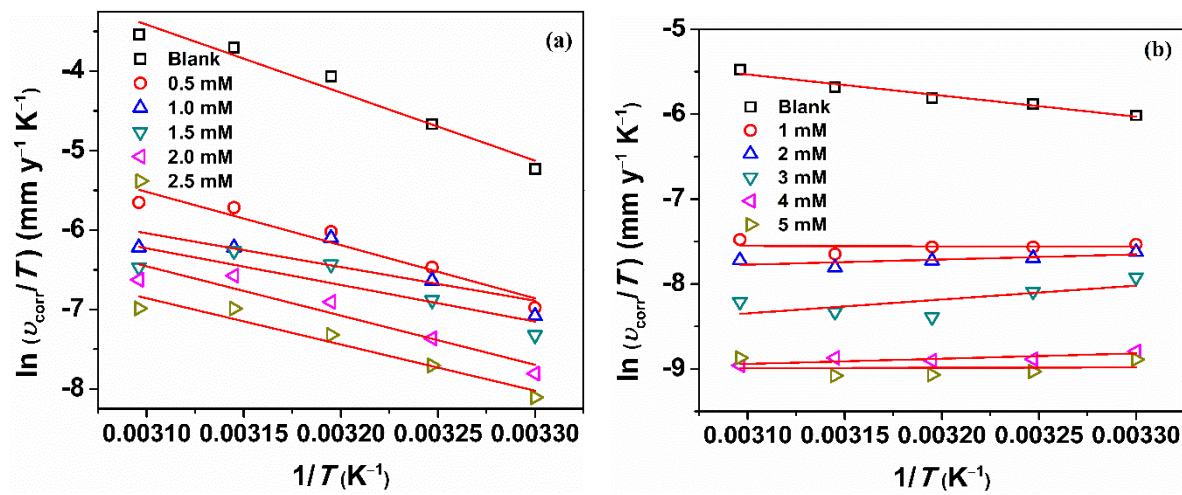
Figure 3.45 Plots of ln (v_{corr}/T) vs. $1/T$ for the corrosion of 6061 Al-15 vol. pct. SiC$_{(P)}$ composite in the presence of different concentrations of [MPOEIm$^+$] [Br$^-$] in 0.1 M (a) HCl and (b) H$_2$SO$_4$.

3.4.4 Adsorption isotherms

Graphical trial and error fitting of surface coverage (θ) and inhibitor concentrations (C_{inh}) to various adsorption isotherms were carried out. The adsorption of the inhibitor on the composite surface followed Langmuir adsorption isotherm with slope and regression value approximately equal to 1. Figures 3.46(a) and 3.46(b) represent the Langmuir adsorption isotherms for the adsorption of [MPOEIm$^+$] [Br$^-$], on the composite surface in 0.1 M HCl and 0.1 M H$_2$SO$_4$, respectively. The thermodynamic parameters for the adsorption of inhibitor on the composite surface in hydrochloric acid and sulfuric acid media are listed in Tables 3.37 and 3.38, respectively. The small deviation of slope values from unity indiactes weak intermolecular interactions among the adsorbed inhibitor molecules (Masel 1996). The values of ΔG^0_{ads} range between −32.2 to −37.2 kJ mol^{-1} in HCl and −29.6 to −34.2 kJ mol^{-1} in H$_2$SO$_4$ medium. These values suggest the adsorption of the inhibitor on the composite surface by both the physisorption and the chemisorption processes. The positive values of enthalpy of adsorption suggest predominant chemisorption mode of adsorption and positive values of entropy of adsorption suggests

increased randomization during adsorption which may be attributed to the displacement of pre-adsorbed water molecules by inhibitor molecules. The values of ΔG^0_{ads}, ΔH^0_{ads}, and the trends in the variation of inhibition efficiency with temperature suggest the adsorption of the inhibitor on the composite surface through both the physisorption and chemisorption modes, but the predominant contribution is by chemisorption.
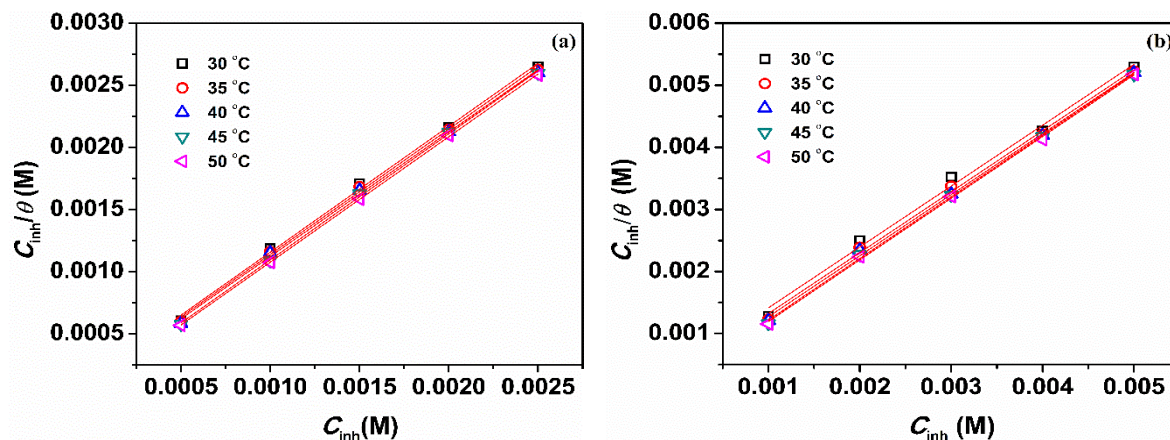
Figure 3.46 Langmuir adsorption isotherms for the adsorption of [MPOEIm⁺] [Br⁻] on the surface of 6061 Al-15 vol. pct. SiC$_{(P)}$ composite in 0.1 M (a) HCl and (b) H$_2$SO$_4$.

3.4.5 Surface analyses

The SEM images of Al alloy composite surface immersed in 0.1 M hydrochloric acid (2 hours) and 0.1 M sulfuric acid (3 hours) in the presence of 2.5 mM and 5 mM of [MPOEIm⁺] [Br⁻], respectively, are given in Figures 3.47(a) and 3.47(b). From the figures it may be observed that in the presence of inhibitor, the surfaces of the composite appear to be smooth and even. However, to support the visual assessment, qualitative support by corresponding EDX is also presented in the Figures 3.48(a) and 3.48(b). The peak corresponding to nitrogen element apart from elemental peaks from composite hints about the presence of adsorbed inhibitor on the composite surface.
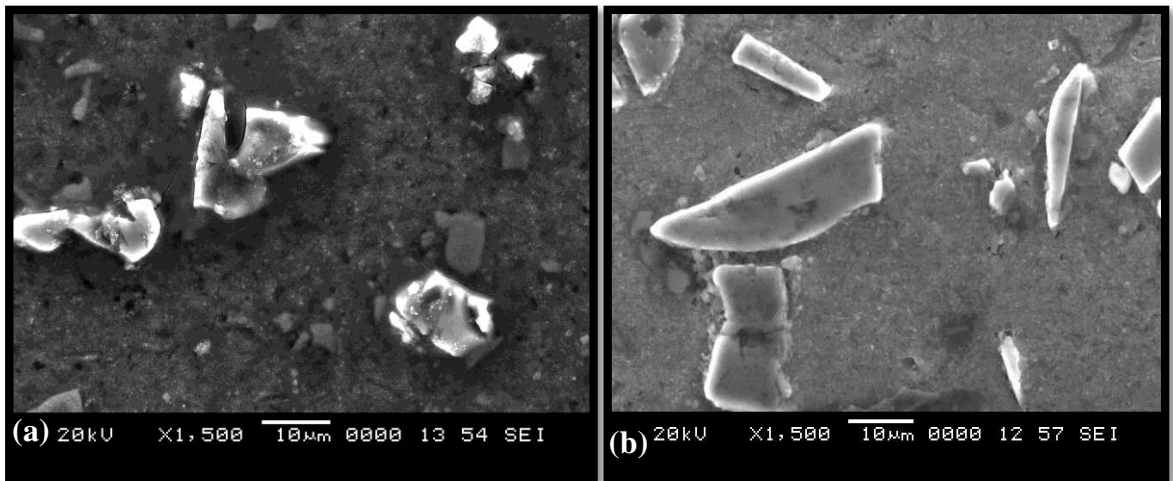
Figure 3.47 SEM images of the 6061 Al-15 vol. pct. SiC$_{(P)}$ composite surface immersed in 0.1 M (a) HCl containing 2.5 mM [MPOEIm$^+$] [Br$^-$] for 2 h and (b) H$_2$SO$_4$ containing 5 mM [MPOEIm$^+$] [Br$^-$] for 3 h.
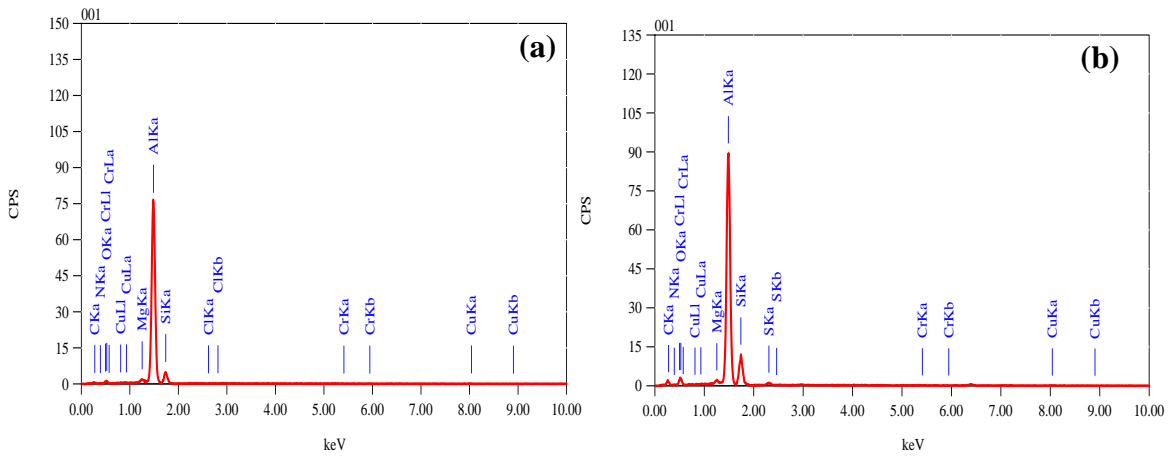
Figure 3.48 EDX spectra of the 6061 Al-15 vol. pct. SiC$_{(P)}$ composite surface immersed in 0.1 M (a) HCl containing 2.5 mM [MPOEIm$^+$] [Br$^-$] for 2 h and (b) H$_2$SO$_4$ containing 5 mM [MPOEIm$^+$] [Br$^-$] for 3 h.

Table 3.23 Potentiodynamic polarization data for the corrosion of 6061 Al-15 vol. pct. SiC$_{(P)}$ composite in 0.025 M HCl solution containing different concentrations of [MPOEIm$^+$] [Br$^-$] at different temperatures.

Temp (°C)	Inh. Conc. (mM)	$-E_{corr}$ (mV vs. SCE)	$-\beta_c$ (mV dec^{-1})	i_{corr} (µA cm^{-2})	η (%)
	Blank	696	215	54.6	-
	0.5	703	187	10.9	80.1
30	1.0	744	184	8.9	83.7
	1.5	761	186	7.1	86.9
	2.0	763	183	4.7	91.4
	2.5	765	181	3.7	93.3
	Blank	676	192	102.6	-
	0.5	709	165	18.7	81.8
35	1.0	731	168	15.2	85.2
	1.5	734	162	13.3	87.1
	2.0	736	168	8.2	92.0
	2.5	737	163	5.3	94.8
	Blank	693	216	134.4	-
	0.5	711	188	21.8	83.8
40	1.0	729	182	18.8	86.0
	1.5	731	178	15.2	88.7
	2.0	734	175	8.4	93.7
	2.5	736	179	6.5	95.2
	Blank	690	225	161.7	-
	0.5	705	189	25.6	84.2
45	1.0	730	192	14.7	90.9
	1.5	734	193	14.0	91.4
	2.0	736	191	10.1	93.8
	2.5	738	194	7.0	95.6
	Blank	714	224	180.8	-
	0.5	714	192	26.2	85.5
50	1.0	735	193	15.2	91.6
	1.5	739	197	10.5	94.2
	2.0	741	191	9.0	95.0
	2.5	743	190	6.1	96.6

Table 3.24 Potentiodynamic polarization data for the corrosion of 6061 Al-15 vol. pct. SiC$_{(P)}$ composite in 0.1 M HCl solution containing different concentrations of [MPOEIm$^+$] [Br$^-$] at different temperatures.

Temp (°C)	Inh. Conc. (mM)	$-E_{corr}$ (mV vs. SCE)	$-\beta_c$ (mV dec^{-1})	i_{corr} (µA cm^{-2})	η (%)
	Blank	664	166	150.8	-
	0.5	682	137	26.3	82.6
30	1.0	695	135	23.7	84.3
	1.5	728	133	18.6	87.7
	2.0	729	136	11.5	92.4
	2.5	731	132	8.5	94.4
	Blank	659	199	269.5	-
	0.5	712	154	44.4	83.5
35	1.0	728	158	37.6	86.1
	1.5	729	157	29.4	89.1
	2.0	731	152	18.2	93.3
	2.5	733	159	12.9	95.2
	Blank	665	188	497.5	-
	0.5	701	167	70.7	85.8
40	1.0	704	169	65.3	86.9
	1.5	738	165	46.7	90.6
	2.0	740	162	29.2	94.1
	2.5	741	165	19.3	96.1
	Blank	691	204	726.3	-
	0.5	705	173	97.2	86.6
45	1.0	715	175	58.8	91.9
	1.5	745	178	56.2	92.3
	2.0	748	171	41.2	94.3
	2.5	750	169	27.3	96.2
	Blank	702	223	874.5	-
	0.5	708	178	105.3	88.0
50	1.0	716	179	59.8	93.2
	1.5	736	182	46.5	94.7
	2.0	737	180	39.8	95.5
	2.5	739	181	27.8	96.8

Table 3.25 Potentiodynamic polarization data for the corrosion of 6061 Al-15 vol. pct. SiC$_{(P)}$ composite in 0.25 M HCl solution containing different concentrations of [MPOEIm$^+$] [Br$^-$] at different temperatures.

Temp (°C)	Inh. Conc. (mM)	$-E_{corr}$ (mV vs. SCE)	$-\beta_c$ (mV dec^{-1})	i_{corr} (µA cm^{-2})	η (%)
	Blank	658	293	898.3	-
	0.5	704	245	132.9	85.2
30	1.0	705	248	114.8	87.2
	1.5	707	246	103.9	88.4
	2.0	711	249	55.2	93.9
	2.5	713	247	46.8	94.8
	Blank	664	224	1239.4	-
	0.5	718	185	169.7	86.3
35	1.0	720	186	146.5	88.2
	1.5	723	182	126.5	89.8
	2.0	725	189	72.1	94.2
	2.5	727	183	54.7	95.6
	Blank	658	308	1807.0	-
	0.5	717	278	235.2	87.0
40	1.0	721	279	171.9	90.5
	1.5	723	281	147.4	91.8
	2.0	725	284	89.1	95.1
	2.5	726	285	70.4	96.1
	Blank	684	277	1878.3	-
	0.5	702	234	217.3	88.4
45	1.0	705	236	145.9	92.2
	1.5	708	237	124.8	93.4
	2.0	716	239	76.6	95.9
	2.5	718	240	63.2	96.6
	Blank	667	246	2135.9	-
	0.5	716	207	216.6	89.9
50	1.0	718	204	129.7	93.9
	1.5	720	205	94.2	95.6
	2.0	720	208	83.7	96.1
	2.5	721	203	64.1	97.0

Table 3.26 Potentiodynamic polarization data for the corrosion of 6061 Al-15 vol. pct. SiC$_{(P)}$ composite in 0.1 M H$_2$SO$_4$ solution containing different concentrations of [MPOEIm$^+$] [Br$^-$] at different temperatures.

Temp (°C)	Inh. Conc. (mM)	$-E_{corr}$ (mV vs. SCE)	$-\beta_c$ (mV dec^{-1})	i_{corr} (µA cm^{-2})	η (%)
	Blank	659	121	68.5	-
	1	661	105	15.1	78.0
30	2	665	106	13.8	79.9
	3	684	104	10.2	85.1
	4	695	108	4.3	93.8
	5	696	105	3.9	94.3
	Blank	665	105	79.5	-
	1	667	105	14.8	81.3
35	2	670	103	13.0	83.6
	3	684	107	8.8	89.0
	4	689	106	4.0	95.0
	5	690	104	3.4	95.7
	Blank	636	155	87.3	-
	1	639	122	15.1	82.7
40	2	640	119	12.8	85.3
	3	643	121	6.6	92.4
	4	646	120	4.0	95.5
	5	646	118	3.4	96.2
	Blank	655	102	100.1	-
	1	657	105	14.1	85.9
45	2	659	107	12.1	88.0
	3	672	106	7.1	92.9
	4	679	106	4.2	95.8
	5	679	105	3.4	96.6
	Blank	653	150	125.7	-
	1	657	148	17.0	86.5
50	2	661	149	13.3	89.4
	3	685	145	8.2	93.5
	4	687	148	5.0	96.1
	5	689	147	4.2	96.6

Table 3.27 Potentiodynamic polarization data for the corrosion of 6061 Al-15 vol. pct. SiC$_{(P)}$ composite in 0.3 M H$_2$SO$_4$ solution containing different concentrations of [MPOEIm$^+$] [Br$^-$] at different temperatures.

Temp (°C)	Inh. Conc. (mM)	$-E_{corr}$ (mV vs. SCE)	$-\beta_c$ (mV dec $^{-1}$)	i_{corr} (μA cm^{-2})	η (%)
	Blank	595	142	209.6	-
	1	596	121	44.3	78.9
30	2	605	122	38.2	81.8
	3	623	125	24.7	88.2
	4	625	124	12.4	94.1
	5	627	125	11.2	94.7
	Blank	595	139	237.6	-
	1	603	129	43.2	81.8
35	2	605	124	39.0	83.6
	3	620	121	25.1	89.4
	4	622	125	11.1	95.3
	5	650	126	10.1	95.8
	Blank	592	141	270.5	-
	1	603	129	45.5	83.2
40	2	604	128	38.2	85.9
	3	607	126	19.4	92.8
	4	613	127	12.1	95.5
	5	614	127	10.0	96.3
	Blank	603	157	273.1	-
	1	607	145	38.0	86.1
45	2	610	146	29.0	89.4
	3	612	145	17.5	93.6
	4	615	145	12.1	95.6
	5	617	147	8.9	96.7
	Blank	605	159	294.8	-
	1	611	146	39.1	86.7
50	2	615	148	29.1	90.1
	3	618	146	13.0	95.6
	4	618	145	11.4	96.1
	5	619	148	9.4	96.8

Table 3.28 Potentiodynamic polarization data for the corrosion of 6061 Al-15 vol. pct. SiC$_{(P)}$ composite in 0.5 M H$_2$SO$_4$ solution containing different concentrations of [MPOEIm$^+$] [Br$^-$] at different temperatures.

Temp (°C)	Inh. Conc. (mM)	$-E_{corr}$ (mV vs SCE)	$-\beta_c$ (mV dec^{-1})	i_{corr} (μA cm^{-2})	η (%)
	Blank	560	129	348.7	-
	1	561	102	59.9	82.8
30	2	564	104	55.1	84.2
	3	567	104	38.2	89.0
	4	572	105	20.3	94.2
	5	576	102	16.1	95.4
	Blank	559	125	372.1	-
	1	562	106	59.0	84.1
35	2	568	109	54.0	85.5
	3	569	104	36.6	90.2
	4	574	102	16.8	95.5
	5	576	107	15.0	96.0
	Blank	557	140	479.8	-
	1	559	113	73.4	84.7
40	2	567	115	65.7	86.3
	3	574	116	29.1	93.9
	4	579	114	20.9	95.6
	5	581	112	17.4	96.4
	Blank	562	164	517.9	-
	1	575	121	70.8	86.3
45	2	577	119	51.5	90.1
	3	579	120	31.8	93.9
	4	584	117	22.5	95.6
	5	587	115	16.5	96.8
	Blank	565	169	564.7	-
	1	567	124	72.7	87.1
50	2	570	126	48.9	91.3
	3	574	125	24.7	95.6
	4	578	123	19.3	96.6
	5	581	126	17.4	96.9

Table 3.29 EIS data for the corrosion of 6061 Al-15 vol. pct. SiC$_{(P)}$ composite in 0.025 M HCl solution containing different concentrations of [MPOEIm$^+$] [Br$^-$] at different temperatures.

Temp (°C)	Inh. Conc. (mM)	R_P (Ω cm^2)	C_{dl} (μF cm^{-2})	η (%)
	Blank	308.7	55.0	-
	0.5	1562.7	50.8	80.2
30	1.0	1775.7	48.0	82.6
	1.5	2742.1	35.5	88.7
	2.0	4319.2	34.2	92.9
	2.5	5350.0	28.1	94.2
	Blank	119.0	119.6	-
	0.5	689.8	56.5	82.7
35	1.0	768.4	46.3	84.5
	1.5	1240.2	37.2	90.4
	2.0	1830.1	36.6	93.5
	2.5	2830.3	32.8	95.8
	Blank	64.6	180.4	-
	0.5	383.9	96.3	83.2
40	1.0	505.6	45.1	87.2
	1.5	908.1	38.9	92.9
	2.0	1173.2	31.9	94.5
	2.5	1604.1	25.0	96.0
	Blank	51.2	251.9	-
	0.5	347.1	155.5	85.2
45	1.0	440.2	69.3	88.4
	1.5	784.2	52.1	93.5
	2.0	1004.1	33.5	94.9
	2.5	1359.2	25.3	96.2
	Blank	48.6	260.2	-
	0.5	388.2	79.7	87.5
50	1.0	419.1	52.9	88.4
	1.5	816.3	35.2	94.0
	2.0	1048.0	29.1	95.4
	2.5	1459.2	27.9	96.7

Table 3.30 EIS data for the corrosion of 6061 Al-15 vol. pct. SiC$_{(P)}$ composite in 0.1 M HCl solution containing different concentrations of [MPOEIm$^+$] [Br$^-$] at different temperatures.

Temp (°C)	Inh. Conc. (mM)	R_P (Ω cm^2)	C_{dl} (μF cm^{-2})	η (%)
	Blank	213.7	83.3	-
	0.5	1311.1	72.2	83.7
30	1.0	1394.7	67.9	84.7
	1.5	2211.3	63.6	90.3
	2.0	3110.1	44.4	93.1
	2.5	4590.3	40.2	95.3
	Blank	100.2	136.5	-
	0.5	647.9	68.2	84.5
35	1.0	732.8	51.3	86.3
	1.5	1116.5	50.7	91.0
	2.0	1616.3	36.4	93.8
	2.5	2528.2	35.6	96.0
	Blank	55.5	201.3	-
	0.5	447.1	84.1	87.6
40	1.0	498.2	67.5	88.9
	1.5	800.8	50.6	93.1
	2.0	1092.2	35.3	94.9
	2.5	1457.2	26.4	96.2
	Blank	41.3	343.2	-
	0.5	355.3	110.5	88.4
45	1.0	421.9	87.4	90.2
	1.5	667.5	71.1	93.8
	2.0	915.3	37.2	95.5
	2.5	1187.2	31.8	96.5
	Blank	21.1	565.1	-
	0.5	204.4	279.9	89.7
50	1.0	224.8	96.2	90.6
	1.5	393.7	61.1	94.6
	2.0	499.2	45.8	95.8
	2.5	654.3	41.9	96.8

Table 3.31 EIS data for the corrosion of 6061 Al-15 vol. pct. SiC(P) composite in 0.25 M HCl solution containing different concentrations of [MPOEIm$^+$] [Br$^-$] at different temperatures.

Temp (°C)	Inh. Conc. (mM)	R_P (Ω cm^2)	C_{dl} (μF cm^{-2})	η (%)
	Blank	126.3	107.8	-
	0.5	821.1	77.5	84.6
30	1.0	1053.2	69.3	88.0
	1.5	1417.4	59.2	91.1
	2.0	1939.2	50.5	93.5
	2.5	2757.2	45.3	95.4
	Blank	71.6	177.8	-
	0.5	489.1	81.3	85.4
35	1.0	774.2	69.5	90.7
	1.5	894.9	60.7	92.0
	2.0	1229.9	37.8	94.2
	2.5	1991.1	35.9	96.4
	Blank	51.4	231.4	-
	0.5	434.8	59.3	88.2
40	1.0	604.2	46.7	91.5
	1.5	786.2	45.4	93.5
	2.0	1066.7	36.6	95.2
	2.5	1524.3	28.4	96.6
	Blank	21.8	413.8	-
	0.5	257.4	87.0	91.5
45	1.0	285.1	61.5	92.4
	1.5	393.8	43.9	94.5
	2.0	490.6	31.9	95.6
	2.5	649.2	28.2	96.6
	Blank	11.7	509.3	-
	0.5	189.3	185.3	93.8
50	1.0	215.3	127.9	94.6
	1.5	237.9	92.3	95.1
	2.0	305.1	73.1	96.2
	2.5	404.0	50.3	97.1

Table 3.32 EIS data for the corrosion of 6061 Al-15 vol. pct. SiC$_{(P)}$ composite in 0.1 M H$_2$SO$_4$ solution containing different concentrations of [MPOEIm$^+$] [Br$^-$] at different temperatures.

Temp (°C)	Inh. Conc. (mM)	R_P (Ω cm^2)	C_{dl} (μF cm^{-2})	η (%)
	Blank	245.5	84.7	-
	1	1059.2	71.6	76.8
30	2	1167.5	68.4	79.0
	3	1894.0	61.2	87.0
	4	4247.0	54.3	94.2
	5	4971.0	52.5	95.1
	Blank	221.2	86.4	-
	1	1032.6	57.0	78.6
35	2	1203.6	54.7	81.6
	3	1998.9	49.3	88.9
	4	4158.0	45.2	94.7
	5	4882.0	43.1	95.5
	Blank	194.1	120.7	-
	1	997.8	95.6	80.5
40	2	1107.5	93.1	82.5
	3	1968.0	89.4	90.1
	4	4062.0	83.2	95.2
	5	4972.0	81.7	96.1
	Blank	121.4	140.4	-
	1	760.0	105.4	84.0
45	2	881.4	103.2	86.2
	3	1330.7	99.3	90.9
	4	2617.0	95.7	95.4
	5	3319.0	93.2	96.3
	Blank	101.3	160.4	-
	1	655.4	118.2	84.5
50	2	744.7	113.5	86.4
	3	1178.8	106.7	91.4
	4	2349.0	101.4	95.7
	5	2736.0	99.3	96.3

Table 3.33 EIS data for the corrosion of 6061 Al-15 vol. pct. SiC$_{(P)}$ composite in 0.3 M H$_2$SO$_4$ solution containing different concentrations of [MPOEIm$^+$] [Br$^-$] at different temperatures.

Temp (°C)	Inh. Conc. (mM)	R_P (Ω cm^2)	C_{dl} (μF cm^{-2})	η (%)
	Blank	103.6	76.5	-
	1	475.8	54.2	78.2
30	2	528.6	51.6	80.4
	3	858.7	43.8	87.9
	4	1832.0	39.3	94.4
	5	2205.1	37.4	95.3
	Blank	73.5	147.9	-
	1	374.4	122.4	80.4
35	2	422.6	120.2	82.6
	3	668.3	116.7	89.0
	4	1507.2	111.6	95.1
	5	1602.1	110.8	95.4
	Blank	62.8	187.0	-
	1	343.7	158.3	81.8
40	2	372.2	155.2	83.2
	3	658.7	146.4	90.5
	4	1353.7	141.3	95.4
	5	1590.2	138.9	96.1
	Blank	59.5	192.7	-
	1	384.2	167.3	84.5
45	2	441.4	164.2	86.5
	3	677.4	159.2	91.2
	4	1337.6	154.7	95.6
	5	1608.7	153.1	96.3
	Blank	45.3	234.3	-
	1	293.7	189.3	84.6
50	2	335.0	186.3	86.5
	3	542.5	181.2	91.6
	4	1057.2	176.3	95.7
	5	1391.3	174.6	96.7

Table 3.34 EIS data for the corrosion of 6061 Al-15 vol. pct. SiC$_{(P)}$ composite in 0.5 M H$_2$SO$_4$ solution containing different concentrations of [MPOEIm$^+$] [Br$^-$] at different temperatures.

Temp (°C)	Inh. Conc. (mM)	R_P (Ω cm^2)	C_{dl} (μF cm^{-2})	η (%)
	Blank	88.6	122.8	-
	1	485.9	96.9	81.8
30	2	533.0	93.2	83.4
	3	798.8	82.9	88.9
	4	1680.7	54.6	94.7
	5	1973.0	53.5	95.5
	Blank	59.6	153.3	-
	1	357.9	122.4	83.3
35	2	417.0	116.6	85.7
	3	582.0	73.7	89.8
	4	1250.0	66.2	95.2
	5	1366.8	57.2	95.6
	Blank	53.7	164.4	-
	1	357.3	117.4	85.0
40	2	403.1	106.3	86.7
	3	597.2	99.0	91.0
	4	1184.6	89.0	95.5
	5	1371.3	63.8	96.1
	Blank	48.9	180.3	-
	1	337.8	82.4	85.5
45	2	397.3	75.9	87.7
	3	566.4	71.2	91.4
	4	1127.1	62.4	95.7
	5	1334.4	50.4	96.3
	Blank	31.2	240.3	-
	1	223.9	119.6	86.1
50	2	243.3	93.2	87.2
	3	381.4	86.0	91.8
	4	742.0	75.9	95.8
	5	909.0	56.3	96.6

Table 3.35 Activation parameters for the corrosion of 6061 Al-15 vol. pct. SiC$_{(P)}$ composite in HCl solutions of different concentrations containing [MPOEIm$^+$] [Br$^-$].

Medium Conc. (M)	Inh. Conc. (mM)	E_a (kJ mol^{-1})	$\Delta H^{\#}$ (kJ mol^{-1})	$-\Delta S^{\#}$ (J K^{-1} mol^{-1})
	Blank	**46.69**	**44.09**	**102.46**
	0.5	33.87	31.27	158.26
0.025	1.0	17.16	14.55	214.45
	1.5	13.98	11.38	226.24
	2.0	24.82	22.21	194.88
	2.5	21.13	18.53	209.47
	Blank	**77.40**	**74.80**	**26.80**
	0.5	58.29	55.69	70.81
0.1	1.0	37.89	35.29	138.39
	1.5	40.90	38.30	130.62
	2.0	54.15	51.55	91.43
	2.5	51.00	48.39	104.55
	Blank	**35.18**	**32.58**	**117.96**
	0.5	20.16	17.55	183.25
0.25	1.0	4.17	1.56	236.88
	1.5	−3.10	−5.70	261.56
	2.0	14.73	12.12	208.43
	2.5	12.75	10.15	216.63

Table 3.36 Activation parameters for the corrosion of 6061 Al-15 vol. pct. SiC$_{(P)}$ composite in H$_2$SO$_4$ solutions of different concentrations containing [MPOEIm$^+$] [Br$^-$].

Medium Conc. (M)	Inh. Conc. (mM)	E_a (kJ mol^{-1})	$\Delta H^{\#}$ (kJ mol^{-1})	$-\Delta S^{\#}$ (J K^{-1} mol^{-1})
	Blank	23.28	20.63	179.49
	0.1	3.04	0.43	258.99
0.1	0.2	−2.41	−5.02	277.73
	0.3	−10.95	−13.55	308.94
	0.4	−2.55	−5.15	287.86
	0.5	−2.24	−0.37	273.43
	Blank	13.33	10.73	202.59
	0.1	−6.11	−8.71	279.80
0.3	0.2	−13.70	−16.31	305.72
	0.3	−26.73	−29.34	352.13
	0.4	−1.48	−4.08	275.52
	0.5	−7.66	−10.27	296.77
	Blank	21.18	18.57	172.84
	0.1	9.28	6.67	−226.72
0.5	0.2	−4.57	−7.18	272.66
	0.3	−16.54	−19.15	315.47
	0.4	3.33	0.73	255.83
	0.5	4.19	1.58	254.66

Table 3.37 Thermodynamic parameters for the adsorption of [MPOEIm$^+$] [Br$^-$] on 6061 Al-15 vol. pct. SiC$_{(P)}$ composite in HCl solutions of different concentrations.

Medium Conc. (M)	Temp (°C)	R^2	Slope	$-\Delta G^0_{ads}$ (kJ mol^{-1})	ΔH^0_{ads} (kJ mol^{-1})	ΔS^0_{ads} (J K^{-1} mol^{-1})
	30	0.997	1.021	32.28		
	35	0.996	1.010	32.86		
0.025	40	0.997	1.003	33.68	25.50	190.0
	45	0.999	1.012	35.12		
	50	0.999	1.002	35.90		
	30	0.996	1.011	32.42		
	35	0.997	1.000	33.17		
0.1	40	0.997	1.001	33.95	33.44	216.6
	45	0.999	1.010	35.56		
	50	0.999	1.000	36.64		
	30	0.997	1.012	33.00		
	35	0.997	1.013	33.72		
0.25	40	0.999	1.011	34.75	31.69	212.8
	45	0.999	1.000	35.82		
	50	0.999	1.011	37.27		

Table 3.38 Thermodynamic parameters for the adsorption of [MPOEIm$^+$] [Br$^-$] on 6061 Al-15 vol. pct. SiC$_{(P)}$ composite in H$_2$SO$_4$ solutions of different concentrations.

Medium Conc. (M)	Temp (°C)	R^2	Slope	$-\Delta G^0_{ads}$ (kJ mol^{-1})	ΔH^0_{ads} (kJ mol^{-1})	ΔS^0_{ads} (J K^{-1} mol^{-1})
	30	0.991	0.980	29.61		
	35	0.996	0.981	30.71		
0.1	40	0.998	0.982	31.65	31.61	202.2
	45	0.998	0.991	32.80		
	50	0.999	0.992	33.62		
	30	0.996	0.983	29.96		
	35	0.996	0.980	30.76		
0.3	40	0.998	0.983	31.77	33.18	208.0
	45	0.999	0.996	33.10		
	50	0.999	0.996	33.99		
	30	0.996	0.993	30.50		
	35	0.997	0.989	31.20		
0.5	40	0.998	0.988	32.06	27.16	189.8
	45	0.999	0.997	33.25		
	50	0.999	0.997	34.22		

3.5 1,3-BIS(2-OXO-2-PHENYLETHYL)-1*H*-BENZIMIDAZOL-3-IUM BROMIDE ([OPEBen⁺] [Br⁻]) AS CORROSION INHIBITOR ON 6061 Al-15 VOL. PCT. SiC(P) COMPOSITE IN ACIDIC MEDIA

3.5.1 Potentiodynamic polarization measurements

The potentiodynamic polarization curves for the corrosion of 6061 Al-15 vol. pct. $SiC_{(P)}$ composite in 0.1 M hydrochloric acid and 0.1 M sulfuric acid media containing different concentrations of [OPEBen⁺] [Br⁻] at 40 °C are given in Figures 3.49(a) and 3.49(b), respectively. The plots obtained in other concentrations of the medium and at other temperatures were also of similar nature.
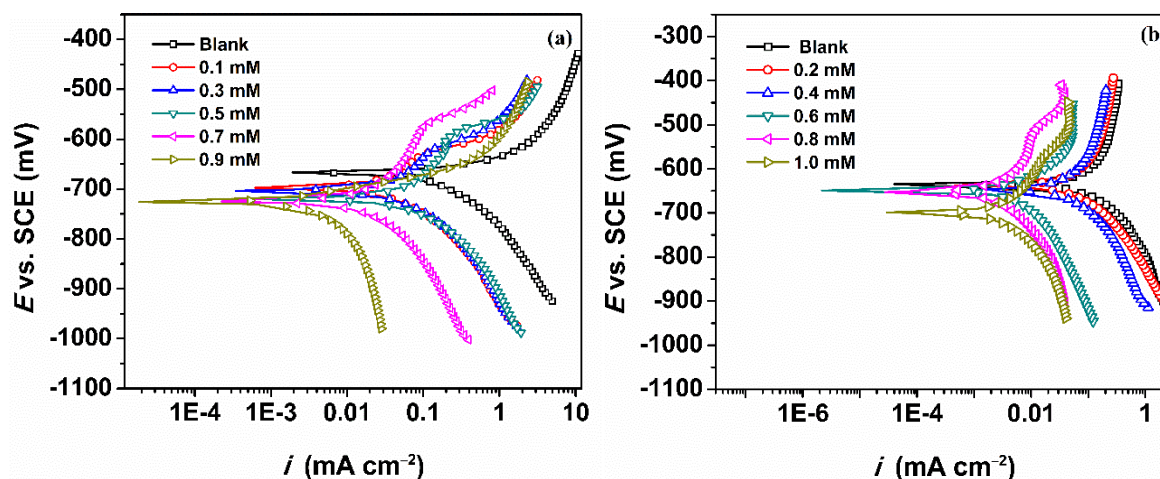
Figure 3.49 Potentiodynamic polarization curves for the corrosion of 6061 Al-15 vol. pct. SiC(P) composite in the presence of different concentrations of [OPEBen⁺] [Br⁻] at 40 °C, in 0.1 M (a) HCl and (b) H₂SO₄.

It is seen from the figures that in the presence of the inhibitor the polarization curves are shifted towards lower current density region in both the media, indicating a decrease in the corrosion rate. The nature of the curves are similar to the one discussed in the section 3.1.1, with the anodic curve in hydrochloric acid showing two inflection points and that in sulfuric acid medium showing passivation (Dindodi and Shetty 2014). The values of corrosion potential (E_{corr}), cathodic slope ($-\beta_c$), corrosion current density (i_{corr}) and

percentage inhibitor efficiency (η %) for the corrosion of the composite in hydrochloric acid and sulfuric acid media are tabulated in Tables 3.39, 3.40, 3.41 and 3.42, 3.43, 3.44, respectively.

It is seen from the results in Tables 3.39-3.41 and 3.42-3.44 that, with the increase in the concentrations of [OPEBen$^+$] [Br$^-$], the inhibition efficiency increases. The small changes in the Tafel slope values suggest no change in the mechanism of the corrosion reaction in the presence of the inhibitor. Distinct from previous sub-sections, here the amount of inhibitor required to control the rate of corrosion in both the media are comparable. About 97.2% inhibition was attained in the presence of 0.9 mM concentration of [OPEBen$^+$] [Br$^-$] in 0.25 M hydrochloric acid medium whereas, the efficiency was about 97.1% in the presence of 1 mM concentration of [OPEBen$^+$] [Br$^-$] in sulfuric acid medium at 50 °C. Hence, [OPEBen$^+$] [Br$^-$] serves as a good inhibitor for corrosion control in both sulfuric and hydrochloric acid media at comparable and lower concentrations. The corrosion inhibition also increases with the increase in the concentration of acids in the medium.

3.5.2 Electrochemical impedance spectroscopy measurements

The Nyquist plots for the corrosion of 6061 Al-15 vol. pct. SiC$_{(P)}$ composite in 0.1 M hydrochloric acid and 0.1 M sulfuric acid containing different concentrations of [OPEBen$^+$] [Br$^-$] at 40 °C are given in the Figures 3.50(a) and 3.50(b), respectively. Similar plots were obtained in different concentrations of the media and at different temperatures. The calculations were made using the same equivalent circuit shown in Figure 3.3. As the concentration of the inhibitor increases, the polarization resistance increases and the double layer capacitance decreases in both the media as it can be seen from Tables 3.45, 3.46, 3.47 for hydrochloric acid medium and 3.48, 3.49, 3.50 for sulfuric acid medium. The decrease in capacitance of the double layer is attributed to the increase in thickness of the electronic double layer which may be due to the adsorbed inhibitor species and reduction in the local dielectric constant (Srinivasan 2006).
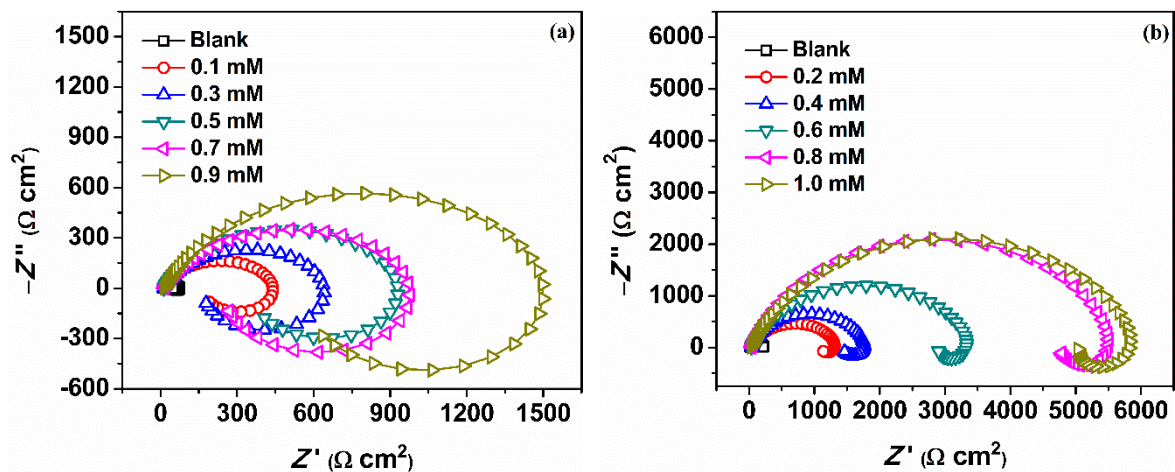
Figure 3.50 Nyquist plots for the corrosion of 6061 Al-15 vol. pct. SiC(P) composite in the presence of different concentrations of [OPEBen⁺] [Br⁻] at 40 °C, in 0.1 M (a) HCl and (b) H₂SO₄.

Bode magnitude plots are represented in Figure 3.51(a) and 3.51(b) for corrosion of 6061 Al-15 vol. pct. $SiC_{(P)}$ composite in the presence of different concentrations of [OPEBen⁺] [Br⁻] at 40 °C in 0.1 M HCl and H_2SO_4, respectively. Bode phase angle plots for the same are given in the Figures 3.52(a) and 3.52(b). From the magnitude and phase angle plots it's seen that for the increasing inhibitor concentrations, there is an increase in impedance modulus (Z_{mod}) and phase maxima (θ'_{max}) (Gao et al. 2010, Hu et al. 2013).
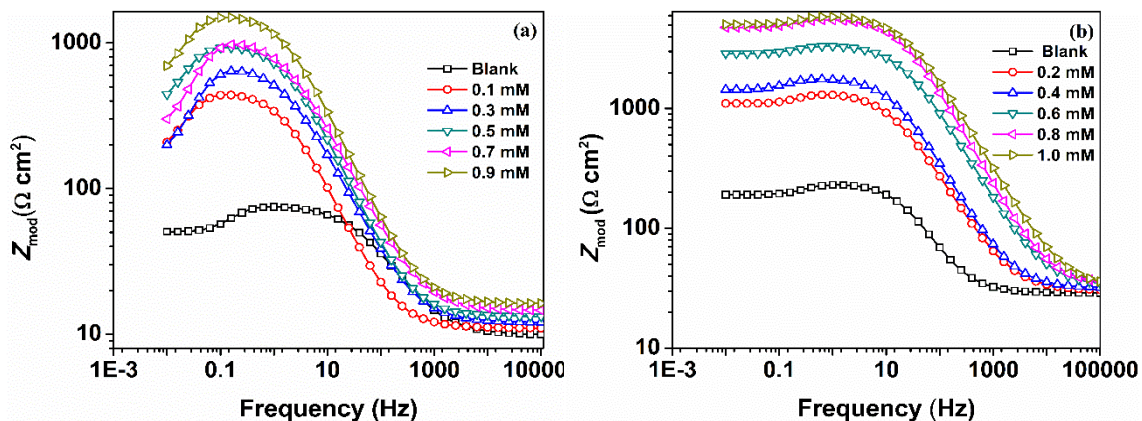
Figure 3.51 Bode magnitude plots for the corrosion of 6061 Al-15 vol. pct. SiC(P) composite in the presence of different concentrations of [OPEBen⁺] [Br⁻] at 40 °C, in 0.1 M (a) HCl and (b) H₂SO₄.
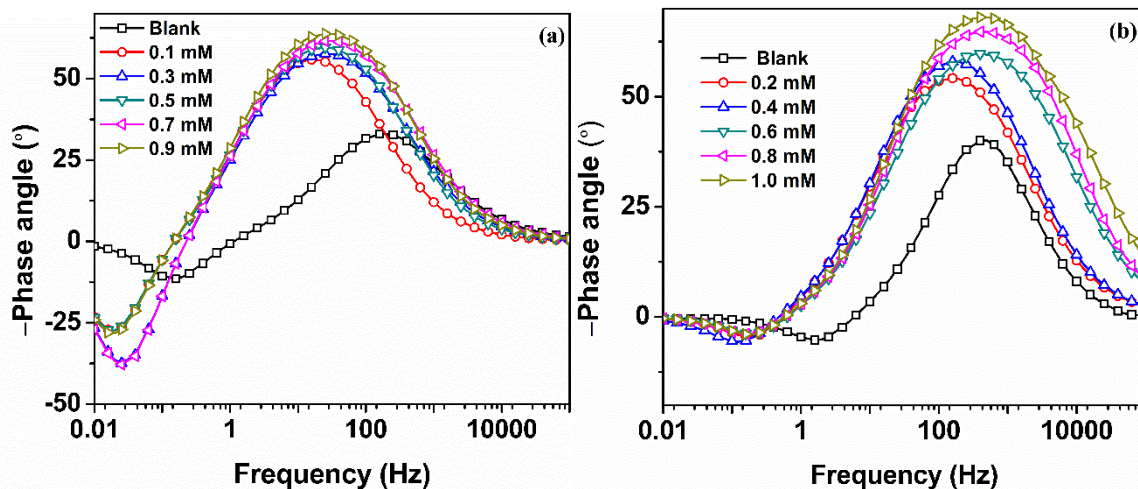
Figure 3.52 Bode phase angle plots for the corrosion of 6061 Al-15 vol. pct. SiC$_{(P)}$ composite in the presence of different concentrations of [OPEBen$^+$] [Br$^-$] at 40 °C, in 0.1 M (a) HCl and (b) H$_2$SO$_4$.

3.5.3 Effect of temperature

From the results of potentiodynamic polarization studies and EIS studies (Tables 3.39-3.50) it is evident that the inhibition efficiency increases with the increase in temperature. This observation is attributed to the adsorption of the inhibitor on the surface of the composite by chemisorption mode (Noor 2007, Adejo et al. 2013). The Arrhenius plots for the corrosion of the composite in 0.1 M hydrochloric acid and 0.1 M sulfuric acid containing different concentrations of [OPEBen$^+$] [Br$^-$] are shown in the Figures 3.53(a) and 3.53(b), respectively. The slopes and intercept values of plot of ln (v_{corr}/T) vs. 1/T were used to deduce the enthalpy and entropy of activation. (Figures 3.54(a) and 3.54(b)). The activation parameters are listed in Tables 3.51 and 3.52. The activation energy in the presence of inhibitor is less or sometimes negative as compared to that in the blank media (Stoyanova et al. 1997, Cicek et al. 2013, Ameer et al. 2014). Large negative values of entropy suggests association step in the formation of reaction intermediates in the rate determining step of the corrosion reaction (Borsato et al. 2014).
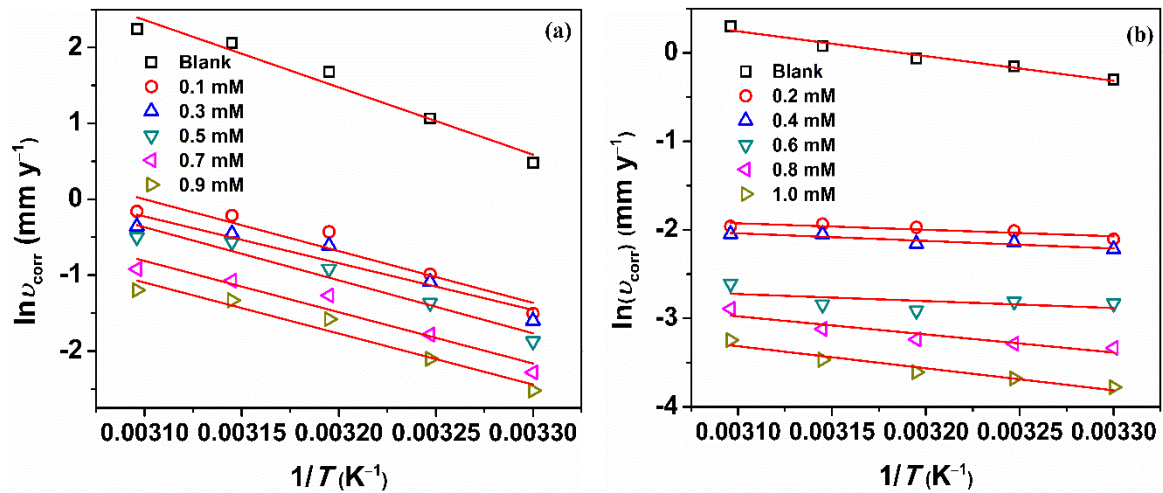
Figure 3.53 Arrhenius plots for the corrosion of 6061 Al-15 vol. pct. SiC(P) composite containing different concentrations of [OPEBen⁺] [Br⁻] in 0.1 M (a) HCl and (b) H₂SO₄.
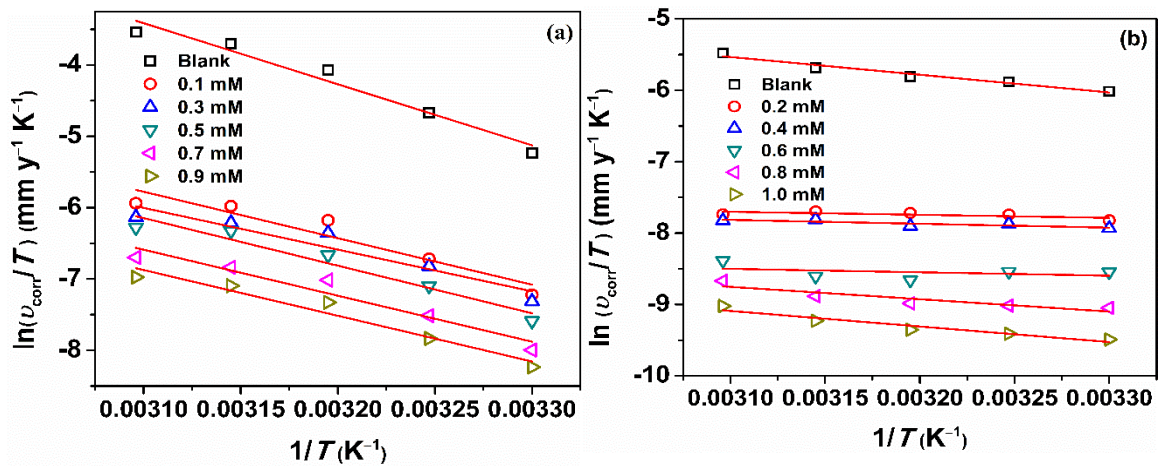
Figure 3.54 Plots of ln (v_{corr}/T) vs. 1/T for the corrosion of 6061 Al-15 vol. pct. SiC(P) composite containing different concentrations of [OPEBen⁺] [Br⁻] in 0.1 M (a) HCl and (b) H₂SO₄.

3.5.4 Adsorption isotherms

The adsorption of the inhibitor on the composite surface follows Langmuir adsorption isotherm. Figures 3.55(a) and 3.55(b) represent the Langmuir adsorption isotherms for the adsorption of [OPEBen$^+$] [Br$^-$], on the composite surface in 0.1 M HCl and 0.1 M H$_2$SO$_4$, respectively. The thermodynamic parameters for the adsorption of inhibitor on the composite surface are listed in Tables 3.53 and 3.54 in hydrochloric acid and in sulfuric acid, respectively. The slope values are very close to unity showing little interactions between the adsorbed inhibitor molecules (Masel 1996). The values of ΔG^0_{ads} ranges between -36.6 to -41.5 kJ mol^{-1} in HCl and -34.6 to -39.2 kJ mol^{-1} in H$_2$SO$_4$ medium. These values suggest the adsorption by both physisorption and chemisorption processes. The positive values of enthalpy of adsorption suggest predominant chemisorption and positive values of entropy of adsorption suggest increased randomization during adsorption which may be attributed to the displacement of pre-adsorbed water molecules by inhibitor molecules. The values of ΔG^0_{ads}, ΔH^0_{ads}, and the trends in the variation of inhibition efficiency with temperature suggest the adsorption of the inhibitor on the composite surface through both the physisorption and chemisorption modes, but the predominant contribution is by chemisorption.
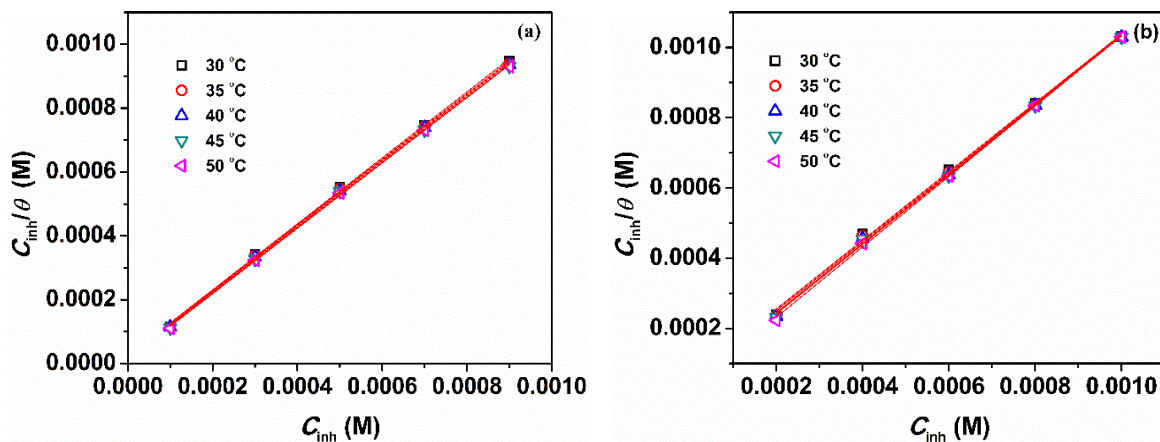
Figure 3.55 Langmuir adsorption isotherms for the adsorption of [OPEBen$^+$] [Br$^-$] on the composite surface in 0.1 M, (a) HCl and (b) H$_2$SO$_4$.

3.5.5 Surface analyses

The SEM images of Al alloy composite surface immersed in 0.1 M hydrochloric acid (2 hours) and 0.1 M sulfuric acid (3 hours) in the presence of 0.9 mM and 1.0 mM of [OPEBen$^+$] [Br$^-$], respectively, are given in Figures 3.56(a) and 3.56(b). From the figures it may be observed that in the presence of inhibitor, the surfaces of the composite appear to be smooth and even. The EDX spectra are represented in the Figures 3.57(a) and 3.57(b). The peak corresponding to nitrogen element apart from the elemental peaks from composite confirms the presence of adsorbed inhibitor on the composite surface.
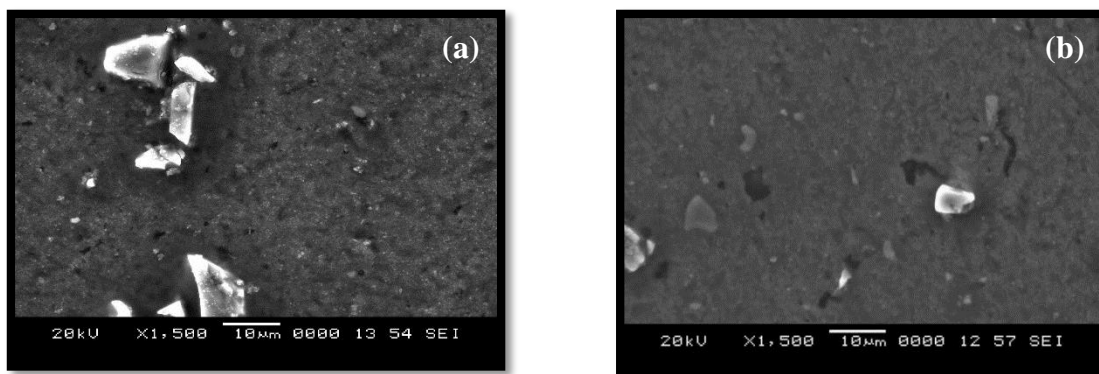
Figure 3.56 SEM images of 6061 Al-15 vol. pct. SiC$_{(P)}$ composite surface immersed in 0.1 M (a) HCl containing 0.9 mM [OPEBen$^+$] [Br$^-$] for 2 h and (b) H$_2$SO$_4$ containing 1 mM [OPEBen$^+$] [Br$^-$] for 3 h.
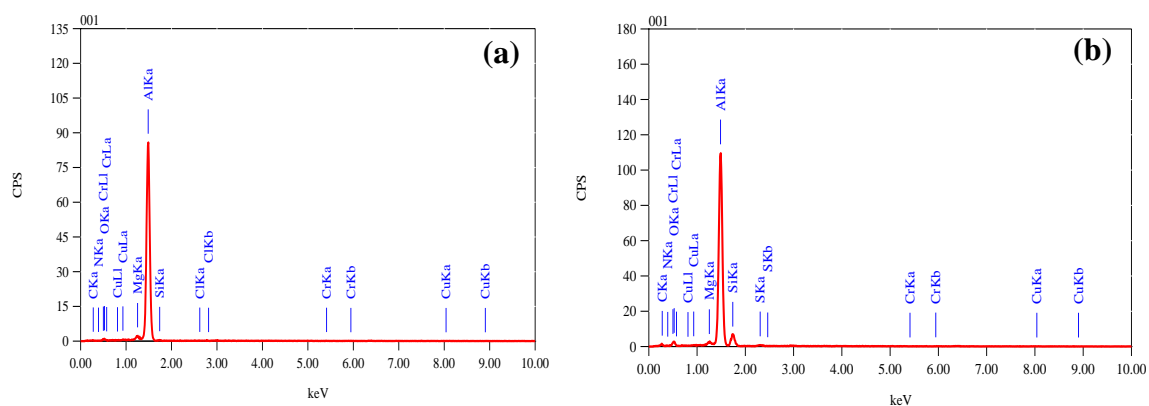
Figure 3.57 EDX spectra of 6061 Al-15 vol. pct. SiC$_{(P)}$ composite surface immersed in 0.1 M (a) HCl containing 0.9 mM [OPEBen$^+$] [Br$^-$] for 2 h and (b) H$_2$SO$_4$ containing 1 mM [OPEBen$^+$] [Br$^-$] for 3 h.

Table 3.39 Potentiodynamic polarization data for the corrosion of 6061 Al-15 vol. pct. SiC$_{(P)}$ composite in 0.025 M HCl solution containing different concentrations of [OPEBen$^+$] [Br$^-$] at different temperatures.

Temp (°C)	Inh. Conc. (mM)	$-E_{corr}$ (mV vs. SCE)	$-\beta_c$ (mV dec^{-1})	i_{corr} (µA cm^{-2})	η (%)
	Blank	696	215	54.6	-
	0.1	721	185	8.5	84.5
30	0.3	723	186	7.4	86.5
	0.5	725	184	5.9	89.2
	0.7	727	179	3.9	92.8
	0.9	728	183	3.1	94.3
	Blank	676	192	102.6	-
	0.1	696	172	14.7	85.7
35	0.3	698	174	13.2	87.1
	0.5	703	175	9.5	90.7
	0.7	706	173	7.0	93.2
	0.9	711	176	5.1	95.0
	Blank	693	216	134.4	-
	0.1	721	196	18.2	86.5
40	0.3	725	193	15.3	88.6
	0.5	726	191	10.8	92.0
	0.7	726	192	8.7	93.5
	0.9	728	196	6.3	95.3
	Blank	690	225	161.7	-
	0.1	713	193	19.6	87.9
45	0.3	716	192	15.3	90.6
	0.5	720	200	12.7	92.2
	0.7	724	193	10.4	93.6
	0.9	726	195	7.2	95.6
	Blank	714	224	180.8	-
	0.1	752	191	20.8	88.5
50	0.3	755	194	15.4	91.5
	0.5	758	193	13.6	92.5
	0.7	763	196	11.0	93.9
	0.9	765	192	6.5	96.4

Table 3.40 Potentiodynamic polarization data for the corrosion of 6061 Al-15 vol. pct. SiC$_{(P)}$ composite in 0.1 M HCl solution containing different concentrations of [OPEBen$^+$] [Br$^-$] at different temperatures.

Temp (°C)	Inh. Conc. (mM)	$-E_{corr}$ (mV vs. SCE)	$-\beta_c$ (mV dec^{-1})	i_{corr} (μA cm^{-2})	η (%)
	Blank	664	166	150.8	-
	0.1	685	134	20.6	86.3
30	0.3	700	135	18.8	87.6
	0.5	709	133	14.3	90.5
	0.7	737	131	9.5	93.7
	0.9	739	135	7.5	95.0
	Blank	659	199	269.5	-
	0.1	686	173	34.6	87.2
35	0.3	690	172	31.3	88.4
	0.5	695	177	23.7	91.2
	0.7	725	174	15.6	94.2
	0.9	728	175	11.3	95.8
	Blank	665	188	497.5	-
	0.1	698	185	60.5	87.8
40	0.3	702	183	50.5	89.9
	0.5	717	186	37.1	92.5
	0.7	725	181	26.1	94.7
	0.9	728	182	19.1	96.2
	Blank	691	204	726.3	-
	0.1	704	197	74.9	89.7
45	0.3	705	195	59.2	91.9
	0.5	710	192	52.9	92.7
	0.7	731	194	31.7	95.6
	0.9	735	192	24.5	96.6
	Blank	702	223	874.5	-
	0.1	710	196	79.1	91.0
50	0.3	702	192	65.0	92.6
	0.5	731	197	56.4	93.6
	0.7	742	194	37.0	95.8
	0.9	745	194	28.1	96.8

Table 3.41 Potentiodynamic polarization data for the corrosion of 6061 Al-15 vol. pct. SiC$_{(P)}$ composite in 0.25 M HCl solution containing different concentrations of [OPEBen$^+$] [Br$^-$] at different temperatures.

Temp (°C)	Inh. Conc. (mM)	$-E_{corr}$ (mV vs. SCE)	$-\beta_c$ (mV dec^{-1})	i_{corr} (µA cm^{-2})	η (%)
	Blank	658	293	898.3	-
	0.1	693	251	113.2	87.4
30	0.3	704	247	94.7	89.5
	0.5	709	253	76.5	91.5
	0.7	712	248	50.4	94.4
	0.9	716	252	37.2	95.9
	Blank	664	224	1239.4	-
	0.1	691	193	143.1	88.5
35	0.3	709	196	113.9	90.8
	0.5	711	192	99.4	92.0
	0.7	714	196	59.5	95.2
	0.9	718	195	48.4	96.1
	Blank	658	308	1807.0	-
	0.1	692	285	196.0	89.2
40	0.3	696	281	153.6	91.5
	0.5	702	283	128.9	92.9
	0.7	705	287	79.6	95.6
	0.9	710	282	65.7	96.4
	Blank	684	277	1878.3	-
	0.1	692	267	173.3	90.8
45	0.3	713	263	141.5	92.5
	0.5	715	265	120.6	93.6
	0.7	718	264	76.8	95.9
	0.9	719	268	57.7	96.9
	Blank	667	246	2135.9	-
	0.1	712	217	191.9	91.0
50	0.3	715	215	116.4	94.5
	0.5	719	218	102.5	95.2
	0.7	723	213	78.8	96.3
	0.9	726	214	60.4	97.2

Table 3.42 Potentiodynamic polarization data for the corrosion of 6061 Al-15 vol. pct. SiC$_{(P)}$ composite in 0.1 M H$_2$SO$_4$ solution containing different concentrations of [OPEBen$^+$] [Br$^-$] at different temperatures.

Temp (°C)	Inh. Conc. (mM)	$-E_{corr}$ (mV vs. SCE)	$-\beta_c$ (mV dec^{-1})	i_{corr} (μA cm^{-2})	η (%)
	Blank	659	121	68.5	-
	0.2	662	104	11.3	83.5
30	0.4	663	105	10.1	85.2
	0.6	674	110	5.5	92.0
	0.8	707	106	3.3	95.2
	1.0	709	112	2.1	96.9
	Blank	665	105	79.5	-
	0.2	669	108	12.4	84.4
35	0.4	672	103	10.9	86.3
	0.6	674	102	5.6	93.0
	0.8	679	108	3.5	95.6
	1.0	682	104	2.3	97.0
	Blank	636	155	87.3	-
	0.2	638	132	12.9	85.2
40	0.4	646	135	10.8	87.7
	0.6	649	134	5.0	94.2
	0.8	653	136	3.6	95.8
	1.0	699	132	2.5	97.1
	Blank	655	102	100.1	-
	0.2	663	102	13.4	86.6
45	0.4	668	109	12.0	88.0
	0.6	675	108	5.4	94.6
	0.8	677	106	4.1	95.9
	1.0	679	105	2.9	97.1
	Blank	653	150	125.7	-
	0.2	660	135	13.1	89.6
50	0.4	667	137	12.0	90.4
	0.6	672	133	6.8	94.6
	0.8	674	137	5.2	95.9
	1.0	675	136	3.6	97.1

Table 3.43 Potentiodynamic polarization data for the corrosion of 6061 Al-15 vol. pct. SiC$_{(P)}$ composite in 0.3 M H$_2$SO$_4$ solution containing different concentrations of [OPEBen$^+$] [Br$^-$] at different temperatures.

Temp (°C)	Inh. Conc. (mM)	$-E_{corr}$ (mV vs. SCE)	$-\beta_c$ (mV dec^{-1})	i_{corr} (µA cm^{-2})	η (%)
	Blank	595	142	209.6	-
	0.2	597	113	32.2	84.6
30	0.4	602	117	28.1	86.6
	0.6	602	115	16.1	92.3
	0.8	605	116	9.3	95.6
	1.0	609	117	6.1	97.1
	Blank	595	139	237.6	-
	0.2	598	105	34.9	85.3
35	0.4	603	104	30.6	87.1
	0.6	605	106	15.6	93.4
	0.8	609	105	9.5	96.0
	1.0	615	107	6.9	97.1
	Blank	592	141	270.5	-
	0.2	595	115	37.0	86.3
40	0.4	598	117	31.8	88.3
	0.6	601	118	14.7	94.6
	0.8	609	116	9.9	96.3
	1.0	613	114	7.6	97.2
	Blank	603	157	273.1	-
	0.2	606	135	34.9	87.2
45	0.4	608	137	31.8	88.4
	0.6	614	137	14.5	94.7
	0.8	616	134	9.8	96.4
	1.0	622	135	7.5	97.2
	Blank	605	159	294.8	-
	0.2	608	124	29.6	89.9
50	0.4	614	122	27.3	90.7
	0.6	615	124	14.5	95.1
	0.8	618	126	10.2	96.6
	1.0	620	125	8.2	97.2

Table 3.44 Potentiodynamic polarization data for the corrosion of 6061 Al-15 vol. pct. SiC$_{(P)}$ composite in 0.5 M H$_2$SO$_4$ solution containing different concentrations of [OPEBen$^+$] [Br$^-$] at different temperatures.

Temp (°C)	Inh. Conc. (mM)	$-E_{corr}$ (mV vs. SCE)	$-\beta_c$ (mV dec^{-1})	i_{corr} (μA cm^{-2})	η (%)
	Blank	560	129	348.7	-
	0.2	565	106	43.9	87.4
30	0.4	568	107	32.0	90.8
	0.6	568	106	21.9	93.7
	0.8	569	105	15.5	95.6
	1.0	572	108	10.9	96.9
	Blank	559	125	372.1	-
	0.2	564	114	42.7	88.5
35	0.4	564	115	33.2	91.1
	0.6	567	116	22.6	93.9
	0.8	569	114	13.9	96.3
	1.0	574	115	10.9	97.1
	Blank	557	140	479.8	-
	0.2	568	117	52.1	89.1
40	0.4	573	115	39.7	91.7
	0.6	575	115	24.8	94.8
	0.8	578	116	16.7	96.5
	1.0	580	118	13.7	97.1
	Blank	562	164	517.9	-
	0.2	565	142	56.1	89.2
45	0.4	568	137	42.3	91.8
	0.6	570	140	27.1	94.8
	0.8	574	139	18.0	96.5
	1.0	576	138	14.9	97.1
	Blank	565	169	564.7	-
	0.2	569	145	57.3	89.9
50	0.4	574	143	41.0	92.7
	0.6	577	145	26.8	95.3
	0.8	583	148	19.4	96.6
	1.0	586	146	16.3	97.1

Table 3.45 EIS data for the corrosion of 6061 Al-15 vol. pct. SiC$_{(P)}$ composite in 0.025 M HCl solution containing different concentrations of [OPEBen$^+$] [Br$^-$] at different temperatures.

Temp (°C)	Inh. Conc. (mM)	R_P (Ω cm^2)	C_{dl} (µF cm^{-2})	η (%)
	Blank	308.7	55.0	-
	0.1	1791.0	42.3	82.8
30	0.3	2072.0	42.0	85.1
	0.5	3277.0	40.0	90.6
	0.7	4204.0	27.0	92.7
	0.9	5390.0	16.7	94.3
	Blank	119.0	119.6	
	0.1	730.0	71.6	83.7
35	0.3	937.0	47.5	87.3
	0.5	1544.0	44.9	92.3
	0.7	1900.0	41.9	93.7
	0.9	2461.0	30.4	95.2
	Blank	64.6	180.4	-
	0.1	418.3	72.0	84.6
40	0.3	630.0	46.3	89.7
	0.5	1013.0	40.4	93.6
	0.7	1039.0	37.1	93.8
	0.9	1518.0	25.8	95.7
	Blank	51.2	251.9	-
	0.1	383.1	63.8	86.6
45	0.3	723.0	43.3	92.9
	0.5	904.0	42.9	94.3
	0.7	951.0	39.9	94.6
	0.9	1267.0	36.7	96.0
	Blank	48.6	260.2	-
	0.1	429.1	58.6	88.7
50	0.3	698.0	50.7	93.0
	0.5	856.0	48.3	94.3
	0.7	949.0	42.5	94.9
	0.9	1405.0	32.2	96.5

Table 3.46 EIS data for the corrosion of 6061 Al-15 vol. pct. SiC$_{(P)}$ composite in 0.1 M HCl solution containing different concentrations of [OPEBen$^+$] [Br$^-$] at different temperatures.

Temp (°C)	Inh Conc. (mM)	R_P (Ω cm^2)	C_{dl} (μF cm^{-2})	η (%)
	Blank	213.7	83.3	-
	0.1	1355.3	58.0	84.2
30	0.3	1497.9	56.8	85.7
	0.5	2580.1	55.5	91.7
	0.7	3477.9	52.6	93.9
	0.9	4560.3	32.9	95.3
	Blank	100.2	136.5	-
	0.1	695.2	65.0	85.6
35	0.3	878.9	58.3	88.6
	0.5	1338.6	54.2	92.5
	0.7	1674.1	52.2	94.0
	0.9	2507.0	28.9	96.0
	Blank	55.5	201.3	-
	0.1	398.5	85.3	86.1
40	0.3	594.9	56.3	90.7
	0.5	875.2	55.2	93.7
	0.7	935.4	54.5	94.1
	0.9	1451.0	53.6	96.2
	Blank	41.3	343.2	-
	0.1	315.3	89.8	86.9
45	0.3	615.6	78.1	93.3
	0.5	740.9	74.0	94.4
	0.7	846.3	59.1	95.1
	0.9	1161.0	32.1	96.4
	Blank	21.1	565.1	-
	0.1	195.4	95.4	89.2
50	0.3	340.4	91.0	93.8
	0.5	378.7	76.9	94.4
	0.7	481.0	57.4	95.6
	0.9	622.0	33.2	96.6

Table 3.47 EIS data for the corrosion of 6061 Al-15 vol. pct. SiC$_{(P)}$ composite in 0.25 M HCl solution containing different concentrations of [OPEBen$^+$] [Br$^-$] at different temperatures.

Temp (°C)	Inh. Conc. (mM)	R_P (Ω cm^2)	C_{dl} (μF cm^{-2})	η (%)
	Blank	126.3	107.8	
	0.1	953.4	73.3	86.8
30	0.3	1116.8	64.2	88.7
	0.5	1624.2	60.5	92.2
	0.7	2284.0	39.7	94.5
	0.9	3322.0	27.4	96.2
	Blank	71.6	177.8	
	0.1	592.7	107.9	87.9
35	0.3	676.0	60.4	89.4
	0.5	1071.3	58.1	93.3
	0.7	1385.0	37.3	94.8
	0.9	1987.0	34.6	96.4
	Blank	51.4	231.4	
	0.1	470.0	80.9	89.1
40	0.3	581.0	79.8	91.2
	0.5	927.4	49.5	94.5
	0.7	1062.1	47.8	95.2
	0.9	1434.2	41.7	96.4
	Blank	21.8	413.8	
	0.1	228.8	72.5	90.5
45	0.3	371.2	68.4	94.1
	0.5	417.4	59.5	94.8
	0.7	546.0	45.1	96.0
	0.9	629.5	40.7	96.5
	Blank	11.7	509.3	
	0.1	133.3	393.9	91.2
50	0.3	239.9	227.1	95.1
	0.5	260.0	225.0	95.5
	0.7	302.0	206.8	96.1
	0.9	424.0	206.3	97.2

Table 3.48 EIS data for the corrosion of 6061 Al-15 vol. pct. SiC$_{(P)}$ composite in 0.1 M H$_2$SO$_4$ solution containing different concentrations of [OPEBen$^+$] [Br$^-$] at different temperatures.

Temp (°C)	Inh. Conc. (mM)	R_P (Ω cm^2)	C_{dl} (μF cm^{-2})	η (%)
	Blank	245.5	84.7	-
	0.2	1346.7	69.0	81.8
30	0.4	1681.4	63.5	85.4
	0.6	2929.0	55.2	91.6
	0.8	5718.0	52.9	95.7
	1.0	6608.0	43.5	96.3
	Blank	221.2	86.4	-
	0.2	1313.1	70.1	83.2
35	0.4	1661.8	64.6	86.7
	0.6	2931.0	51.4	92.5
	0.8	5852.0	48.3	96.2
	1.0	6331.0	46.5	96.5
	Blank	194.1	120.7	-
	0.2	1248.1	98.5	84.4
40	0.4	1697.7	95.2	88.6
	0.6	3271.0	91.4	94.1
	0.8	5445.0	88.3	96.4
	1.0	5766.0	86.5	96.6
	Blank	121.4	140.4	-
	0.2	948.8	112.9	87.2
45	0.4	1152.9	107.6	89.5
	0.6	2196.0	104.5	94.5
	0.8	3367.0	97.6	96.4
	1.0	3707.0	92.8	96.7
	Blank	101.3	160.4	-
	0.2	913.3	104.3	88.9
50	0.4	1116.2	102.8	90.9
	0.6	2098.0	96.3	95.2
	0.8	2815.8	94.6	96.4
	1.0	3101.0	92.5	96.7

Table 3.49 EIS data for the corrosion of 6061 Al-15 vol. pct. SiC$_{(P)}$ composite in 0.3 M H$_2$SO$_4$ solution containing different concentrations of [OPEBen$^+$] [Br$^-$] at different temperatures.

Temp (°C)	Inh. Conc. (mM)	R_P (Ω cm^2)	C_{dl} (μF cm^{-2})	η (%)
	Blank	103.6	76.5	-
	0.2	585.7	67.1	82.3
30	0.4	734.2	64.4	85.9
	0.6	1354.7	60.6	92.4
	0.8	2476.7	57.4	95.8
	1.0	2818.7	56.4	96.3
	Blank	73.5	147.9	-
	0.2	446.5	124.6	83.6
35	0.4	534.4	120.7	86.3
	0.6	629.0	117.5	88.3
	0.8	995.7	114.7	92.6
	1.0	2122.6	109.4	96.5
	Blank	62.8	187.0	-
	0.2	415.5	145.7	84.9
40	0.4	583.6	142.4	89.3
	0.6	1185.3	138.4	94.7
	0.8	1728.0	136.3	96.4
	1.0	1905.8	135.8	96.7
	Blank	59.5	192.7	-
	0.2	481.4	152.3	87.7
45	0.4	620.3	151.7	90.4
	0.6	766.0	149.4	92.2
	0.8	1133.3	146.8	94.8
	1.0	1782.4	145.1	96.7
	Blank	45.3	234.3	-
	0.2	469.9	195.3	90.4
50	0.4	541.3	192.4	91.6
	0.6	1076.1	189.4	95.8
	0.8	1358.0	183.5	96.7
	1.0	1378.5	179.3	96.7

Table 3.50 EIS data for the corrosion of 6061 Al-15 vol. pct. SiC$_{(P)}$ composite in 0.5 M H$_2$SO$_4$ solution containing different concentrations of [OPEBen$^+$] [Br$^-$] at different temperatures.

Temp (°C)	Inh. Conc. (mM)	R_P (Ω cm^2)	C_{dl} (μF cm^{-2})	η (%)
	Blank	88.6	122.8	-
	0.2	588.5	119.4	84.9
30	0.4	683.8	115.3	87.0
	0.6	1199.2	112.4	92.6
	0.8	2153.3	108.5	95.9
	1.0	2374.1	106.9	96.3
	Blank	59.6	153.3	-
	0.2	409.9	135.9	85.5
35	0.4	546.5	132.4	89.1
	0.6	820.7	129.5	92.7
	0.8	1571.5	126.8	96.2
	1.0	1860.8	121.4	96.8
	Blank	53.7	164.4	-
	0.2	392.9	147.3	86.3
40	0.4	548.5	141.3	90.2
	0.6	1159.5	134.5	95.4
	0.8	1478.0	132.7	96.4
	1.0	1660.3	131.4	96.8
	Blank	48.9	180.3	-
	0.2	413.3	160.5	88.2
45	0.4	546.7	157.3	91.1
	0.6	1108.4	152.1	95.6
	0.8	1401.8	150.1	96.5
	1.0	1548.0	149.4	96.8
	Blank	31.2	240.3	-
	0.2	359.0	196.2	91.3
50	0.4	382.5	195.3	91.8
	0.6	747.0	189.3	95.8
	0.8	948.2	187.4	96.7
	1.0	1055.2	186.3	97.0

Table 3.51 Activation parameters for the corrosion of 6061 Al-15 vol. pct. SiC$_{(P)}$ composite in HCl solutions of different concentrations containing [OPEBen$^+$] [Br$^-$].

Medium Conc. (M)	Inh. Conc. (mM)	E_a (kJ mol^{-1})	$\Delta H^{\#}$ (kJ mol^{-1})	$-\Delta S^{\#}$ (J K^{-1} mol^{-1})
	Blank	**46.69**	**44.09**	**102.45**
	0.1	34.12	31.51	159.42
0.025	**0.3**	26.64	24.03	184.94
	0.5	32.10	29.49	169.50
	0.7	40.36	37.76	145.31
	0.9	29.83	27.22	181.90
	Blank	**77.40**	**74.80**	**26.80**
	0.1	56.74	54.13	77.77
0.1	**0.3**	51.21	48.60	96.79
	0.5	58.08	55.48	76.66
	0.7	56.20	53.59	86.19
	0.9	55.89	53.29	89.50
	Blank	**35.18**	**32.58**	**117.96**
	0.1	20.49	17.89	183.62
0.25	**0.3**	10.54	7.94	217.67
	0.5	12.99	10.38	211.20
	0.7	18.86	16.25	195.97
	0.9	18.85	16.25	198.07

Table 3.52 Activation parameters for the corrosion of 6061 Al-15 vol. pct. SiC$_{(P)}$ composite in H$_2$SO$_4$ solutions of different concentrations containing [OPEBen$^+$] [Br$^-$].

Medium Conc. (M)	Inh. Conc. (mM)	E_a (kJ mol^{-1})	$\Delta H^{\#}$ (kJ mol^{-1})	$-\Delta S^{\#}$ (J K^{-1} mol^{-1})
	Blank	23.28	20.63	179.49
	0.1	6.12	3.51	250.70
0.1	0.2	7.10	4.50	248.58
	0.3	6.57	3.97	255.93
	0.4	16.99	14.39	225.71
	0.5	20.71	18.11	217.00
	Blank	13.33	10.73	202.59
	0.1	−2.55	−5.15	270.24
0.3	0.2	−0.20	−2.81	263.74
	0.3	−4.79	−7.39	284.07
	0.4	3.54	0.94	261.10
	0.5	11.23	8.62	239.00
	Blank	21.18	18.57	172.84
	0.1	13.12	10.51	216.86
0.5	0.2	12.18	9.57	222.29
	0.3	9.58	6.97	234.10
	0.4	11.51	8.91	231.18
	0.5	18.07	15.46	212.15

Table 3.53 Thermodynamic parameters for the adsorption of [OPEBen$^+$] [Br$^-$] on 6061 Al-15 vol. pct. SiC$_{(P)}$ composite in HCl solutions of different concentrations.

Medium Conc. (M)	Temp (°C)	R^2	Slope	$-\Delta G^0_{ads}$ (kJ mol^{-1})	ΔH^0_{ads} (kJ mol^{-1})	ΔS^0_{ads} (J K^{-1} mol^{-1})
	30	0.998	1.031	36.62		
	35	0.998	1.032	37.42		
0.025	40	0.999	1.030	38.44	20.25	187.6
	45	0.999	1.031	39.62		
	50	0.999	1.020	40.21		
	30	0.998	1.030	36.89		
	35	0.998	1.020	37.56		
0.1	40	0.999	1.020	38.58	23.02	197.2
	45	0.999	1.020	39.68		
	50	0.999	1.021	40.76		
	30	0.999	1.021	37.19		
	35	0.999	1.020	38.16		
0.25	40	0.999	1.021	39.04	27.04	211.6
	45	0.999	1.020	40.00		
	50	0.999	1.020	41.56		

Table 3.54 Thermodynamic parameters for the adsorption of [OPEBen$^+$] [Br$^-$] on 6061 Al-15 vol. pct. SiC$_{(P)}$ composite in H$_2$SO$_4$ solutions of different concentrations.

Medium Conc. (M)	Temp (°C)	R^2	Slope	$-\Delta G^0_{ads}$ (kJ mol^{-1})	ΔH^0_{ads} (kJ mol^{-1})	ΔS^0_{ads} (J K^{-1} mol^{-1})
	30	0.997	0.978	34.61		
	35	0.998	0.979	35.41		
0.1	40	0.998	0.984	36.34	24.91	196.0
	45	0.998	0.988	37.17		
	50	0.999	1.002	38.63		
	30	0.998	0.981	34.85		
	35	0.998	0.982	35.63		
0.3	40	0.998	0.985	36.54	22.18	187.8
	45	0.998	0.987	37.26		
	50	0.999	1.000	38.73		
	30	0.996	1.001	35.99		
	35	0.999	1.000	36.72		
0.5	40	0.999	1.001	37.61	12.70	160.6
	45	0.999	1.001	38.23		
	50	0.999	1.005	39.25		

3.6 1,3-BIS[2-(4-METHOXYPHENYL)-2-OXOETHYL]-1*H*-BENZIMIDAZOL-3-IUM BROMIDE [MPOEBen⁺] [Br⁻] AS CORROSION INHIBITOR ON 6061 Al-15 VOL. PCT. SiC$_{(P)}$ COMPOSITE IN ACIDIC MEDIA

3.6.1 Potentiodynamic polarization measurements

The potentiodynamic polarization curves for the corrosion of 6061 Al-15 vol. pct. SiC$_{(P)}$ composite containing different concentrations of [MPOEBen⁺] [Br⁻] in 0.1 M hydrochloric acid and 0.1 M sulfuric acid at 40 °C are given in the Figure 3.58(a) and 3.58(b), respectively. Similar plots were obtained in other medium concentrations and at different temperatures.
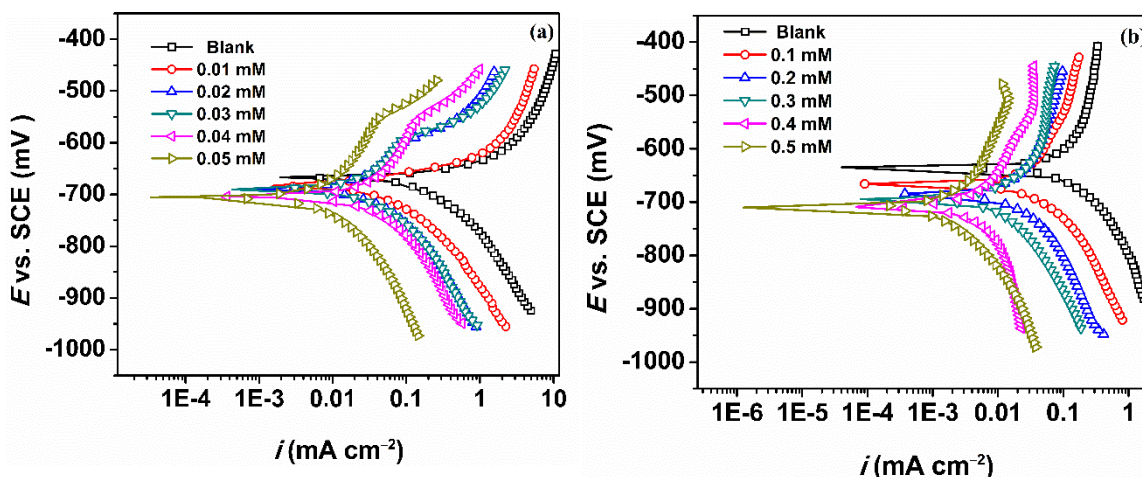
Figure 3.58 Potentiodynamic polarization curves for the corrosion of 6061 Al-15 vol. pct. SiC$_{(P)}$ composite in the presence of different concentrations of [MPOEBen⁺] [Br⁻] at 40 °C, in 0.1 M (a) HCl and (b) H$_2$SO$_4$.

In the figures, it is clearly seen that for increasing concentrations of the inhibitor in both the media, the curves evidently shift to lower current densities indicating lesser rate of corrosion. Also, the cathodic curves seem to be more affected than the anodic curve, as it is seen by the overlapping of the anodic curves.

The electrochemical parameters, E_{corr}, i_{corr}, β_c, and η %, are tabulated in the Tables 3.55, 3.56 and 3.57 for the corrosion of the composite in hydrochloric acid medium and

Tables 3.58, 3.59 and 3.60 for the corrosion of the composite in sulfuric acid medium. It is observed that in the presence of inhibitors, the corrosion potential value shifts towards the cathodic side, but not more than -85 mV from the blank value. Such a shift in corrosion potential indicates mixed control on anodic dissolution and cathodic hydrogen evolution reaction, but with predominant control on the cathodic reaction (Arukalam et al. 2014). Minor changes in the Tafel slope indicates change in the corrosion mechanism in the presence of the inhibitor. Although the inhibition efficiencies in both the medium are comparable, the amount of inhibitor required in hydrochloric acid medium is less than that required in the sulfuric acid medium. The inhibition efficiency of 98.7% at 0.05 mM and 98.8% at 0.5 mM concentration of [MPOEBen$^+$] [Br$^-$] at 50 °C in 0.25 M hydrochloric and in sulfuric acid media, respectively was achieved. The efficiency of the inhibitor increases with the increase in the concentration of both HCl and H$_2$SO$_4$ corrosive media.

3.6.2 Electrochemical impedance spectroscopy measurements

The Nyquist plots for the corrosion of 6061 Al-15 vol. pct. SiC$_{(P)}$ composite containing different concentrations of [MPOEBen$^+$] [Br$^-$] in 0.1 M hydrochloric acid and 0.1 M sulfuric acid at 40 °C are given in the Figure 3.59(a) and 3.59(b), respectively. Similar plots were obtained in other medium concentrations and at different temperatures
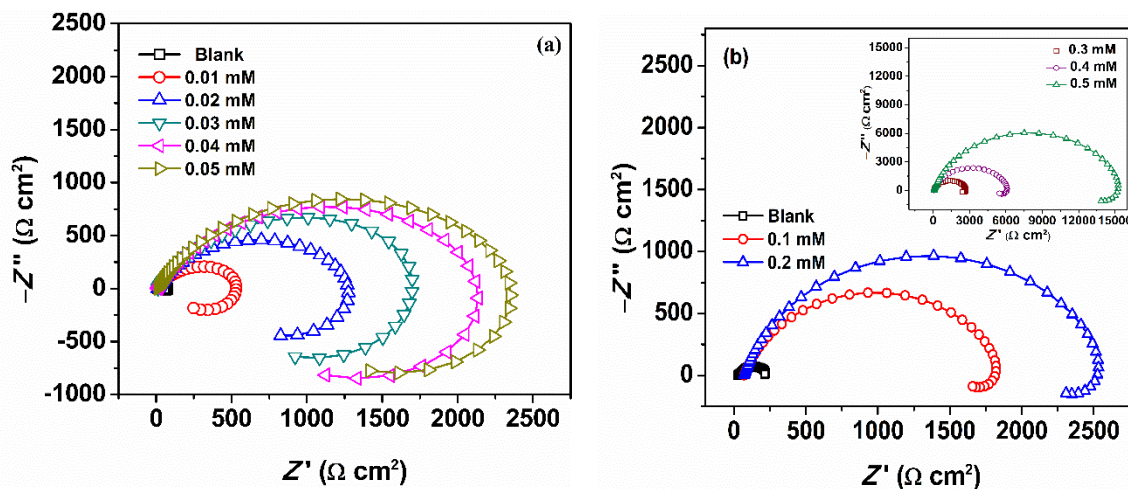
Figure 3.59 Nyquist plots for the corrosion of 6061 Al-15 vol. pct. SiC$_{(P)}$ composite in the presence of different concentrations of [MPOEBen$^+$] [Br$^-$] at 40 °C, in 0.1 M (a) HCl and (b) H$_2$SO$_4$.

It is observed from the plots that in both the media that in the presence of the inhibitor, the capacitive and inductive loops are enlarged to a large extent. The impedance parameters were calculated by simulation with the equivalent circuit shown in the Figure 3.3. The R_P, C_{dl} and η % for the corrosion of the composite in hydrochloric acid medium are tabulated in the Tables 3.61, 3.62 and 3.63 and for the corrosion of the composite in sulfuric acid medium are tabulated in Tables 3.64, 3.65 and 3.66. The variations of polarization resistance and capacitance of the double layer follow similar trend as discussed under section 3.3.2.

Figures 3.60(a) and 3.60(b) show Bode magnitude plots for the corrosion of alloy composite in 0.1 M hydrochloric acid and 0.1 M sulfuric acid at 40 °C, respectively. The corresponding Bode phase angle plots are shown in the Figures 3.61(a) and 3.61(b), respectively. The Figures 3.60 and 3.61 clearly show increase in the values of impedance modulus (Z_{mod}) and phase maxima (θ'_{max}) with the increase in the inhibitor concentration suggesting an increased inhibition efficiency (Gao et al. 2010, Hu et al. 2013).
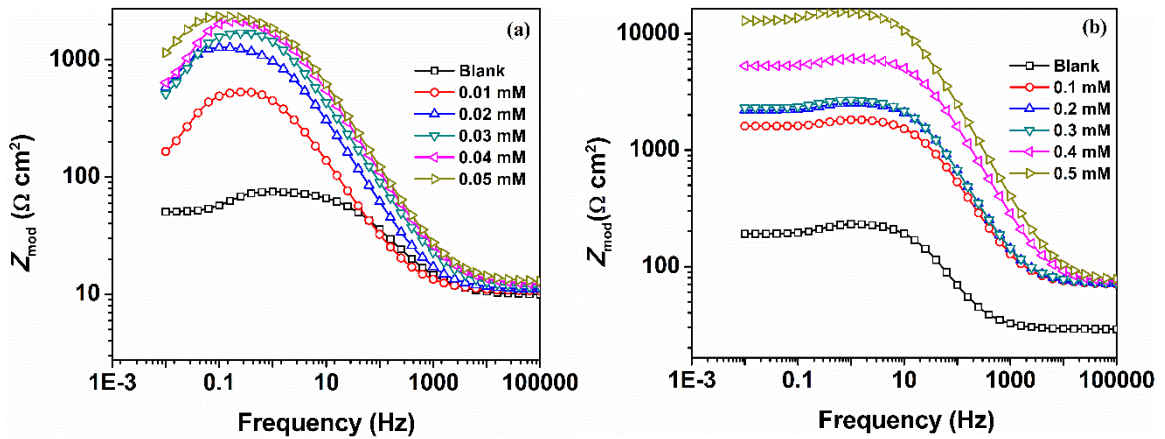
Figure 3.60 Bode magnitude plots for the corrosion of 6061 Al-15 vol. pct. SiC$_{(P)}$ composite in the presence of different concentrations of [MPOEBen$^+$] [Br$^-$] at 40 °C, in 0.1 M (a) HCl and (b) H$_2$SO$_4$.
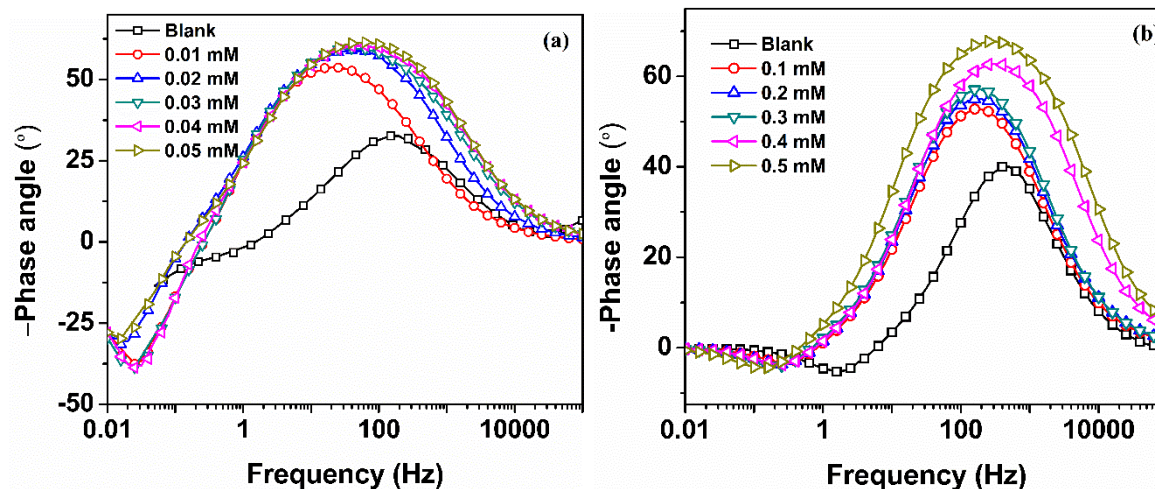
Figure 3.61 Bode phase angle plots for the corrosion of 6061 Al-15 vol. pct. SiC(P) composite in the presence of different concentrations of [MPOEBen⁺] [Br⁻] at 40 °C, in 0.1 M (a) HCl and (b) H₂SO₄.

3.6.3 Effect of temperature

From the results of the potentiodynamic polarization studies and EIS (Tables 3.55-3.66) it is observed that the inhibition efficiency increases with the temperature. This observation is attributed to the chemisorption of the inhibitor on the surface of the composite. The Arrhenius plots for the corrosion of the composite in hydrochloric acid and in sulfuric acid media containing different concentrations of [MPOEBen⁺] [Br⁻] are shown in the Figures 3.62(a) and 3.62(b), respectively. The slopes and intercept values of plot of ln (v_{corr}/T) vs. $1/T$ were used to deduce the enthalpy of activation and entropy of activation (Figures 3.63(a) and 3.63(b)). The activation parameters are listed in Tables 3.67 and 3.68. The activation energy in the presence of inhibitor is lower/negative than that in the blank media (Shimomura 1967). Large negative values of entropy suggests association step in the formation of reaction intermediates in the rate determining step of the corrosion reaction (Borsato et al. 2014).
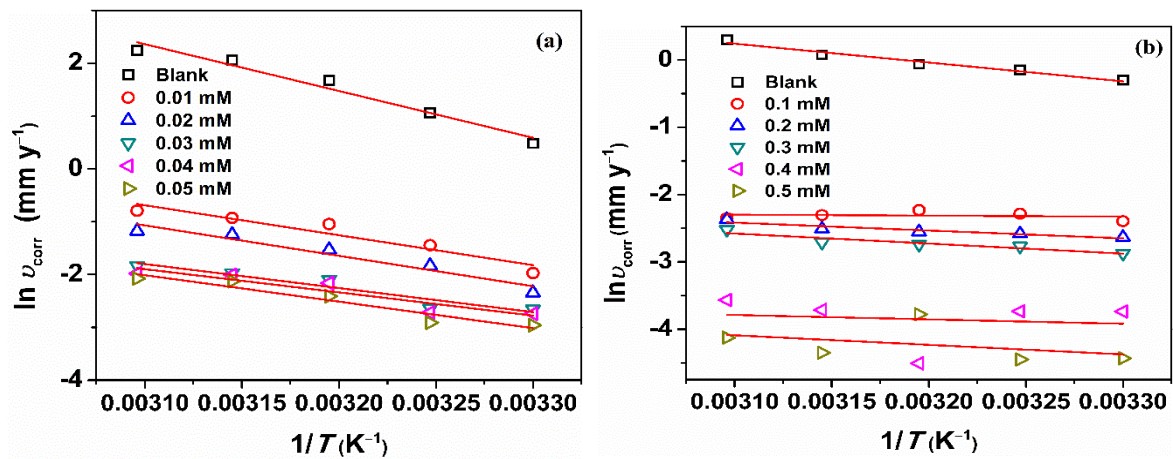
Figure 3.62 Arrhenius plots for the corrosion of 6061 Al-15 vol. pct. SiC(P) composite containing different concentrations of [MPOEBen+] [Br−] in 0.1 M (a) HCl and (b) H2SO4.
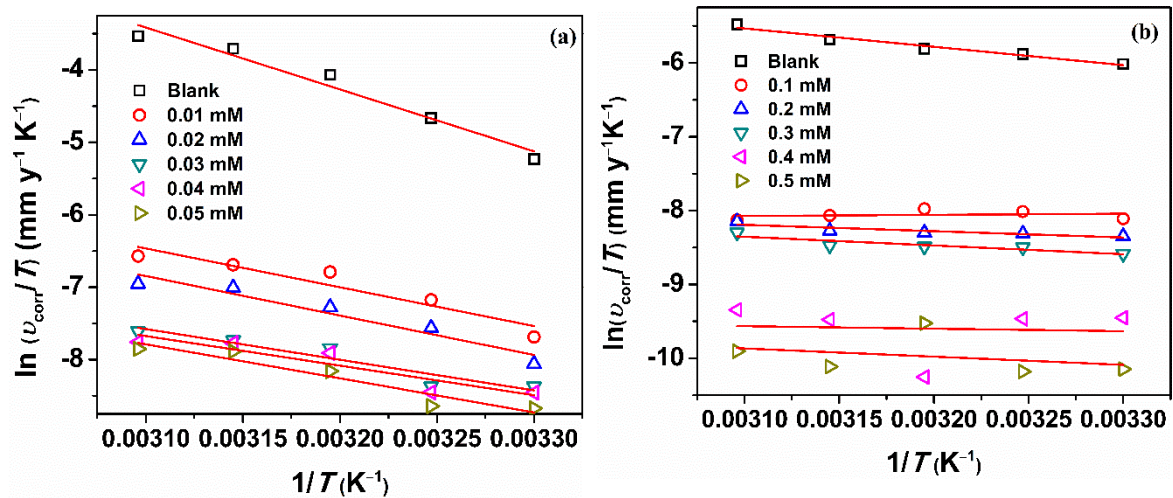
Figure 3.63 Plots of ln (v_{corr}/T) vs. 1/T for the corrosion of 6061 Al-15 vol. pct. SiC(P) composite containing different concentrations of [MPOEBen+] [Br−] in 0.1 M (a) HCl and (b) H2SO4.

3.6.4 Adsorption isotherms

Similar to all other inhibitors studied, the adsorption of the inhibitor on the composite surface followed Langmuir adsorption isotherm. Figures 3.64(a) and 3.64(b)

represent the Langmuir adsorption isotherms for the adsorption of [MPOEBen$^+$] [Br$^-$], on the composite surface in 0.1 M HCl and 0.1 M H$_2$SO$_4$, respectively. The thermodynamic parameters for the adsorption of inhibitor on the composite surface in hydrochloric acid and in sulfuric acid medium are listed in Tables 3.69 and 3.70, respectively. The slope values are very close to unity showing minor deviations from ideal Langmuir adsorption behavior (Masel 1996). The values of ΔG^0_{ads} ranges between -45.2 to -50.4 kJ mol^{-1} in HCl and -36.1 to -41.8 kJ mol^{-1} in H$_2$SO$_4$ medium. These values suggest the adsorption of the inhibitor on the composite surface by predominant chemisorption processes. The positive values of enthalpy of adsorption suggests predominant chemisorption and positive entropy of adsorption suggests increased randomization during adsorption which may be attributed to the displacement of pre-adsorbed water molecules by inhibitor molecules (Manamela et al. 2014).
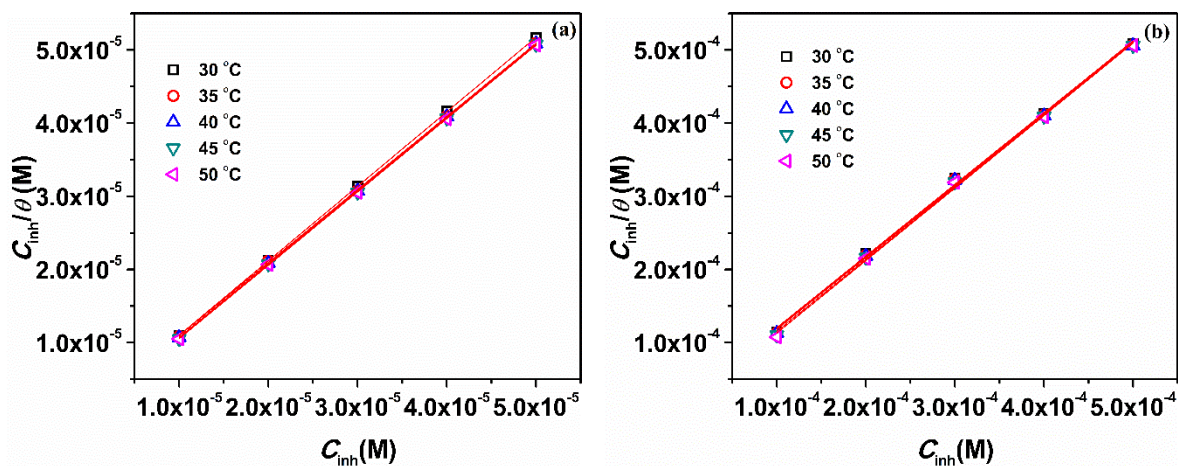
Figure 3.64 Langmuir adsorption isotherms for the adsorption of [MPOEBen$^+$] [Br$^-$], on the 6061 Al-15 vol. pct. SiC$_{(P)}$ composite surface in 0.1 M, (a) HCl and (b) H$_2$SO$_4$.

3.6.5 Surface analyses

The SEM images of Al alloy composite surface immersed in 0.1 M hydrochloric acid (2 hours) and 0.1 M sulfuric acid (3 hours) in the presence of 0.05 mM and 0.5 mM of [MPOEBen$^+$] [Br$^-$], respectively, are given in Figures 3.65(a) and 3.65(b). From the figures it may be observed that in the presence of inhibitor, the surfaces of the composite appear

to be smooth and even. The corresponding EDX spectra are represented in the Figures 3.66(a) and 3.66(b). The peak corresponding to nitrogen element apart from elemental peaks from composite confirms the presence of adsorbed inhibitor on the composite surface.
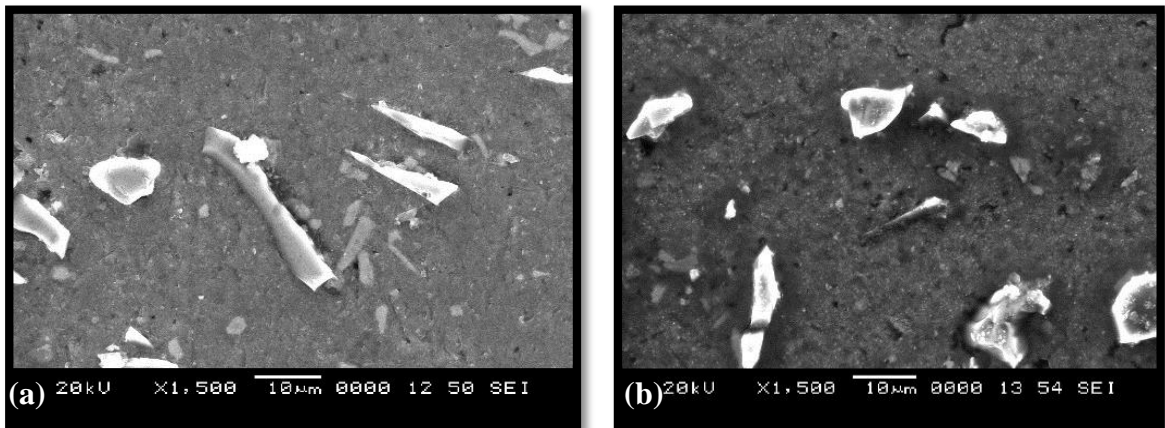
Figure 3.65 SEM images of 6061 Al-15 vol. pct. SiC(P) composite surface immersed in 0.1 M (a) HCl containing 0.05 mM [MPOEBen⁺] [Br⁻] for 2 h and (b) H₂SO₄ containing 0.5 mM [MPOEBen⁺] [Br⁻] for 3 h.
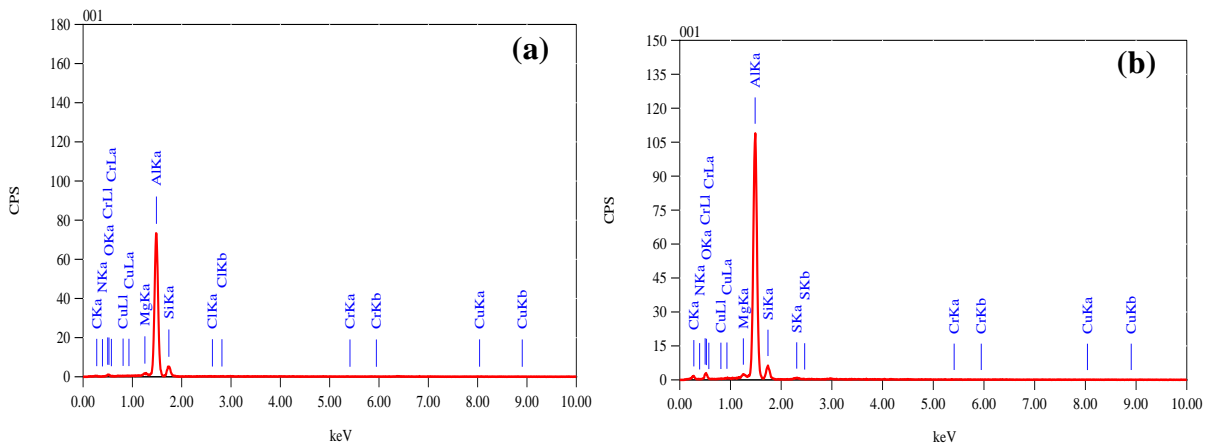
Figure 3.66 EDX spectra of 6061 Al-15 vol. pct. SiC(P) composite surface immersed in 0.1 M (a) HCl containing 0.05 mM [MPOEBen⁺] [Br⁻] for 2 h and (b) H₂SO₄ containing 0.5 mM [MPOEBen⁺] [Br⁻] for 3 h.

Table 3.55 Potentiodynamic polarization data for the corrosion of 6061 Al-15 vol. pct. SiC$_{(P)}$ composite in 0.025 M HCl solution containing different concentrations of [MPOEBen$^+$] [Br$^-$] at different temperatures.

Temp (°C)	Inh. Conc. (mM)	$-E_{corr}$ (mV vs. SCE)	$-\beta_c$ (mV dec^{-1})	i_{corr} (µA cm^{-2})	η (%)
	Blank	696	215	54.6	-
	0.01	698	192	5.0	90.8
30	0.02	699	191	3.3	93.8
	0.03	708	193	2.6	95.1
	0.04	711	198	2.3	95.8
	0.05	715	195	1.9	96.5
	Blank	676	192	102.6	-
	0.01	726	186	9.0	91.2
35	0.02	728	187	5.8	94.3
	0.03	729	181	3.2	96.8
	0.04	731	187	3.1	97.0
	0.05	738	183	2.6	97.4
	Blank	693	216	134.4	-
	0.01	745	194	9.3	93.1
40	0.02	746	192	5.9	95.6
	0.03	747	195	4.8	96.4
	0.04	750	191	3.0	97.8
	0.05	752	196	2.9	97.8
	Blank	690	225	161.7	-
	0.01	752	195	8.7	94.6
45	0.02	753	193	6.4	96.1
	0.03	754	191	4.9	96.9
	0.04	756	194	3.2	98.0
	0.05	758	199	2.8	98.3
	Blank	714	224	180.8	-
	0.01	724	199	9.2	94.9
50	0.02	726	193	6.4	96.5
	0.03	728	194	4.3	97.6
	0.04	731	197	2.8	98.4
	0.05	734	192	2.5	98.6

Table 3.56 Potentiodynamic polarization data for the corrosion of 6061 Al-15 vol. pct. SiC(P) composite in 0.1 M HCl solution containing different concentrations of [MPOEBen⁺] [Br⁻] at different temperatures.

Temp (°C)	Inh. Conc. (mM)	$-E_{corr}$ (mV vs. SCE)	$-\beta_c$ (mV dec^{-1})	i_{corr} (μA cm^{-2})	η (%)
	Blank	664	166	150.8	-
	0.01	665	156	12.9	91.4
30	0.02	666	157	8.9	94.1
	0.03	681	151	6.5	95.7
	0.04	686	159	6.0	96.0
	0.05	701	153	4.8	96.8
	Blank	659	199	269.5	-
	0.01	660	142	21.9	91.9
35	0.02	701	149	14.9	94.5
	0.03	702	141	6.6	97.5
	0.04	703	144	6.1	97.7
	0.05	704	149	5.1	98.1
	Blank	665	188	497.5	-
	0.01	682	139	32.7	93.4
40	0.02	688	137	20.1	96.0
	0.03	690	134	11.4	97.7
	0.04	704	137	10.7	97.9
	0.05	705	134	8.3	98.3
	Blank	691	204	726.3	-
	0.01	694	172	36.7	94.9
45	0.02	696	173	26.8	96.3
	0.03	701	176	12.9	98.2
	0.04	702	174	12.5	98.3
	0.05	703	173	11.1	98.5
	Blank	702	223	874.5	-
	0.01	714	186	42.1	95.2
50	0.02	725	187	28.6	96.7
	0.03	768	185	14.8	98.3
	0.04	769	188	12.8	98.5
	0.05	779	186	11.7	98.7

Table 3.57 Potentiodynamic polarization data for the corrosion of 6061 Al-15 vol. pct. SiC$_{(P)}$ composite in 0.25 M HCl solution containing different concentrations of [MPOEBen$^+$] [Br$^-$] at different temperatures.

Temp (°C)	Inh. Conc. (mM)	$-E_{corr}$ (mV vs. SCE)	$-\beta_c$ (mV dec^{-1})	i_{corr} (μA cm^{-2})	η (%)
	Blank	658	293	898.3	-
	0.01	688	242	69.8	92.2
30	0.02	705	245	49.8	94.5
	0.03	707	246	33.2	96.3
	0.04	709	244	29.7	96.7
	0.05	712	243	23.7	97.4
	Blank	664	224	1239.4	-
	0.01	680	198	85.5	93.1
35	0.02	702	194	63.3	94.9
	0.03	714	195	27.2	97.8
	0.04	715	196	22.1	98.2
	0.05	716	193	19.7	98.4
	Blank	658	308	1807.0	-
	0.01	695	295	90.4	95.0
40	0.02	716	293	65.7	96.4
	0.03	724	294	38.5	97.9
	0.04	725	295	28.2	98.4
	0.05	726	294	27.0	98.5
	Blank	684	277	1878.3	-
	0.01	685	267	88.4	95.3
45	0.02	702	264	59.8	96.8
	0.03	724	261	30.5	98.4
	0.04	725	269	28.9	98.5
	0.05	726	265	26.7	98.6
	Blank	667	246	2135.9	-
	0.01	699	208	83.6	96.1
50	0.02	700	205	60.7	97.2
	0.03	720	206	31.4	98.5
	0.04	721	207	29.1	98.6
	0.05	722	209	27.7	98.7

Table 3.58 Potentiodynamic polarization data for the corrosion of 6061 Al-15 vol. pct. SiC$_{(P)}$ composite in 0.1 M H$_2$SO$_4$ solution containing different concentrations of [MPOEBen$^+$] [Br$^-$] at different temperatures.

Temp (°C)	Inh. Conc. (mM)	$-E_{corr}$ (mV vs. SCE)	$-\beta_c$ (mV dec^{-1})	i_{corr} (μA cm^{-2})	η (%)
	Blank	659	121	68.5	-
	0.1	661	116	8.5	87.6
30	0.2	663	113	6.7	90.3
	0.3	680	114	5.3	92.3
	0.4	688	111	2.2	96.8
	0.5	702	113	1.1	98.4
	Blank	665	105	79.5	-
	0.1	673	137	9.5	88.1
35	0.2	677	138	7.0	91.2
	0.3	679	131	5.8	92.7
	0.4	682	140	2.2	97.2
	0.5	702	141	1.1	98.6
	Blank	636	155	87.3	-
	0.1	666	154	10.0	88.6
40	0.2	684	152	7.2	91.7
	0.3	694	150	6.0	93.1
	0.4	709	138	2.1	97.6
	0.5	710	142	1.0	98.8
	Blank	655	102	100.1	-
	0.1	664	136	9.3	90.7
45	0.2	679	135	7.5	92.5
	0.3	689	135	6.2	93.8
	0.4	698	135	2.3	97.7
	0.5	702	182	1.2	98.8
	Blank	653	150	125.7	-
	0.1	658	147	8.9	92.9
50	0.2	662	157	8.7	93.1
	0.3	666	164	7.5	94.1
	0.4	675	169	2.6	97.9
	0.5	676	148	1.5	98.8

Table 3.59 Potentiodynamic polarization data for the corrosion of 6061 Al-15 vol. pct. SiC$_{(P)}$ composite in 0.3 M H$_2$SO$_4$ solution containing different concentrations of [MPOEBen$^+$] [Br$^-$] at different temperatures.

Temp (°C)	Inh. Conc. (mM)	$-E_{corr}$ (mV vs. SCE)	$-\beta_c$ (mV dec^{-1})	i_{corr} (µA cm^{-2})	η (%)
	Blank	595	142	209.6	-
	0.1	596	143	25.1	88.0
30	0.2	598	133	19.7	90.6
	0.3	601	144	15.2	92.7
	0.4	608	138	6.6	96.9
	0.5	611	138	3.2	98.5
	Blank	595	139	237.6	-
	0.1	599	124	27.5	88.4
35	0.2	604	124	19.9	91.6
	0.3	607	132	16.3	93.2
	0.4	615	122	5.6	97.6
	0.5	618	121	3.4	98.6
	Blank	592	141	270.5	-
	0.1	595	137	30.4	88.8
40	0.2	598	125	21.3	92.1
	0.3	604	127	17.5	93.5
	0.4	611	128	6.2	97.7
	0.5	615	131	3.2	98.8
	Blank	603	157	273.1	-
	0.1	605	143	24.1	91.2
45	0.2	607	140	20.1	92.6
	0.3	614	134	15.8	94.2
	0.4	618	140	6.0	97.8
	0.5	624	142	3.3	98.8
	Blank	605	159	294.8	-
	0.1	610	145	20.5	93.1
50	0.2	617	139	19.4	93.4
	0.3	620	140	17.0	94.2
	0.4	624	136	5.8	98.0
	0.5	625	133	3.4	98.8

Table 3.60 Potentiodynamic polarization data for the corrosion of 6061 Al-15 vol. pct. SiC$_{(P)}$ composite in 0.5 M H$_2$SO$_4$ solution containing different concentrations of [MPOEBen$^+$] [Br$^-$] at different temperatures.

Temp (°C)	Inh. Conc. (mM)	$-E_{corr}$ (mV vs. SCE)	$-\beta_c$ (mV dec^{-1})	i_{corr} (µA cm^{-2})	η (%)
	Blank	560	129	348.7	-
	0.1	564	114	41.2	88.2
30	0.2	568	115	29.9	91.4
	0.3	570	117	23.5	93.3
	0.4	573	118	10.9	96.9
	0.5	583	120	4.2	98.8
	Blank	559	125	372.1	-
	0.1	562	109	42.5	88.6
35	0.2	573	106	31.0	91.7
	0.3	576	113	24.6	93.4
	0.4	582	114	8.2	97.8
	0.5	584	113	4.4	98.8
	Blank	557	140	479.8	-
	0.1	573	113	50.0	89.6
40	0.2	576	113	34.4	92.8
	0.3	581	115	29.8	93.8
	0.4	584	117	10.8	97.8
	0.5	586	114	5.9	98.8
	Blank	562	164	517.9	-
	0.1	565	144	39.8	92.3
45	0.2	566	138	33.5	93.5
	0.3	569	137	26.9	94.8
	0.4	578	141	11.6	97.8
	0.5	579	139	6.1	98.8
	Blank	565	169	564.7	-
	0.1	576	136	31.1	94.5
50	0.2	577	135	29.6	94.8
	0.3	578	137	23.6	95.8
	0.4	581	135	12.4	97.8
	0.5	586	138	7.0	98.8

Table 3.61 EIS data for the corrosion of 6061 Al-15 vol. pct. SiC$_{(P)}$ composite in 0.025 M HCl solution containing different concentrations of [MPOEBen$^+$] [Br$^-$] at different temperatures.

Temp (°C)	Inh. Conc. (mM)	R_P (Ω cm^2)	C_{dl} (μF cm^{-2})	η (%)
	Blank	308.7	55.0	-
	0.01	2014.2	38.6	84.7
30	0.02	5085.0	32.0	93.9
	0.03	6367.0	30.4	95.2
	0.04	7667.0	30.2	96.0
	0.05	10030.0	29.5	96.9
	Blank	119.0	119.6	-
	0.01	915.8	47.1	87.0
35	0.02	2115.1	36.9	94.4
	0.03	2992.4	35.3	96.0
	0.04	3551.3	32.9	96.6
	0.05	4177.1	31.4	97.2
	Blank	64.6	180.4	-
	0.01	556.2	53.4	88.4
40	0.02	1295.2	44.1	95.0
	0.03	1787.0	42.6	96.4
	0.04	2308.1	38.6	97.2
	0.05	2670.1	36.7	97.6
	Blank	51.2	251.9	-
	0.01	675.3	52.6	92.4
45	0.02	1188.1	45.4	95.7
	0.03	1788.3	38.8	97.1
	0.04	2007.2	36.3	97.4
	0.05	2797.1	33.3	98.2
	Blank	48.6	260.2	-
	0.01	684.4	56.3	92.9
50	0.02	1289.1	48.4	96.2
	0.03	2236.1	43.2	97.8
	0.04	3256.2	35.3	98.5
	0.05	3554.3	32.4	98.6

Table 3.62 EIS data for the corrosion of 6061 Al-15 vol. pct. SiC$_{(P)}$ composite in 0.1 M HCl solution containing different concentrations of [MPOEBen$^+$] [Br$^-$] at different temperatures.

Temp (°C)	Inh. Conc. (mM)	R_P (Ω cm²)	C_{dl} (µF cm^{-2})	η (%)
	Blank	213.7	83.3	-
	0.01	1536.9	34.5	86.1
30	0.02	3647.4	31.3	94.1
	0.03	4842.7	28.6	95.6
	0.04	5867.4	23.6	96.4
	0.05	7573.9	21.2	97.2
	Blank	100.2	136.5	-
	0.01	796.5	54.6	87.4
35	0.02	2075.3	48.4	95.2
	0.03	2859.4	46.3	96.5
	0.04	3174.7	42.3	96.8
	0.05	3852.9	38.2	97.4
	Blank	55.5	201.3	-
	0.01	523.5	65.4	89.4
40	0.02	1265.3	54.3	95.6
	0.03	1695.2	52.5	96.7
	0.04	2126.4	51.2	97.4
	0.05	2340.3	45.3	97.6
	Blank	41.3	343.2	-
	0.01	555.3	72.4	92.6
45	0.02	1024.3	65.2	96.0
	0.03	1487.1	63.2	97.2
	0.04	1747.3	62.3	97.6
	0.05	2493.4	60.3	98.3
	Blank	21.1	565.1	-
	0.01	313.6	76.4	93.3
50	0.02	583.6	64.3	96.4
	0.03	1026.9	59.2	97.9
	0.04	1474.6	55.3	98.6
	0.05	1493.2	54.9	98.6

Table 3.63 EIS data for the corrosion of 6061 Al-15 vol. pct. SiC$_{(P)}$ composite in 0.25 M HCl solution containing different concentrations of [MPOEBen$^+$] [Br$^-$] at different temperatures.

Temp (°C)	Inh. Conc. (mM)	R_P (Ω cm^2)	C_{dl} (μF cm^{-2})	η (%)
30	Blank	126.3	107.8	-
	0.01	984.3	43.2	87.2
	0.02	2294.2	41.7	94.5
	0.03	3022.4	38.4	95.8
	0.04	3668.3	36.3	96.6
	0.05	4782.4	32.7	97.4
35	Blank	71.6	177.8	-
	0.01	636.4	56.3	88.7
	0.02	1634.2	45.1	95.6
	0.03	2208.8	42.3	96.8
	0.04	2744.0	41.4	97.4
	0.05	4071.0	32.4	98.2
40	Blank	51.4	231.4	-
	0.01	623.5	67.4	91.8
	0.02	1336.4	54.3	96.2
	0.03	1740.10	52.1	97.0
	0.04	2163.5	51.3	97.6
	0.05	3264.0	49.3	98.4
45	Blank	21.8	413.8	-
	0.01	314.7	60.6	93.1
	0.02	641.8	57.2	96.6
	0.03	867.4	55.2	97.5
	0.04	1246.3	45.3	98.3
	0.05	1524.1	44.6	98.6
50	Blank	11.7	509.3	-
	0.01	264.7	44.2	95.6
	0.02	366.8	42.4	96.8
	0.03	620.4	40.3	98.1
	0.04	862.2	39.3	98.6
	0.05	870.4	38.9	98.7

Table 3.64 EIS data for the corrosion of 6061 Al-15 vol. pct. SiC$_{(P)}$ composite in 0.1 M H$_2$SO$_4$ solution containing different concentrations of [MPOEBen$^+$] [Br$^-$] at different temperatures.

Temp (°C)	Inh. Conc. (mM)	R_P (Ω cm^2)	C_{dl} (μF cm^{-2})	η (%)
	Blank	245.5	84.7	-
	0.1	2036.0	44.8	87.9
30	0.2	2618.8	43.4	90.6
	0.3	3079.4	42.2	92.0
	0.4	6177.0	35.2	96.0
	0.5	16570.0	25.1	98.5
	Blank	221.2	86.4	-
	0.1	1905.8	46.5	88.4
35	0.2	2589.1	46.0	91.5
	0.3	2838.0	44.2	92.2
	0.4	5923.0	37.9	96.3
	0.5	15998.3	29.8	98.6
	Blank	194.1	120.7	-
	0.1	1738.4	40.3	88.8
40	0.2	2449.5	37.4	92.1
	0.3	2590.4	32.1	92.5
	0.4	5905.4	31.2	96.7
	0.5	15165.1	28.6	98.7
	Blank	121.4	140.4	-
	0.1	1416.6	89.0	91.4
45	0.2	1695.8	82.4	92.8
	0.3	2159.3	78.5	94.4
	0.4	3874.1	45.0	96.9
	0.5	8997.2	21.4	98.7
	Blank	101.3	160.4	-
	0.1	1361.2	90.1	92.6
50	0.2	1476.7	89.2	93.1
	0.3	1846.5	88.3	94.5
	0.4	3618.0	33.5	97.2
	0.5	7856.4	23.8	98.7

Table 3.65 EIS data for the corrosion of 6061 Al-15 vol. pct. SiC$_{(P)}$ composite in 0.3 M H$_2$SO$_4$ solution containing different concentrations of [MPOEBen$^+$] [Br$^-$] at different temperatures.

Temp (°C)	Inh. Conc. (mM)	R_P (Ω cm^2)	C_{dl} (μF cm^{-2})	η (%)
	Blank	103.6	76.5	-
	0.1	874.5	53.2	88.2
30	0.2	1110.1	51.3	90.7
	0.3	1392.3	50.2	92.6
	0.4	2849.7	47.3	96.4
	0.5	7975.0	36.8	98.7
	Blank	73.5	147.9	-
	0.1	641.1	125.6	88.6
35	0.2	883.9	119.3	91.7
	0.3	1015.1	117.8	92.8
	0.4	2295.2	112.7	96.8
	0.5	4989.3	110.5	98.7
	Blank	62.8	187.0	-
	0.1	569.7	163.7	89.0
40	0.2	823.3	161.4	92.4
	0.3	929.1	154.3	93.3
	0.4	2193.4	143.7	97.1
	0.5	4984.8	141.7	98.7
	Blank	59.5	192.7	-
	0.1	701.7	173.5	91.5
45	0.2	862.7	164.6	93.1
	0.3	1152.9	159.3	94.8
	0.4	2172.4	153.2	97.3
	0.5	4406.6	145.3	98.7
	Blank	45.3	234.3	-
	0.1	626.4	187.4	92.8
50	0.2	657.1	182.5	93.1
	0.3	867.6	178.2	94.8
	0.4	1678.8	175.2	97.3
	0.5	3476.8	169.3	98.7

Table 3.66 EIS data for the corrosion of 6061 Al-15 vol. pct. SiC$_{(P)}$ composite in 0.5 M H$_2$SO$_4$ solution containing different concentrations of [MPOEBen$^+$] [Br$^-$] at different temperatures.

Temp (°C)	Inh. Conc. (mM)	R_P (Ω cm^2)	C_{dl} (μF cm^{-2})	η (%)
	Blank	88.6	122.8	-
	0.1	774.4	94.4	88.6
30	0.2	991.0	90.6	91.1
	0.3	1226.6	85.3	92.8
	0.4	2767.6	83.2	96.8
	0.5	7467.1	69.3	98.8
	Blank	59.6	153.3	-
	0.1	561.5	124.2	89.4
35	0.2	751.1	115.2	92.1
	0.3	963.5	109.5	93.8
	0.4	1960.5	103.6	97.0
	0.5	4858.2	98.3	98.8
	Blank	53.7	164.4	-
	0.1	547.7	135.3	90.2
40	0.2	747.1	123.3	92.8
	0.3	895.1	117.8	94.0
	0.4	1951.9	112.8	97.2
	0.5	4447.7	104.3	98.8
	Blank	48.9	180.3	-
	0.1	642.3	154.7	92.4
45	0.2	794.6	147.2	93.8
	0.3	959.4	142.3	94.9
	0.4	1944.8	132.5	97.5
	0.5	4049.4	130.7	98.8
	Blank	31.2	240.3	-
	0.1	532.3	184.5	94.1
50	0.2	602.3	179.3	94.8
	0.3	622.8	171.5	95.0
	0.4	1235.3	167.7	97.5
	0.5	2634.1	165.3	98.8

Table 3.67 Activation parameters for the corrosion of 6061 Al-15 vol. pct. SiC$_{(P)}$ composite in HCl solutions of different concentrations containing [MPOEBen$^+$] [Br$^-$].

Medium Conc. (M)	Inh. Conc. (mM)	E_a (kJ mol^{-1})	$\Delta H^{\#}$ (kJ mol^{-1})	$-\Delta S^{\#}$ (J K^{-1} mol^{-1})
	Blank	46.69	44.09	102.46
	0.01	19.18	16.58	212.66
0.025	0.02	22.34	19.73	205.81
	0.03	22.83	20.23	207.06
	0.04	7.60	4.99	258.28
	0.05	10.76	8.15	249.20
	Blank	77.40	74.80	26.80
	0.01	47.16	44.5	113.19
0.1	0.02	47.92	45.31	114.00
	0.03	37.83	35.22	151.36
	0.04	36.57	33.97	156.06
	0.05	41.71	39.11	141.06
	Blank	35.18	32.58	117.96
	0.01	6.55	3.95	233.61
0.25	0.02	5.68	3.08	239.17
	0.03	0.09	−2.51	262.23
	0.04	3.59	0.98	252.32
	0.05	10.00	7.40	232.66

Table 3.68 Activation parameters for the corrosion of 6061 Al-15 vol. pct. SiC$_{(P)}$ composite in H$_2$SO$_4$ solutions of different concentrations containing [MPOEBen$^+$] [Br$^-$].

Medium Conc. (M)	Inh. Conc. (mM)	E_a (kJ mol^{-1})	$\Delta H^{\#}$ (kJ mol^{-1})	$-\Delta S^{\#}$ (J K^{-1} mol^{-1})
	Blank	23.28	20.63	179.49
	0.1	−0.02	1.33	268.79
0.1	0.2	−1.28	−7.13	243.55
	0.3	0.01	−9.84	236.50
	0.4	−9.74	−2.82	268.33
	0.5	0.02	−9.22	250.99
	Blank	13.33	10.73	202.59
	0.1	−8.58	−11.19	291.88
0.3	0.2	−0.41	−3.02	267.68
	0.3	3.10	0.50	258.18
	0.4	−3.37	−5.98	287.18
	0.5	−1.54	−1.06	276.40
	Blank	21.18	18.57	172.84
	0.1	−10.08	−12.69	292.79
0.5	0.2	0.99	−1.61	259.44
	0.3	1.81	−0.80	258.59
	0.4	9.73	7.12	240.53
	0.5	18.77	18.66	206.63

Table 3.69 Thermodynamic parameters for the adsorption of [MPOEBen$^+$] [Br$^-$] on 6061 Al-15 vol. pct. SiC$_{(P)}$ composite in HCl solutions of different concentrations.

Medium Conc. (M)	Temp (°C)	R^2	Slope	$-\Delta G^0_{ads}$ (kJ mol^{-1})	ΔH^0_{ads} (kJ mol^{-1})	ΔS^0_{ads} (J K^{-1} mol^{-1})
	30	0.999	1.020	45.23		
	35	0.999	1.000	45.96		
0.025	40	0.999	1.007	47.29	19.78	214.0
	45	0.999	1.006	48.41		
	50	0.999	1.002	49.30		
	30	0.999	1.018	45.42		
	35	0.999	0.999	45.75		
0.1	40	0.999	1.003	47.35	24.78	230.6
	45	0.999	1.004	48.80		
	50	0.999	1.002	49.66		
	30	0.999	1.012	45.45		
	35	0.999	0.997	46.02		
0.25	40	0.999	1.003	47.90	33.96	261.1
	45	0.999	1.004	49.14		
	50	0.999	1.004	50.42		

Table 3.70 Thermodynamic parameters for the adsorption of [MPOEBen$^+$] [Br$^-$] on 6061 Al-15 vol. pct. SiC$_{(P)}$ composite in H$_2$SO$_4$ solutions of different concentrations.

Medium Conc. (M)	Temp (°C)	R^2	Slope	$-\Delta G^0_{ads}$ (kJ mol^{-1})	ΔH^0_{ads} (kJ mol^{-1})	ΔS^0_{ads} (J K^{-1} mol^{-1})
	30	0.998	0.979	36.12		
	35	0.998	0.978	39.05		
0.1	40	0.998	0.977	41.74	93.26	428.8
	45	0.998	0.984	43.03		
	50	0.998	0.990	44.85		
	30	0.998	0.980	37.18		
	35	0.998	0.979	37.97		
0.3	40	0.998	0.979	38.68	19.18	185.6
	45	0.998	0.985	39.81		
	50	0.998	0.990	40.90		
	30	0.998	0.979	37.28		
	35	0.998	0.977	37.95		
0.5	40	0.999	0.983	38.95	32.72	230.0
	45	0.999	0.990	40.25		
	50	0.999	0.998	41.88		

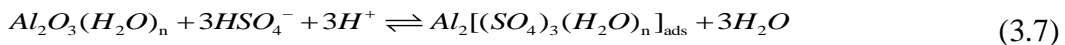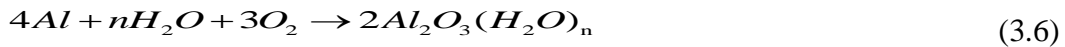## 3.7 PLAUSIBLE MECHANISM OF CORROSION INHIBITION

The following mechanism is proposed for the inhibition action on Al alloy composite in acidic medium taking into consideration, the interaction of [MPOEBen$^+$] [Br$^-$] in sulfuric acid medium with the composite surface.

3.7.1 Corrosion inhibition of the alloy composite by [MPOEBen$^+$] [Br$^-$] in sulfuric acid medium

The corrosion inhibition of the composite is the consequence of the adsorption of the ionic liquid [MPOEBen$^+$] [Br$^-$] on the alloy composite-solution interface. Pure aluminum readily reacts with oxygen in aqueous solution and gets converted into aluminum oxide. The oxide layer thus formed serves as a protective layer preventing corrosion. In dilute solutions of sulfuric acid, the oxide layer may become porous and pervious without complete dissolution as per the results of potentiodynamic polarization measurements. The increase in the corrosion rate with the increase in the concentration of the acid indicates the enhanced corrosion probably due to the increased adsorption of aggressive anions like SO$_4^{2-}$ ions, as discussed under section 3.1.4.1. The corrosion of aluminum in aqueous solution is dependent on the concentration of corrosive anions present in the electrolyte.

3.7.1.1 Anodic reactions

In the absence of [MPOEBen$^+$] [Br$^-$], the protective oxide film undergoes partial dissolution in the presence of 0.1 M sulfuric acid, by the interaction of the hydrated film of aluminum oxide with bisulfate anions when the complex Al$_2$[(SO$_4$)$_3$(H$_2$O)$_n$]$_{ads}$ is formed, as per Equations 3.6 and 3.7 (Arellanes-Lozada et al. 2014). The complex thus formed is soluble in aqueous conditions and therefore gets desorbed from the surface leaving behind free active sites for further attack by the anions like HSO$_4^-$ or SO$_4^{2-}$.

$$4Al + nH_2O + 3O_2 \rightarrow 2Al_2O_3(H_2O)_n \tag{3.6}$$

$$Al_2O_3(H_2O)_n + 3HSO_4^- + 3H^+ \rightleftharpoons Al_2[(SO_4)_3(H_2O)_n]_{ads} + 3H_2O \tag{3.7}$$

In the presence of [MPOEBen$^+$] [Br$^-$], the anodic reactions are modified. The Al$_2$[(SO$_4$)$_3$(H$_2$O)$_n$]$_{ads}$ complex can adsorb HSO$_4^-$ ion and interact electrostatically with the organic cation [MPOEBen$^+$] of the [MPOEBen$^+$] [Br$^-$] molecule (Equation 3.8). Such

interaction between the composite and inhibitor leads to inhibition by physisorption phenomenon. Similarly, the counter ion Br^- present in [MPOEBen$^+$] [Br$^-$] molecule may also be adsorbed on alloy composite surface (Equation 3.9). The $Al_2[Br_6(H_2O)_n]_{ads}$ could also interact electrostatically with the organic cation [MPOEBen$^+$] of [MPOEBen$^+$] [Br$^-$] Equation 3.10 (Arellanes-Lozada et al. 2014). However, the concentration of Br^- in the solution is very less as compared to HSO_4^- ions, and therefore the presence of $Al_2H[SO_4)_4^-(H_2O)_n$ MPOEBen$^+]_{ads}$ is more likely.

$$Al_2[(SO_4)_3(H_2O)_n]_{ads} + HSO_4^- + MPOEBen^+ \rightleftharpoons Al_2H[(SO_4)_4^-(H_2O)_n MPOEBen^+]_{ads} \qquad (3.8)$$

$$Al_2O_3(H_2O)_n + 6Br^- + 6H^+ \rightleftharpoons Al_2[Br_6(H_2O)_n]_{ads} + 3H_2O \qquad (3.9)$$

$$Al_2[Br_6(H_2O)_n]_{ads} + Br^- + MPOEBen^+ \rightleftharpoons Al_2[(Br_7^-(H_2O)_n MPOEBen^+]_{ads} \qquad (3.10)$$
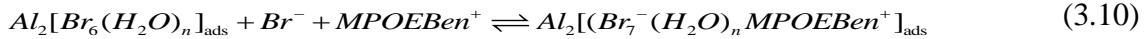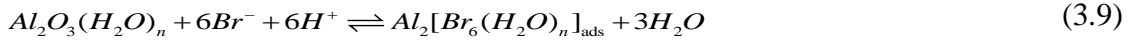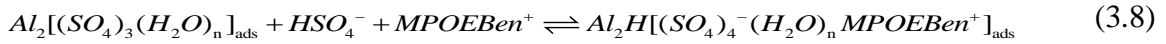
3.7.1.2 Cathodic reactions

In the presence of [MPOEBen$^+$] [Br$^-$], the macromolecular cations [MPOEBen$^+$] compete with protons to occupy active cathodic sites, leading to the formation of [Al-MPOEBen$_{ads}$] Equation 3.11. The size of protons are very less compared to the macromolecular [MPOEBen$^+$] [Br$^-$], therefore, [MPOEBen$^+$] [Br$^-$] can cover larger surface area of the composite and thereby reduces the rate of cathodic reaction and thus helps in controlling the rate of corrosion.

$$Al + MPOEBen^+ + e^- \rightleftharpoons [AlMPOEBen_{ads}] \qquad (3.11)$$
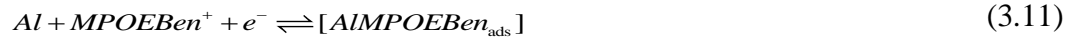
Also, there is pi electron cloud and lone pair of electrons on the O and N atoms of the organic cation. The donation of electrons to the vacant p-orbitals of aluminum atoms may lead to a bond formation between the metal and inhibitor molecule resulting in blocking of metal surface via chemisorption phenomenon (Al-Turkustani et al. 2010). The anchoring of the inhibitor cation either by physisorption or chemisorption provides an 'umbrella' effect on the composite surface due to its large molecular size thereby providing the barrier effect. As stated earlier, the inhibition of corrosion of alloy composite is of mixed type, with both anodic and cathodic control, however, with predominant cathodic control. The thermodynamic parameters and the variation of inhibition efficiency with temperature, suggests predominant chemisorption of the inhibitor, as discussed in earlier

sections. Therefore, it can be concluded that the extent of chemisorption by the inhibitor is more than physisorption.

The inhibition mechanism in hydrochloric acid medium may also occur similar to that of sulfuric acid. The adsorption of the inhibitor cation on the anodic region is given by the Equations 3.12 and 3.13.

$$Al_2O_3(H_2O)_n + 6Cl^- + 6H^+ \rightleftharpoons Al_2[Cl_6(H_2O)_n]_{ads} + 3H_2O \qquad (3.12)$$

$$Al_2[Cl_6(H_2O)_n]_{ads} + Cl^- + MPOEBen^+ \rightleftharpoons Al_2[(Cl_7^-(H_2O)_n MPOEBen^+]_{ads} \qquad (3.13)$$
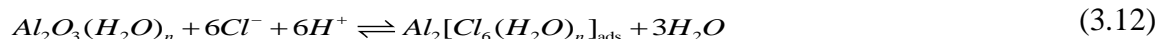
The adsorption of the inhibitor at the cathodic region and chemisorption on the composite surface are same as that in the case of sulfuric acid.

3.7.2 Effect of ionic concentration of the medium

In both the electrolyte media, on increasing the medium concentration (i.e. 0.025 M to 0.25 M HCl and 0.1 M to 0.5 M H_2SO_4), it was observed that the efficiency of the inhibitor is increased. This observation could be attributed to the enhanced mode of physisorption due to the increased concentration of HSO_4^- and Cl^- as per Equations 3.8 and 3.13 apart from chemisorption phenomenon. Also, as the concentration of sulfate or chloride increases, the active dissolution of the surface oxide film increases, which in turn would bring about increased adsorption of the inhibitor as per Equation 3.8 and 3.13, respectively. The dissolution of the surface protective oxide layer also exposes more neutral aluminum atoms to inhibitor molecules for the chemisorption process through electron rich center of the inhibitor. For all the ILs, the inhibition efficiencies achieved in both the chloride and the sulfate media are comparable. However, chloride media require lower concentrations of inhibitors as compared to that required in sulfate medium.

3.8 DIFFERENCE IN THE INHIBITION EFFICIENCIES AMONG THE SYNTHESIZED ILs

The inhibition abilities of synthesized ionic liquids towards corrosion of 6061 Al-15 vol. pct. SiC$_{(P)}$ composite in acidic media are schematically presented in Figure 3.67. The figure shows four ILs with same basic chain group skeleton but with different substituted functional groups. The overall inhibition of corrosion may be attributed the interaction of electron rich centers (i.e., aromatic rings) in the ILs with the metal surface as depicted in

the figure. The order of the inhibition efficiency was [OPEIm$^+$] [Br$^-$] < [MPOEIm$^+$] [Br$^-$] < [OPEBen$^+$] [Br$^-$] < [MPOEBen$^+$] [Br$^-$].

Of the four synthesized ILs, the [OPEIm$^+$] [Br$^-$], is with the simplest skeleton. This is a symmetric molecule containing benzyl and imidazole groups. These pi electron rich centers interact with the electron deficient composite surface and inhibit corrosion. When this molecule was substituted with methoxy (−OCH$_3$) group, [MPOEIm$^+$] [Br$^-$] was obtained. The methoxy group is an electron donor due to lone pairs of electrons on oxygen atom and is involved in resonance increasing the electron density of the benzyl group (Noor and Al-Moubaraki 2008). This causes increased interaction of the benzyl group with the composite surface. Further, in the case of [OPEBen$^+$] [Br$^-$] the imidazole of the basic skeleton chain is replaced with benzimidazole. This adds to the bulk of the molecule as well as increased pi electron cloud on the basic skeleton. The effect of larger molecular structure along with pi electron rich benzimidazole moiety fulfils the pre-requisite for a good corrosion inhibitor as compared to other two ILs. However, both methoxy and benzimidazole substitutions on the basic skeleton of [MPOEBen$^+$] [Br$^-$] contributed largely to the resonance as well as increased molecular size thereby enriching the electron donor ability of the molecule and larger surface coverage on the composite. This results in higher efficiency of the inhibitor. Apart from the pi electron rich centers, lone pairs of N/O atoms in all the four ILs may also interact with the vacant orbitals of aluminum. All ILs effectively controlled the corrosion in both the media when present in their respective concentrations. However, the difference in optimal concentration of the ILs may be attributed to change in molecular weight and structure. Molecules with high molecular weight and larger structure are known to inhibit corrosion at relatively lower concentrations as they cover larger surface area of the corroding surface as compared to low molecular weight and smaller molecules. The efficiency of all the ILs in both the media increased with both concentration of the medium and temperature. The Figure 3.68 (a) and 3.68 (b) represent the optimal concentrations and inhibition efficiencies for ILs as corrosion inhibitors at 50 °C in 0.25 M hydrochloric acid and 0.5 M sulfuric acid media, respectively.
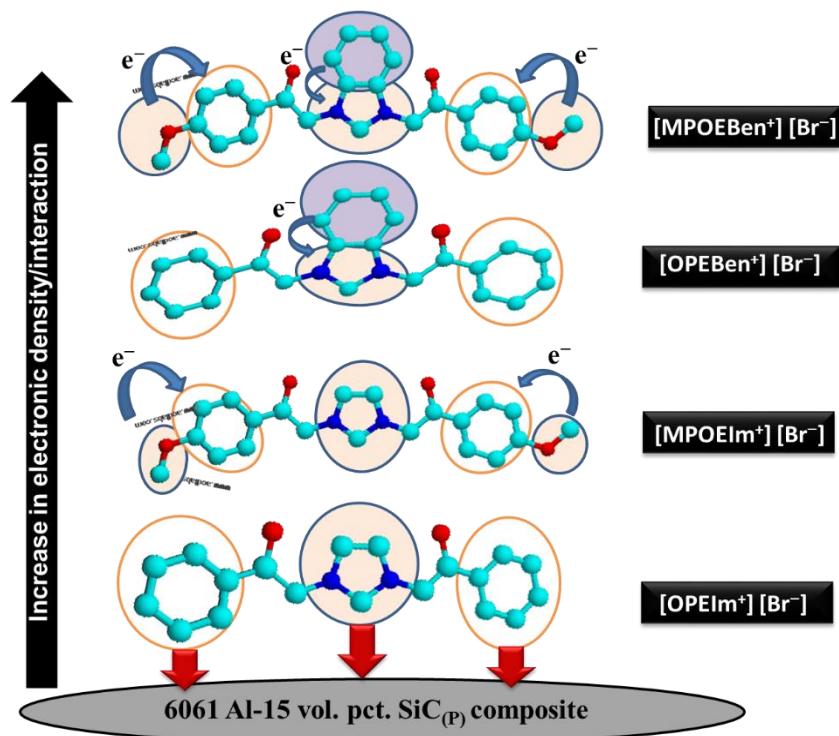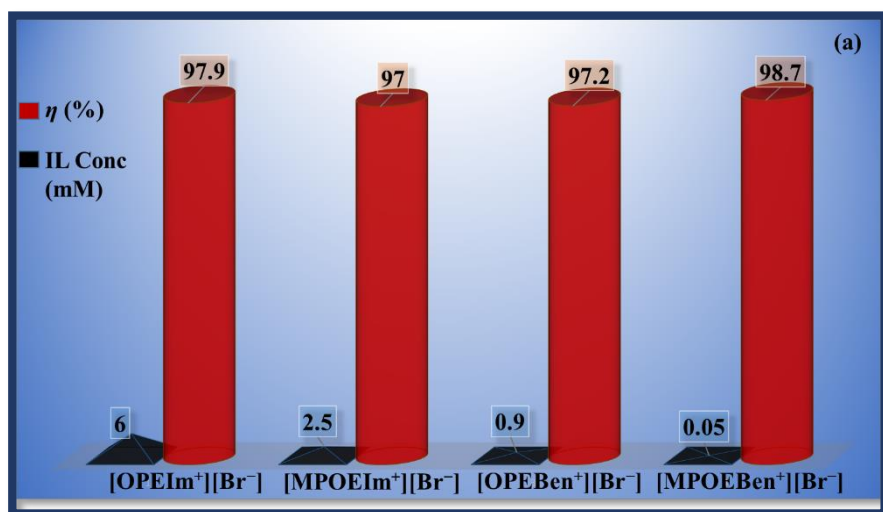
Figure 3.67 The schematic representation of the inhibition abilities of synthesized ionic liquids towards corrosion of 6061 Al-15 vol. pct. SiC$_{(P)}$ composite in acidic media.
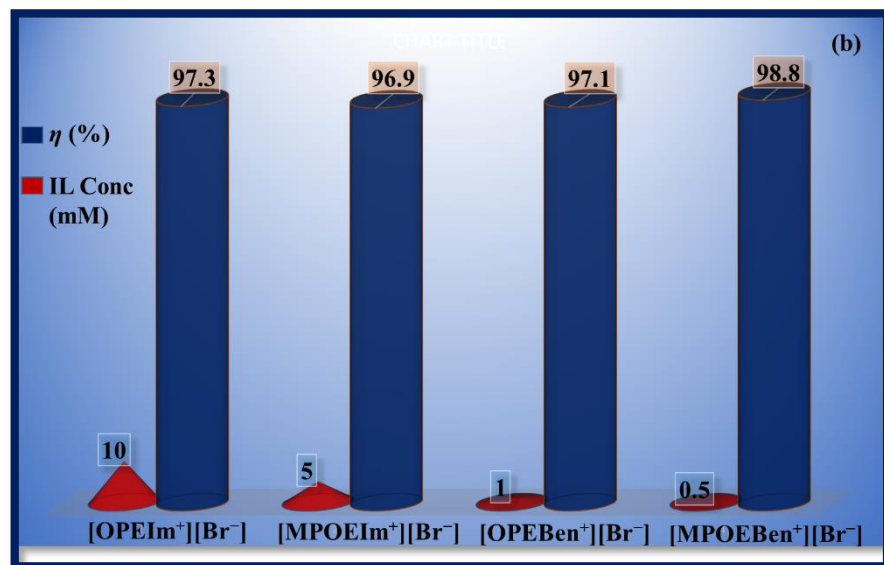
Figure 3.68 The optimal concentrations and inhibition efficiencies of ILs as corrosion inhibitors at 50 °C in (a) 0.25 M HCl and (b) 0.5 M H$_2$SO$_4$ media.

4.1 SUMMARY

The corrosion behavior of 6061 Al-15 vol. pct. $SiC_{(P)}$ composite in hydrochloric acid and sulfuric acid media was investigated using electrochemical techniques like potentiodynamic polarization measurements and electrochemical impedance spectroscopy. The effect of variation in the medium concentration and temperature were studied. The activation parameters for the corrosion reaction were evaluated. Surface morphology and surface compositional analyses were carried out by recording SEM images and EDX spectra. The destabilization of the oxide film due to the corrosive anions was found to contribute to the corrosion of the composite in the acidic media. The surface analyses results also indicated surface unevenness and severe pitting around the SiC particles. Presence of corrosive anion peaks in the EDX as compared to freshly polished composite surface affirmed the attack of anions on the surface of the composite.

Four ionic liquids namely, 1,3-bis(2-oxo-2-phenylethyl)-1*H*-imidazol-3-ium bromide ([OPEIm$^+$] [Br$^-$]), 1,3-bis[2-(4-methoxyphenyl)-2-oxoethyl]-1*H*-imidazol-3-ium bromide ([MPOEIm$^+$] [Br$^-$]), 1,3-bis(2-oxo-2-phenylethyl)-1*H*-benzimidazol-3-ium bromide ([OPEBen$^+$] [Br$^-$]) and 1,3-bis[2-(4-methoxyphenyl)-2-oxoethyl]-1*H*-benzimidazol-3-ium bromide ([MPOEBen$^+$] [Br$^-$]) were synthesized by slight modification of the procedure from the literature (Roman et al. 2010). The synthesized ILs were characterized using NMR, LC-MS and FT-IR spectroscopy. Single crystal XRD was analyzed to confirm the structure of the new IL. The ILs were then investigated for their corrosion inhibition ability on the 6061 Al-15 vol. pct. $SiC_{(P)}$ composite in hydrochloric acid and sulfuric acid media using potentiodynamic polarization and EIS methods. The inhibitors showed mixed control on both the anodic and the cathodic reactions, but predominantly on the cathodic reaction, as reflected by the shift of the corrosion potential to the cathodic side in the Tafel plots. The surface morphologies of the corroded composite surface in the presence of inhibitors were analyzed by recording their SEM images and the surface compositions were determined by EDX spectral analyses. The effect of temperature, concentration of acids in the corrosive medium and concentration of the ionic

liquids on the inhibition efficiencies of the ILs were evaluated. The activation parameters for the corrosion of the composite and thermodynamic parameters for the adsorption of ionic liquids on the surface of the composite were also calculated. The corrosion inhibition by ILs were both by physisorption and chemisorption modes, but predominantly by chemisorption and were affirmed from the results of electrochemical measurements where, inhibition efficiencies increased with the increase in temperature. The adsorption of the inhibitor followed Langmuir adsorption isotherm with minor deviation of slope values from unity, indicating possible weak intermolecular interactions of the adsorbed inhibitor molecules. The plausible inhibition mechanism was also proposed. The surface protective oxide film dissolution at increasing medium concentrations facilitated more neutral aluminum atoms to interact with electron rich centers of the inhibitor IL and promoted the chemisorption mode of adsorption. Physisorption of inhibitor occurred through mere attraction of inhibitor cations towards the previously adsorbed corrosive anions on the surface of the composite. SEM and EDX analyses provided sufficiently fair, visual and qualitative support to the corrosion inhibition by adsorption phenomenon. Out of the four synthesized ILs, the new IL i.e. $[MPOEBen^+]$ $[Br^-]$ showed highest inhibition ability of 98.8% in both the media at relatively lower concentrations, due to the presence of electron rich moieties and also due to its macro-molecular size which cover the larger surface area of the composite.

4.2 CONCLUSIONS

On the basis of the research data, the following conclusions are drawn:

1. The higher medium concentration and higher temperature causes dissolution/destabilization of surface protective oxide layer and increases the rate of corrosion.

2. All the four synthesized ionic liquids are good corrosion inhibitors for the corrosion of 6061 Al-15 vol. pct. $SiC_{(P)}$ composite in hydrochloric acid and sulfuric acid in the concentration ranges of acids studied.

3. Potentiodynamic polarization measurements indicate that the inhibitors act as mixed inhibitors with predominant cathodic control in both the media.

4. The inhibition efficiency increases both with the increase in acid concentration and with the increase in temperature.

5. The inhibitors adsorb on the composite surface by both physisorption and chemisorption mode, but with predominant chemisorption and follow Langmuir adsorption isotherm.

6. The amount of inhibitor required for effective inhibition is less in HCl medium than in H_2SO_4 medium, however extent of inhibition is comparable in both the media.

7. The order of inhibition efficiency is [OPEIm$^+$] [Br$^-$] < [MPOEIm$^+$] [Br$^-$] < [OPEBen$^+$] [Br$^-$] < [MPOEBen$^+$] [Br$^-$] in both the media.

4.3 SCOPE FOR FURTHER WORK

1. Theoretical investigations by modeling and simulation studies may be carried out for accomplishing details on effect of medium concentration, temperature and inhibitor concentration variation.

2. Synthesis of novel eco-friendly ILs as corrosion inhibitors which may be tested for micro/nano-capsulation in shell-layers of the self-healing polymer coatings that can be released during break in the coating and inhibit corrosion in the presence of corrosive species.

3. Application of ILs as corrosion inhibitors in real examples like industrial water heaters, pickling baths, etc., may be explored.

Abdallah, M. (2004). "Antibacterial drugs as corrosion inhibitors for corrosion of aluminium in hydrochloric solution." *Corros. Sci.*, 46, 1981-1996.

Adejo, S.O., Yiase, S.G., Ahile, T.G., Tyohemba, T.G. and Gbertyo, J.A. (2013). "Inhibitory effect and adsorption parameters of extract of leaves of *Portulaca oleracea* of corrosion of aluminum in H_2SO_4 solution." *Arch. Appl. Sci. Res.*, 5(2013), 25–32.

Ahmad, Z., Paulette, P.T. and Aleem, B.J.A. (2000). "Mechanism of localized corrosion of aluminium- silicon carbide composites in a chloride containing environment." *J. Mater. Sci.*, 35, 2573–2579.

Aircraft accident report, Aloha Airlines, flight 243, Boeing 737-200, N73711, Near Maui, Hawaii, April 28, 1988, NTSB Report No. NTSB/AAR-89/03, National Transportation Safety Board, Washington, D.C., June 1989.

Akbarzadeh, E., Ibrahim, M.N.M. and Rahim, A.A. (2011). "Corrosion inhibition of mild steel in near neutral solution by Kraft and Soda lignins extracted from oil palm empty fruit bunch." *Int. J. Electrochem. Sci.*, 6, 5396–5416.

Alaneme, K.K. and Bodunrin, M.O. (2011). "Corrosion behavior of alumina reinforced aluminium (6063) metal matrix composites." *JMMCE*, 10(12), 1153-1165.

Al-Turkustani, A.M., Arab, S.T. and Al-Dahiri, R.H. (2010). "Aloe plant extract as environmentally friendly inhibitor on the corrosion of aluminum in hydrochloric acid in absence and presence of iodide ions." *Mod. Appl. Sci.*, 4(5), 105–124.

Ameer, M.A., Fekry, A.M. and Othman, A. (2014). "Electrochemical investigation of green inhibitor adsorption on low-carbon steel in produced water." *Int. J. Electrochem. Sci.*, 9, 1964–1985.

Ansari, K.R, Yadav, D.K., Ebenso, E.E. and Quraishi, M.A. (2012). "Novel and effective pyridyl substituted 1,2,4-triazole as corrosion inhibitor for mild steel in acid solution." *Int. J. Electrochem. Sci.*, 7, 4780–4799.

Aoun, S.B. (2013). "Gravimetric and temperature effect studies of a novel imidazolium-based ionic liquid as a corrosion inhibitor for carbon steel in molar hydrochloric acid." *Der. Pharm. Chemica.*, 5(3), 294-304.

Arellanes-Lozada, P., Olivares-Xometl, O., Guzman-Lucero, D., Likhanova, N., Dominguez-Aguilar, M., Lijanova, I. and Arce-Estrada, E. (2014). "The inhibition of aluminum corrosion in sulfuric acid by poly(1-vinyl-3-alkyl-imidazolium hexafluorophosphate)." *Materials (Basel)*, 7(2014), 5711–5734.

Arshadi, M., Amiri, M.J. and Mousavi, S. (2014). "Kinetic, equilibrium and thermodynamic investigations of Ni(II), Cd(II), Cu(II) and Co(II) adsorption on barley straw ash." *Water. Res. Ind.*, 6, 1-17.

Arukalam, I.O., Madu, I.O., Ijomah, N.T., Ewulonu, C.M. and Onyeagoro, G.N. (2014). "Acid corrosion inhibition and adsorption behavior of ethyl hydroxyethyl cellulose on mild steel corrosion, *J. Mater.*, 2014, 1–11.

Ashassi-Sorkhabi, H. and Es'haghi, M. (2009). "Corrosion inhibition of mild steel in acidic media by [BMIm] Br ionic liquid." *Mater. Chem. Phys.*, 114, 267-271.

Ashassi-Sorkhabi, H., Ghasemi, Z. and Seifzadeh, D. (2005). "The inhibition effect of some amino acids towards the corrosion of aluminum in 1 M HCl + 1 M H_2SO_4 solution." *Appl. Surf. Sci.*, 249, 408-418.

Ashassi-Sorkhabi, H., Shabani, B., Aligholipour, B. and Seifzadeh D. (2006). "The effect of some Schiff bases on the corrosion of aluminum in hydrochloric acid solution." *Appl. Surf. Sci.*, 252, 4039-4047.

ASTM Standard G102. (1999). "Standard practice for calculation of corrosion rates and related information from electrochemical measurements." *ASTM International*, West Conshohocken, PA.

Ating, E.I., Umoren, S.A., Udousoro, I.I., Ebenso, E.E. and Udoh, A.P. (2010). "Leaves extract of *Ananas sativum* as green corrosion inhibitor for aluminium in hydrochloric acid solutions." *Green. Chem. Lett. Rev.*, 3(2), 61-68.

Atta, A.M., El-Mahdy, G.A., Al-Lohedan, H.A. and Ezzat, A.R.O. (2015). "A new green ionic liquid-based corrosion inhibitor for steel in acidic environments." *Molecules*, 20, 11131-11153.

Avci, G. (2008). "Inhibitor effect of N,N′-methylenediacrylamide on corrosion behavior of mild steel in 0.5 M HCl." *Mater. Chem. Phys.*, 112, 234–238.

Aytac, A., Ozmen, U. and Kabasakaloglu, M. (2005). "Investigation of some Schiff bases as acidic corrosion of alloy AA3102." *Mater. Chem. Phys.*, 89, 176-181.

Babic, R., Metikos, M. and Grubac, Z. (1998). "Corrosion protection of aluminum in acidic chloride solutions with nontoxic inhibitors." *J. Appl. Electrochem.*, 28(1998), 433–439.

Behpour, M., Ghoreishi, S.M., Soltani, N. and Salvati-Niasari, M. (2009). "The inhibitive effect of some bis-N, S-bidentate Schiff bases on corrosion behavior of 304 stainless steel in hydrochloric acid solution." *Corros. Sci.*, 51, 1073-1082.

Bentiss, F., Lebrini, M. and Lagrenee, M. (2005). "Thermodynamic characterization of metal dissolution and inhibitor adsorption processes in mild steel/ 2,5-bis(n-thienyl)-1,3,4-thiadiazoles/hydrochloric acid system." *Corros. Sci.*, 47, 2915–2931.

Bhat, M.S.N., Surappa, M.K. and Sudhaker Nayak, H.V. (1991). "Corrosion behaviour of silicon carbide particle reinforced 6061/Al alloy composites." *J. Mater. Sci.*, 26(18), 4991-4996.

Bobic. B., Mitrovic, S., Babic, M. and Bobic, M. (2010). "Corrosion of metal-matrix composites with aluminium alloy substrate." *Tribol. Ind.*, 32, 3-9.

Borsato, D., Galvan, D., Pereira, J.L., Orives, J.R., Angilelli, K.G. and Coppo, R.L. (2014). "Kinetic and thermodynamic parameters of biodiesel oxidation with synthetic antioxidants: Simplex centroid mixture design." *J. Braz. Chem. Soc.*, 25, 1984–1992.

Boukerch, I., Djerad S., Benmansour, L., Tifouti, L. and Saleh, K. (2014). "Degradability of aluminum in acidic and alkaline solutions." *Corros. Sci.*, 78, 343-352.

Campbell, C. (2010). *"Introduction to composite materials, structural composite Materials."* ASM International, Ohio, 1–29.

Candan, S. and Bilgic, E. (2004). "Corrosion behavior of Al–60 vol.% SiC$_{(p)}$ composites in NaCl solution." *Mater. Lett.*, 58, 2787-2790.

Cicek, V. (2013). "Cathodic Protection." *Cathodic protection industrial solutions for protecting against corrosion*, Scrivener, M. and Carmical, P., eds., Scrivener Publishing LLC, Salem, Massachusetts, 83–84.

Cullinan, P. (2004). *Environmental toxicology and human health – Vol. I -Case Study of the Bhopal Incident,* Eolss Publishers, Paris, France.

Deng, S. and Li, S. (2012). "Inhibition by *Jasminum nudiflorum* Lindl. leaves extract of the corrosion of aluminium in HCl solution." *Corros. Sci.*, 64, 253-262.

Dinodi, N. and Shetty, A.N. (2014). "Alkyl carboxylates as efficient and green inhibitors of magnesium alloy ZE41 corrosion in aqueous salt solution." *Corros. Sci.*, 85, 411–427.

Earle, M.J. and Seddon, K.R. (2002). "Ionic liquids:Green solvents for the future, in: In clean solvents." Abraham, M., ed., *ACS Symposium Series; American Chemical Society*: Washington, DC, 10–25.

Eid, S., Abdallah, M. and Kamar, E.M. (2015). "Corrosion inhibition of aluminum and aluminum silicon alloys in sodium hydroxide solutions by methyl cellulose." *J. Mater. Environ. Sci.*, 6, 892–901.

El Bribri, A., Tabyaoui, M., Tabyaoui, B., El Attari, H. and Bentiss, F. (2013). "The use of *Euphorbia falcata* extract as eco-friendly corrosion inhibitor of carbon steel in hydrochloric acid solution." *Mater. Chem. Phy.*, 141, 240-247.

El Etre, A.Y. (2001). "Inhibition of acid corrosion of aluminum using vanillin." *Corros. Sci.*, 43, 1031-1039.

El Mouden, O. ID., Anejjar, A., Messali, M., Salghi, R., Ismat, H.A. and Hammouti, B. (2014). "The effect of new pyridazinium-based ionic liquid derivative as corrosion inhibitor for carbon steel in 1M HCl solution." *Chem. Sci. Rev. Lett.*, 3(11), 579-588.

El Rehim, S.S.A., Hassan, H.H. and Amin, M.A. (2001). "Corrosion inhibition of aluminum by 1,1(lauryl amido)propyl ammonium chloride in HCl solution." *Mater. Chem. Phys.*, 70, 64-72.

El-Mahdy, G.A., Atta, A.M., Al-Lohedan, H.A. and Ezzat, A.R.O. (2015). "Influence of green corrosion inhibitor based on chitosan ionic liquid on the steel corrodibility in chloride solution." *Int. J. Electrochem. Sci.*, 10, 5812 – 5826.

El-Sherbini, E.E.F., Abd-El-Wahab, S.M. and Deyab, M.A. (2003). "Studies on corrosion inhibition of aluminum in 1.0 M HCl and 1.0 M H_2SO_4 solutions by ethoxylated fatty acids." *Mater. Chem. Phys.*, 82, 631-637.

Evans, U.R. (1923). *Metals and metallic compounds*, Longmans and Green, eds., London.

Fares, M.F., Maayta, A.K. and Al-Qudah, M.M. (2012). "Pectin as promising green corrosion inhibitor of aluminum in hydrochloric acid solution." *Corros. Sci.*, 60, 112-117.

Ferrando, W.A. (1989). "Review of corrosion and corrosion control of magnesium alloys and composites." *J. Mater. Eng.*, 11, 299-313.

Fischer, H. (1972). "Modes of inhibiting electrode processes (corrosion included) and their experimental discrimination. Definition, nomenclature and classification of modes of inhibition in electrochemical electrode reactions." *Mater. Corros.*, 23, 445-452.

Flick, E.W. (1993). *Corrosion inhibitors: An industrial guide*, Second edition, Noyes Publications, Park Ridge, New Jersey.

Fontana, M.G. (1986). *Corrosion engineering*, Third edition, Mc Graw Hill, New York.

Ford, F.P., Burstein, G.T. and Hoar T.P. (1980). "Bare surface reaction rates and their relation to environment controlled cracking of aluminum alloys." *J. Electrochem. Soc.*, 127(6), 1325-1331.

Fouda, A.S. and Abdallah, A.M. (2014). "Corrosion inhibition of aluminum–silicon alloy in 1 M HCl solution using phenazone and aminophenazone." *Arab. J. Sci. Eng.*, 39(7), 5363-5371.

Fouda, A.S., Al-Sarawy, A.A., Ahmed, F. Sh. and El-Abbasy, H.M. (2009). "Corrosion inhibition of aluminum 6063 using some pharmaceutical compounds." *Corros. Sci.*, 51, 485–492.

Gadag, R.V. and Shetty, A.N. (2010). *Engineering chemistry*, Second edition, I.K. International Publishing house Pvt. Ltd, New Delhi.

Gao, H., Li, Q., Dai, Y., Luo, F. and Zhang, H.X. (2010). "High efficiency corrosion inhibitor 8-hydroxyquinoline and its synergistic effect with sodium dodecylbenzenesulphonate on AZ91D magnesium alloy." *Corros. Sci.*, 52, 1603–1609.

Gnecco, F. and Beccaria, A.M. (1999). "Corrosion behaviour of Al-Si/SiC composite in sea water." *Br. Corros. J.*, 34 (1), 57-62.

Guzman-Lucero, D., Olivares-Xometl, O., Martinez-Palou, R., Likhanova, N.V., Dominguez-Aguilar, M.A. and Garibay-Febles, V. (2011). "Synthesis of selected vinylimidazolium ionic liquids and their effectiveness as corrosion inhibitors for carbon steel in aqueous sulfuric acid." *Ind. Eng. Chem. Res.*, 50(12), 7129-7140.

Hakerman, N. (1962). "Recent advances in understanding of organic inhibitors." *Corrosion*, 18, 332-335.

Hameed, R.S.A., Ismail, E.A., Abu- Nawwas, A.H. and Al-Shafey, H. (2015). "Expired voltaren drugs as corrosion inhibitor for aluminium in hydrochloric acid." *Int. J. Electrochem. Sci.*, 10, 2098-2109.

Han, X., Lee, R., Chen, T., Luo., J., Lu, Y. and Huang, K.-W. (2013). "Kinetic evidence of an apparent negative activation enthalpy in an organocatalytic process." *Sci. Rep.*, 3, 2557, doi: 10.1038/srep02557.

Hegazy, M.A., Abd El Rehim, S.S., Badawia, A.M. and Ahmed, M.Y. (2015). "Studying the corrosion inhibition of carbon steel in hydrochloric acid solution by 1-dodecyl-methyl-1H-benzo [d] [1,2,3]triazole-1-ium bromide." *RSC Adv.*, 5, 49070-49079.

Hickling, A. and Salt, F.W. (1941). "Studies in hydrogen overvoltage at high current densities: Part IV- The influence of concentration, anions, temperature and catalytic poisons." *Trans. Faraday Soc.*, 37, 333-339.

Hihara, L.H. and Latanision, R.M. (1994). "Corrosion of metal matrix composites." *Int. Mater.Rev.*, 39, 245-264.

Hoar, T.P. (1948). *Pittsburg Int. Conf. of surface reactions*, Pittsburg corrosion publishing co.,127.

Hu, J., Zeng, D., Zhang, Z., Shi, T., Song, G.-L. and Guo, X. (2013). "Hydroxy-4-methoxy-acetophenone as an environment-friendly corrosion inhibitor for AZ91D magnesium alloy." *Corros. Sci.*, 74, 35–43.

Ibrahim, M.A.M., Messali, M., Moussa, Z., Alzahrani, A.Y., Alamry, S.N. and Hammouti, N. (2011). "Corrosion inhibition of carbon steel by imidazolium and pyridinium cations ionic liquids in acidic environment." *Port. Electrochim. Acta*, 29(6), 375-389.

Ibrahim, T.H. and Zour, M.A. (2011). "Corrosion inhibition of mild steel using Fig leaves extract in hydrochloric acid solution." *Int. J. Electrochem. Sci.*, 6, 6442–6455.

Ihom, A.P., Nyior, G.B., Nor Iv, J., Segun, S. and Ogbodo. J. (2012). "Evaluation of the corrosion resistance of aluminum alloy matrix/ 2.5% particulate glass reinforced composite in various media." *IJST*, 1(10), 560-568.

Iofa, Z.A., Batrakov, V.V. and Cho-Ngok-Ba. (1964). "Influence of anion adsorption on the action of inhibitors on the acid corrosion of iron and cobalt." *Electrochim. Acta*, 9, 1645-1653.

Ismail, A.S. (2015). "Corrosion behavior of aluminum-silicon-copper-manganese alloy in sulfuric acid medium." *Silicon*, doi: 10.1007/s12633-014-9226-y.

Khaled, K.F. (2010). "Electrochemical investigation and modelling of corrosion inhibition of aluminum in molar nitric acid using some sulphur-containing amines." *Corros. Sci.*, 52, 2905–2916.

Khupse, N.D. and Kumar, A. (2010). "Ionic liquids : New materials with wide applications", *Indian J. Chem. A.*, 49(A), 635–648.

Kini, A.U., Shetty, P., Shetty, S.D. and Isloor, M.A. (2011). "Corrosion inhibition of 6061 aluminium alloy/SiCp composite in hydrochloric acid medium using 3-chloro-1-benzothiophene-2-carbohydrazide". *Ind. J. Chem. Tech.*, 18(November), 439–445.

Kini, A.U., Shetty, P., Shetty, S.D., Isloor, M.A. and Herle, R. (2012). "Propanoyl(1*Z*)-N-(2,6-dimethylphenyl)-2 oxopropanehydrazonoate as inhibitor for corrosion of 6061 Al alloy 15 % (v) SiC$_{(p)}$ composite in hydrochloric acid media." *IIUM Eng. J.*, 13(2), 121-129.

Kini, A.U., Shetty, P., Shetty, S.D., Isloor, M.A. and Herle, R. (2010). "The inhibition action of ethyl-2-phenyl hydrozono-3-oxobutyrate on the corrosion of 6061 Al alloy / SiCp composite in hydrochloric acid medium." *J. Chil. Chem. Soc.*, 1, 56–60.

Knag, M. (2006). "Fundamental behavior of model corrosion inhibitors." *J. Dispers. Sci. Technol.*, 27, 587-597.

Ku, S.-Y. and Lu, S.-Y. (2011). "Inexpensive room temperature ionic liquids for low volatility electrolytes of dye-sensitized solar cells." *Int. J. Electrochem. Sci.*, 6, 5219–5227.

Kumari, P.D.R, Nayak, J. and Shetty, A.N. (2012). "Corrosion behavior of 6061/Al-15 vol. pct. SiC$_{(p)}$ composite and the base alloy in sodium hydroxide solution." *Arab. J. Chem.*, doi: 10.1016/j.arabjc.2011.12.003.

Kumari, P.D.R., Nayak, J. and Shetty, A.N. (2011a). "3-Methyl-4-amino-5-mercapto-1,2,4-triazole as corrosion inhibitor for 6061/Al-15 (vol.%) SiC$_{(p)}$ composite in 0.5 M sodium hydroxide solution." *J. Mater. Environ. Sci.*, 2(4), 387-402.

Kumari, P.D.R., Nayak, J. and Shetty, A.N. (2011b). "3-Ethyl-4-amino-5-mercapto-1,2,4-triazole as corrosion inhibitor for 6061-alloy in sodium hydroxide solution." *Port. Electrochim. Acta*, 29(6), 445-462.

Kumari, P.D.R., Nayak, J. and Shetty, A.N. (2014). "Corrosion inhibition of 6061 Al-15 vol. pct. SiCp composite in sodium hydroxide solution by 4-amino-5-(4-nitrophenyl)-4H-1,2,4-triazole-3-thiol." *Procedia Mater. Sci.*, 5, 181-187.

Lamaka, S.V., Zheludkevich, L., Yasakau, K.A., Montemorb, M.F. and Ferreira, M.G.S. (2007). "High effective organic corrosion inhibitors for 2024 aluminium alloy." *Electrochim. Acta*, 52, 7231-7247.

Lebrini, M., Traisnel, M., Lagrenee, M., Mernari, B. and Bentiss F. (2008). "Inhibitive properties, adsorption and a theoretical study of 3,5-bis(n-pyridyl)-4-amino-1,2,4-triazoles as corrosion inhibitors for mild steel in perchloric acid." *Corros. Sci.*, 50(2), 4473-4479.

Li, X., Deng, S. and Fu, H. (2011a). "Triazolyl blue tetrazolium bromide as a novel corrosion inhibitor for steel in HCl and H_2SO_4 solutions." *Corros. Sci.*, 53, 302-309.

Li, X., Deng, S. and Fu, H. (2011b). "Inhibition by tetradecylpyridinium bromide of the corrosion of aluminium in hydrochloric acid solution." *Corros. Sci.*, 53(4), 1529-1536.

Likhanova, N.V., Olivares-Xometl, O., Guzman-Lucero, D., Dominguez-Aguilar, M.A., Nava1, N., Corrales-Luna, M. and Mendoza, M.C. (2011). "Corrosion inhibition of carbon steel in acidic environment by imidazolium ionic liquids containing vinyl-hexafluorophosphate as anion." *Int. J. Electrochem. Sci.*, 6, 4514-4536.

Maayta, A.K. and Al-Rawashdeh, N.A.F. (2004). "Inhibition of acidic corrosion of pure aluminum by some organic compounds." *Corros. Sci.*, 46, 1129-1140.

Manamela, K.M., Murulana, L.C., Kabanda, M.M. and Ebenso, E.E. (2014). "Adsorptive and DFT studies of some imidazolium based ionic liquids as corrosion inhibitors for zinc in acidic medium." *Int. J. Electrochem. Sci.*, 9, 3029–3046.

Mansfeld, F., Tsai, C.H. and Shih, H. (1992). "Software for simulation and analysis of electrochemical impedance spectroscopy (EIS) data." *Computer modeling in corrosion*, Munn, R.S., ed., ASTM, Philadelphia, 186-196.

Masel, R.I. (1996). "Adsorption II – Adsorption isotherms." *Principles of adsorption and reaction on solid surfaces*, Wiley Interscience, New York, 235-302.

McCafferty, E. (2010). *Introduction to corrosion science*, Springer, New York.

Mercier, D., Herinx, M., and Barthes-Labrousse, M.-G. (2010). "Influence of 1,2-diaminoethane on the mechanism of aluminium corrosion in sulphuric acid solutions." *Corros. Sci.*, 52, 3405–3412.

Messaadia, L., El Mouden, O. ID., Anejjar, A., Messali, M., Salghi, R., Benali, O., Cherkaoui, O. and Lallam. A. (2015). "Adsorption and corrosion inhibition of new

synthesized pyridazinium-based ionic liquid on carbon steel in 0.5 M H_2SO_4." *J. Mater. Environ. Sci.*, 6(2), 598-606.

Mizuno, K., Nylund, A. and Olefjord, I. (2001). "Surface reactions during pickling of an aluminium-magnesium-silicon alloy in phosphoric acid." *Corros. Sci.*, 43, 381-396.

Musa, A.Y., Mohamad, A.B., Kadhum, A.A.H. and Chee, E.P. (2011). "Galvanic corrosion of aluminum alloy (Al2024) and copper in 1.0 M nitric acid." *Int. J. Electrochem. Sci.*, 6, 5052–5065.

Naeem, H.T., Mohammed, K.S. and Ahamad, K.R. (2014). "The role of cobalt and nickel intermetallic phases on the mechanical properties and microstructure evolution of Al-Zn-Mg-Cu alloys." *Mater. Res.*, 17(6), 1663-1676.

Nayak, J. and Hebbar, K.R. (2008). "Corrosion inhibition of T-6 treated 6061 Al $SiC_{(p)}$ composite in hydrochloric acid". *Trans. Indian Inst. Met.*, 61(June), 221–224.

Neil, W. and Garrard, C. (1994). "The corrosion behaviour of aluminium-silicon carbide composites in aerated 3.5% sodium chloride." *Corros. Sci.*, 36, 837-851.

Noor, E. A. (2007). "Temperature effects on the corrosion inhibition of mild steel in acidic solutions by aqueous extract of fenugreek leaves." *Int. J. Electrochem. Res.*, 2, 996–1017.

Noor, E.A. (2009). "Evaluation of inhibitive action of some quaternary N-heterocyclic compounds on the corrosion of Al–Cu alloy in hydrochloric acid." *Mater. Chem. Phys.*, 114, 533-541.

Noor, E.A. and Al-Moubaraki, A.H. (2008). "Thermodynamic study of metal corrosion and inhibitor adsorption processes in mild steel/1-methyl-4[4'(-X)-styryl pyridinium iodides/hydrochloric acid systems." *Mater. Chem. Phys.*, 110,145-154.

Nunez-Lopez, C.N., Habazaki, H., Skeldon, P., Thompson, G.E., Karimzadeh, H., Lyons, P. and Wilks, T.E. (1996). "An investigation of microgalvanic corrosion using a model magnesium-silicon carbide metal." *Corros. Sci.*, 38, 1721–1729.

Obot, I.B. and Obi-Egbedi, N.O. (2008). "Fluconazole as an inhibitor for aluminium corrosion in 0.1M HCl." *Colloids and Surfaces A: Physicochem. and Eng. Aspects*, 330(2-3), 207–212.

Obot, I.B., Obi-Egbedi, N.O. and Umoren, S.A. (2009). "The synergistic inhibitive effect and some quantum chemical parameters of 2, 3-diaminonaphthalene and iodide ions on the hydrochloric acid corrosion of aluminium." *Corros. Sci.*, 51(2), 276–282.

Obot, I.B., Umoren, S.A. and Obi-Egbedi, N.O. (2011). "Corrosion inhibition and adsorption behaviour for aluminum by extract of *Aningeria robusta* in HCl solution: Synergistic effect of iodide ions." *J. Mater. Env. Sci.*, 2(1), 60-71.

Olivares-Xometl, O., Lopez-Aguilar, C., Herrasti, P., Likhanova, V.N., Lijanova, I. Martínez-Palou, R. and Marquez, J.R. (2014). "Adsorption and corrosion inhibition performance by three new ionic liquids on API 5L X52 steel surface in acid media." *Ind. Eng. Chem. Res.*, 53(23), 9534–9543.

Ovat, F.A., David, F.O. and Anyandi, A.J. (2012). "Corrosion behaviour of Al (6063) alloy (as-cast and age hardened) in H_2SO_4 solution." *J. Mater. Sci. Res.*, 1(4), 35-40.

Palou, R.M., Olivares-Xomelt, O. and Likhanova, N.V. (2014). *Environmentally friendly corrosion inhibitors, in: Development in corrosion protection*, InTech, Croatia, Europe, 431-465.

Papavinasam, S. (1999). "Corrosion inhibitors." *Uhlig's corrosion handbook*, Revie, R.W., ed., John Wiley & Sons, New Jersey, 1089-1096.

Papavinasam, S. (2011). "Evaluation and selection of corrosion inhibitors." *Uhlig's corrosion handbook*, Revie, R.W., ed., John Wiley & Sons, New Jersey, 1169-1178.

Pardo, A., Merino, M.C., Arrabal, R., Feliu, S. and Viejo, F. (2007). "Oxidation behavior of cast aluminum matrix composites with Ce surface coatings." *Corros. Sci.*, 49, 3118–3133.

Patel, A.S., Panchal, V.A., Mudaliar, G.V. and Shah, N.K. (2013). "Impedance spectroscopic study of corrosion inhibition of Al-Pure by organic Schiff base in hydrochloric acid". *J. Saudi Chem. Soc.*, 17, 53–59.

Pinto, G. M., Nayak, J. and Shetty, A. N. (2011a). "Corrosion inhibition of 6061 Al–15 vol. pct. $SiC_{(p)}$ composite and its base alloy in a mixture of sulphuric acid and hydrochloric acid by 4-(N,N-dimethyl amino) benzaldehyde thiosemicarbazone". *Mater. Chem. and Phy.*, 125(3), 628–640.

Pinto, G.M. (2010). "Studies on corrosion inhibition of 6061 Al-15 vol.pct. $SiC_{(p)}$ composite in acid medium". *Ph.D thesis, National Institute of Technology Karnataka*, Surathkal, Mangalore.

Pinto, G.M., Nayak, J. and Shetty, A.N. (2009). "Corrosion behaviour of 6061 Al-15 vol. pct. SiC composite and its base alloy in a mixture of 1:1 hydrochloric and sulphuric acid medium." *Int. J. Electrochem. Sci.*, 4, 1452 – 1468.

Pinto, G.M., Nayak, J. and Shetty, A.N. (2011b). "Adsorption and inhibitor action of 4-(N,N-dimethylamino)benzaldehyde thiosemicarbazone on 6061 Al SiC composite and its base alloy in sulfuric acid medium." *Synth. React. Inorg. M.*, 41, 37–41.

Pinto, G.M., Nayak, J. and Shetty, A.N. (2011c)."4-(N,N-Diethylamino) benzaldehyde thiosemicarbazone as corrosion inhibitor for 6061 Al–15 vol .pct. $SiC_{(p)}$ composite and its base alloy, *JOM*, 21, 53–71.

Poornima, T., Nayak, J. and Shetty, A.N. (2011). "Effect of 4-(N,N-diethylamino)benzaldehyde thiosemicarbazone on the corrosion of aged 18 Ni 250 grade maraging steel in phosphoric acid solution." *Corros. Sci.*, 53(11), 3688-3696.

Rao, S.A., Padmalatha, Nayak, J. and Shetty, A.N. (2005). "3-Methyl-4-amino-5 mercapto-1, 2, 4-triazole as inhibitor of corrosion of 6061 Al-15 vol. pct. SiC$_{(p)}$ composite." *J. Met. Mater. Sci.*, 47, 51-56.

Ravari, F.B. and Dadgareenezhad, A. (2013). "Synergistic influence of propargyl alcohol and zinc sulfate on inhibition of corrosion of aluminum in 0.5 M H$_2$SO$_4$." *J. Chil. Chem. Soc.*, 58, 1853-1857.

Roberge, P.R. (2007). "Defects and failures." *Corrosion inspection and monitoring*, John Wiley & Sons, Inc., Hoboken, New Jersy.

Roman, G., Vlahakis, J.Z., Vukomanovic, D., Nakatsu, K. and Szarek, W.A. (2010). "Heme-oxygenase inhibition by 1-aryl-2-(1H-imidazol-1-yl/1H-1,2,4-triazol-1-yl)ethanones and their derivatives." *Chem. Med. Chem.*, 5, 1541–1555.

Şafak, S., Duran, B., Yurt, A. and Turkoglu, G. (2012). "Schiff bases as corrosion inhibitor for aluminium in HCl solution." *Corros. Sci.*, 54, 251–259.

Sastri, V.S. (1998). *Corrosion inhibitors: Principles and applications*, Wiley, New York.

Sastri, V.S. (2012). *Green corrosion inhibitors: Theory and practice*, Wiley, New York.

Sastri, V.S., Ghali, E. and Elboujdaini, M. (2007). *Corrosion prevention and protection: Practical solutions*, John Wiley & Sons, New York.

Sato, N. (2012). "Basics of corrosion chemistry." *Green corrosion chemistry and engineering: opportunities and challenges*, First edition, Sharma, K.S., ed., Wiley-VCH Verlag GmbH & Co. KGaA, Weinheim.

Scendo, M. and Uznanska, J. (2011). "The effect of ionic liquids on the corrosion inhibition of copper in acidic chloride solutions." *Int. J. Corros.*, 2011, 1–13.

Sharma, A., Sharma, A., Choudhary, G. and Yadav, S. (2012). "Effect of mineral acids on corrosive propensity of metals." *Int. J. Sci. Adv. Technol.*, 2(12), 68-74.

Shetty, H. (2009). "Corrosion is a national calamity: declares NIGIS at World CORCON 2009 Seeks Government, industry and citizen support to fight corrosion." *India PRwire*, http://www.indiaprwire.com.

Shimomura, T., Tolle, K.J., Smid, J. and Szwarc, M. (1967). "Energy and entropy of activation of propagation by the free polystyryl anions and their ion pairs. The phenomenon of "negative" activation energy." *J. Am. Chem. Soc.*, 89(4), 796-803.

Shreir, L.L., Jarman, R.A. and Burstien G.T. (1994), "Corrosion." Vol I and II, *Metal/Environment Reactions*, Third edition, Butterworth-Heinemann, Jordan Hill, Woburn, MA.

Song, P., Guo, X.-Y., Pan, Y.-C., Shen, S., Sun, Y., Wen, Y. and Yang, H.-F. (2013). "Insight in cysteamine adsorption behaviors on the copper surface by electrochemistry and Raman spectroscopy." *Electrochim. Acta*, 89, 503–509.

Srinivasan, S. (2006). "Electrode/electrolyte interfaces:Structure and kinetics of charge transfer." *Fuel cells: from fundamentals to applications*, Springer, New York, 28.

Stoyanova, A.E., Sokolova, E.I. and Raicheva, S.N. (1997). "The inhibition of mild steel corrosion in 1 M HCl in the presence of linear and cyclic thiocarbamides-Effect of concentration and temperature of the corrosion medium on their protective action." *Corros. Sci.*, 39, 1595–1604.

Trabanelli, G., Montecelli, C., Grassi, V. and Frignani, A. (2005). "Electrochemical study on inhibitors of rebar corrosion in carbonated concrete." *J. Cem. Concr. Res.*, 55, 1804-1809.

Trowsdale, A.J., Noble, B., Harris, S.J., Gibbins, I.S.R., Thompson, G.E. and Woods, G.C. (1996). "The influence of silicon carbide reinforcement on the pitting behavior of aluminum." *Corros. Sci.*, 38, 177–191.

Turnbull, A. (1992). "Review of corrosion studies on aluminium metal matrix composites." *Br. Corros. J.*, 27, 27-35.

Turner, D.R. (1953). "The effect of temperature on the cathode potential during nickel plating." *J. Electrochem. Soc.*, 100(1), 15-21.

Uerdingen, M., Treber, C., Balser, B., Schmitt, G. and Wernerbd, C. (2005). "Corrosion behaviour of ionic liquids." *Green. Chem.*, 7, 321-325.

Uhlig, H.H and Revie, R.W. (1991). *Corrosion and corrosion control*, Third edition, John Wiley & Sons, New York.

Wang, F., Fan, R., Jia, M. and Wang, J. (2014). "Corrosion inhibition of triazinedithoil for aluminum alloy in hydrochloric acid solution." J. *Material Sci. Eng.*, 4(1), 1-5.

Winkler, S.L. and Flower, H.M. (2004). "Stress corrosion cracking of cast 7XXX aluminum fibre reinforced composites." *Corros. Sci.*, 46, 903–915.

Xu, B., Liu, Y., Yin, X., Yang, W. and Chen, Y. (2013). "Experimental and theoretical study of corrosion inhibition of 3-pyridinecarbozalde thiosemicarbazone for mild steel in hydrochloric acid, *Corros. Sci.*, 74, 206–213.

Yousefi, A., Javadian, S., Dalir, N., Kakemama, J. and Akbari, J. (2014). "Imidazolium-based ionic liquids as modulators of corrosion inhibition of SDS on mild steel in hydrochloric acid solutions: experimental and theoretical studies." *RSC Adv.*, 5, 11697-11713.

Yurt, A. and Aykın, O. (2011). "Diphenolic schiff bases as corrosion inhibitors for aluminium in 0.1M HCl: Potentiodynamic polarisation and EQCM investigations."*Corros. Sci.*, 53, 3725–3732.

Zaid, B., Saidi, D., Benzaid, A. and Hadji, S. (2008). "Effects of pH and chloride concentration on pitting corrosion of AA6061 aluminum alloy." *Corros. Sci.*, 50(7), 1841-1847.

Zarrouk, A., Messali, M., Aouad, M.R., Assouag, M., Zarrok, H., Salghi, R., Hammouti, B. and Chetouani, A. (2012). "Some new ionic liquids derivatives: Synthesis, characterization and comparative study towards corrosion of C-steel in acidic media." *J. Chem. Pharm. Res.*, 4(7), 3427-3436.

Zarrouk, A., Zarrok, H., Salghi, R., Hammouti, B., Ebenso, E.E., Bentiss, F., Oudda, H., Elbakri, M. and Touir, R. (2013). "Inhibition of copper corrosion by 2-aminobenzenethiol in aerated 2 M HNO$_3$ medium." *Int. J. Electrochem. Sci.*, 8, 11000–11018.

Zhang, Q.B. and Hua, Y.-X. (2009). "Corrosion inhibition of mild steel by alkylimidazolium ionic liquids in hydrochloric acid." *Electrochim. Acta,* 54, 1881-1887.

Zhang, Q.B. and Hua, Y.-X. (2010). "Corrosion inhibition of aluminum in hydrochloric acid solution by alkylimidazolium ionic liquids." *Mater. Chem. Phys.*, 119(1-2), 57-64.

Zhang, S., Sun, J., Zhang, X., Xin, J., Miao, Q. and Wang, J. (2014). "Ionic liquid-based green processes for energy production." *Chem. Soc. Rev.*, 43, 7838–69.

Zheng, X., Zhang, S., Li, W., Yin, L., He, J. and Wua, J. (2014). "Investigation of 1-butyl-3-methyl-1*H*-benzimidazolium iodide as inhibitor for mild steel in sulfuric acid solution." *Corros. Sci.*, 80, 383-392.

Zhu, J. and Hihara, L.H. (2010). "Corrosion of continuous alumina-fibre reinforced Al–2 wt. % Cu–T6 metal–matrix composite in 3.15 wt. % NaCl solution." *Corros. Sci.*, 52, 406–415.

LIST OF PUBLICATIONS

1. Shetty K.S. and Shetty A.N. (2014). "Studies on corrosion behavior of 6061 Al-15 vol. pct. SiC$_{(P)}$ composite in HCl medium by electrochemical technique." *Surf. Eng. Appl. Electrochem.*, 51(4), 374-381.

2. Shetty K.S. and Shetty A.N. (2015). "Ionic liquid as an effective corrosion inhibitor on 6061 Al-15 vol. pct. SiC$_{(P)}$ composite in 0.1 M H$_2$SO$_4$ medium – An ecofriendly approach." *Can. Chem. Trans.*, 3(1), 41-64.

3. Shetty K.S. and Shetty A.N. (2015). "New benzimidazolium based ionic liquid as a corrosion inhibitor for aluminum alloy composite in acidic media." *Corros. Sci.* [Communicated]

PAPER PRESENTED IN CONFERENCES/SYMPOSIUM

1. Shetty K.S. and Shetty A.N. (2014). "Electrochemical analysis on the corrosion behavior of 6061 Al-15 vol. pct. SiC$_{(P)}$ composite in hydrochloric acid medium." International Corrosion Prevention Symposium for Research Scholars (CORSYM-2014), February 18th-21st, 2014, Indian Institute of Technology Bombay, Mumbai.

2. Shetty K.S. and Shetty A.N. (2014). "Ionic liquid as corrosion inhibitor on 6061 Al-15 vol. pct. SiC$_{(P)}$ composite in 0.1 M H$_2$SO$_4$ medium- An ecofriendly approach." International Corrosion Conference (CORCON -2014), November 12th-15th, 2014, NACE event, Hotel Grand Hyatt, Mumbai.

3. Shetty K.S. and Shetty A.N. (2015). "Ionic liquid as corrosion inhibitor on 6061 Al-15 vol. pct. SiC$_{(P)}$ composite in 0.1 M HCl medium- An ecofriendly approach." International Conference on Green Chemistry: Catalysis. Energy and Environment, January 22nd-24th, 2015, ICGC-2015, Goa University, Goa.

CURRICULUM VITAE

Kshama Shetty S

'Devidaya', D/No: 1-14/4, Kottara Chowki, Mangalore-575006
+91-9901723368
kshama3021@gmail.com

ACADEMIC PROFILE

DOCTOR OF PHILOSOPHY (Ph.D.), National Institute of Technology Karnataka, Surathkal (July 2012-Present).

Research Area: Studies on some ionic liquids as corrosion inhibitors on Al 6061-SiC$_{(P)}$ composite in acidic media.

Research Publications/Presentations:

In Journals

1. Shetty K.S. and Shetty, A.N. (2015). "Studies on corrosion behavior of 6061 Al-15 vol. pct. SiC$_{(p)}$ composite in HCl medium by electrochemical techniques." *Surf. Eng. Appl. Electrochem.*, 51(4), 374–381.

2. Shetty K.S. and Shetty A.N. (2015). "Ionic liquid as an effective corrosion inhibitor on 6061 Al-15 vol. pct. SiC$_{(p)}$ composite in 0.1 M H$_2$SO$_4$ medium – An ecofriendly approach." *Can. Chem. Trans.*, 3(1), 41-64.

3. Shetty, K.S. and Shetty, A.N. "New benzimidazolium based ionic liquid as a corrosion inhibitor for aluminum alloy composite in acidic media", Communicated to *Corros. Sci.*

In Conferences

1. Shetty K.S. and Shetty A.N. (2014). "Electrochemical analysis on the corrosion behavior of 6061 Al-15 vol. pct. SiC$_{(p)}$ composite in hydrochloric acid medium." International Corrosion Prevention Symposium for Research Scholars (CORSYM-2014), NACE event, February 18-21, Indian Institute of Technology Bombay, Powai.

2. Shetty K.S. and Shetty A.N. (2014). "Ionic liquid as corrosion inhibitor on 6061 Al-15 vol. pct. SiC$_{(p)}$ composite in 0.1 M H$_2$SO$_4$ medium- An ecofriendly approach." International Corrosion Conference (CORCON -2014), November 12th-15th, NACE event, Hotel Grand Hyatt, Mumbai.

3. Shetty K.S. and Shetty A.N. (2015). "Ionic liquid as corrosion inhibitor on 6061 Al-15 vol. pct. SiC$_{(p)}$ composite in 0.1 M HCl medium- An ecofriendly approach." International Conference on Green Chemistry: Catalysis. Energy and Environment, January 22nd-24th, ICGC-2015, Goa University, Goa.

MASTER OF SCIENCE, St. Aloysius College (Autonomous) Mangalore, (2010-2012)

Area: Analytical Chemistry, **Aggregate:** 81%

BACHELOR OF SCIENCE, St. Aloysius College (Autonomous) Mangalore, (2007- 2010)

Area: Chemistry, Microbiology, Zoology, **Aggregate:** 81%